MRI and behavioural investigations of auditory function and cognition in naïve and expert listeners

MRI and behavioural investigations of auditory function and cognition in naïve and expert listeners

Francesco Caprini

Thesis submitted for the degree of Doctor of Philosophy (Ph.D.) in Psychology

Department of Psychological Sciences

Birkbeck College, University of London

2023

Originality Statement

I, Francesco Caprini, declare that except where due acknowledgement has been made to other sources, the work presented in this thesis is my own.

_____

Francesco Caprini

Abstract

The morphology, histology, and tonotopic organisation of the human auditory cortex vary significantly across individuals. Similarly, auditory perception and cognition are also characterised by considerable variability in both naive and expert listeners. Focusing on both the behavioural and neural domains, this thesis explores how individual differences in auditory perception and expertise relate to the functional and structural properties of the human auditory cortex.

In the first experimental chapter, we investigate the auditory perception and cognition of two groups of auditory experts: music instrumentalists and audio engineers. We find that musicians and audio engineers have lower thresholds than controls across several psychoacoustic measures. We also see an advantage across three auditory scene analysis tasks: musicians performed best in a sustained selective attention task with two competing streams of tones and a speech-in-babble-noise task, while audio engineers could better memorise and recall auditory scenes composed of non-musical sounds.

Next, we present a series of MRI investigations on the structural and functional properties of the human auditory cortex. We introduce an automated pipeline for the classification of Heschl's gyrus' duplication patterns and alignment of individuals with similar morphologies. After testing the pipeline's validity, we classify the morphology of 58 subjects and compare results with previous benchmarks and publicly available data. We then localise functional and structural homologies across gyri with different morphologies, align homologous regions, and compare the resulting average maps with those generated by existing curvature-based alignment techniques.

Finally, we explore whether the structural characteristics of Heschl's gyrus are associated with auditory perception and musical training. We find that individuals with a single gyrus in the left hemisphere have lower pitch discrimination thresholds, and that greater myelination of the right Heschl's gyrus is associated with lower duration discrimination thresholds. Conversely, there were no differences in musical training between individuals with different gyral morphologies.

Acknowledgements

I am deeply grateful to my supervisors, Professor Fred Dick and Dr Adam Tierney, whose support and guidance throughout all stages of my PhD allowed these research projects to reach fruition. Thank you, Fred, for coming along this -seriously- long journey and allowing me to grow as a scientist and a person.

I would also like to extend my gratitude to the Department of Psychological Sciences at Birkbeck, whose patience and acceptance allowed me to fulfil my academic goals; The Bloomsbury Colleges for funding my research program; the Society for Education, Music and Psychology Research (Arnold Bentley New Initiatives Fund); and the British Psychological Society Research Board (Postgraduate Study Visits Scheme).

I want to thank Dr Trevor Agus, who generously welcomed me in Belfast and played a pivotal role in the success of my projects; Professor Daniel Müllensiefen, who supported and mentored me through my academic transition from Italy to the UK; and Professor Susan Hallam, who with Fred allowed me to begin this journey.

I want to thank my family, who has supported me unconditionally since setting foot in frozen Canary Wharf until the final weeks of "*studio matto e disperatissimo*". Eric, no words could ever express my gratitude (or maybe I'm just terrible with words). Thank you for always being my rock. A heartfelt thank you to my extended family, Elena, Michela, Giulia, Giulia, Ioanna, Carlo, and Ilaria.

Finally, I am sincerely grateful to my examiners Professor Narly Golestani and Professor Robert Leech for taking the time to read my thesis, providing valuable feedback, and allowing me to end my PhD on such a positive note.

Table of contents

List of figures

Chapter 1.

General introduction

1.0 Preface

The elusive correspondence of structure and function in the brain has captivated philosophers' and scientists' curiosity for centuries. From Galen's ventricular flow of *pneuma psychicon* (Arribas, 2017), the interaction of *res extensa* and *res cogitans* in Descartes' enlightened depiction of the pineal gland (Berhouma, 2013), the misguided intuition of Gall's phrenology (Zola-Morgan, 1995), to the field-defining descriptions of cortical myelo- and cytoarchitectonics by pioneers Ramón y Cajal (Ramón y Cajal, 1923), Oskar and Cécile Vogt's (Kreutzberg et al., 1992), and Brodmann (Brodmann, 1909; Nieuwenhuys, 2013), the human ambition to capture tangible traces of the mind remains one of the essential drivers of modern neuroscience.

The introduction of radionuclide-free functional magnetic resonance imaging (fMRI) in the early '90s (Bandettini, 2012; Belliveau et al., 1991) propelled us into a new era of non-invasive, in-vivo exploration of task-dependent brain activity. By measuring the local changes in blood deoxyhaemoglobin (HbR) concentrations which follow neuronal activity (Ogawa et al., 1990), fMRI could *seemingly* map any psychological function onto a specific brain region or set of regions. Additionally, the development of streamlined visualisation and processing packages such as AFNI (Cox, 2012), SPM (Eickhoff et al., 2005), and Freesurfer (Fischl, 2012) allowed researchers from any background to solve complex tasks (e.g. automated segmentation of white and grey matter, parcellation of gyral patterns, cortical surface reconstruction, curvature-based inter-subject alignment, statistical

modelling, etc.) with simple commands. The combined enthusiasm for the potential of functional neuroimaging and the great accessibility provided by the software toolboxes led to the publication of an enormous amount of studies, with PubMed returning some 613,678 results for "fMRI" in the 31 years between 1991 and 2021.

Perhaps due to the luring simplicity of its "activation maps" and the many details and assumptions lost in translation in the journey from scanner to pop science magazines, the field has been at times criticised for reducing the study of the functional specialisation of the brain to a "neophrenology" (e.g. Uttal, 2001; but see Hubbard, 2003), that is a strongly modular cartography of the brain where area *X* is assigned function *Y*. The criticism sometimes also extended to the -well-known- technical limitations of fMRI (for a summary, see Logothetis, 2008) and improper statistical inference (Yarkoni, 2009). Nonetheless, beyond the constraints posed by measuring instruments or statistics (or whether neuroscientists might have occasionally overindulged in simplistic interpretations), the conclusions we draw from neuroimaging data build on a deeply interconnected set of philosophical assumptions and theoretical models.

More specifically, at a fundamental level, the neuroscientific practice of matching mental faculties and neural substrate involves combining elements of two ontologies[1] (Bard & Rhee, 2004; Gruber, 1993): one that defines the biological units (e.g. cortical regions defined by morphology or cytoarchitecture, nuclei, networks, genetic variants of a receptor)

[1] This exercise requires at least two assumptions: one ontological, which states the existence and overlap of *some* form of modularity in both the psychological and biological domains, and one epistemological, which states that neuroscientific methods allow us to gather knowledge on the ontology of the psyche by studying the brain and on the ontology of the brain by studying the psyche.

and one that establishes psychological constructs (e.g. sensory processing, memory, language, personality), as well as their relationships.

In terms of cortical ontology, Brodmann's study or cytoarchitecture famously led to a mosaic-like parcellation (Zilles & Amunts, 2010), still used over a century later to localise function[2]. Since individual cytoarchitecture is not available *in vivo* through MRI, the gyral and sulcal patterns of the cortex are usually what is used to identify discrete regions of the cortex. However, the correspondence between cortical morphology, cytoarchitecture, myeloarchitecture, and function is not univocal and is further obfuscated by the variability in cortical morphology across individuals (Amunts et al., 2007; Steinmetz et al., 1989), especially in higher-order areas (Fischl et al., 2008). For instance, in Broca's area, the borders separating Brodmann area (BA) 44 and 45 cannot be accurately predicted by sulcal morphology alone in individuals (Amunts & Zilles, 2006). Similarly, Heschl's gyrus (HG), the anterior-most transverse temporal gyrus, shows a high degree of morphological variability, with frequent occurrence of partial duplications (Marie et al., 2015). In such cases, automatic gyral parcellation and alignment could lead to invalid comparisons of structurally and functionally heterologous areas across individual brains. Expanding on this issue, in this thesis, we explore how individual differences in the morphology of HG relate to its histological and functional properties, how to leverage these properties to improve the alignment of gyri with different morphologies, and the relationship between variation in cortical structure and auditory skills.

[2] More recent probabilistic parcellation methods take into account multiple cortical properties instead of just cytoarchitecture (e.g. Glasser et al., 2016).

On the behavioural side, the deconstruction and classification of mental functions are possibly even more complex, partially due to the compounding effect of the ambiguous definition of psychological constructs and the multitude of tasks used to measure them. Efforts have been made to create systematic ontologies of mental processes (e.g. Poldrack et al., 2011; Poldrack & Yarkoni, 2016), although these are not widely adopted and several constructs remain poorly defined[3]. The issue of construct classification is also central in the study of learning and the transfer of expertise across–supposedly–different domains. For instance, several perceptual and cognitive abilities have been associated with musical instrument training[4]. However, the processing "modules" involved in playing a musical instrument, whose activity might affect non-musical skills, are not clearly defined or understood. In this thesis, we explore how the ability to understand speech in noisy environments, which has been somewhat inconsistently associated with musical expertise (Coffey et al., 2017b), relates to different facets of auditory scene analysis and perceptual skills in auditory experts (musicians and audio engineers) and non-experts.

The manuscript is structured as follows. In Chapter 1, we first review the literature on the biological mechanisms that drive corticogenesis, the emergence of individual differences in cortical morphology, and its relationship with local cytoarchitecture and histology. Second, we review the structural and functional properties of the auditory central nervous system across species, focusing on the human auditory cortex. Third, we review current data on the development of auditory skills and the interplay between expertise, brain plasticity, and

[3] For instance, www.cognitiveatlas.org (Poldrack et al., 2011) has an entry for "auditory scene analysis" but shows no associated tasks or related constructs other than "music perception".

[4] A literature review on the "effects" of musical training is provided in the introduction of Chapter 2.

genetics. In Chapter 2, we present the results of a behavioural study which explores differences and interactions between auditory-based perceptual and cognitive skills of two groups of auditory experts (i.e. music instrumentalists and audio engineers) and controls. In Chapter 3, we evaluate the inter-subject variability and association of cortical myelination and tonotopy in the human auditory cortex. Chapter 4 presents a pipeline to automatically classify and align Heschl's gyri based on their morphology. In Chapter 5, apply this technique to illustrate the individual differences in morphology, myelination, and functional properties of Heschl's gyrus, and how they relate to each other. We then evaluate whether gyral parcellation alone is sufficient to define functionally and structurally homologous regions across individuals. Based on these results, we compute group-average maps of the homologous HG regions and compare them with the maps obtained with curvature-based alignment. In Chapter 6, we explore the correlation between HG morphology, auditory perception, and musical training. Chapter 7 discusses the experimental findings in the context of recent literature, their limitations, and potential next steps in researching auditory expertise and the auditory cortex.

1.1 Development and biological significance of gyrencephaly

1.1.1 Ontogeny

Neurogenesis begins with the asymmetric proliferation of neuroepithelial stem cells in the ventricular zone (VZ), which lines the lateral ventricles of the developing embryo. The asymmetric division leads to the production of new progenitor stem cells or apical radial glia (aRG) (Noctor et al., 2002), a multipotent type of stem cell characterised by an apical process connected to the ventricular wall, and a longer basal process that extends radially

connected to the pial surface. ARG further undergo asymmetric division to produce intermediate progenitor cells (IPC), basal radial glia (bRG), or a neuron (Betizeau et al., 2013). Following the scaffolding provided by the aRG, IPCs and bRG migrate radially to form a new germinal layer called the subventricular zone (SVZ). In contrast, neurons migrate further, populating what would become the infragranular layers of the cortex (Lewitus et al., 2013).

An additional lamination into two distinct outer (OSVZ) and inner (ISVZ) zones was first observed in the larger SVZ of primates (Smart et al., 2002), but its presence was later confirmed in several other gyrencephalic species (Fietz et al., 2010; Gilardi & Kalebic, 2021; Reillo et al., 2011; Toda et al., 2016). The OSVZ is characterised by a high density and morphological diversity of basal progenitors, namely non-polar IPCs and several types of bRG defined by the presence and length of their apical and basal fibres. Interestingly, bRG was initially described as having a single basal process (e.g. Fietz et al., 2010; Hansen et al., 2010), but later studies not only described several morphological variants but also identified this variability as a critical regulatory component of proliferative behaviour (Betizeau et al., 2013; Borrell & Götz, 2014; Kalebic et al., 2019; Kalebic & Huttner, 2020): by determining the type of extrinsic input that the cell receives, the morphology of the bRG affects its transcriptional activity and mitotic fate. For instance, apically connected cells can respond to proliferative signals from the cerebrospinal fluid in the ventricles (Fame et al., 2020), while basal processes are sensitive to neuronal activity in the forming cortical plate and thalamocortical axons (Arai & Taverna, 2017; Reillo et al., 2017). More generally, the role of bRG in gyrencephalic animals seems to be two-fold: on the one hand, the symmetric and asymmetric mitotic properties of these progenitors allow them to

simultaneously self-sustain and dramatically amplify neuronal production (Martínez-Cerdeño et al., 2006); on the other hand, the abundance of bRG basal fibres causes them to orient in a fan-like fashion, increasing the tangential dispersion of neurons migrating towards the cortical plate and the formation of gyral patterns (Borrell & Reillo, 2012; Hevner & Haydar, 2012; Lui et al., 2011). Conversely, bRG make up a much smaller percentage of the progenitor pool of the mouse, tends to have a more uniform morphology with single basal processes organised in parallel, and mainly divide symmetrically to produce two neurons rather than self-renewing (Wang et al., 2011; Shitamukai et al., 2011; Dehay et al., 2015).

1.1.2 Phylogeny

Although the striking differences in corticogenesis between mice and primates would intuitively implicate bRG and SVZ expansion as an evolutionary stepping stone in the expansion and complexification of the cerebral cortex, the actual phylogeny of brain morphology across species appears to be much more complex (Cárdenas & Borrell, 2020). A comparable lamination and size of the germinal layers, as well as an abundance of bRG, to that observed for gyrencephalic primates and ferrets, was also observed in the marmoset, a lissencephalic primate, and the agouti, a gyrencephalic rodent (Garcia-Moreno et al., 2012; Kelava et al., 2012). Therefore, the presence of an OSVZ and the number of basal progenitors during corticogenesis might be necessary for developing gyrencephaly but not sufficient. Other species-specific adaptations must have occurred during evolution (Borrell & Calegari, 2014; Laguesse et al., 2015). Lewitus et al. (Lewitus et al., 2014) modelled the degree of gyrification of the cortex with several neurophysiological and life-history traits in mammals. They found that the main discriminant factor between species with high and low

degrees of gyrification is the ability of progenitor cells to undergo symmetric division. In their model, this proliferative mode alone could explain the 14-fold difference in brain weight gain per day between the high and low gyrification groups. Conversely, variability within these two groups could be best explained by differences in the duration of neurogenesis during gestation. In other words, the phenotype of cortical size and folding in mammals appears to follow a bimodal rather than linear distribution determined by discrete modalities of neurogenesis. In contrast, other adaptations, such as the duration of gestation, might instead explain variability across species that share the same proliferative modality. Finally, the authors estimated the mammal ancestor to be moderately gyrencephalic, in contrast with the classic notion that the mammalian brain might have evolved from a small lissencephalic brain to a large gyrencephalic one. Additional evidence supports the hypothesis that the mammal ancestor was large-bodied (Luo, 2007; Romiguier et al., 2013) and gyrencephalic (O'Leary et al., 2013). If the brain evolved linearly from lissencephaly to gyrencephaly, it must have done so independently across all mammalian orders. Alternatively, a more parsimonious explanation would be that the ancestral brain was already gyrified, and individual orders and species evolved towards a more or less gyrified morphology according to individual evolutionary pressure. Mice and marmosets might have lost the gyrencephalic phenotype in their miniaturisation process, albeit through different processes: the former by altering the cytoarchitecture of its germinal layers, the latter by maintaining the same architecture but tuning progenitor activity or shrinking the neurogenic period (Kelava et al., 2012; Kelava et al., 2013). Notably, large-bodied sirenians (manatees and dugongs) also possess a lissencephalic cortex, as opposed to the highly gyrated cortex of cetaceans (Butti et al., 2011; Reep & O'Shea, 1990). Thus other

evolutionary pressures other than miniaturisation, such as adaptation to aquatic life or diet, can result in lissencephaly. For instance, sirenians also possess very large ventricles, which might exert pressure on the skull, impede the formation of gyri, and double the cortical thickness of cetaceans, largely increasing cortical volume without increasing cortical area (Manger et al., 2012).

1.1.3 Genetics

Several genetic and epigenetic components have been implicated in the development of brain morphology. Evidence from twin studies points to high heritability for intracranial, white and grey matter volumes (Baare, 2001; Gilmore et al., 2010; Peper et al., 2007), corpus callosum and ventricular size (Jansen et al., 2015; Pfefferbaum et al., 2004), and sulcal depth (Van Der Meer et al., 2021). Local grey matter volume in Heschl's Gyrus, medial frontal cortex, and postcentral gyrus also show high heritability (Peper et al., 2007). On the other hand, sulcal patterns appear to be moderately heritable (White et al., 2002) but also display significant environmental components (Bartley, 1997; Mohr et al., 2004), with genetic heritability being highest for deeper sulci (Lohmann, 1999).

At the cellular level, the healthy development and gyrification of the cortex are orchestrated by a carefully coordinated sequence of changes in transcriptional activity, which determine critical components of corticogenesis such as progenitor proliferation and fate, mitotic cycle length, delamination from the VZ, basal progenitor amplification, neuronal migration, composition of extracellular matrix, and mechanical tissue properties (Borrell, 2018; Franchini, 2021; Llinares-Benadero & Borrell, 2019). In more detail, Trnp1 expression in aRG regulates their proliferative activity, with low levels leading to asymmetric division into bRG and high levels promoting self-renewal instead. Downregulation of Trnp1 in the

lissencephalic murine cortex has been shown to augment the proliferation and delamination of bRG and induce gyrification (Stahl et al., 2013). The downregulation of Trnp1 in gyrencephalic species is epigenetically controlled by H3 acetylation, which appears to be high in human bIPCs but low in murine bIPCs (Kerimoglu et al., 2021). The timing of transcriptional activity also plays a crucial role in correct cortex development. In the developing ferret embryo, aRG generates a large number of bRG within a critical time window of only 3-4 days in response to the downregulation of Trnp1 and Cdh1, after which bRG begins to self-renew and proliferate independently, forming the oSVZ. Disruption of aRG asymmetric division during this specific time window leads to the absence of oSVZ and cortical malformation (Martínez-Martínez et al., 2016).

Studies using knockout animal models or gene overexpression allowed the identification of several other molecular pathways implicated in the modulation of progenitor behaviour and gyral formation (Cárdenas & Borrell, 2020). Non exhaustively, these include TAG1, whose knockdown leads to retraction of the basal process of RG, disrupting histogenesis (Okamoto et al., 2013); Slit-Robo signalling, which regulates neuronal migration and the balance between direct neurogenesis and production of IPCs (Cárdenas et al., 2018; Gonda et al., 2020); fibroblast growth factor (FBF) signalling, which amplifies progenitor proliferation in the oSVZ and enhances gyrification (Matsumoto et al., 2017); Insm1, responsible for promoting NPC delamination by altering the structure of the apical adherens junction belt (Tavano et al., 2018); sonic hedgehog (SHH) signalling, whose overexpression in the mouse promotes the novel generation of bRG and self-renewal of IPCs, inducing cortical expansion and folding (Wang et al., 2016); and Pax6 expression in the aRG, which alters their cleavage plane orientation, promoting asymmetric division and

generation of bRG in the mouse (Wang et al., 2009; Wong et al., 2015). Additionally, in the mouse, the ectopic expression of primate-specific TBC1D3 (Ju et al., 2016) and TMEM14B (Liu et al., 2017) also increases the production of bRG, size of SVZ, and cortical thickness. Similarly, expression of human-specific ARHGAP11B has been shown to increase the bRG pool (Florio et al., 2016) and induce cortical gyrification in mice (Florio et al., 2015), ferrets (Kalebic et al., 2018), and marmosets (Heide et al., 2020).

Neuronal migration also plays a fundamental role in the development of cortical morphology, and mutations in several genes involved in this process are known to be associated with cortical malformations (Ross & Walsh, 2001). More specifically, mutations in the gene coding for Reelin (RELN), an extracellular protein involved in neuronal terminal translocation (i.e. guiding the final position of the migrating neuron) and cortical stratification (Nomura et al., 2008; Rice & Curran, 2001; Sekine et al., 2014), is associated to lissencephaly in humans (Hong et al., 2000). Cdk5 knockout in the ferret also disrupts the organisation of upper-layer neurons and cortical folding (Shinmyo et al., 2017). Conversely, Del Toro et al. (del Toro et al., 2017) demonstrated that the ablation of cell adhesion molecules FLRT1 and FLRT3 promotes neuronal migration in the mouse, leading to the formation of cortical gyri, notably without affecting progenitor morphology or amplification. Additionally, they found that expression of FLRT1 and FLRT3 in the ferret is lower in sulci than in gyri, indicating that cortical folding, to some degree, reflects alternating patterns of neuronal transcriptional activity. Corroborating this hypothesis, alternating patterns of differentially expressed genes have also been identified in regions of the oSVZ of the ferret corresponding to prospective gyral and sulcal regions (de Juan Romero et al., 2015; Reillo et al., 2011; Toda et al., 2016; Matsumoto et al., 2020).

These findings suggest that the modulation of genes shared across mammal phylogeny can give rise to a broad spectrum of morphologies. These genetic pathways coordinate key morphogenetic processes such as progenitor morphology and proliferation, as well as neuronal radial and tangential expansion. Additionally, the correspondence between alternating patterns of differentially expressed genes within the germinal layers and prospective gyri and sulci implies that cortical morphology is, to some degree, genetically predetermined. Importantly, this line of evidence only applies to phylogenetically and ontogenetically older landmarks such as the central sulcus, the Sylvian fissure, or the calcarine sulcus, but cannot be extended to more superficial gyral and sulcal patterns, which vary considerably across individuals.

1.1.4 Folding mechanics

Multiple mechanisms have been proposed to explain the forces and tissue properties that might lead to the formation of cortical convolution (Garcia et al., 2018; Ronan & Fletcher, 2015). It was initially hypothesised that the expanding cortex crumples in response to the spatial constraint imposed by the skull (Welker, 1990). This hypothesis has been largely dismissed due to observing that the cortex folds even without volumetric restrictions (Barron, 1950). Another theory implicated the pulling force resulting from axonal tension as a cause of cortical folding (Van Essen, 1997). Empirical evidence also contradicts this theory, as axons are mainly oriented radially within gyri and could not realistically exert sufficient force to drive folding directly (Xu et al., 2010). However, this does not exclude the potential role of axonal tension, cell body deformation, and cortico-cortical connectivity as mediators of other neurotrophic processes (Foubet et al., 2019; Javier-Torrent et al., 2021; Van Essen, 2020). For instance, the co-variation of micro- and macro-anatomical

characteristics (i.e. grey matter volume, cortical size, myelination) of distant cortical areas in humans can be explained by their degree of structural connectivity (Fenchel et al., 2020; Smith et al., 2019; Yang et al., 2021); similarly, the degree of cytoarchitectonic similarity of distant areas in the cortex of the mouse correlates with their cortico-cortical connectivity, both ipsilaterally and contralaterally (Goulas et al., 2017).

Another proposed driver of cortical folding is the differential expansion of cortical and subcortical layers; that is, a higher rate of tangential expansion of superficial layers would increase their compressive stress, leading to buckling and the formation of sulci (Ronan et al., 2014). This mechanism is compatible with the physical modelling of layered expanding tissues with similar viscoelastic properties (Tallinen et al., 2016; Tallinen et al., 2014), which can predict the shape, orientation, and wavelength of resulting convolutions. However, these models cannot predict the exact location or patterns of convolutions as they appear in actual brains. Although initial shape, tissue viscoelasticity, and differential expansion *across* layers can predict the overall formation and frequency of convolutions, local differences in the growth rates *within* layers are needed to predict their actual location (Bayly et al., 2013). This heterogeneity of cortical expansion could be explained by the different patterns of neurogenesis and transcriptional activity in the oSVZ of prospective sulci and gyri in gyrencephalic species (Reillo et al., 2011), but also by tissue development after neurogenesis, such as apoptosis, neuronal differentiation and translocation, and development of connectivity, or, more generally, the development of local cytoarchitecture. For instance, longitudinal diffusion tensor imaging (DTI) studies revealed a co-occurrence of gyral formation and reduction of local fractional anisotropy (FA) (Kroenke et al., 2009). Combining FA measurements with staining of cortical tissue at different phases of

morphogenesis, these studies (Jespersen et al., 2012; Wang et al., 2017) linked FA reduction to the development of dendritic arborisation: during early corticogenesis, undifferentiated neurons possess mainly radially oriented processes, constraining water diffusion in one specific direction, while the subsequent formation of tangentially oriented dendrites leads to an average isotropic mode of diffusion. More generally, cytoarchitectural and folding patterns are roughly co-localised, with the correspondence being more consistent for primary and secondary convolutions (Fischl et al., 2008; Fischl, 2013). Seminal enucleation (i.e. removal of the eye) studies demonstrated a reduction (70%) in the size of the primary visual cortex (Dehay et al., 1991) and a concurrent increase in gyrification (Rakic, 1988) following enucleation during the first half of gestation, but no change if enucleation occurred in the second half. Notably, the patterns of gyrification induced by enucleation appeared to be consistent across animals, and the increase in folding did not correspond to an increase in cortical size (Dehay et al., 1996). These results highlight the importance of the timing of thalamocortical signals in the development of local cytoarchitecture (Sato et al., 2022) and its influence on macro-anatomical morphology.

In summary, current evidence identifies local variability in the rate and timing of cortical expansion as one of the leading forces driving cortical gyrification. Regional differences in rates of neurogenesis and cytoarchitecture are considered to be the primary sources of this variability. Furthermore, tissue organisation and microanatomy are affected by the biomechanical forces induced by cortical folding and thalamocortical and cortico-cortical connectivity.

1.1.5 Function and pathology

Cortical folding emerges from the interaction of tightly regulated genetic and biomechanical events. Disruption of any of the components involved in this process (i.e. progenitor proliferation, neuronal migration, terminal translocation, connectivity, etc.) can lead to severe malformations, such as microcephaly, lissencephaly, polymicrogyria, and heterotopias. The related clinical presentation usually includes epilepsy and severe cognitive disability (Guerrini & Dobyns, 2014; Subramanian et al., 2020), although there are cases, such as focal cortical dysplasia, where cognitive impairment can be mild or absent, depending on the specific area affected (Blackmon et al., 2015).

Without clear developmental malformations, it is possible to trace gross gyral and sulcal regularities across individuals or, in the case of phylogenetically older landmarks, even species. These regularities underpin the creation of standard atlases of human cortical morphology (e.g. Destrieux et al., 2010), commonly used to identify homologous regions across individuals. However, one major limitation of this approach is that it underweights the importance of individual differences in local morphology, which are widespread even in typically developed bran and especially pronounced in higher-order cortical areas (Fischl et al., 2008): on the one hand, this variability undermines the ability to determine a true homology (e.g. in function or cytoarchitecture) across individuals for a given standardised anatomical region; on the other hand, the approximations introduced by standard atlases can potentially conceal critical information about brain function and behaviour that is embedded in individual morphology.

Several studies have explored the relationship between regional morphological variability, functional localisation, and behaviour, employing either measure of average local curvature

like the local gyrification index (LGI) or by explicitly examining specific sulcal variants of a given region.

For instance, the exact location of the peak activation of the default mode network in the ventromedial prefrontal cortex (vmPFC) was found to depend on the individual configuration of sulcal patterns, specifically on the presence of an additional rostral sulcus (Lopez-Persem et al., 2019). Li et al. (2015) identified the location of two types of reward-dependent activation (i.e. monetary and erotic) in the orbitofrontal cortex (OFC), which could only be detected when local variations in sulcal morphology were taken into account, highlighting potential limitations of group-average analyses. Similarly, Amiez et al. (2013) found reward-related activity in the midcingulate cortex (MCC) to be located in the cingulate sulcus in participants with a single sulcus configuration but in the additional paracingulate sulcus in participants who exhibit one. The sensorimotor representation of different effectors (e.g. tongue, larynx, lips, hand) was also shown to be dependent on the individual sulcal configuration of the central gyrus (Eichert et al., 2021; Germann et al., 2020), while the local anatomical variability of the precentral gyrus predicted the locus of activation for visuomotor hand conditional activity and saccadic eye movement.

Several associations have also been reported between indices of local and global cortical gyrification and perception, cognitive ability, and motor control, but also neurodevelopmental and psychiatric disorders. In terms of general cognitive ability, putative associations with gyrification, both global and local within frontoparietal regions, have been proposed (Chung et al., 2017; Lamballais et al., 2020), although these effects appear to be mediated by age and very small (Mathias et al., 2020). Mathematical abilities appear to be associated with cortical surface complexity of the right temporal gyrus

(Heidekum et al., 2020) as well as the left postcentral gyrus, right insular sulcus and left lateral orbital sulcus (Polspoel et al., 2020). As for language, a negative correlation was reported between phonetic ability (i.e. discrimination of fricatives) and gyrification in the transverse temporal gyrus bilaterally (Fuhrmeister & Myers, 2021), while age-related reduction of gyrification in the right cingulate and entorhinal cortices was identified in monolinguals, but not in bilinguals (Del Maschio et al., 2019). Unique morphological patterns also appear to co-occur with specific neurodevelopmental and psychiatric disorders (Sasabayashi et al., 2021). More specifically, altered gyrification has been identified for schizophrenia in several cortical regions, including the supramarginal gyrus, inferior frontal gyrus, insula, and prefrontal cortex (Madeira et al., 2020; Rollins et al., 2020; Sasabayashi et al., 2020; Spalthoff et al., 2018). Autism spectrum disorder has been reportedly associated with reduced gyrification of the left supramarginal gyrus (Libero et al., 2014) and specific morphological variants of the orbitofrontal sulcal patterns, namely a reduced number of intermediate and posterior orbital sulci, which is considered to be associated with social behaviour (Nakamura et al., 2020). Increased gyrification of the left occipitotemporal cortex -which hosts the visual word form area- has been observed in children with dyslexia (Williams et al., 2018), with variability in the morphology of the occipitotemporal sulcus showing an association with reading fluency (i.e. better fluency for discontinuous sulci).

These studies highlight the sheer amount of functional information that can potentially be derived from a brain's unique cortical morphology, including early markers of psychopathology. For instance, using a neural network trained on structural imaging data from 591 subjects obtained from the Human Connectome Project (HCP), Ellis and

Aizenberg (2022) found that cortical and subcortical morphology alone was sufficient to predict individual activation maps across 47 different tasks. More generally, it is clear that cortical localisation based on rough anatomical landmarks can severely reduce the range of questions that one can ask about brain function and conceal essential information rooted in individual differences. Indeed, the integration of several sets of data, such as brain morphology, cytoarchitecture, connectivity, and function, will be essential for the identification of precise homologies across individual brains (Glasser et al., 2016).

1.2 The auditory cortex: characteristics, definitions, and theoretical framework

1.2.1 The auditory pathway

The auditory pathway comprises a series of interconnected structures collectively responsible for capturing, amplifying, abstracting, and integrating the dynamic stream of information contained in the material waves that constantly surround us. Unlike the visual system, which has just one relay station (the lateral geniculate nucleus in the thalamus) between the eye and the primary visual cortex, the auditory pathway includes several subcortical structures, including the cochlear nucleus, superior olivary complex, lateral lemniscus, inferior colliculus, and medial geniculate body in the thalamus. These subcortical structures are small in size and contain several functionally distinct subnuclei (Glendenning & Masterton, 1998), which severely limits the ability to study their structure and function in vivo, particularly in humans. For this reason, most of the research on subcortical auditory structures has focused on animal and ex-vivo methodologies (Kandler, 2019). Briefly, these studies have identified the role of cochlear nuclei in the processing of sound intensity, pitch, and location (Blackburn & Sachs, 1990; Reiss & Young, 2005).

Ascending on the auditory pathway, the superior olivary complex receives bilateral input from both cochlear nuclei and processes location cues such as interaural time and level difference (Tollin, 2003), while the inferior colliculus is sensitive to spectral and temporal information (Versnel et al., 2009) and to have a potential role in the integration of auditory and sensorimotor inputs (Aitkin et al., 1978). Finally, neuronal activity in the medial geniculate body has been implicated in the modulation of information to and from the auditory cortex in a task-oriented way (Antunes & Malmierca, 2011; Chen et al., 2019; Kommajosyula et al., 2021). Clusters of neurons that fire in response to specific sound frequencies have been identified across all structures of the auditory pathway (Bajo et al., 1999; Hackett et al., 2011; Merzenich et al., 1975; e.g. Ryugo & Parks, 2003), mirroring the tonotopic configuration of the cochlea from the cochlear nuclei to the auditory cortex. Although structural homologies exist between the auditory pathway of humans and other mammals (Malmierca & Hackett, 2010; Schofield, 2010), the findings of invasive animal research don't necessarily generalise to the small-scale organisation or function of each structure in humans (Moore, 1987). Nevertheless, the high resolution granted by MRI (Moerel et al., 2020) has provided some in-vivo insight into the structure (García-Gomar et al., 2019), connectivity (Javad et al., 2014; Maffei et al., 2018; Sitek et al., 2019) and function of subcortical auditory structures in humans, such as the presence of tonotopic gradients in the inferior colliculus (De Martino et al., 2013) and the medial geniculate body (Mihai et al., 2019; Moerel et al., 2015).

1.2.2 A "primary" auditory cortex

The parcellation of the auditory cortex into discrete functional-structural units is also grounded in animal research. The definition of a primary auditory area, or "A1", was first

proposed by Woolsey & Walzl (1942), who identified a primary (A1) and non-primary (A2) auditory cortex in the cat by tracing cortical activation in response to cochlear stimulation. The cortical representation of the cochlea followed a posterior-anterior gradient from low to high frequencies. Other distinguishing characteristics of A1 in the cat are its direct connection with the ventral division of the medial geniculate nucleus (Lee et al., 2004), a thick granular layer (Winer, 1984) typical of koniocortical primary sensory cortices, and greater myelin density and expression of acetylcholinesterase (AChE), cytochrome oxidase (CO), and parvalbumin in middle layers (III and IV) compared to non-primary areas. A1 is surrounded anteriorly by an additional primary field (AAF), which is similar in cytoarchitecture to A1, directly connected to the thalamus, and tonotopic, albeit with an inverted high-to-low gradient and broader frequency tuning (Imaizumi et al., 2004). A primary-like posterior (P) field characterised by a direct connection to the medial geniculate nucleus and a mirrored (i.e. compared to A1) tonotopic gradient has also been described (Lee & Winer, 2008). A set of similar primary-like auditory fields like A1 and AAF have been observed in other mammals such as dogs (Malinowska & Kosmal, 2003) and ferrets (Bizley et al., 2005). As in cats, dogs' tonotopic gradients in A1 and AAF are also mirrored and separated by a region of high-frequency selective response, while in the ferret, tonotopic gradients extend mediolaterally in parallel across both fields. This functional difference is an important example of how primary auditory fields of different species might not share the same characteristics despite the use of the same nomenclature, such as "A1". In particular, the correspondence of tonotopic gradient reversals and cytoarchitectonic boundaries does not appear to be maintained across all species. From a phylogenetic perspective, homologous structures are defined based not on structural or

functional similarity per se but on the existence of a common ancestor from which those structures have evolved. In fact, homologous structures might present distinct functional characteristics in different species as a result of unique environmental pressures (Kaas, 2011). Conversely, structures that serve similar functions in different species could be the product of parallel or convergent evolution rather than the existence of a common ancestor. In this case, these functionally similar structures (e.g. the wings of a bee and a hummingbird) are classified as analogous rather than homologous (Nixon & Carpenter, 2012). The practical relevance of this distinction is that, even in the presence of a true homology, animal models do not necessarily generalise well to the small-scale organisation of the human auditory cortex and that, conversely, structures with similar characteristics are not necessarily homologous. This issue also underlies the decades-long search for a correspondence between the topography of the primary auditory fields of non-human primates and humans.

1.2.3 Human and non-human primates

The primate auditory cortex has been studied extensively (Baumann et al., 2015; Hackett et al., 2001; Imig et al., 1977; Merzenich & Brugge, 1973; Morel et al., 1993; Petkov et al., 2006; Rauschecker et al., 1995). Using the cat model, Woolsey (1971) initially identifies two primary fields in the money: A1 and A2. The use of the "A2" was eventually deprecated with the definition of a tonotopic, primary-like rostral[5] (R) field (Imig et al., 1977; Merzenich & Brugge, 1973), and an additional frontotemporal (RT) field (Morel & Kaas, 1992). These three regions constitute the auditory "core", distinguished by direct

[5] It was defined as rostrolateral (RL) in the original study by Merzenich & Brugge (1973).

connectivity with the ventral division of the medial geniculate body, primary-like cytoarchitecture, and tonotopic organisation (Hackett et al., 1998; Kosaki et al., 1997). The core region is connected to a surrounding set of secondary fields, known as the "belt", which is then connected to an additional surrounding "parabelt" region (Galaburda & Pandya, 1983; Hackett et al., 1998). In both New and Old World monkeys, tonotopic gradients of core fields follow a posterior-anterior high-to-low gradient in A1, with the first reversal in R and the second reversal in RT (Kajikawa et al., 2005; Philibert et al., 2005). These tonotopic patterns were also replicated in monkeys using fMRI (Baumann et al., 2010; Tanji et al., 2010). Inverted tonotopic gradients were reported in A1 in squirrel monkeys (Cheung et al., 2001); however, this could also be the product of inconsistent labelling of R as A1 (Kaas, 2011).

A similar keyhole-shaped auditory core was also identified in chimpanzees and humans ex vivo (Hackett et al., 2001) using observer-independent cytoarchitectonic staining techniques (Amunts et al., 2000, 1999). Cytoarchitectonic data on the human auditory cortex is scarce overall. Additionally, methodologies and nomenclatures vary across studies, which has resulted in several partially-overlapping parcellation schemes being proposed over the past century (Moerel et al., 2014). Although probabilistic cytoarchitectonic atlases are available (Amunts & Zilles, 2015), whether it is possible to delineate the borders of the primary auditory fields in vivo has been debated and researched for decades. Two main candidates have been investigated for this purpose: cortical myelination and tonotopy. The auditory core is marked by a high myelin content, particularly within A1, when compared to the surrounding belt and parabelt regions (Nieuwenhuys, 2013), which can be tracked using a selection of quantitative MRI

parameters that are sensitive to variation in myelin density (Lutti et al., 2014; Mancini et al., 2020; Weiskopf et al., 2021, 2013). Similarly, tonotopic gradients can be measured in vivo with fMRI (Formisano et al., 2003; Talavage et al., 2014; Talavage et al., 2004). These measurements have been used in isolation or combination to identify a putative auditory core or A1 (e.g. Dick et al., 2012; Moerel et al., 2020), although both have limitations. In the case of myelin, it is difficult to determine which threshold should be used to distinguish core fields from surrounding secondary fields, especially considering quantitative MRI myelin proxies vary across individuals and acquisition protocols (Carey et al., 2018). The use of tonotopic reversals as markers of cytoarchitectonic regionalisation is arguably even more controversial. Patterns of mirrored tonotopic gradients in humans were initially described as extending parallel to HG (Formisano et al., 2003; Talavage et al., 2004), which was seen as evidence of an underlying core also extending mediolaterally across HG, compatibly with cytoarchitectonic evidence (Hackett, 2007). However, later studies challenged this view, suggesting that human tonotopic gradients follow a posterior-anterior axis perpendicular (Humphries et al., 2010; Striem-Amit et al., 2011) or oblique (Langers & van Dijk, 2012; Woods et al., 2010) with respect to HG. In all of these studies, the observed tonotopic gradients extended posteriorly to HG into the planum temporale. Although unified frameworks have been proposed (Baumann et al., 2013), the homologies between the non-human primate and human auditory fields are still being questioned (Besle et al., 2019).

More generally, the application of non-human primate models to in vivo human data is driven by the lack of large-scale histological data or invasive neurophysiological recordings in humans. However, it is questionable whether the use of cross-species analogy is fully

warranted or informative, as homologous regions may differ considerably across specie due to divergent evolutionary pathways (Kaas, 2011). In other words, it is a working hypothesis, rather than a fact, that the human auditory core should follow the shape, function, or cytoarchitectonic configuration of other primates. Furthermore, the establishment of a generalised model of the human auditory cortex is further complicated by the gyral variability of the superior temporal plane in humans, which differs substantially from non-human primates.

1.2.4 Morphological variability

In monkeys, the location of the core, belt, or parabelt fields is not indicated by gross anatomical landmarks. The superior temporal plane of humans, on the other hand, is characterised by the presence of one or more convolutions, known as transverse gyri (of Heschl, HG), that extend anterolaterally to posteromedially. The morphology of HG itself varies across individuals, with the most common configurations being a single gyrus, two partially duplicated gyri connected at their medial end (also known as common stem duplication), and two or more fully duplicated gyri [6]. In chimpanzees, who possess a primitive single HG, the auditory core is aligned with the main mediolateral axis of the gyrus (Hackett et al., 2001). However, the observation of anterior-posterior tonotopic gradients in humans has challenged this view, suggesting either a different core orientation (e.g. Humphries et al., 2010) or a similar orientation but with gradients parallel to the core's axis (Besle et al., 2019).

[6] A more detailed review of the classification of HG morphology in humans can be found in the introduction of Chapter 4.

The exact correspondence of cytoarchitectonic and gyral topographies in this region varies across individuals (Morosan et al., 2001; Rademacher et al., 1993), and the location of homologous auditory fields relative to each morphological variant is currently unknown. However, the morphology of HG has been associated with several other neural and behavioural measures, such as myelination (Tzourio-Mazoyer et al., 2019), musicianship (Benner et al., 2017), learning non-native speech sounds (Golestani et al., 2007), dyslexia (Serrallach et al., 2016), and schizophrenia (Takahashi et al., 2022a). These studies highlight the importance of taking into account individual differences in HG morphology when studying the human auditory cortex, as they may be indicative of predisposition towards certain behavioural traits.

1.3 The auditory cortex: development, expertise, and plasticity

1.3.1 Perinatal development

The development of auditory processing in humans begins in the womb and continues after birth. The ear canal in humans typically opens around the 21st week of pregnancy (Anthwal & Thompson, 2016). Fetal movement and physiological response to sound are present since the end of the second trimester (Voegtline et al., 2013), with low-frequency sounds being perceived earlier (i.e. 19th gestational week) than high-frequency sounds (i.e. 27th gestational week; Hepper & Shahidullah, 1994). In the first six months after birth, children can detect differences in speech contour (Fernald & Kuhl, 1987) and timing (Aslin et al., 1981). On the other hand, the ear canal of altricial animals such as cats opens after birth. However, neural activity in response to sound is present in the first week after birth (i.e.

before the opening of the ear canal) in cats (Walsh et al., 1986), ferrets (Wess et al., 2017), and rats (de Villers-Sidani et al., 2007).

During neurogenesis, the auditory cortex develops earlier than the somatosensory and visual areas in several species. For example, in marsupials, all auditory cortical neurons form and migrate by around 46 days after birth, which is about three weeks earlier than in the visual cortex (Sanderson & Aitkin, 1990), while in rats, the formation of adult cortical laminae in the auditory cortex also develops earlier than in the visual cortex (Chang et al., 2018). Thalamocortical axons also reach the subplate neurons of the auditory cortex earlier than the visual and somatosensory cortex, but they reach the cortical layer 4 later, indicating an extended period of thalamic-subplate interaction (McConnell et al., 1994). Subplate neurons also form early connections with layer 4 of the developing auditory cortex (Zhao et al., 2009) and are the first to respond to sound before the opening of the ear canal and the development of a direct connection between the thalamus and cortical layer 4 (Wess et al., 2017). Cochlear manipulation or exposure to sound during this critical period can significantly alter the circuitry of subplate neurons (Meng et al., 2021). Furthermore, projections from the ventral medial geniculate body to the subplate of the auditory cortex can be observed in mice about two weeks before birth when projections from the inferior colliculus have not fully connected to the ventral medial geniculate body (Gurung & Fritzsch, 2004), suggesting that the direction of thalamocortical projections may be regulated by intrinsic programs or spontaneous activity in the thalamus, irrespective of any activity in lower regions of the ascending auditory pathway. Interestingly, spontaneous tonotopic signalling from the cochlea to the auditory cortex is present even before hearing onset, i.e. before the cochlea begins to sense and process sound (Babola et al., 2018), and

altering this activity has been found to disrupt the proper development tonotopic projections to the auditory brainstem (Kandler et al., 2009).

More generally, different onsets of deafness or timing of exposure to specific auditory environments have been shown to have different effects on the development of the auditory cortex. For instance, cats that are born deaf show a thinning of cortical layers 4 to 6 (Wong et al., 2014). However, early-onset deafness and late-onset deafness do not appear to affect laminar architecture or total cortical volume of the auditory cortex per se, but rather the relative volume of primary and secondary areas differed, with secondary areas growing thicker than primary areas (Wong et al., 2014). Additionally, congenital deafness in cats does not appear to affect thalamocortical projections between the medial geniculate body and A1, while deafness onset after birth reduces thalamocortical connectivity, in particular in the case of early onset (Chabot et al., 2015). Earlier research has also shown an effect of sound exposure, rather than deprivation, during critical windows. For instance, exposure to noise after birth can alter the tonotopic response in the inferior colliculus (Sanes & Constantine-Paton, 1985) and A1 (Zhang et al., 2002), while repeated exposure to sound pulses at a given frequency leads to an expansion of the cortical representation of that frequency (Zhang et al., 2001).

1.3.2 Myelination

Myelin is a lipidic sheath that envelops and insulates nerve cell axons. Myelin is produced by oligodendrocytes and Schwann cells in the central and peripheral nervous systems (Emery, 2010). Myelin makes up approximately 40% of the dry brain weight. Its primary role is to increase the speed and efficiency of electric signalling through a mechanism known as saltatory conduction: by only allowing action potentials to propagate through

small unmyelinated openings rich in voltage-gated sodium channels, known as nodes of Ranvier, rather than continuously along the entire length of axonal fibres, signalling speed is increased from 0.5-10 m/s up to 150 m/s. In the CNS, myelination begins with a pre-myelination phase, in which oligodendrocytes proliferate, migrate, and align their processes with target axons (Dubois et al., 2014). Axonal myelination starts before birth, with visible (ex-vivo) myelin in the pons and bulb around the 20th week of gestation and the cerebellum and internal capsule around the 37th (Baumann & Pham-Dinh, 2001). Myelination continues post-natally in the optic radiation, corpus callosum splenium, and posterior limb of the internal capsule (3rd month), the anterior limb of the internal capsule and corpus callosum genu (6th month), the occipital lobe (15th month), and frontal and temporal lobes (23rd month). Myelination across the auditory pathway mirrors the developmental milestones of auditory skill acquisition. For example, hearing onset co-occurs with the myelination of the cochlear nerve and the brainstem (Moore et al., 1995; Moore & Linthicum, 2001), while myelin development within the auditory cortex and its associated white matter tracts coincides with vocabulary acquisition in toddlers (i.e. about 1.5 years old; Su et al., 2008; Long et al., 2018). Cortical myelin content in developed brains also varies across different cortical regions (Dinse et al., 2015), with primary sensory areas such as the auditory cortex showing the highest degree of myelination (De Martino et al., 2015; Dick et al., 2012).

MRI studies in vivo showed that cortical myelination continues to increase at a rate of 0.5-1% until early adulthood (Carey et al., 2018) and declines afterwards (Callaghan et al., 2014). However, beyond physiological changes, myelination is also dynamically influenced by neuronal activity and is believed to mediate plastic changes in brain connectivity in an

experience-dependent way (Kaller et al., 2017; Long et al., 2018; Ullén, 2009). Studies on congenital deafness have shown a decrease in white matter to grey matter ratio and connectivity within HG and the temporal lobe (Hribar et al., 2014; Smith et al., 2011). Sinclair et al. (2017) observed that, in mice, ear plugging before the onset of hearing led to the development of thinner and less myelinated trapezoid body fibres. Ear plugging in adult mice also led to thinning of the same axonal fibres, indicating a potential effect of age-related hearing loss in the decline of myelination along the auditory pathway. Auditory enrichment during critical developmental periods might also affect myelination of the CNS. Increased connectivity in the corpus callosum was found in musicians who began training before the age of 7 compared to those who started after (Steele et al., 2013). Additionally, intense auditory training in rats is sufficient to reverse age-related decline in parvalbumin and myelin basic protein expression in A1 (de Villers-Sidani et al., 2010).

1.3.3 Auditory expertise in the brain

A number of differences in the brain's function and structure have been described in a variety of expert groups, such as sommeliers (Castriota-Scanderbeg et al., 2005) and perfumers (Plailly et al., 2011), racers (Lappi, 2015) and taxi drivers (Maguire et al., 2006), or karate black belts (Roberts et al., 2013). The brain of musicians has been studied extensively as a model of brain predisposition or plastic adaptation to intensive training (Schlaug, 2015). Evidence from cross-sectional studies has shown a greater cortical volume and thickness across several cortical regions of musicians compared to non-musicians, including the auditory cortex. (Bermudez et al., 2009; Gaser & Schlaug, 2003 ; e.g. Schneider et al., 2002). Although the issue of nature and nurture is still very much an open question (Olszewska et al., 2021), evidence suggests at least a partial experience-related

adaptation in response to musical training. For example, cross-sectional studies found that the effect of musical training on brain structure differed based on training onset (Steele et al., 2013), duration (Groussard et al., 2014), or intensity (Gaser & Schlaug, 2003). Furthermore, longitudinal studies found structural cortical changes in children who underwent instrument training compared to children who didn't (Habibi et al., 2020; Hyde et al., 2009).

Structural correlates of other types of auditory expertise have also been studied. For example, years of training in piano tuning were found to be associated with an increase in grey matter volume in the hippocampus and superior temporal gyrus (Teki et al., 2012). Furthermore, expert phoneticians were shown to have greater grey matter volume in the left pars opercularis (Golestani et al., 2011) as a function of years of training and alterations in frontotemporal connectivity (Vandermosten et al., 2016). The occurrence of left HG duplications was also higher in phoneticians (Golestani et al., 2011), indicating a potential predisposition to phonetic expertise. A similar increase in HG duplications was also previously observed in musicians (Schneider et al., 2002).

Chapter 2.

Generalization of auditory expertise in audio engineers and instrumental musicians[7]

2.1. Introduction

2.1.1 Musical expertise

2.1.1.1 Current literature

The training of a professional musician normally begins very early in life and is estimated to entail over 10000 hours of training by early adulthood (Ericsson & Charness, 1994; Macnamara & Maitra, 2019). Playing a musical instrument involves a multifaceted ensemble of skills, including acoustic processing (e.g. pitch, duration, timbre), cognitive processing of melodic and harmonic content (e.g. selective attention, grouping, auditory scene analysis), fine motor control, sensory-motor coordination, sequence memorisation, musical interpretation and expression, and development of learning strategies (Hallam, 2001, 2010; Norton et al., 2005). Over the past few decades, the perceptual and cognitive advantages associated with musical training have been studied extensively. Reported examples of such advantages include pitch perception (Kishon-Rabin et al., 2001; Spiegel & Watson, 1984), temporal information processing (Cicchini et al., 2012; Güçlü et al., 2011; Rammsayer & Altenmüller, 2006), phonological processing (Chobert et al., 2014; Tierney et al., 2015; Wong et al., 2007), attention (Kaganovich et al., 2013; Román-

[7] A pre-print version of this chapter is available online: Caprini, F., Zhao, S., Chait, M., Agus, T., Pomper, U., Tierney, A., & Dick, F. (2021, June 24). Generalization of auditory expertise in audio engineers and instrumental musicians. https://doi.org/10.31234/osf.io/7fg5h

Caballero et al., 2020; Strait et al., 2010, 2015; Zendel & Alain, 2009), speech in noise perception (Parbery-Clark et al., 2009; Slater & Kraus, 2016; Tierney et al., 2020; Yoo & Bidelman, 2019; for a review, see e.g. Coffey et al., 2017a), statistical learning (Mandikal Vasuki et al., 2016; Schön & François, 2011), working memory (Bugos et al., 2007; Talamini et al., 2017, p. 201), auditory-motor synchronisation (Chen et al., 2008; Zatorre et al., 2007), visuospatial cognition (Douglas & Bilkey, 2007; Hassler et al., 1985; Lidji et al., 2007), reading (Flaugnacco et al., 2015; Tierney & Kraus, 2013), and metacognition (Hallam, 2001). The educational and clinical implications of these findings (François et al., 2015) and their relevance in the study of brain plasticity and learning (Hyde et al., 2009; Zatorre, 2005) are some of the reasons that underlie the widespread adoption of musicianship[8] as a model of how expertise in one domain might develop and affect supposedly unrelated[9] and/or more general domains of perception and cognition. This phenomenon is known as transfer of expertise (either near or far based on the relatedness of the skills' contexts and cognitive demands; Barnett & Ceci, 2002; Mestre, 2005) and commonly serves as the epistemological construct underlying the literature on the effects of music training on both musical and nonmusical abilities.

2.1.1.2 Limitations

However, the conclusions that can be drawn from the current literature on the topic are somewhat limited by conflicting evidence and theoretical issues. An example is speech-in-

[8] At least in the compartmentalised or quasi-Platonic Western notions of "music" and "being a musician" (Cross, 2012; Wiggins et al., 2010).

[9] These domains might in fact share perceptual and cognitive processing in the brain, despite appearing superficially unrelated (e.g. the OPERA hypothesis for music and speech processing) (Patel, 2011, 2014).

noise perception. As noted above, a number of studies have reported musician advantages in perceiving speech in noisy or distracting environments, but equally, several studies have failed to detect an association with musical training across multiple experimental conditions (e.g. Boebinger et al., 2015; MacCutcheon et al., 2020; Madsen et al., 2017, 2019; Ruggles et al., 2014). It has been suggested that the advantage of musicians for speech-in-noise perception might depend on the relevance of pitch discrimination for the given task (Fuller et al., 2014), along with rhythmic skills (Slater et al., 2018) and the presence of spatial cues (Bidelman & Yoo, 2020; Clayton et al., 2016; but see Madsen et al., 2019), and may be partially negated by musicians' high levels of chronic noise exposure (Skoe et al., 2019). Importantly, the musicians' advantage for speech-in-noise perception could also be mediated by other and possibly pre-existing cognitive abilities (e.g. working memory, attention) rather than being a direct effect of musical experience (Escobar et al., 2020; Yoo & Bidelman, 2019). Thus, despite the interest in the topic and promising clinical applications (e.g. the rehabilitation of sensorineural and age-related hearing loss; Alain et al., 2014; Lo et al., 2020; Parbery-Clark et al., 2011), current evidence does not unequivocally support the hypothesis that musical training enhances speech-in-noise perception. Another example is the musicians' advantage for auditory sequence memorisation and reproduction (Krishnan et al., 2021; Tierney et al., 2008), which Carey et al. (2015) did not replicate using the same general paradigm, despite testing a relatively large number of highly trained violinists and pianists. More generally, many studies have only observed expertise-related skill transfer closely related to the original training context (for a review, see Green & Bavelier, 2008), although a lack of granularity in the definition of population characteristics and behavioural measurements might in itself make it difficult

to reach conclusive and replicable results (Green et al., 2014). For example, simple comparisons of musically trained and untrained individuals cannot explain whether any of the observed advantages are specifically associated with unique features of musical training or could instead be observed (or even enhanced) with other types of training. Evidence from single-task randomised controlled training studies on non-musicians shows that several auditory perceptual thresholds (i.e. pitch, duration, intensity, interaural time and level difference) can indeed be individually improved with training (Wright & Fitzgerald, 2005; Wright & Sabin, 2007) and match those of musicians (Micheyl et al., 2006). Non-musical forms of auditory training have been investigated in the enhancement of speech intelligibility in adults with hearing loss (e.g. Fu et al., 2005; Henshaw & Ferguson, 2013; Whitton et al., 2017; but see Stacey & Summerfield, 2007), language processing in children with learning difficulties (for a review, see Loo et al., 2010), as well as neurocognitive improvements of psychiatric patients (Adcock et al., 2009; Bettison, 1996; Fisher et al., 2009). Training profile variations within the musician population also appeared to be associated with specific perceptual advantages. A number of studies have reported perceptual differences between musicians who play different instruments and genres, such as lower (i.e. better) frequency discrimination thresholds for classical musicians compared to jazz musicians (Kishon-Rabin et al., 2001; cf. Tervaniemi et al., 2016; Vuust et al., 2012), a frequency discrimination advantage for players of a variable pitch instrument (i.e. string and woodwind) compared to a fixed-pitch instrument (Micheyl et al., 2006) or percussion instruments (Zaltz et al., 2017), an instrument-specific preference for a musical temperament (i.e. tuning system; Carey et al., 2015), and better perception of speech harmonics for vocalists as opposed to speech timing for percussionists

(Slater et al., 2017). Additionally, other types of musical performers, such as professional club disk jockeys, have been shown to match trained percussionists in rhythmic ability (Butler & Trainor, 2015). Neuroplastic and behavioural correlates of other forms of auditory expertise unrelated to musical training have also been studied. For instance, 60 minutes of birdsong identification training was shown to lead to a decrease in early (200-300 ms) neural activity in the left superior temporal gyrus and middle frontal gyrus in response to trained stimuli, but also a later (500-550 ms) increase in activity in the cingulate cortex bilaterally for untrained songbird stimuli (De Meo et al., 2015). Additionally, scalp topography of P2 auditory-evoked potentials of songbird experts revealed more frontal positivity than naive subjects in response to not only birdsongs but also voice and environmental stimuli, which might reflect a generalised difference in processing strategy (Chartrand et al., 2007). Another example is learning to decode Morse code, which has been associated with an increase in neural activity in the inferior and medial parietal cortex bilaterally and in grey matter density in the fusiform gyrus (Schmidt-Wilcke et al., 2010), while musicians have been shown to reproduce Morse code at variable speeds more accurately than non-musicians after training at a static speed (Slayton et al., 2020). Nonetheless, very little attention has been paid to other populations whose profession depends on high levels of auditory sophistication, such as audio engineers.

2.1.2 Audio engineering

2.1.2.1 Population characteristics

Audio engineers attempt to create, capture, and modify the sound in order to resolve technical issues and meet multiple artists' objectives (e.g. a musician, a producer, or their own), ultimately curating the listener's experience (Zwicker & Zwicker, 1991). This

process can involve the discrimination and manipulation of psychoacoustic attributes such as pitch and timbre via equalisation and filtering, loudness and dynamic range via compression and expansion, but also synchronicity, phase, filtering, masking, and spatial features via custom configurations of hardware and software tools (Corey & Benson, 2016). Other than professional practice, this level of perceptual expertise is usually achieved via technical ear training, which involves exercises designed to improve the ability to focus on and identify discrete elements of auditory sensations, and associate them with objective acoustical measurements (Corey, 2013; Iwamiya et al., 2003; Letowski, 1985), although this practice is not yet fully standardised (Kaniwa et al., 2011; Kim et al., 2013; Marui & Kamekawa, 2013, 2019; McKinnon-Bassett & Martens, 2013). Additionally, audio engineers must learn to deliberately direct their attention to individual elements of sounds or auditory scenes and to maintain them in memory. For example, the practice of mixing in music production can involve listening to a complex auditory scene (e.g. an instrument group), scanning the scene to identify a source of potential acoustic issues in the global sound (e.g. phase interference, tonal imbalance, lack of definition or "muddy" sound, timing issues, etc.), applying a fix at the level of individual instruments or elements, reintegrating them into the scene, and re-evaluating the updated auditory scene (for a detailed description of what mixing entails, see, e.g. Case, 2012; Izhaki, 2008). This process requires considerable sustained selective attention (auditory scene segregation and integration) and auditory working memory (mental sound manipulation and pre-post comparison); the relevant tasks are supported by visual cues provided by screening devices like spectrum analysers.

2.1.2.2 A different model of auditory expertise

Musicians who play in ensembles must also be able to track the auditory scene and, in large ensembles, interpret the conductor's cues in order to synchronise with the group and adapt their sound to the collective performance. By comparison, audio engineers are responsible for several sound sources at the same time, have a much larger toolbox for acoustic manipulation that is not constrained by the physical construction of a musical instrument and can work either synchronously (e.g. live performance) or asynchronously (e.g. studio work). Furthermore, the process of mixing can be nonlinear, and there can be multiple ways of achieving similar acoustic outcomes depending on the available gear, personal workflow, and creative process (De Man et al., 2015). For instance, the adjustment of a sound's intensity could correspond to the turn of a knob or a push of a slider on a mixing board, the click of a mouse in a digital audio workstation, or the repositioning of a microphone. Moreover, these gestures can affect the sound in real time or with any amount of delay. Conversely, the correspondence between an instrumentalist's gestures and acoustic outcomes is narrower in terms of the range of motion and temporal co-occurrence of action and sound, which may promote auditory-motor coupling (Alluri et al., 2017; de Manzano et al., 2020; Li et al., 2018; Palomar-García et al., 2017; Zatorre et al., 2007). Audio engineers are also equipped with domain-specific knowledge such as signal processing, electronics, audio theory, and psychoacoustics (Howard & Angus, 2009), as well as technical language and professional jargon (Porcello, 2004), which can provide context and assist the interpretation of sensory perception. Taken together, the skills of these professionals correspond to a model of auditory expertise that is very different in nature from that of musical instrument training. In contrast to performing musicians, audio

engineers do not need high proficiency in playing a musical instrument to excel in their profession. These unique characteristics of audio engineers can be exploited to test the specificity of some of the auditory advantages associated with musical training described in the literature, in particular fine auditory perception and auditory scene analysis.

2.1.3 Current study

The current study aims to contrast two different ecologically valid, auditory-based forms of expertise: audio engineering and playing a musical instrument. First, we tested the hypothesis that both audio engineers and musicians would show superior auditory skills compared to matched controls across a broad set of auditory-based measures that are both associated with musical training and essential for the practice of audio engineering. We included six psychophysical measurements (i.e. pitch, duration, intensity, sinusoidal amplitude modulation, interaural level difference, and interaural difference) and four measurements of auditory scene analysis. The latter were: 1) a sustained auditory selective attention task (Laffere et al., 2020) where subjects discriminate between two concurrent streams of tonal sequences; 2) a working memory and sound segregation task that involves the memorisation and matching of three concurrent sounds varying in frequency and amplitude modulation with a target sound; 3) a task that involves the detection of changes in the statistical properties of an auditory scene; and 4) a monaural speech-in-babble-noise task.

Second, we ran a set of exploratory analyses to identify and describe the unique attributes of our auditory expert cohorts. In order to complement the observational nature of this study and detect cohort qualities that may contribute to self-selection and performance, we also included self-report measures of personality and musical sophistication. The latter is

particularly important as musicians and audio engineers can present partially overlapping forms of auditory expertise, thus posing a challenge to the interpretation of observational data. It is possible, for instance, for audio engineers to be excellent instrumentalists and vice-versa, for musicians to be knowledgeable in the field of audio engineering, although we aimed to partially reduce the overlap between these two populations by explicitly recruiting musicians with no expertise in audio engineering, including recording, mixing, and mastering. We then evaluated the associations between different levels of audio engineering experience, musical experience, and auditory skill.

Third, we explored whether and to what extent low-level perceptual ability, auditory scene analysis, and speech-in-babble perception correlate with each other and compared how these associations manifest between groups.

2.2. Methods

2.2.1 Participants

Participants (n=64) were undergraduate students of either audio engineering, a musical instrument degree, or any other non-musical degree. All subjects were native English speakers between 19 and 26 years old and reported no history of hearing impairments. Audiometric thresholds were verified manually (see 2.2.2.1).

2.1.1 Audio engineering students

Students of audio engineering (n = 20, 17M; age range = 19-26, mean (SD) = 21.3 (1.9)) were recruited first through email and flyer advertising. At the time of testing, they were enrolled full-time (year 1, n=2; year 2, n=8; year 3, n=10) in the Music Technology and

Sonic Arts (BSc) program at Queen's University Belfast, where they were tested in a sound-insulated recording studio. They reported having, on average, 3.9 years of experience with audio recording, mixing or mastering (SD = 1.7, range = 1-7; see Table 2.1).

2.1.2 Musical instrument students

Musicians (n = 24, 16M; age range = 20-26, mean (SD) = 23.9 (1.69)) were students of a musical instrument degree (see Table 2.1 for instruments) recruited in London through flyer advertising and UCL/Birkbeck SONA systems. Recruitment criteria included the practice of any musical instrument other than percussion for four or more years, with an average daily practice of at least 2 hours a day and no experience with audio engineering, mixing, mastering, or recording. Despite efforts being made to match all cohorts' demographics, participants in the musician group included five more female subjects and were, on average, 2.5 years older than engineers and controls. The effects of these potential confounds on the auditory measurements were evaluated post-hoc via nonparametric univariate testing (see 2.2.4.2) for gender and Spearman correlations for age. No association was found for either demographic variable.

2.1.3 Control group

Controls (n = 20, 17M; age range = 19-25, mean (SD) = 21.6 (1.9)) were also recruited in London through the UCL and Birkbeck SONA systems. They were undergraduate students of non-musical degrees (i.e. psychology, anthropology, pharmacy, history, management, mathematics, social sciences, finance, jewellery design, computer science, medicine) with no formal training or history of regular practice playing a musical instrument or audio

engineering, mixing, mastering, or recording. Both music instrumentalists and controls were tested in a quiet testing booth at Birkbeck, University of London.

***Table 2.1**: Demographics, years of formal training (i.e. musical instrument lessons), years of regular practice of a musical instrument, and years of audio engineering experience.*

GroupID	Age	Sex	Course	Formal Training	Regular Practice	Audio Engineering
E1	20	Male	Music Technology	3-5	2	6
E2	20	Male	Music Technology	3-5	4-5	4
E3	19	Female	Music Technology	10+	10+	1
E4	21	Male	Music Technology	0	4-5	3
E5	26	Male	Music Technology	0	3	7
E6	21	Male	Music Technology	1	4-5	4
E7	22	Male	Music Technology	0	4-5	1
E8	21	Male	Music Technology	6-9	6-9	4
E9	19	Male	Music Technology	10+	10+	6
E10	22	Male	Music Technology	2	6-9	3
E11	21	Female	Music Technology	10+	10+	3
E12	22	Male	Music Technology	0	6-9	5
E13	20	Male	Music Technology	6-9	10+	3
E14	20	Male	Music Technology	0	4-5	3

GroupID	Age	Sex	Course	Formal Training	Regular Practice	Audio Engineering
E15	21	Male	Music Technology	6-9	6-9	6
E16	20	Male	Music Technology	0	6-9	3
E17	23	Male	Music Technology	1	4-5	6
E18	21	Female	Music Technology	10+	10+	3
E19	21	Male	Music Technology	0	1	3
E20	26	Male	Music Technology	3-5	6-9	3
C1	20	Female	Psychology	0	0	0
C2	24	Male	Anthropology	0	0	0
C3	23	Female	Pharmacy	0	1	0
C4	22	Female	Medicine	0.5	0	0
C5	20	Male	History	0	0	0
C6	22	Male	Mathematics	0	0	0
C7	25	Male	Management	0	0	0
C8	21	Male	Computing	0.5	0	0
C9	24	Male	Medicine	1	0	0
C10	22	Male	Social Policy	0.5	0	0
C11	23	Male	Medicine	0	0	0
C12	21	Male	Computer Science	0	0	0
C13	24	Male	Banking and Finance	0	0	0
C14	20	Male	Mathematics	1	1	0
C15	19	Male	Economics	0	0	0
C16	20	Male	Engineering	0	0	0
C17	23	Male	Jewellery Design	1	0	0

GroupID	Age	Sex	Course	Formal Training	Regular Practice	Audio Engineering
C18	21	Male	Natural Sciences	0	0	0
C19	19	Male	Neuroscience	0	0	0
C20	19	Male	History and Politics	2	1	0
M1	25	Female	Piano	6-9	10+	0
M2	25	Female	Piano	6-9	10+	0
M3	22	Male	Trumpet	6-9	6-9	0
M4	26	Female	Voice	6-9	10+	0
M5	25	Male	Piano	10+	10+	0
M6	24	Male	NA	NA	NA	0
M7	24	Male	Guitar	3-5	4-5	0
M8	22	Male	NA	NA	NA	0
M9	26	Male	NA	NA	NA	0
M10	24	Female	Piano	6-9	6-9	0
M11	26	Female	Piano	6-9	6-9	0
M12	22	Male	Violin	3-5	6-9	0
M13	23	Female	Violin	3-5	6-9	0
M14	24	Male	Oboe	3-5	6-9	0
M15	26	Male	Guitar	6-9	10+	0
M16	25	Male	Piano	3-5	4-5	0
M17	26	Male	Violin	3-5	4-5	0
M18	23	Male	Violin	3-5	6-9	0
M19	25	Male	Piano	3-5	6-9	0
M20	23	Male	Guitar	6-9	10+	0
M21	20	Male	Piano	6-9	10+	0
M22	21	Female	Piano	6-9	10+	0
M23	24	Male	Guitar	3-5	4-5	0
M24	23	Female	Oboe	6-9	6-9	0

2.2.2 Procedure

The test battery was composed of one audiometric screening, ten behavioural tasks, and two questionnaires. Each testing session lasted up to 2 hours, with the average duration being about 1 hour and 45. To minimise differences across individuals due to task order, tasks and questionnaires were run in the same order for all subjects, which is the order they are presented below. The study was approved by the Birkbeck Department of Psychological Sciences ethics committee, and all participants gave their informed consent before the start of the experiment.

2.2.2.1 Audiology

Two different tools were used to measure audiometric thresholds. Students of audio engineering were tested with a Kamplex KC35 Audiometer, while musicians and non-musicians were tested with an Otopod system paired with Symphony software on a Windows XP laptop. In both cases, a 10 dB-down, 5 dB-up adaptive staircase procedure (British Society of Audiology, 2018) was used, and thresholds were measured using pure tones from a range of frequencies presented in this order: 1 kHz, 1.5 kHz, 2 kHz, 3 kHz, 4 kHz, 6 kHz, 8 kHz, 125 Hz, 250 Hz, 500 Hz, 750 Hz. After manually checking that they could hear a sample sound from both ears, subjects were asked to listen carefully and to press the provided response button whenever they could hear a tone, starting at 10 dB HL. All frequencies were presented monaurally, starting with the left ear. For each frequency, a threshold was determined when the subject performed two reversals at the same intensity.

2.2.2.2 Speech in babble noise (SIN)

Subjects were instructed to listen carefully to a target sentence in the presence of four-talker babble and repeat that sentence out loud to the experimenter. Subjects were encouraged to repeat any word they heard, regardless of whether that was a single word or an entire sentence. Target sentences spoken by a British male were sampled from the Bamford-Kowal-Bench Speech-in-Noise (BKB-SIN) sentences (Bench et al., 1979; Research, 2005) and included three keywords. All stimuli were presented diotically. Unlike the original BKB-SIN test, we estimated speech/babble SNR thresholds using an in-house adaptive staircase procedure implemented in MATLAB (2013b). The initial SNR value was set to +10dB and changed adaptively up or down according to the subjects' response. A response was considered correct if at least two keywords were identified by the subject. After recording the participant's response, a new sentence was presented. The first step size was set to 8 dB and reduced to 6 dB, 4 dB, and 2 dB after each reversal. SNR changes were obtained by increasing or decreasing the amplitude of the target sentence while the amplitude of the babble mask was kept constant. The experiment terminated after six 2-dB-step reversals or when the limit of 20 sentences was reached. A final SNR threshold was calculated as the average SNR ratio of the stimuli presented after the first three reversals (i.e. the final set of stimuli presented with a 2 dB step size).

2.2.2.3 Sustained auditory selective attention (SASA)

This task was designed to quantify participants sustained selective attention (Dick et al., 2017; Holt et al., 2018; Laffere et al., 2020). Each block consisted of a stream of 30 short sequences, each made of six 125 ms cosine-ramped sine tones sampled with replacement from two frequency bands in an alternating pattern (Figure 2.1). Each band was composed

of three tones set two semitones apart: 185, 207.7, and 233.1 Hz (F#3, G#3, and A#3) for the lower band and 370, 415.3, and 466.2 Hz (F#4, G#4, and A#4) for the higher band (i.e. one octave above). Tones were presented at regular intervals at a rate of 8 Hz followed by a 250 ms pause, and the first tone was always sampled from the lower band. As higher-frequency stimuli tend to be perceived as louder, a ratio of 4:10 was set between the amplitudes of the tones in the high and low bands. A total of 30 sequences were presented in each block. For the first 10 blocks, subjects were asked to respond by pressing the space bar when they heard two consecutive sequences in the high band. After a short break, subjects completed another 10 blocks, this time detecting repetitions in the low band while ignoring tones in the high band. Each trial included between 3 and 6 repetitions. The experiment was preceded by 4 training blocks for each condition, during which the amplitude of the confounding stream was initially set to zero and linearly increased until it matched the amplitude of the attended stream in the fourth trial. Answers were evaluated within a 1s window starting at the onset of the third tone of a sequence (i.e. between 0.5s and 1.5s after a sequence's onset). Subjects received feedback on screen immediately after responding. Sensitivity to repetitions in the attended band was calculated as d'.

2.2.2.4 Goldsmiths Musical Sophistication Index (Gold-MSI)

A digital version of the Goldsmiths Musical Sophistication Index (Gold-MSI) (Müllensiefen et al., 2014) was administered. This extensively normed questionnaire quantifies individual differences in musical sophistication according to five dimensions, Active Engagement, Perceptual Abilities, Musical Training, Singing Abilities, Emotions, and one common factor, General Sophistication. Subjects rated on a 7-point Likert scale how much they agreed with a statement that described their experience with music. Scores

for each dimension were calculated as the sum of the ratings given to each item belonging to that dimension after inverting negative-score items.

2.2.2.5 Ten Item Personality Inventory (TIPI).

A computerised version of the Ten Item Personality Inventory (TIPI) (Gosling et al., 2003) was administered. In this brief questionnaire, each of the Big Five personality dimensions (i.e. extraversion, agreeableness, conscientiousness, emotional stability, and openness to experience) is represented by two pairs of adjectives, one positive (e.g. "sympathetic, warm" for conscientiousness) and one negative (e.g. "reserved, quiet" for extraversion). Subjects were asked to indicate how much they identified with each pair of adjectives on a scale from 1 (Strongly disagree) to 7 (Strongly agree). The final scores were calculated by taking the average of the 2 items representing each dimension after inverting the ratings of the negative items.

2.2.2.6 Auditory scene recall (ASR)

This task was designed to measure participants' ability to segregate different sounds in an auditory scene analysis and maintain them in memory for a short period of time. Each trial was made of three phases. During the first phase ("encoding phase"), subjects listened to an auditory scene (2s) composed of three amplitude-modulated pure tones ("streams") drawn from a fixed pool of 20 log-spaced frequencies between 200 Hz and 3000 Hz, with square-wave amplitude modulations rates set at either 3 Hz, 7 Hz, or 19 Hz. Tone frequencies and modulation frequencies were set so that they would not be multiples of each other. The second phase consisted of 1.5s of silence. During the third phase ("test phase"), a single stream (2s) was presented: in half the trials, the stream was identical in both frequency and

amplitude modulation rate to one of the streams presented in the encoding phase, whereas in the other half, it had a new unique combination of frequency (sampled from the three frequencies presented in the encoding phase) and modulation rate (Figure 2.1). For each trial, subjects were asked to memorise the three streams presented simultaneously in the encoding phase and determine whether the single stream heard in the retrieval phase was one of the three tones they memorised. Subjects responded by pressing the "F" key if they believed the target tone was present in the encoding phase and the "D" key if it was not. Subjects were allowed to respond as soon as they heard the target stream and up to 4s after the stream offset. Before the task was administered, the experimenter played several sample sounds to make sure subjects understood the task. 100 trials were generated for each subject using MATLAB (2015b). Stimuli were generated at a 44.1 kHz sampling rate, saved as WAV files, and subsequently presented to subjects in the form of two blocks of 50 trials each, with a break in between the two blocks. Visual feedback was provided for each trial, and a summary score of false alarms, correct, and invalid responses was displayed at the end of each block. Target detection sensitivity was calculated as d' following a "1/2N" correction for extreme proportions of hit or false alarm rates (Macmillan & Kaplan, 1985; Stanislaw & Todorov, 1999).

2.2.2.7 Psychophysics

Six psychophysical tasks were administered using the Maximum Likelihood Procedure (MLP) for auditory threshold estimation implemented in the Psychoacoustics toolbox (Soranzo & Grassi, 2014) in MATLAB 2013b running on a MacBook computer. During the pitch, duration, intensity, and sinusoidal amplitude modulation (SAMD) discrimination tasks, subjects were asked to listen carefully to three randomly ordered sounds in a

sequence: 2 comparison sounds set to a fixed value and one target sound whose value changed adaptively across trials. They then identified the sound that differed ('odd one out') by pressing 1, 2 or 3 on the keyboard. For the interaural level difference (ILD) and interaural time difference (ITD) tasks, only two sounds were presented, and subjects were asked to identify whether the first of the two sounds was perceived as coming from the left or from the right (with the second sound having the same parameter magnitude but coming from the opposite side). All six psychophysical tasks were administered in two blocks of 20 trials each, and no feedback was provided. Details of all six psychophysical tasks are reported in Table 2.2.

The MLP aims to achieve an optimal compromise between speed and accuracy in the estimation of several psychophysical thresholds through a nonparametric staircase adaptive procedure (details of stimulus selection and threshold estimations are described in Grassi & Soranzo, 2009). However, the adaptive procedure can fail if the subject gives a pattern of invalid responses at the beginning of a block due to attentional lapses or random guessing. The validity of each block was evaluated manually at the end of the experiment by examining the steps and thresholds for each block. Final thresholds were calculated as the average of the two blocks unless one of the blocks was determined to be invalid.

***Table 2.2**: Details of the six psychophysical tasks.*

Task	Stimulus	Parameter	Parameter range: Min (best), Max (worst)	Target stimulus
Pitch discrimination (PD)	250 ms complex tones with four harmonics	Frequency	330hz, 390hz	Highest-pitched tone

Task	Stimulus	Parameter	Parameter range: Min (best), Max (worst)	Target stimulus
Duration discrimination (DD)	Complex tones with four harmonics (f0 =330Hz)	Duration	250ms, 450ms	Longest tone
Intensity discrimination (ID)	Complex tones with four harmonics (f0=330Hz)	Intensity	-30 dB FS, -20 dB FS	Loudest tone
Sinusoidal amplitude modulation discrimination (SAMD)	500 ms Gaussian noise with 60 Hz sinusoidal amplitude modulation	Depth of modulation expressed as 20log(m)	m = 0 (no modulation), m = 1 (max modulation)	Amplitude-modulated tone
Interaural level difference (ILD)	5000Hz 250ms pure tones	Intensity (opposite signs for left and right ear)	±0.1dB, ±5dB	First tone (either left or right)
Interaural time difference (ITD)	330Hz 250ms pure tones	Phase (opposite signs for left and right ear)	±0.0001ms, ±0.3ms	First tone (either left or right)

2.2.2.8 Stochastic auditory scene (StAS)

This task aimed at measuring subjects' sensitivity to statistical changes in auditory sequences. Subjects were presented with random sequences of concatenated 50 ms tone pips (gated on and off with 5 ms raised cosine ramps), selected with replacement from a pool of 20 distinct log-spaced frequencies between 222–1912Hz (12% steps or 1/6 of an octave). All trials began with a series of randomly selected tones drawn from the pool. In half the trials, after 40-50 tones (with the number drawn randomly per trial), the sequence would then switch to a halved pool of only ten frequencies for 40 tones (i.e. 2 seconds).

There were two conditions: in the "full-to-middle" (F-M) condition, the halved pool consisted of the ten middle frequencies (391-1085Hz) of the original pool, whereas in the "full-to-edge" (F-E) condition, it consisted of the five highest (1215-1912Hz) and five lowest (222-349Hz) frequencies (Figure 2.1). Listeners were instructed to press the spacebar as soon as they heard a change in the auditory scene. Although they were not given information on what exactly would change, participants were provided with several examples and one practice trial per condition, as well as receiving visual accuracy feedback on the screen at the end of each sequence. Overall detection sensitivity was obtained by calculating d' for the two conditions, correcting for extreme proportions of hit and false alarm rates (Macmillan & Kaplan, 1985; Stanislaw & Todorov, 1999), and averaging them.

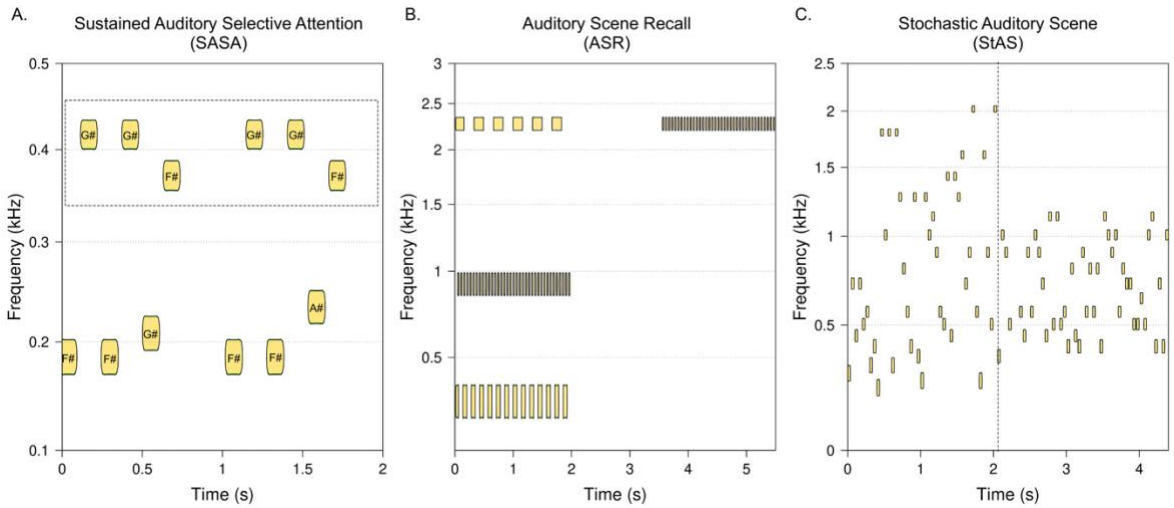

Figure 2.1*: Schematic representation of auditory scene analysis stimuli. A. Sustained auditory selective attention. Three-tone repetition in the high band marked by a black rectangle. B. Auditory scene recall. Three tones with different frequencies and square-wave amplitude modulation rates followed by a target tone with a new combination of frequency and modulation rate. C. Stochastic auditory scene. Example of a "full to middle" (F-M) transition. The vertical dotted line represents the change in the frequency sampling pool for the random tones.*

2.2.3 Data preprocessing

Scores for all behavioural tasks were screened for univariate outliers and patterns of missing data using JMP 15.2.1.

2.2.3.1 Outliers

Extreme data points were evaluated manually based on overall data distributions, previous benchmarks, and a combination of robust measures of centre and spread. More specifically, values over one interdecile range from the first or ninth decile or over 4 robust spreads from the centre (M-estimates; Huber, 1973; Huber, 2011) were initially flagged as extreme. A total of 5 outlier data points were detected: pitch discrimination (29.52 Hz, or about 8.9% of the 330 Hz reference stimulus) for subject 46 (musician); intensity discrimination (7.08 dB SPL) for subject 40 (control); sinusoidal amplitude modulation discrimination (-35.75; 20log(m)) for subject 49 (musician); interaural level difference (4.54 dB) for subject 35 (control); and speech-in-babble (-24.5 dB SNR) for subject 62 (musician). The first 4 observations correspond to exceptionally high (i.e. poor) psychoacoustic threshold estimates, by far higher than any other subject or benchmark (e.g. Kidd et al., 2007). Further inspection revealed that these were due to mistakes (e.g. attentional lapse, wrong button pressed, random guessing) made by participants within the first few trials of both blocks, which the MLP staircase procedure is particularly sensitive to (Soranzo & Grassi, 2014). For this reason, these measurements were judged as invalid and excluded from further analyses. The speech-in-babble outlier, on the other hand, corresponds to an extremely low SNR threshold (i.e. exceptionally good) which cannot be ruled out as a measurement error and it was retained. None of the other potential outliers identified by manual inspection of data distributions could be attributed to a technical error and so they were retained as valid measurements.

2.2.3.2 Missing data

A total of 15 out of 640 (2.3%) missing data points were identified across the behavioural dataset, due to either outlier exclusion, technical issues during testing, or time constraints. Missing data points were distributed across nine subjects who failed to complete one of the tasks and one subject (ID=1) from the audio engineers' group who failed to complete six tasks (auditory scene recall and all psychophysical tasks except interaural time difference). Gold-MSI data for 3 participants from the musician group was also missing due to data corruption during the online questionnaire saving process. When using statistical methods that require complete data vectors for every subject (e.g. 2.2.4.3), Subject E1 (audio engineers) was entirely excluded; for the remaining subjects, multivariate normal imputation based on a least squares prediction from the non-missing variables with shrinkage (Schäfer & Strimmer, 2005) was calculated for the rest of the dataset using JMP (15.2.1) and employed as an alternative to listwise deletion to retain as much information as possible (Schafer, 1999). While imputation can generate redundancy in data and increase the risk of Type 1 error, listwise deletion can increase Type 2 error and reduce statistical power (Cheema, 2014; Mishra & Khare, 2014). Where applicable, both methods were utilised and results compared to verify whether missing data would cause critical differences in statistical analyses. Pairwise deletion was employed when calculating correlations (see 2.2.4.5).

2.2.4 Statistical analyses

Statistical analyses are divided into two sections. First, we tested the *a priori* global hypothesis that groups do not come from the same auditory population, followed by the more specific hypothesis that auditory experts (i.e. musicians and audio engineers) will

outperform controls across each of the auditory tasks, with emphasis on inferential statistics and control of Type 1 error. Second, we ran a series of exploratory analyses to uncover any meaningful patterns in the dataset, as well as to test finer-grained hypotheses regarding the specific differences between the musician and audio engineer populations, relationships between auditory tasks, and the role of musical and audio engineering experience. Methods for data exploration included graphical methods, descriptive statistics, point estimates of relevant sample statistics, and data-driven models (Behrens, 1997; Szucs & Ioannidis, 2017). Any *a posteriori* hypothesis formulated during data exploration was made explicit in order for the associated confidence intervals and p-values to be interpreted as per their descriptive content (Amrhein et al., 2017; Lavine, 2014), rather than as confirmatory evidence for inference at the population level (Cohen, 1994; Gaus, 2015). Robust metrics and/or nonparametric methods were preferred across all statistical analyses to accommodate for differences in distribution characteristics across tasks and groups, unbalanced classes, heteroscedasticity, and presence of outliers without recurring to arbitrary data transformations or post-hoc analytic choices. Finally, the signs of all psychophysical and speech-in-babble thresholds were reversed before analyses in order for a greater number to always represent a better performance across all tasks and improve readability.

2.2.4.1 Multivariate differences (nonparametric MANOVA)

The global null hypothesis of no group differences in auditory skills was tested with the *nonpartest* function in the *npmv* R package (version 2.4.0) (Ellis et al., 2017), which employs a multivariate ANOVA-type test statistic based on ranks (Brunner et al., 1997; Brunner & Munzel, 2000) and p-values calculated via an asymptotic F-distribution

approximation (Bathke & Harrar, 2008) or resampling. This is a nonparametric equivalent of a MANOVA.

2.2.4.2 Univariate multiple comparisons and relative effects

In the case of a rejection of the multivariate null hypothesis, a set of univariate tests was planned to test whether experts outperform controls in each auditory task. This was done with a rank-based nonparametric multiple contrast test procedure (MCTP) implemented in the *mctp* function in the *nparcomp* R package (version 3.0; Konietschke et al., 2015; Noguchi et al., 2020). This procedure was selected for all univariate comparisons as it does not make assumptions on distribution shape, heteroscedasticity, or class imbalance. The MCTP tests hypotheses of stochastic inequality, that is the probability of a random observation from one sample being larger (or smaller) than a random observation from another sample. This operationalises the notion that one group will tend to outperform another without reference to measures of central tendency and spread (Cliff, 1993; Delaney & Vargha, 2002). This probability is referred to as relative effect and was calculated for each group against a reference unweighted mean distribution of all group distributions so that a random measurement from one group is always evaluated in the context of the entire dataset. Relative effects were used to formulate hypotheses about group inequalities. Specifically, for each auditory task, we tested the one-tailed null hypothesis that control subjects will show equal or better performance compared to musicians or audio engineers, which is an equal or higher relative effect. The rejection of a null hypothesis for a given task would then support the alternative hypothesis that one or both auditory expert cohorts scored significantly higher than controls for that task. This was done by setting *type = "Dunnett"* (i.e. many-to-one comparisons) and *alternative = "greater"* in the *mctp*

function. In addition to the simple difference between relative effects, a point estimate of a transformed log odds-type effect size comparable in magnitude to Cohen's d was also calculated and reported to facilitate interpretation (Noguchi et al., 2020). The MCTP is a single-step procedure, in that overall and specific contrasts are evaluated at the same time with no contradiction (i.e. a statistically significant omnibus test always corresponds to a significant "post-hoc" test and vice-versa) and under strong control of the family-wise error rate (FWER). Asymptotic estimates of adjusted p-values and simultaneous confidence intervals were calculated following a multivariate t-based approximation with adjusted degrees of freedom (Noguchi et al., 2020). The p-values of the overall effects, which always correspond to the lowest p-value of any pairwise comparison, were further corrected following the Benjamini-Hochberg false discovery rate (FDR) (Benjamini & Hochberg, 1995) adjustment implemented in the *p.adjust* function from the stats R package. An equivalent testing procedure for simple pairwise comparisons (i.e. a studentised permutation test (Neubert & Brunner, 2007) with the *npar.t.test* function from the same package) was used to complement plots and descriptive statistics during exploratory analyses between audio engineers and musicians. In these cases, p-values were left uncorrected and explicitly reported as such to suggest an appropriate interpretation.

2.2.4.3 Classification of musicians and audio engineers: variable importance

To further explore the different characteristics of our expert cohorts on a multivariate basis, we extracted variable importance from a random forest classifier (Breiman, 2001) trained with personality scores, Gold-MSI sub-dimensions, and auditory measures as predictors. Random forests are non-parametric algorithms that aggregate predictions from binary decision trees constructed on bootstrap samples or sub-samples of the original dataset and a

random subset of predictors (for an overview, see e.g. Strobl et al., 2009). We selected a class of random forests that utilises conditional inference trees as base classifiers (Torsten et al., 2006). These perform permutation tests (Strasser & Weber, 1999) at each node to identify the predictor most strongly associated with the response variable along with the optimal split point that maximises the discrepancy between the subnodes (Torsten et al., 2006). This method, when applied with subsampling without replacement, has been shown to be unbiased to the nature of a predictor (e.g. categorical, scale, ordinal). This differs from other types of binary decision trees that rely on measures of impurity reduction such as classification and regression trees (Strobl et al., 2007). This feature is particularly important as our predictors include both continuous variables and low-cardinality questionnaire data. We grew our forest with *cforest* from the *partykit* R package (Hothorn & Zeileis, 2015), with hyperparameters set to *ntree* = 10000 (number of trees in the forest), *mtry* = 4 (number of random predictors tested at each node of a tree; default is $\sqrt{p}$ where p is the number of predictors), and perturb set to a subsampling fraction of 0.632 with no replacement to achieve unbiasedness to predictor type (see above). Trees in the forest were allowed to fully grow by setting *minsplit* = *minbucket* = 1 (minimum size of a node), only limited by a minimum significance of a permutation test set with *mincriterion* = 0.95 (1-p-value). These were set with the goal of achieving a compromise between variance (i.e. node size of 1) and bias (i.e. high criterion of 0.95) (see guidelines in Probst et al., 2019). The importance of each predictor in the model was calculated as conditional permutation importance (Strobl et al., 2008). Permutation importance corresponds to the mean decrease in prediction accuracy when the values of a predictor are randomly permuted. Conditional permutation importance also accounts for collinearity between variables by measuring associations between

predictors and permuting collinear ones together. This was calculated using the *varimp* function in *partykit* with parameters *nperm* = 5 (number of permutations), conditional = TRUE, and threshold = 0.95. As per default, prediction accuracy and importance were calculated on the "out-of-box" data (i.e. OOB = TRUE), that is on the data excluded during subsampling. Random forests were employed here as a fully nonparametric tool for data exploration (Jones & Linder, 2015) which, given a high number of predictor variables and a low number of observations, specifically serves the purpose of identifying and ranking a subset of variables (i.e. feature selection) that can best describe the differences between musicians and audio engineer. As multiple imputations and listwise deletion lead to interchangeable results, only results following listwise deletion are reported. This corresponds to a total of 40 subjects, 19 audio engineers and 21 musicians. Variables with importance above 2.5%, corresponding to a mean decrease in accuracy equivalent to at least one subject (i.e. 100%/40), were included in an alternative reduced model. For replicability, results were obtained using a random seed of 1112.

2.2.4.4 Musical and audio engineering experience

To draw a more direct comparison between musicians and audio engineers with a similar musical background, we clustered participants into two groups based on their scores in the Musical Training sub-dimension of the Gold-MSI questionnaire. Specifically, with the exception of one musician who scored 31, musicians scored between 37 and 49 (Figure 2.2). Therefore, using a cut-off of 37, we were able to match all but this one musician with 8 audio engineers with a similar musical background. The underlying meaning of this cutoff was further examined using two items of the Gold-MSI questionnaires that contribute to the musical training score, namely "I engaged in regular,

daily practice of a musical instrument (including voice) for___years" and "I have had___years of formal training on a musical instrument (including voice) during my lifetime", in order to qualify possible differences in formal or informal training between cohorts (Figure 2.2). We then re-examined differences in behavioural measures between musicians and engineers with a similar level of musical training, as well as audio engineers with different levels of musical training, using the same methods described in paragraph 2.2.4.2. Additionally, we explored associations between mixing and mastering experience and behavioural measures with Spearman correlations.

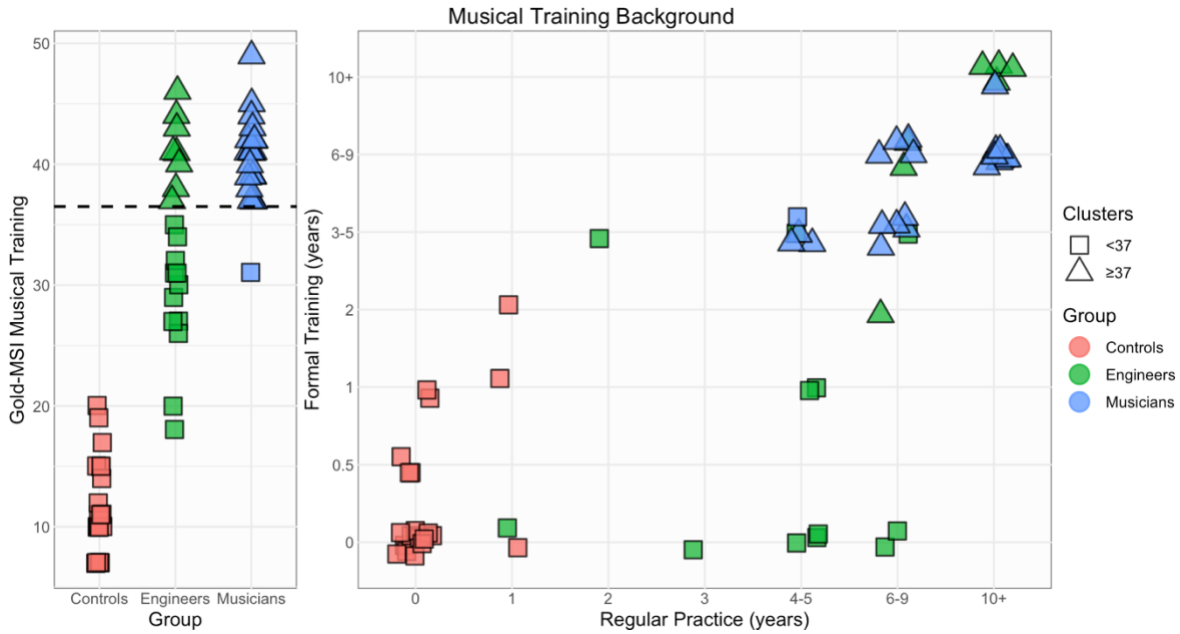

***Figure 2.2**: Musical training background. The left plot represents Musical Training dimension scores from the Gold-MSI questionnaire. Data points above the dashed line correspond to musicians and audio engineers with a matching degree of musical training, defined by a Gold-MSI score higher or equal to 37, which captures all but one musician. The right plot shows the musical training background of the three cohorts, as well as musical training clusters, in terms of years of formal training and regular practice of a musical instrument.*

2.2.4.5 Correlations between auditory tasks

Monotonic relationships between behavioural variables were estimated using Spearman's rank correlations coefficients (ρ) separately for each group. Empirical confidence intervals

for individual bivariate ρ were calculated via bootstrapping (Haukoos & Lewis, 2005; Wright et al., 2011). Relevant correlations, as well as their differences across groups, were assessed graphically with a series of correlograms as well as bivariate scatterplots on both raw data and ranked data. To facilitate comparisons between groups, data were ranked within groups and centred at the median rank before plotting.

2.3. Results

2.3.1 Auditory expertise: multivariate and univariate tests

The multivariate null hypothesis that participants come from the same population was rejected (ANOVA-type test statistic = 4.254, df1 = 11.616, df2 = 301.082, p-value < 0.0001), confirming that groups do indeed exhibit overall different degrees of auditory ability. After FDR correction, the null hypothesis of stochastic equality between experts and controls was rejected at the 0.05 level on all tasks except duration discrimination, intensity discrimination, and stochastic auditory scene (full details of test statistics can be found in Table 2.3). On perceptual tasks, both students of audio engineering and musical instrumentalists had significantly lower thresholds for pitch discrimination and interaural time difference tasks than controls. Musicians also showed significantly lower thresholds than controls on sinusoidal amplitude modulation discrimination and interaural level difference tasks (Figure 2.3). On auditory scene tasks, musicians were more accurate than controls on the sustained auditory selective attention task, while audio engineers were more accurate than controls on the auditory scene recall task. Finally, musicians, but not engineers, showed significantly lower SNR thresholds for the speech-in-babble-noise task (Figure 2.4). Pitch discrimination had the largest expertise-related effect size across all

auditory tasks for both expert cohorts compared to the control group, with median thresholds for audio engineers (median = 3 Hz, or 0.9% difference reference tone, MAD = 1.659 Hz (0.5%) and musicians (median = 3 Hz (0.9%), MAD = 1.248 Hz (0.37%) being approximately half of those of control subjects (median = 6.667 Hz (2%), MAD = 3.983 Hz (1.2%).

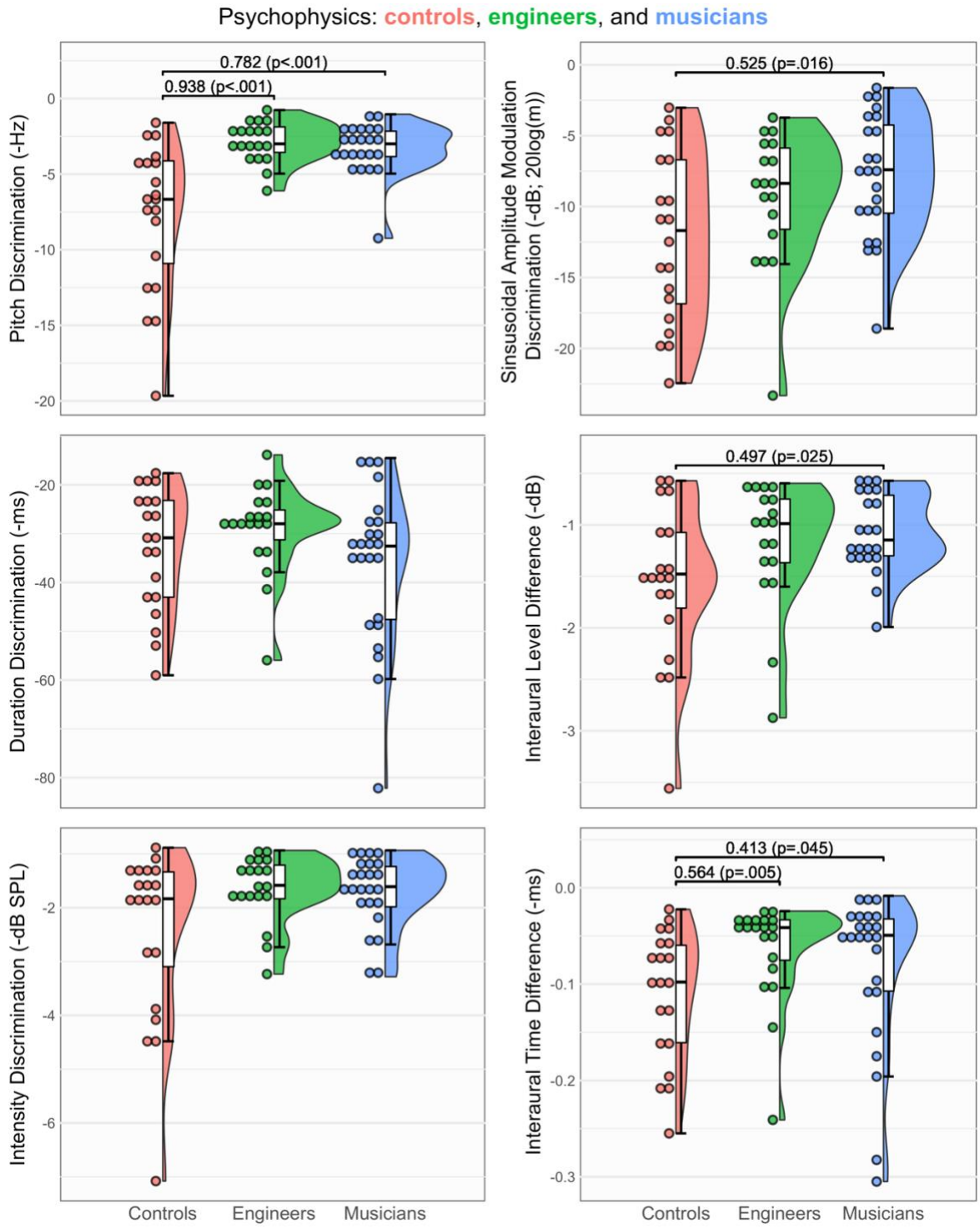

Figure 2.3*: Dot plots, same area violin plots, and box plots for all psychophysical measures by group. Just noticeable differences are reported on the y-axes with opposite signs in order for a positive effect size to consistently correspond to better performance across tasks. The brackets above graphs display log-odds-type effect size and one-tailed p values when p<0.05.*

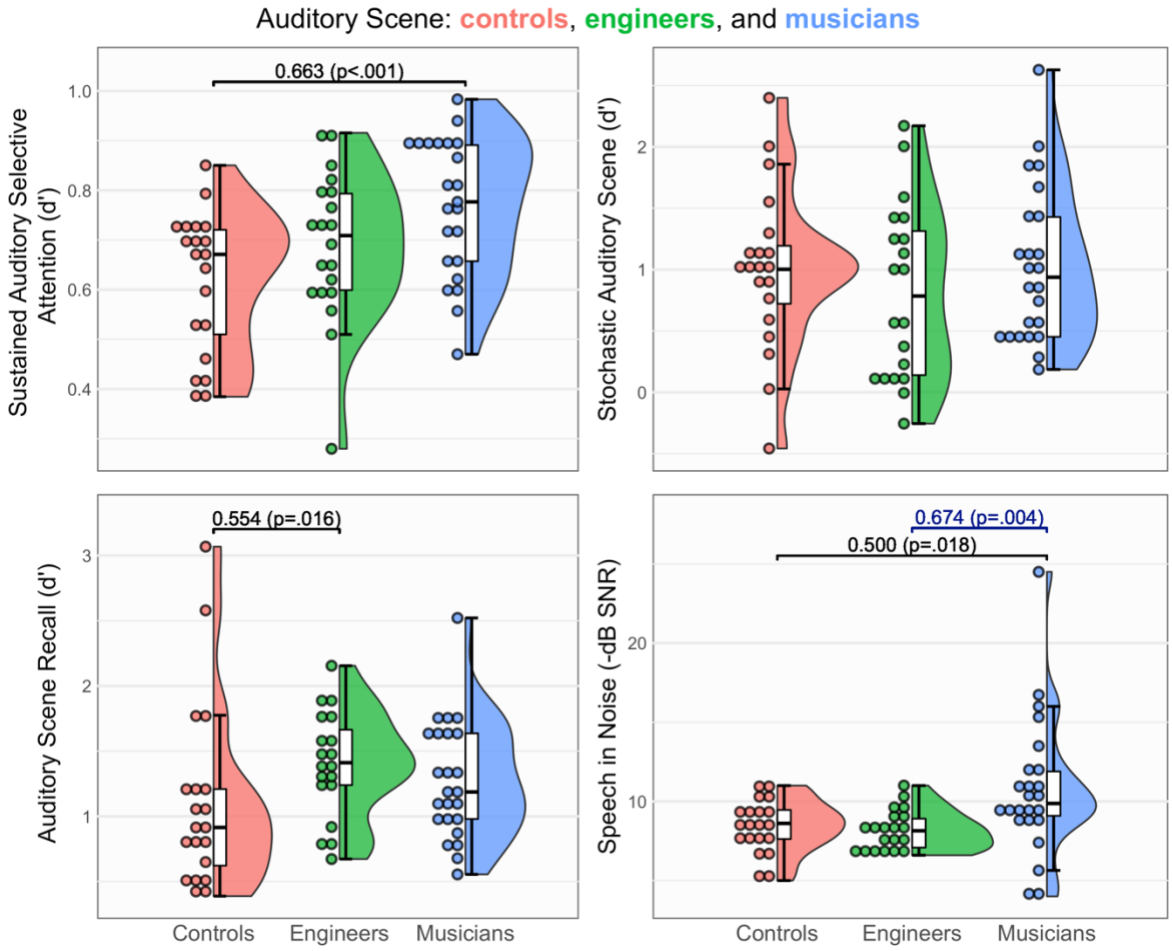

Figure 2.4*: Dot plots, same area violin plots, and box plots for all auditory scene tasks by group. Speech-in-babble thresholds are reported with opposite signs in order for a positive effect size to consistently correspond to better performance across tasks. The brackets above graphs display log-odds-type effect size and one-tailed p values when p<0.05. Values in blue brackets correspond to post-hoc two-tailed tests and are not corrected for multiple comparisons. Note that for the Auditory Scene Recall task, audio engineers' d' is significantly higher than that of controls overall, despite the two outlier control participants showing high d' values.*

***Table 2.3**: Results of many-to-one testing procedure between audio engineers (E) and musicians (M) compared to controls (C). Tasks: pitch discrimination (PD), duration discrimination (DD), intensity discrimination (ID), sinusoidal amplitude modulation discrimination (SAMD), interaural level difference (ILD), interaural time difference (ITD), sustained auditory selective attention (SASA), auditory scene recall (ASR), stochastic auditory scene (StAS), speech in babble noise (SIN). H_a: Alternative hypotheses expressed as the probability that a random participant from the audio engineer group (E > C) or musician group (M > C) would have a higher score than a random participant from the control group. Rel. Effect [95% CI]: relative effects with one-tailed 95% confidence interval. Effect size: log-odds type effect size comparable in magnitude to Cohen's d. Statistic: test statistic. p: test significance with strong control of the family-wise error rate within each task. p_{omni}: significance of the omnibus test. p_{FDR}: significance of the omnibus test corrected for false discovery rate across all tasks.*

Task	Ha	Rel. Effect [95% CI]	Effect Size	Statistic	p	p_{omni}	p_{FDR}
Pitch Discrimination	E > C	0.376 [0.236; 1.000]	0.938	5.316	<.001	<.001	<.001
Duration Discrimination	E > C	0.081 [-0.098; 1.000]	0.192	0.888	.288	.288	.320
Intensity Discrimination	E > C	0.150 [-0.031; 1.000]	0.355	1.631	.094	.094	.118
Sin. Amplitude Modulation Discr.	E > C	0.136 [-0.046; 1.000]	0.324	1.466	.125	.016	.030
Interaural Level Difference Discr.	E > C	0.177 [-0.019; 1.000]	0.423	1.783	.072	.025	.036
Interaural Time Difference Discr.	E > C	0.235 [0.079; 1.000]	0.564	2.984	.005	.005	.016
Sustained Auditory Selective Attention	E > C	0.132 [-0.034; 1.000]	0.318	1.575	.109	<.001	.004
Auditory Scene Recall	E > C	0.231 [0.049; 1.000]	0.554	2.491	.016	.016	.030
Stochastic Auditory Scene	E > C	-0.084 [-0.278; 1.000]	-0.199	-0.866	.918	.689	.689
Speech in Noise	E > C	-0.063 [-0.220; 1.000]	-0.151	-0.785	.900	.018	.030

2.3.2 Differentiating auditory expert cohorts: exploratory analyses

2.3.2.1 Random forests: variable importance

To summarise the variables in our dataset that can best discriminate between musicians and audio engineers and rank their relevance, we calculated conditional permutation importance - i.e. mean decrease in classification accuracy following a permutation of a given predictor - of a random forest classifier built on all variables in our dataset. The overall accuracy of the full model including all 20 predictors was 80%. A reduced model (Figure 2.5) which only included variables with importance above 2.5% had an accuracy of 82.5%. The predictor with the largest influence on prediction accuracy was singing abilities (25.6%), followed by speech-in-babble-noise thresholds and musical training (~15%), and emotional stability (5.4%). Minor contributions between 2.5% and 5% were obtained for active engagement and 2 psychophysical tasks, interaural time difference and duration discrimination. Bivariate Spearman correlations among the top three predictors revealed that while singing abilities and musical training were strongly correlated for both musicians ($\rho = 0.53$, 90% CI [0.14, 0.83]) and audio engineers ($\rho = 0.62$, 90% CI [0.20, 0.86]), speech-in-babble-noise thresholds did not correlate with either predictor.

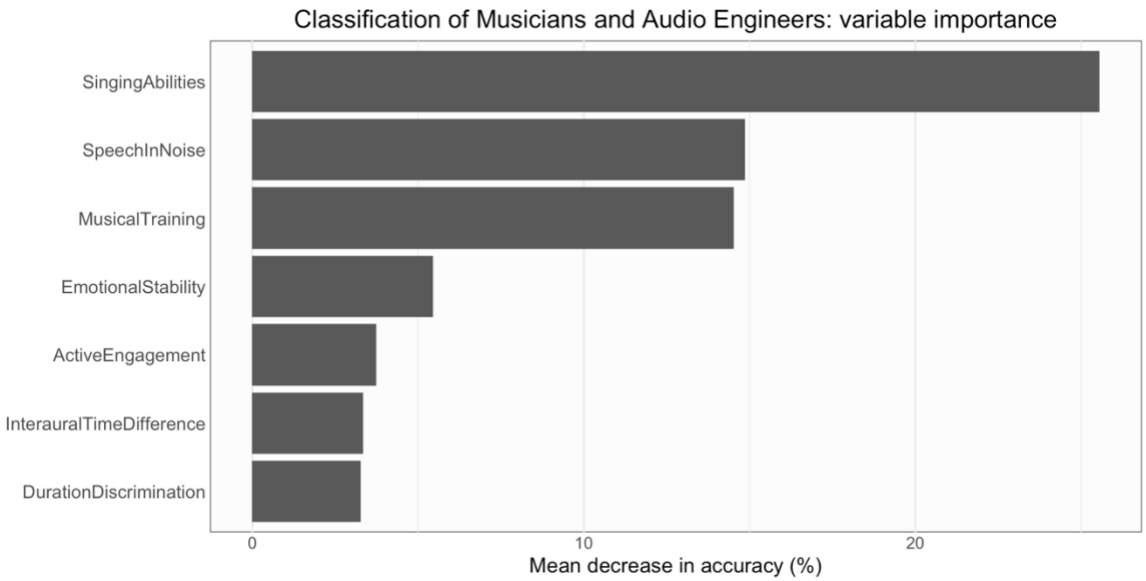

Figure 2.5*: Mean decrease in prediction accuracy (i.e. conditional permutation importance) of a random forest classifier with predictors including auditory tasks, personality traits, and musical sophistication sub-dimensions. Only the predictors with importance over 2.5% are shown.*

2.3.2.2 Auditory tasks

Data plots (Figure 2.3 and Figure 2.4) and descriptive statistics were used to integrate the results from the random forest importance classification and interpret the directionality of its prediction. In terms of behavioural variables, speech-in-babble-noise thresholds of musicians (median = -9.87 dB SNR, MAD = 1.82 dB SNR) were significantly lower than both controls (median = -8.61 dB SNR, MAD = 1.42 dB SNR) and engineers (median = -8.15 dB SNR, MAD = 1.62 dB SNR; post-hoc Brunner-Munzel, effect size = 0.674, test statistic = 3.347, p = 0.003), although musicians were also the most inconsistent within group and displayed the largest range (20.5 dB SNR) of responses on this task. As for the other auditory scene performance tasks which did not add a unique contribution to classification accuracy according to the random forest model, median sustained auditory selective attention d' was marginally higher for the musician group (0.777, MAD = 0.173) than audio engineers (0.709, MAD = 0.148), while the opposite was true for the auditory

scene recall task (audio engineers: median = 1.411, MAD = 0.307; musicians: median = 1.187, MAD = 0.519), although these differences were not statistically significant[10]. As for psychophysical tasks, with the exception of sinusoidal amplitude modulation discrimination, audio engineers' median thresholds were the lowest across all tasks, albeit by also a very small margin. The most apparent difference between expert cohorts (Figure 2.3) was duration discrimination (audio engineers: median = 29.03 ms, MAD = 5.98 ms; musicians: median = 32.55 ms, MAD = 9.47 ms), although a post-hoc test showed this difference was also not statistically significant at the 0.05 level (post-hoc Brunner-Munzel, effect size = 0.408 test statistic = 1.927, p = 0.063).

2.3.2.3 Musical expertise and personality

Musical sophistication (Figure S1) and personality traits (Figure S2) were among the most important variables in the discrimination of musicians and audio engineers. Unsurprisingly, musicians scored substantially higher than audio engineers in the musical training (post-hoc Brunner-Munzel, effect size = 0.693, test statistic = 3.311, p = 0.004) and singing abilities dimensions (post-hoc Brunner-Munzel, effect size = 1.1486983, test statistic = 6.505, p < 0.001) of the Gold-MSI questionnaire, bus also marginally higher in the perceptual abilities (post-hoc Brunner-Munzel, effect size = 0.498, test statistic = 2.393, p = 0.028) and emotions (post-hoc Brunner-Munzel, effect size = 0.448, test statistic = 2.134, p = 0.041) dimensions. However, a comparable level of active engagement with music was present in musicians compared to audio engineers. Results from the TIPI questionnaire revealed significant differences in emotional stability (post-hoc Brunner-Munzel, effect size=-0.523,

[10] An experiment with much larger sample sizes would be needed to appropriately test the statistical significance of such small effect sizes.

test statistic = -2.569, p = 0.015), with musicians on average seeing themselves as less emotionally stable than audio engineers. Musicians and audio engineers also appeared to cluster around equally higher scores compared to controls in the openness to experience dimension, which included an item about creativity.

2.3.3 Musical training and audio engineering experience

Clustering participants based on their musical training background (see 2.2.4.4) did not affect previous results: musicians displayed lower speech-in-babble thresholds than audio engineers with a matched degree of musical training (post-hoc Brunner-Munzel, effect size = 0.733, test statistic = 2.93, p = 0.019) and there were no significant differences in auditory ability between audio engineers with different musical backgrounds (nonparametric MANOVA, permutation test of ANOVA-type statistic with 10000 replications, p = 0.687). On the other hand, audio engineering experience was moderately correlated with both stochastic auditory scene ($\rho = 0.43$, 90% CI [0.08, 0.70]) and speech in babble noise ($\rho = 0.49$, 90% CI [0.13, 0.78]) performance, although even the most trained participants' scores fell within the range of control participants.

2.3.4 Associations between fine perception, auditory scene analysis, and speech in noise

Among the auditory scene tasks, sustained auditory selective attention d' scores appeared to be the most consistently (i.e. across groups) associated with psychophysical thresholds, in particular with pitch discrimination, intensity discrimination, and interaural time difference (Figure 2.6). Correlations between speech-in-babble-noise thresholds and psychophysical tasks were mixed across groups and overall negligible. Correlations between the auditory scene and speech-in-babble-noise tasks also appeared fairly inconsistent across groups,

with stochastic auditory scene showing the largest correlation with speech-in-babble thresholds in both engineers and musicians.

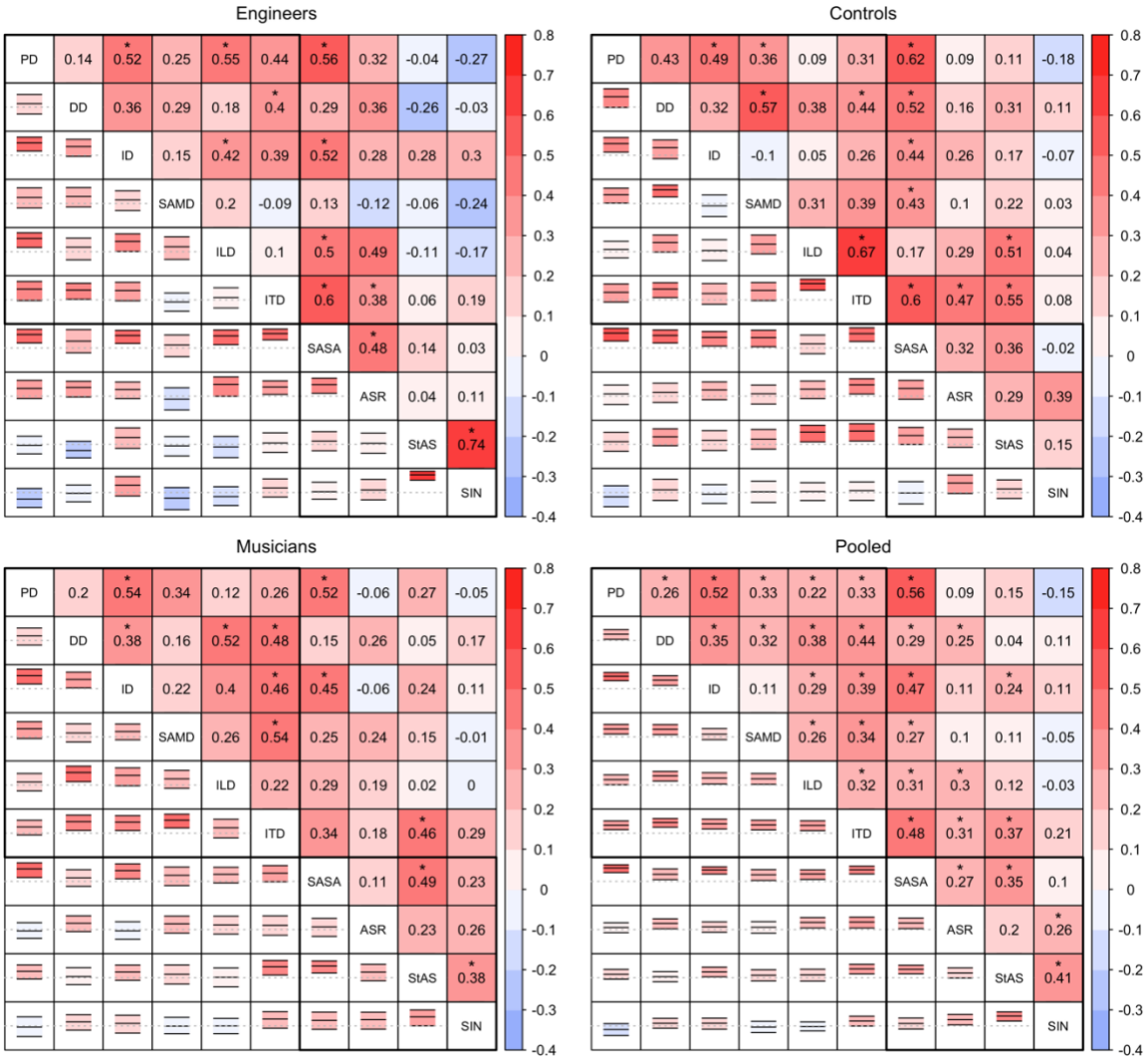

Figure 2.6*: Correlograms of behavioural tasks for all groups and pooled correlations obtained by median-centring ranks by group. Top triangles: Spearmans' ρ. Positive correlations correspond to red-coloured cells, negative correlations to blue-coloured cells, while colour saturation reflects correlation magnitude. Correlations whose 90% empirical confidence interval does not include the null are marked with *. Bottom triangles: 90% empirical confidence intervals. Dashed horizontal lines represent ρ=0. Thicker black margins identify psychophysical tasks and auditory scene tasks. Acronyms: PD = pitch discrimination; DD = duration discrimination: ID = intensity discrimination; SAMD = sinusoidal amplitude modulation discrimination; ILD = interaural level difference; ITD = interaural time difference; SASA = sustained auditory selective attention; ASR = auditory scene recall; StAS = stochastic auditory scene; SIN = speech in babble noise.*

2.4. Discussion

2.4.1 Study summary

We first tested the hypothesised superiority of their fine perceptual and auditory scene analysis skills in relation to naive subjects and contrasted their performance to that of music instrumentalists. We found that when compared to naive subjects, both auditory expert cohorts had lower thresholds for pitch discrimination and interaural time difference discrimination, while musicians also had lower thresholds for sinusoidal amplitude modulation discrimination and interaural level difference discrimination. Audio engineers performed better than controls in auditory scene recall, which requires subjects to determine whether a target sound matches one of three sounds presented earlier in terms of pitch and amplitude modulation frequency. On the other hand, musicians outperformed controls in sustained auditory selective attention, during which participants identified repetitions of three-tone sequences in an auditory stream while ignoring a competing stream one octave apart. Musicians also had significantly lower thresholds for speech-in-babble-noise perception than both naive subjects and audio engineers. Both auditory expert cohorts showed higher levels of openness to experience and audio engineers had higher levels of emotional stability compared to musicians. Audio engineers had a wider variety of musical backgrounds, although controlling for this did not affect previous conclusions about group differences. The number of years of audio engineering experience was moderately associated with better sensitivity in the stochastic auditory scene task and lower speech-in-babble-noise thresholds, but overall scores for both tasks fell within the normal range. Finally, psychophysical scores were the most associated with sustained auditory selective

attention and speech in babble noise was associated with stochastic auditory scene, particularly for audio engineers.

In sum, we gathered evidence supporting the hypothesis that audio engineers' auditory expertise, similarly to musical training, corresponds to generalised advantages in fine auditory discrimination and auditory scene analysis. However, the advantage for speech in noise perception, at least for the present cohort, seems to be specifically associated with musical instrument training.

2.4.2 Fine perception

Musicians and audio engineers showed superior fine auditory perception, with pitch discrimination having the largest effect size and clear-cut separation between experts and controls. Thresholds for the control group followed generally a wider distribution, as reflected by a higher median absolute deviation across all psychophysical tasks, and the top performers always matched the performance of the expert groups. These results reflect one challenging aspect of designing a control group for expert populations in a cross-sectional study, as pseudo-randomly sampling from the general population will unavoidably correspond to a wider spectrum of responses and include highly skilled individuals, despite controlling for musical training (Law & Zentner, 2012). Overall, we could not detect a clear advantage of musicians over audio engineers or vice versa in fine auditory perception.

2.4.3 Auditory scene analysis and speech in babble noise

While musicians significantly outperformed controls in sustained auditory selective attention (SASA), audio engineers performed better than controls in auditory scene recall

(ASR).[11] In addition to the differences in cognitive loads for each task (i.e. SASA relies more heavily on sustained selective attention and ASR on working memory), SASA stimuli are comparatively more "musical", in that the two competing auditory streams are constructed from the first three tones of a major scale separated by an octave, which might resemble competing melodies. ASR stimuli, on the other hand, are simple pure tones defined by a pitch and an amplitude modulation frequency but have no tonal relation with each other. Audio engineers' selective attention ability in this case might benefit from a more technical understanding of sound components and a more generalised experience working with any type of sound, musical and non-musical. Furthermore, this task required participants to analyse and maintain the whole auditory scene (i.e. three sounds) in memory, as no distinction between target and foil can be made until the target sound is heard. This type of mental sound manipulation and asynchronous pre-post comparison is common during mixing practices (see paragraph 2.1.2.1) and could in part account for the audio engineers' advantage. Musicians showed significantly lower SNR thresholds for speech-in-babble-noise perception compared to both controls and audio engineers, even accounting for differences in musical training. This effect was also robust to the exclusion of one outlier musician whose threshold was -24.5 dB SNR (see 2.2.3.1 and Figure 2.4). Furthermore, musical training and general musical sophistication (as measured by the Gold-MSI questionnaire) showed no association with speech-in-babble-noise thresholds within each group, implying that the musician effect might be due to characteristics intrinsic to the group not detected by our test battery. One confounding variable could be the difference in

[11] The effect sizes for the direct comparison between expert cohorts were much smaller and did not reach statistical significance.

regional accent between audio engineers (Belfast, UK) and musicians (London, UK), which could have put audio engineers at a disadvantage given that target sentences were spoken in a standard British accent (e.g. Smith et al., 2014). However, the only behavioural measure in our data that showed a fairly consistent positive correlation across groups with speech-in-babble-noise perception was sensitivity to statistical changes in a stochastic auditory scene. This could be explained by a better ability to detect changes in higher-order statistics of a sound sequence (Barascud et al., 2016; Skerritt-Davis & Elhilali, 2018), spectral entropy (Overath et al., 2007; Stilp & Kluender, 2010) or, more generally, informational content in a noisy signal, which is a strategy implemented for instance in speech-in-noise recognition algorithms (e.g. Misra et al., 2004; Toh et al., 2005). However, this is speculative and a dedicated experiment is needed to test this specific hypothesis. In this vein, Oberfeld and Klöckner-Nowotny (2016), found that individual differences in selective attention — measured in both auditory and visual modes — could explain variations in speech-in-noise perception abilities in their sample. However, their stimuli consisted of two individual competing speakers presented binaurally and one central target speaker, which might more explicitly depend on the ability to pay selective attention to one of multiple intelligible elements. Similarly, Tierney et al. (2020) found a correlation between non-verbal sustained selective attention and the perception of speech masked by one distractor talker. On the other hand, De Kerangal et al. (2021) found an association between musical training and sustained attention, but not between sustained attention and speech in noise perception.

2.4.4 Personality and musical sophistication

Not surprisingly, students of audio engineering had higher levels of musical sophistication compared to the general population, with about half of the participants reporting a similar degree of formal musical training as musicians. According to random forest variable importance, Gold-MSI Singing Abilities is the measure that can best discriminate between musicians and audio engineers in our dataset. Items that contribute to this sub-dimension include questions on singing itself (e.g. "I am able to hit the right notes when I sing along with a recording"), but also melodic memory (e.g. "I only need to hear a new tune once and I can sing it back hours later" or "I can sing or play music from memory") and performance anxiety (e.g. "I don't like singing in public because I'm afraid that I would sing wrong notes"). In terms of personality, both musicians and audio engineers scored higher in openness to experience, which is associated with creative abilities (McCrae, 1987) and musical sophistication (Greenberg et al., 2015) and has been shown to predict auditory and musical abilities by predicting engagement with music and musical training (Corrigall et al., 2013; Swaminathan & Schellenberg, 2018; Thomas et al., 2015). Neuroticism, which is the reverse of emotional stability, was significantly higher in musicians than in audio engineers. The association between musicianship and neuroticism has been observed before (Gillespie & Myors, 2000; e.g. Vaag et al., 2018), although the connection between the two is not yet fully understood (for a review, see Miranda, 2020). These findings imply that there can be several covariates specific to the musician population that are not normally controlled during the recruitment process or considered in the interpretation of musicians' data. For instance, differences in musical sophistication profiles and personality could be interpreted as an effect of self-selection of creative individuals (i.e. high openness) who

chose a stage-oriented career as music instrumentalists as opposed to a more studio-oriented or "behind-the-scenes" profession such as audio engineering (i.e. emotional stability and singing abilities).

2.4.5 Limitations and future directions

One limitation of this study was the inclusion of students of audio engineering who might still be relatively inexperienced, as they reported having between 1 and 6 years of experience with recording, mixing, and mastering, while musicians had from 4 to over 10 years of regular practice of a musical instrument. For instance, speech-in-babble-noise thresholds showed an association with years of audio engineering experience, although the performance of even the more experienced audio engineers in our sample was entirely within the range achieved by controls. Data from more experienced professionals could clarify whether audio engineering training can be associated with speech-in-noise perception abilities beyond the levels of the general population. Additionally, the inclusion of only one diotic speech-in-babble-noise test somewhat limits the generality of the conclusions that can be reached with our data. The inclusion of a wider range of tests in future experiments will allow us to determine whether cohort differences should be interpreted at a construct level rather than at a single task level (Green et al., 2014) and to pinpoint which auditory abilities might benefit specific aspects of speech-in-noise perception. Finally, cross-sectional experiments like the one presented in this paper cannot enable conclusions to be drawn about the causality of an observed group effect. Despite this, the legitimacy of causal inference in this category of music training studies has been often erroneously assumed (Schellenberg, 2019), underestimating the complexity of the interaction between individual differences and environment (Schellenberg, 2015). For

instance, the association between musical training and IQ could be explained by genetic pleiotropy (Mosing et al., 2016) and the undertaking and duration of music practice itself can be predicted by general cognitive ability, personality, socioeconomic status (e.g. Corrigall et al., 2013; Schellenberg, 2011; Swaminathan & Schellenberg, 2018), and genetics (Mosing et al., 2014). Genetic variability accounts for individual differences across several musical skills (Gingras et al., 2015) and even in the absence of actual musical training, auditory and musical abilities are associated respectively with the enhanced neural encoding of speech (Mankel & Bidelman, 2018) and emotion recognition (Correia et al., 2020). In the current study, by contrasting musicians with another population of auditory experts, we were able to draw a more nuanced and specific picture of musicians' profiles in terms of auditory ability, personality, and musical sophistication. More generally, despite not being able to directly test causality, we showed that the inclusion of additional control groups and covariates in cross-sectional studies on musical expertise can help clarify the implicit assumptions about the musically trained population, challenge the specificity of the observed perceptual or cognitive advantages, and form new hypotheses on the potential source of such advantages beyond musical training itself.

Chapter 3.

In-vivo tonotopic and myeloarchitectonic mapping of the human auditory cortex: individual differences and interactions

3.1 Introduction

A long-standing issue in auditory neuroscience is the identification of primary auditory fields in humans, particularly in-vivo. Unlike vision (e.g. Sereno et al., 1995), there isn't an agreed set of functional or structural localisers that can be reliably used to identify the primary auditory cortex across individuals. In non-human primates, the hierarchical cytoarchitectonic model of the auditory cortex includes three primary "core" fields (i.e. A1, R, RT) surrounded by several belt and parabelt secondary fields (Hackett et al., 1998; Hackett et al., 2001). Core regions are typically characterised by a greater myelin density in middle cortical layers, particularly A1 (Hackett, 2007; Nieuwenhuys, 2013), while topographical boundaries between core fields tend to align with isofrequency contour reversals in non-human primates (Merzenich & Brugge, 1973; Morel et al., 1993; Kaas & Hackett, 2000; Bendor & Wang, 2006; but see 1.2.2). The use of tonotopic reversals as a tool to delineate the primary fields in the human auditory cortex has been the object of controversy for decades (Baumann et al., 2013; Besle et al., 2019). On the one hand, several studies have attempted to interpret the orientation of human tonotopic gradients (e.g. perpendicular or parallel to HG's mediolateral axis) to infer the location of a putative auditory core, but no collective agreement has been reached yet. On the one hand, the topographical correspondence of human and non-human primate cytoarchitecture and tonotopic maps remains a working hypothesis rather than an empirical fact, as current

methodological limitations don't allow the acquisition of both detailed cytoarchitectonic and functional data in humans. Furthermore, the superior temporal plane in humans has expanded substantially compared to non-human primates and is characterised by great inter-individual macro-anatomical variability, which affects the underlying cytoarchitecture (Hackett et al., 2001). This variability in gyral and sulcal topography also limits the utility of probabilistic cytoarchitectonic atlases (e.g. Morosan et al., 2001), which don't necessarily generalise well to individual macro-anatomy.

Another approach that has been adopted to characterise the human auditory cortex is the combined use of in-vivo MRI measures of cortical myelination and tonotopy (De Martino et al., 2014; Dick et al., 2012; Glasser & Van Essen, 2011). Unlike cytoarchitecture, information on cortical myelin content can be obtained non-invasively with several quantitative MRI parameters (Lazari & Lipp, 2021; Weiskopf et al., 2015). For example, relaxation rates such as R1 (1/T1) are influenced by the macromolecules (i.e. lipids and proteins) that compose myelin sheets (Callaghan et al., 2015; Weiskopf et al., 2013). Magnetisation transfer, by measuring the energy transferred by excited protons of macromolecules to the local unbound protons spins, can also be used to estimate tissue myelin content (Hagiwara et al., 2018; Henkelman et al., 2001). FMRI has also allowed the acquisition of tonotopic data in vivo in humans (Da Costa et al., 2011; Dick et al., 2012; Dick et al., 2017; e.g. Formisano et al., 2003; Talavage et al., 2004). The general configuration of tonotopic gradients is consistent across the literature (Moerel et al., 2014), with a region of low-frequency preference within HG surrounded anteriorly, medially, and posteriorly with regions of high-frequency preference. Furthermore, it is possible to quantify the tuning width of cortical tonotopic activation, that is the range of frequencies

below and above the main preferred frequency that elicits cortical activation (De Martino et al., 2013; e.g. Moerel et al., 2012). In the monkey, core regions are known to have narrower tuning widths compared to belt regions (Hackett et al., 1998; Kajikawa et al., 2005; Kusmierek & Rauschecker, 2009; Rauschecker et al., 1995).

This is the first of three chapters dedicated to the analysis of the structural and functional characterisation of the human auditory cortex, with an emphasis on individual differences. The aim of this chapter is to present the average distribution of tonotopic gradients, tuning widths, and myelin-sensitive R1 and MT maps in a sample of 58 healthy subjects sampled from the general population and evaluate, qualitatively and quantitatively, their spatial covariance. An initial estimation of group variability for each of these maps is provided.

3.2 Methods

3.2.1 Subjects

Participants (n = 58; age (mean ± SD): 23.9 ± 4.9; 32 female) were healthy, right-handed adults recruited from local participant pools.

3.2.2 Multi-parameter mapping

3.2.2.1 MPM acquisition protocol and preprocessing

Structural MRI data were acquired according to the multi-parameter mapping protocol (Lutti et al., 2010; Weiskopf et al., 2013) with a 3T whole-body Tim Trio system (Siemens Healthcare) and a 32-channel head coil (data acquisition protocol is also described in detail in Carey et al., 2018, cohort 2). The protocol consists of three 3D spoiled multi-echo fast low angle shot (FLASH) volume acquisitions at 0.8 mm isometric resolution and the

additional acquisition of the RF transmit field map and a static magnetic (B0) field map (total scan time of 26 minutes). Three different weightings: magnetisation transfer (MT), longitudinal relaxation rate (R1 = 1/T1), and proton density (PD). For each participant, 3D EPI spin-echo and stimulated echo images were acquired to estimate individual inhomogeneities in the RF transmit field (B1+) as well as a B0 field map to remove the off-resonance effect from the B1+ map (Lutti et al., 2010).

R1, MT, PD, and R2* maps were calculated using the Voxel-Based Quantification (VBQ) toolbox in SPM 8. R2* maps were estimated through the ordinary least squares ESTATICS approach (Weiskopf et al., 2014). R1, MT and PD weighted volumes were calculated as the average of all echoes for each weighting to increase the signal-to-noise ratio (Helms & Dechent, 2009), which were then used to calculate R1, MT, and PD maps (Weiskopf et al., 2013).

3.2.2.2 Cortical surface reconstruction

Each participant's cortical surface was reconstructed in freesurfer (version 5.3; Dale A. M., 1999). MPM maps were first pre-processed to optimise freesurfer's grey matter segmentation procedure (see Carey et al., 2018). The skull was removed from the PD volumes using csurf's (i.e. in-house version of freesurfer) skull stripping procedure. Skull-stripped volumes were manually inspected for excessive stripping (i.e. stripping cortical tissue) and adjusted accordingly by lowering the shrinking factor. The resulting volumes were normalised with freesurfer's *mri_normalize* routine and inspected to verify correct ranges for white (110) and grey (50-70) matter. Volumes were then registered (*mri_em_register*) and normalised (-*canorm* option in *recon-all*). An additional multi-dimensional Talairach transformation was calculated (*recon-all* with options -*careg*, -

careginv) using the first Talairach transform, skull-stripped volume, and normalised volume as inputs. The cortical surface was then reconstructed using the full *recon-all* routine (all parameters of the "autorecon-2" and the first six of the "autorecon-3" steps; these parameters can be found at: https://surfer.nmr.mgh.harvard.edu/fswiki/ReconAllDevTable). The resulting pial and white matter surfaces were superimposed on the normalised volume and manually inspected for any inaccuracies in tissue segmentation.

3.2.3 Tonotopy

3.2.3.1 Stimuli

Subjects were asked to listen to bandpass-swept non-linguistic vocalisations adapted from the Montreal Affective Voices (Belin et al., 2008) and press a response button whenever they heard a laughter sound (actual responses were not recorded). These stimuli were selected because fMRI activation is positively modulated by stimulus complexity and attentional demands (Dick et al., 2017; Woods et al., 2009). Tokens of these vocalisations were randomly recombined in 8-minute and 32-second long passages with no token repeating twice within a single passage. Passages were compressed and a cycling bandpass filter was applied with a period of 64 seconds and centre frequencies ascending logarithmically from 150 Hz to 9600 Hz (quality factor Q = 2, expanding to Q = 3 at tails), for a total of 8 sweeps per block. Stimuli were then further filtered using bandpass filters one octave above and below the centre frequency. A final filter was applied to correct for the specific acoustic transfer function of the Sensimetrics S14 earphones used to deliver the stimuli. The amplitude envelope of the frequency sweeps was adjusted to match the loudness of the scanner. Each subject completed 4 blocks, 2 of which had the frequency

direction of the bandpass sweep reversed (i.e. 9600 Hz to 150 Hz). Memory foam pillows (NoMoCo Inc.) were fit around participants' heads to improve the stability of the head and earbud position and provide passive isolation from scanner noise.

3.2.3.2 Data acquisition protocol

Tonotopic data were acquired at the Birkbeck/UCL Centre for Neuroimaging (BUCNI) with a 1.5T whole-body Tim Avanto System (Siemens Healthcare) and a 32-channel head coil. Echo-planar images (EPI) were acquired with the following parameters: 28 slices, voxel size = 3x3x3 mm^3, matrix = 64 x 64, excitation flip angle = 90°, bandwidth = 1474 Hz/pixel, TR = 2000 ms, TE = 39 ms. Each block consisted of 262 volumes in total, with 6 initial volumes for longitudinal relaxation to reach equilibrium and 256 (i.e. 8 minutes and 32 seconds) volumes for tonotopic data. Using the same orientation and slice block centre, an additional short (3 minutes) 3D MPRAGE (88 partitions, voxel resolution 1 × 1 × 2 mm3, flip angle = 7°, TE = 4 ms, TI = 1000 ms, TR = 8.2 ms, mSENSE acceleration = 2×, slab-selective excitation) was also acquired to run an initial alignment with the high-resolution MPM structural data.

3.2.3.3 Preprocessing

All functional volumes were manually inspected for blink motion artefacts or other quick movements. Affected volumes were removed and substituted with the average of the volumes immediately before and after the discarded volume. Each block was further motion corrected using AFNI's 3dvolreg (with options -heptic -twodup -twopass) by registering all EPI volumes in each block to a reference volume (i.e. 128th, middle of the time series). The T1-weighted volume acquired in the functional scanning session was used

to calculate the 4 x 4 affine transformation required to align EPI data to the high-resolution structural data using freesurfer's bbregister (Greve & Fischl, 2009), with an additional manual blink comparison to ensure alignment quality.

3.2.3.3 Data analysis

For each block, a fast Fourier transform (FFT) was calculated to extract at each voxel the stimulus phase with the highest magnitude (Sereno et al., 1995; Sereno & Huang, 2006). Magnitudes at each stimulus phase were calculated as the square root of the F ratio of signal amplitude and amplitude of the remaining phase spectrum. The second and third harmonics were also considered part of the stimulus frequency. After inverting the phases of the two reversed blocks (i.e. descending bandpass sweeps), the four blocks were averaged by calculating the vector average of the complex signals, that is by calculating the arithmetic average of the real and imaginary components of the Fourier transforms and calculating the phase (atan2(imaginary, real)) and magnitudes (sqrt(real^2 + imaginary^2)) of the resulting vector. Cross-subject averages were also calculated as the vector average of individual complex data, albeit by first resampling (mri_surf2surf) each subject's data onto freesurfer's standard icosahedron (order 7) using nearest neighbour forward and reverse (nnfr) mapping and one step of smoothing. During cross-subject averaging, an additional dispersion statistic was calculated to quantify the loss of magnitude at each vertex due to phase incoherence across participants. Finally, the resulting phase-encoded group-average tonotopic maps and dispersion maps were resampled back onto a representative surface (fsaverage).

3.2.3.4 Population receptive fields

Data from the four EPI blocks of each participant were concatenated and matched with the log-spaced discrete spectrogram (100 bins) or the corresponding auditory stimuli. The frequency centre (mu) and width (sigma) parameters of tonotopic population receptive fields (pRF) were calculated according to a 2-stage iterative process (Dumoulin & Wandell, 2008; van Dijk et al., 2016). In the first phase, a coarse estimate of the pRF parameters was calculated on a spatially smoothed (FWHM = 5 mm) inflated spherical surface. A set of predicted time series was generated by calculating the overlap between the stimulus time series and the pRF parameters in the parameter space and convolving with a standard hemodynamic response function (HRF). The parameters that generated the best predicted time series were identified by calculating the Pearson correlation of the predicted and observed time series. In the second phase, a more accurate parameter estimation was obtained by minimising the sum of squared errors between predicted and observed time series using a simplex optimisation algorithm. Individual data were thresholded by setting parameters for any vertex with a poor fit (R^2<0.04) to zero. Cross-subject averages were calculated using the same technique as phase-encoded data. Additionally, a t-test statistic was calculated at each vertex to test whether the group mean was different from zero and used to visualise significant (p<10^-6) vertices.

3.2.4 Searchlight spatial cross-correlation

Spatial cross-correlations between R1 and tonotopic magnitude were calculated in csurf using a searchlight radius of 5 mm. This procedure calculates the Pearson correlation between any two datasets within a searchlight area centred at each vertex across the entire cortical surface of each hemisphere. The resulting cross-correlation maps represent, at each

vertex, the covariance (or correlation) between the two datasets in a small region surrounding that vertex.

3.3 Results

3.3.1 MPM: R1 and MT group average maps

R1 and MT (Figure 3.1 and Figure 3.2, bottom row), known to be sensitive to cortical myelin density, were expectedly greatest in primary somatosensory, motor, visual (not shown) cortices, as well as auditory regions in group-average maps. More specifically, a "keyhole" shaped peak in R1 and MT was present medially within HG, which is compatible with the notion of a highly myelinated putative auditory core present within the medial two-thirds of the gyrus.

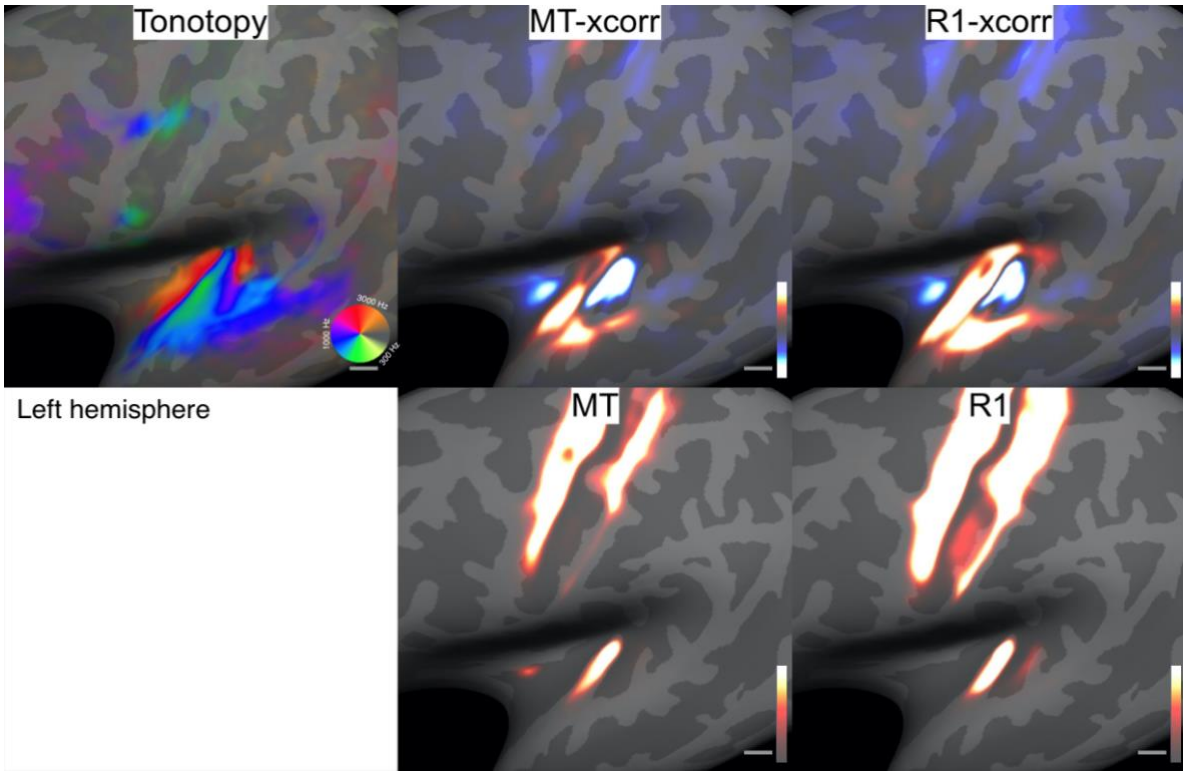

Figure 3.1*: Left-hemisphere group-average maps of tonotopic phase, R1, and MT data, with corresponding spatial covariance maps (MT-xcorr, R1-xcorr). Spatial covariance was calculated between MPM parameters and tonotopic magnitude.*

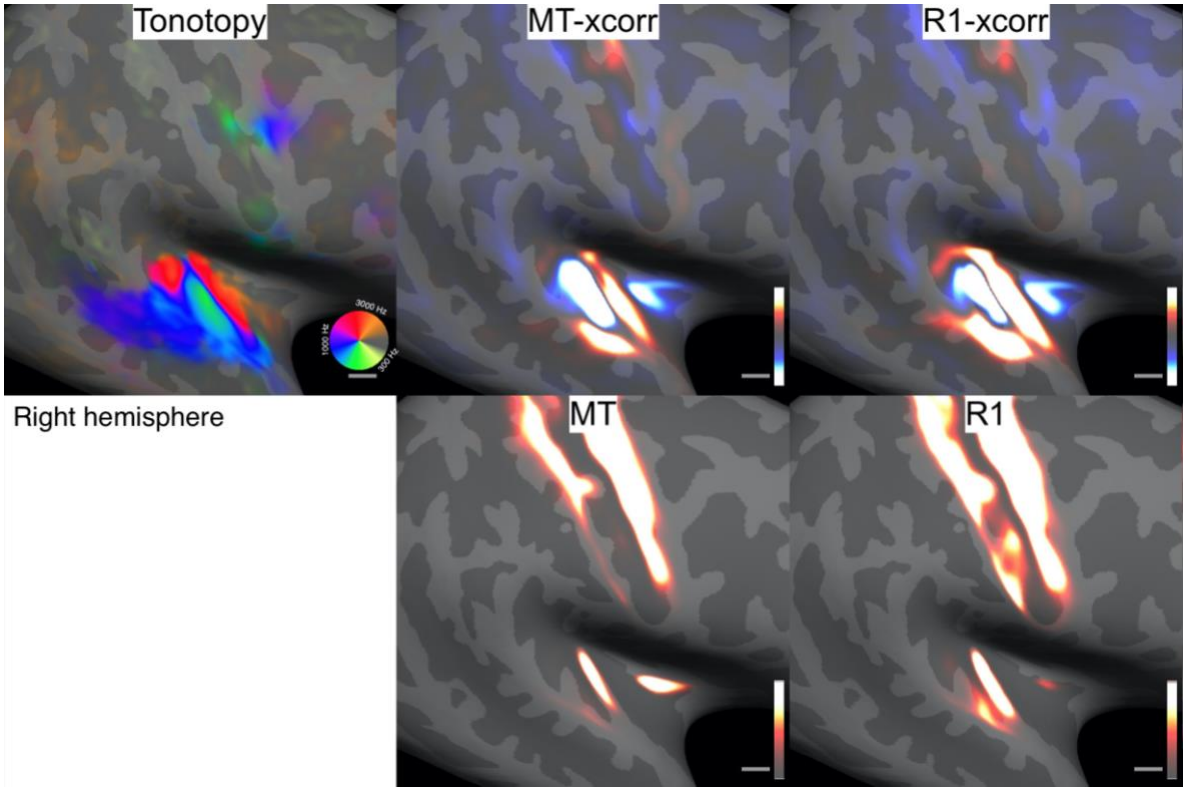

Figure 3.2*: Right-hemisphere group-average maps of tonotopy phase, R1, and MT data, with corresponding spatial covariance maps (MT-xcorr, R1-xcorr). Spatial covariance was calculated between MPM parameters and tonotopic magnitude.*

3.3.2 Tonotopy: phase-encoded and pRF average maps

Group-average phase-encoded data (Figure 3.1 and Figure 3.2) showed typical anterior-posterior gradient reversals (De Martino et al., 2014; Dick et al., 2012), with high-frequency regions forming an inverted "V" shape around the most medial portion of HG in both hemispheres. Specifically within HG, tonotopic gradients are highest anteromedially and decrease posterolaterally and the full frequency spectrum appears to be represented within the boundaries of the gyrus. Group-average pRF centre frequency maps (Figure 3.3), unsurprisingly, also followed the same characteristics observed in phase-encoded maps, forming the same inverted "V" high-frequency-preference region around the medial extremity HG. On the other hand, tuning widths (Figure 3.4) appeared narrower anteromedially and wider posterolaterally.

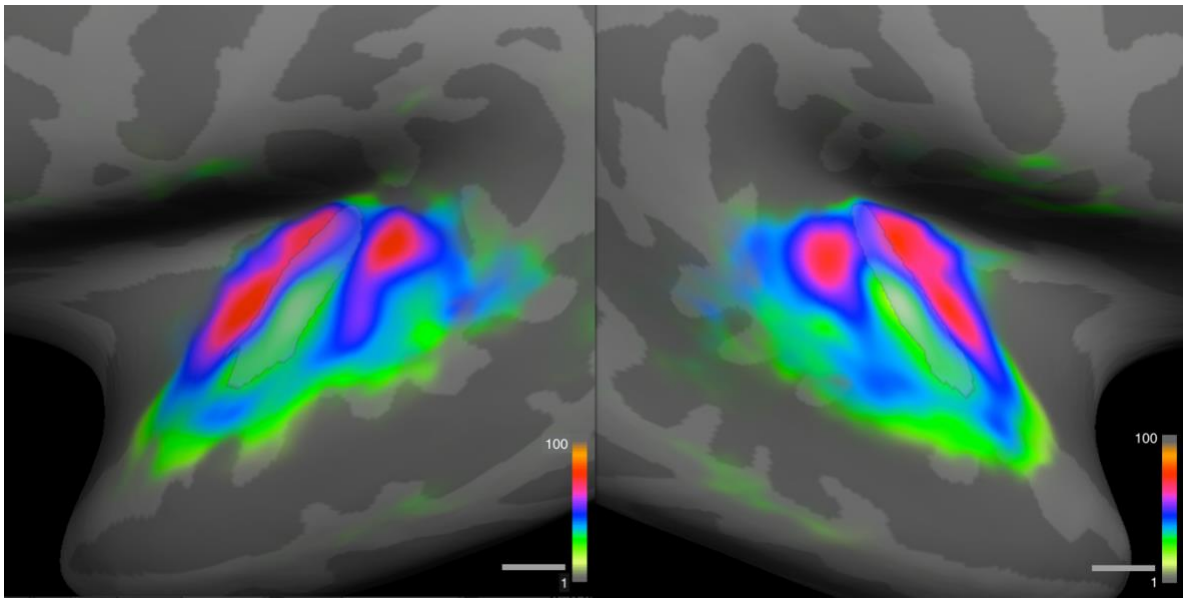

Figure 3.3*: Centre-frequency group-average maps of tonotopic population receptive fields mapped onto a representative surface (fsaverage). The surface of HG is superimposed transparently for reference.*

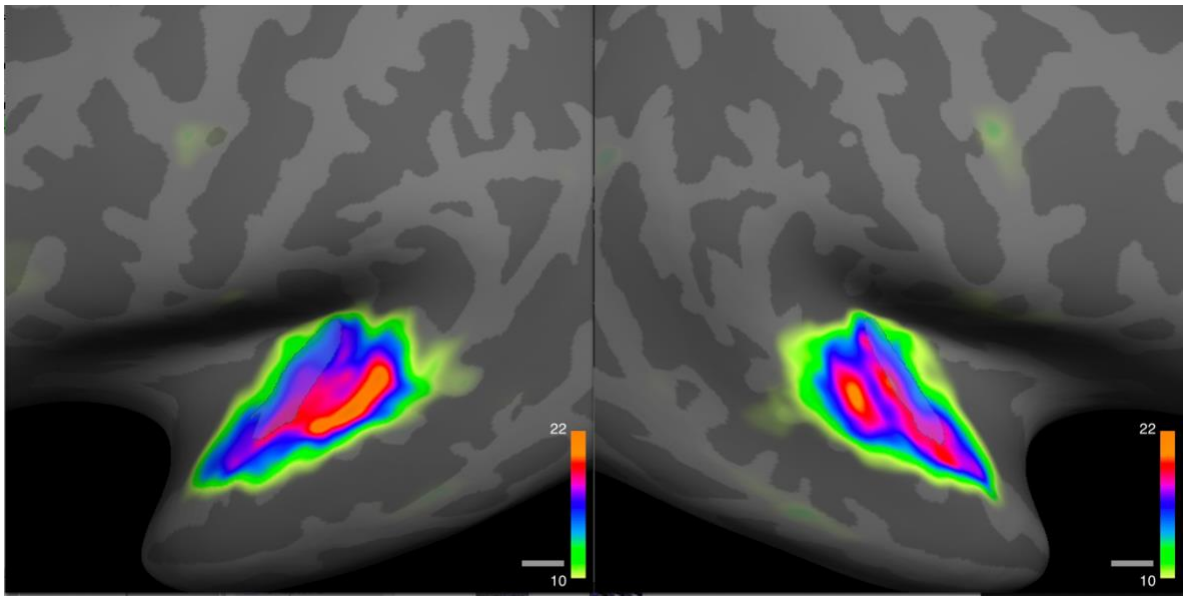

Figure 3.4*: Tuning width group-average maps of tonotopic population receptive fields mapped onto a representative surface (fsaverage). The surface of HG is superimposed transparently for reference.*

3.3.3 Tonotopy: inter-subject variability

Representative examples of individual tonotopic maps are reported in Figure 3.5. Although the anterior-posterior high-to-low-to-high gradients were generally traceable across

participants, there were also substantial differences in the configuration of high and low-frequency preference regions and their relative size. For instance, subject 82 displayed thin regions of low-frequency preference parallel to the mediolateral axis of HG, surrounded anteriorly and posteriorly by much wider regions of high-frequency preference. This was in contrast with the tonotopic configuration of group-average maps and individual maps such as subjects 79 and 90. Interestingly, the relative surface area of high and low-frequency regions within individuals appeared to be consistent across hemispheres. Additional anterior-posterior gradient reversals were also visible across participants posteriorly to the canonical high-to-low-to-high gradients. In particular, an additional posterior region of low-frequency preference was present posterolaterally across most participants, which is somewhat reflected in group-average maps in a region of low-frequency preference extending into the superior temporal sulcus. Although not as frequent, an additional reversal towards high-frequency preference was present in the right hemisphere of subject 69 and, albeit noisier, subject 93. Overall phase agreement across subjects (Figure 3.6) appeared lowest anteromedially and increased gradually posterolaterally in both hemispheres. This gradient mirrored the pattern observed in tonotopic gradients, with a lower cross-subject agreement for high-frequency regions and a higher cross-subject agreement for low-frequency regions.

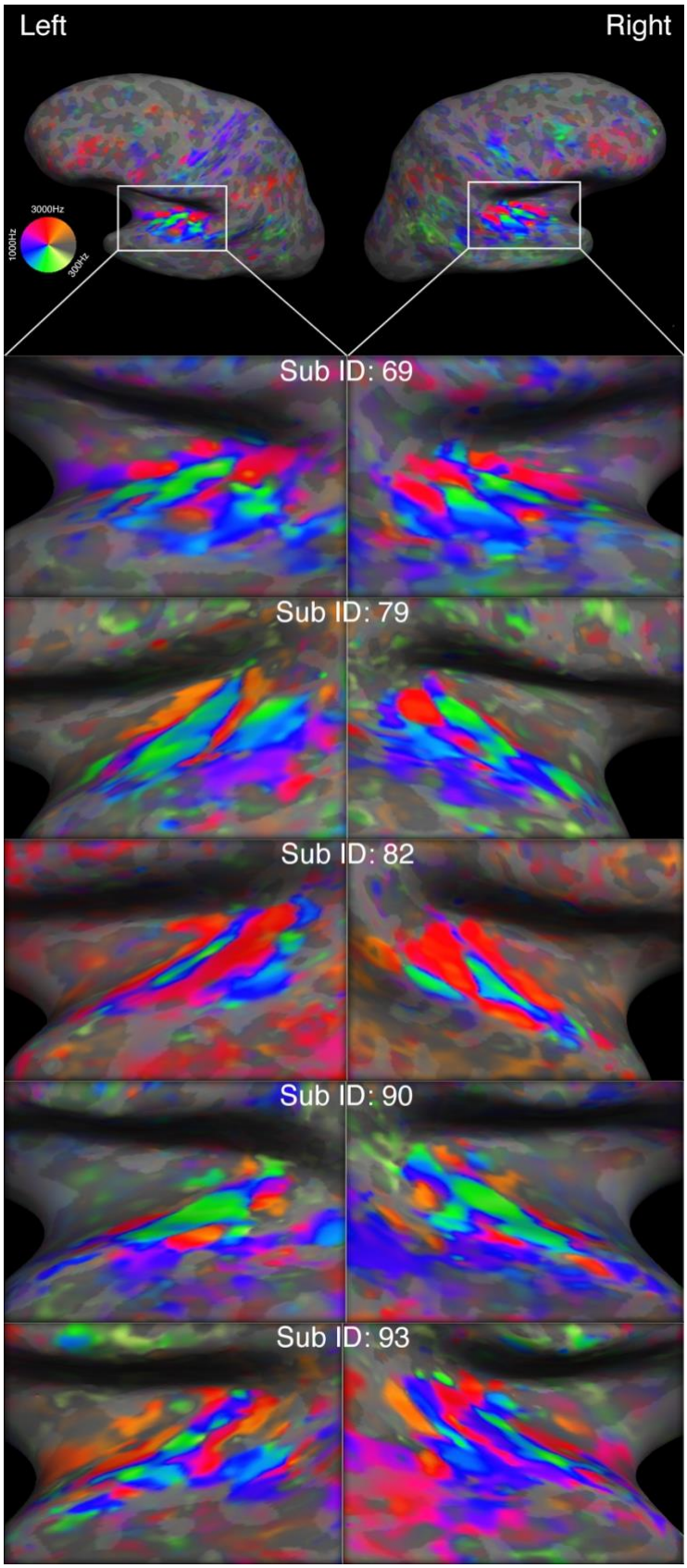

Figure 3.5*: Representative examples of individual tonotopic maps.*

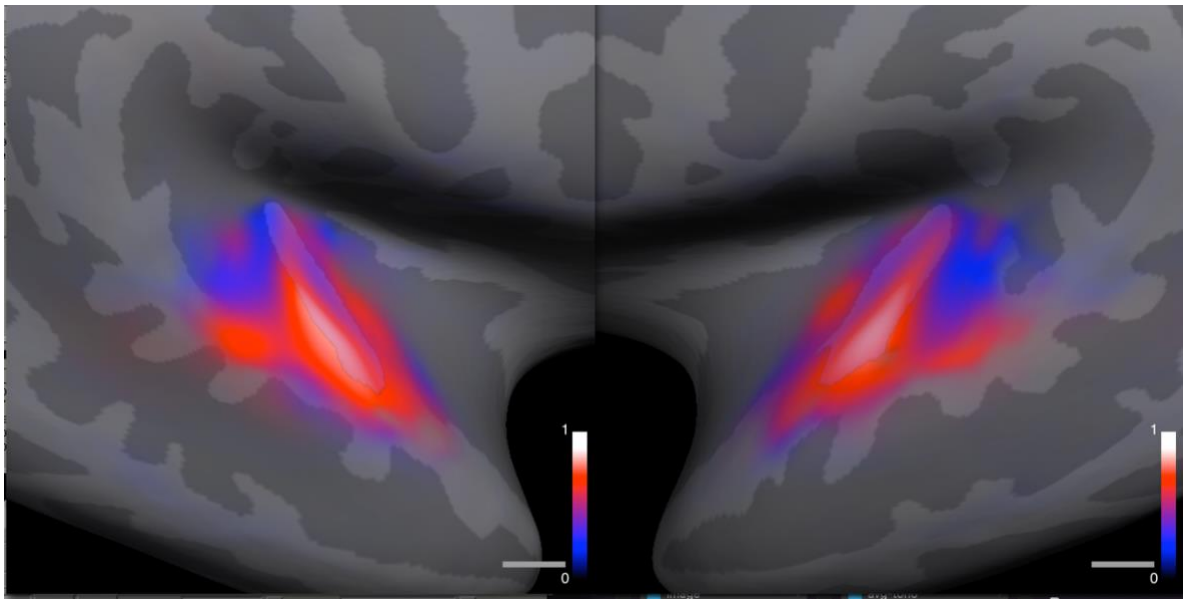

***Figure 3.6**: Cross-subject phase agreement of phase-encoded data. The HG label is superimposed with transparency for reference.*

3.3.4 Local covariance of R1 and tonotopic magnitude

Average cross-correlation maps showed a systematic relationship between R1[12] and tonotopic magnitude across hemispheres (Figure 3.7). These results closely replicate those found by Dick et al. (2017), namely the presence of an arc-shaped region of positive covariance surrounding medially (circular insula), anteriorly (anterior half of HG and planum polare), and laterally (STG) a circular region of negative covariance centred at the posterolateral border between HG and HS. The region of positive covariance was mainly driven by a mutual decrease in both R1 and tonotopic magnitude, whereas negative covariance emerged from opposing gradients of increasing tonotopic magnitude and decreasing R1. The border between regions of high and low covariance corresponded to the crown of HG, effectively splitting it into two halves along its mediolateral axis. This topographical aspect of R1-tonotopy covariance maps can be recapitulated by the

[12] All results were equivalent when using MT instead of R1. For the sake simplicity, only R1 results are discussed.

association between R1 and cortical curvature (Carey et al., 2018; Dick et al., 2012; Sereno et al., 2013): while R1 always decreased from HG's crown anteriorly towards the first transverse sulcus and posteriorly towards HS, tonotopic magnitude increased anteromedially to posterolaterally irrespective of curvature gradients.

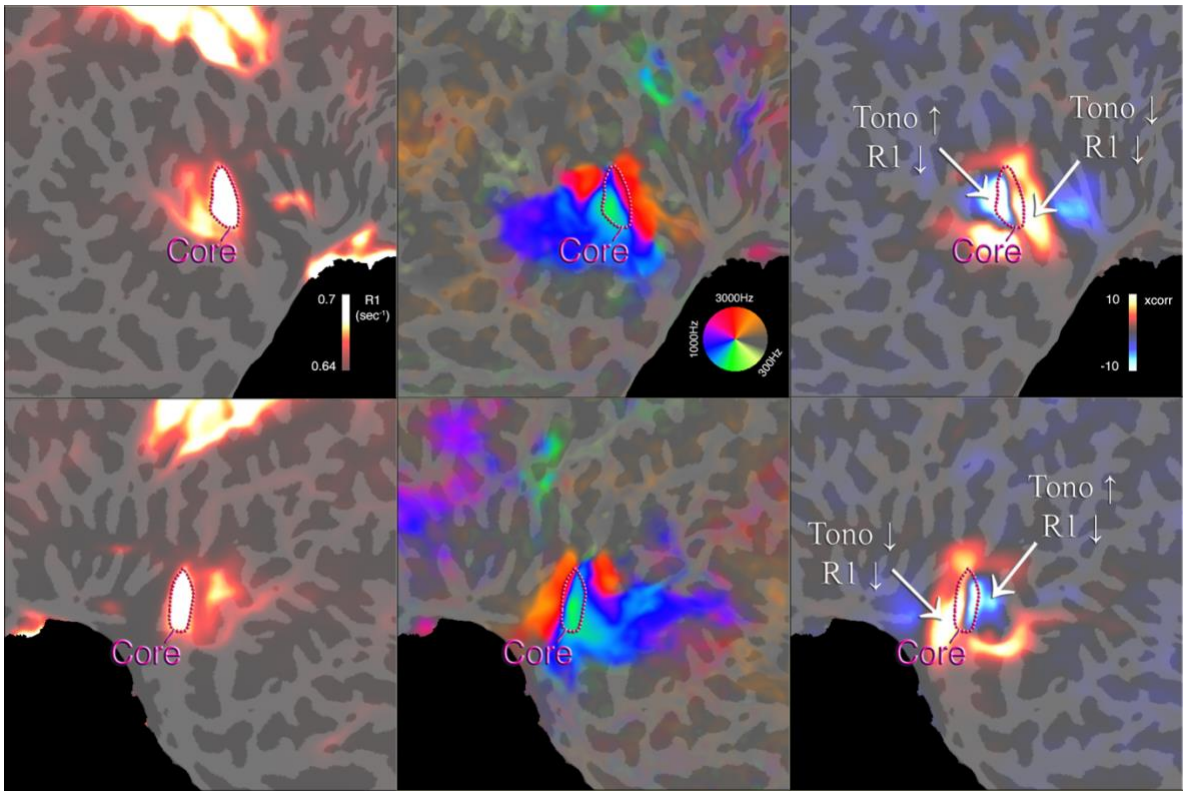

Figure 3.7*: Group-average R1, tonotopy (phase-encoded), and spatial covariance of R1 and tonotopy. The "Core" region marked by a dotted purple line corresponds to a putative auditory core identified using an R1 threshold of 0.69* s^{-1}.

3.4 Discussion

3.4.1 Average maps: comparison with previous studies

Group average maps for tonotopy and MPM data largely replicated previous findings (e.g. Dick et al., 2012; Dick et al., 2017). More specifically, the gradients of myelin-sensitive R1 and MT across the superior temporal plane were largely interchangeable. Both parameters showed strong signals confined within the boundaries of HG, greatest medially and

decreasing laterally. Tonotopic gradients were characterised by low-frequency preference across most of the surface of HG, with adjacent regions of high-frequency preference anteromedially and posteromedially. The spatial covariance of the magnitude of tonotopic response with R1 (also applicable to MT) was also in line with previous data (Dick et al., 2017), with a region of negative spatial covariance around lateral HG surrounded anteriorly and laterally by an arc of positive covariance. Finally, tuning width maps were also compatible with previous reports (Moerel et al., 2012, 2014), showing narrow tuning anteromedially within and around HG and broader tuning posterolaterally, extending into the planum temporale.

3.4.2 Association between tonotopic phase and magnitude

Tonotopic magnitude was greatest posterolaterally, extending into the superior temporal sulcus and planum temporale, and lowest anteromedially, in a pattern that resembles inverted tonotopic frequency gradients. Indeed, spearman correlation coefficients between average phase and average magnitude within HG[13] were -0.91 in the left hemisphere and -0.92 in the right hemisphere, which is in stark contrast with the overall correlations obtained with whole-hemisphere data (i.e. left hemisphere, r = -0.13; right hemisphere, r = -0.10). In other words, the magnitude of high-frequency selective cortical activation appeared to be systematically lower than low-frequency activation and localised within tonotopic HG only. Additionally, this association appears to be inflated by freesurfer's alignment and averaging procedure, as correlations distributions for individual data appeared much less extreme (i.e. approximately null for whole-hemisphere coefficients,

[13] HG was labelled according to the procedure described in Chapter 4.

and -0.41 and -0.38 within HG in the left and right hemispheres respectively; see Figure 3.8). On the one hand, the localised nature of this relationship excludes the possibility of a simple measurement artefact, as phase and magnitude are not systematically related across the whole cortical surface. On the other hand, cross-subject phase agreement was also lowest around the anteromedial portion of HG (Figure 3.6), and the average magnitude of two or more vectors decreases as a function of their phase disagreement. It is possible for the cross-subject alignment around the medial half of HG to be particularly challenging, given its deep location within the lateral sulcus. However, this localised increase in phase disagreement in the medial HG could also emerge from true individual differences in tonotopy around this region.

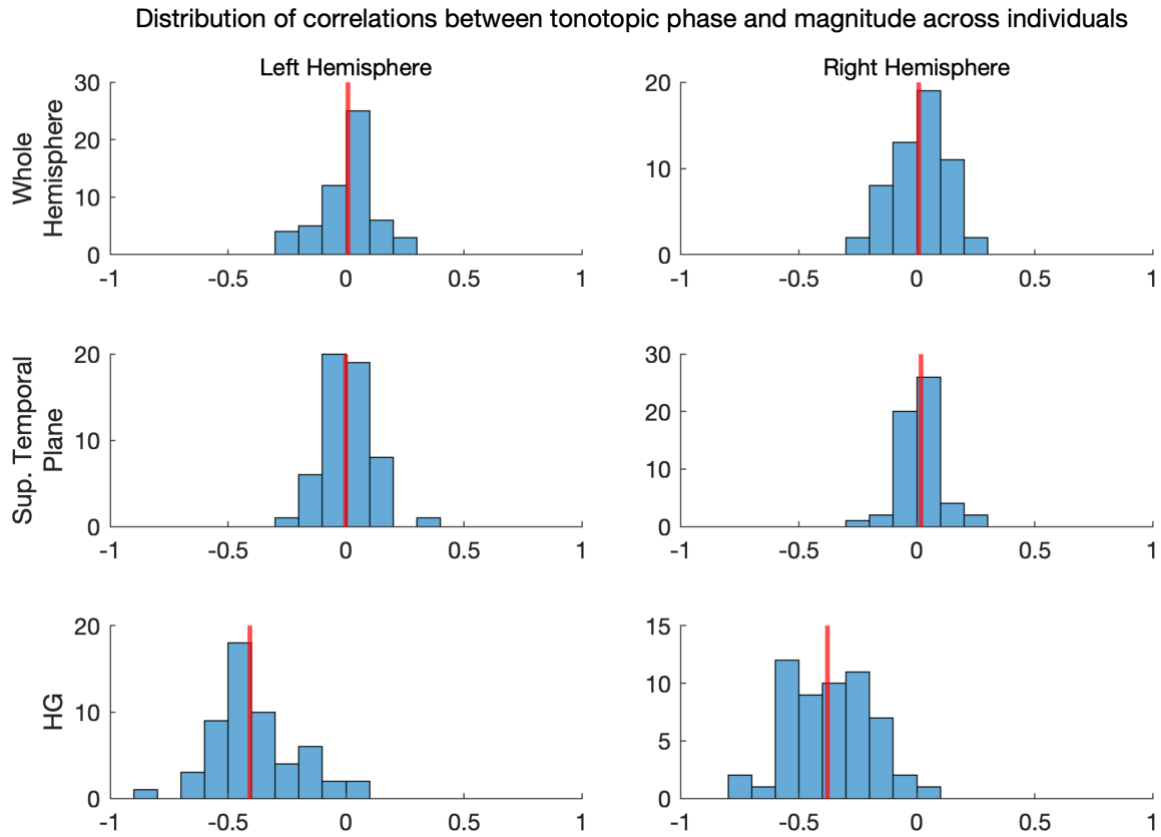

***Figure 3.8**: Histogram of the Spearman correlation coefficients between tonotopic phase and magnitude. The left and right columns correspond to the left and right hemispheres. The three rows correspond to the correlation coefficients calculated including vertices from the whole hemisphere*

(top row), the superior temporal plane (middle row), and Heschl's gyrus (bottom row). Vertical red lines indicate the average correlation coefficient.

3.4.3 Association between centre frequency and tuning width

A similar inverse relationship was also observed between the tuning width and centre frequency of pRF maps in HG, although in this case, this relationship extended not just to HG but the whole superior temporal plane (Figure 3.9). Importantly, pRF tuning widths only measure the selectivity of voxel activation around a single centre frequency. However, the spectral tuning of neuronal populations in the auditory cortex includes several types of response profiles, including multi-peak responses to several frequencies (Moerel et al., 2013). At the population level, multi-peak responses could simply emerge from clusters of neurons that are tuned to different frequencies. However, single-neuron recordings in the A1 of mice (Romero et al., 2020) and ferrets (Gaucher et al., 2020) also showed heterogeneous patterns of frequency selectivity, such as single frequency, double frequency, or a more complex response. In this chapter, pRFs were modelled according to a symmetric Gaussian defined by two parameters, the mean (centre frequency) and standard deviation (tuning width). However, it is possible to model more complex patterns of population response, such as the presence of multiple peaks or attenuation bands (Moerel et al., 2013). Finally, spectrally-directed attention in complex auditory scenes has been shown to produce similar tonotopic maps to those obtained with simple sensory stimulation (Da Costa et al., 2013; Dick et al., 2017; Riecke et al., 2016) and lead to the narrowing of frequency-selective response to a given frequency in animals through both augmenting response in neurons tuned to the attended frequency and suppressing response in neurons tuned to the competing frequencies (Ahrens et al., 2008; e.g. Fritz et al., 2005; O'Connell et al., 2014; Wehr & Zador, 2003). Exploring multiple modalities of pRF frequency response

and the effects of top-down cognitive control could improve our understanding of the regionalisation of the auditory cortex beyond tonotopic mapping gradients.

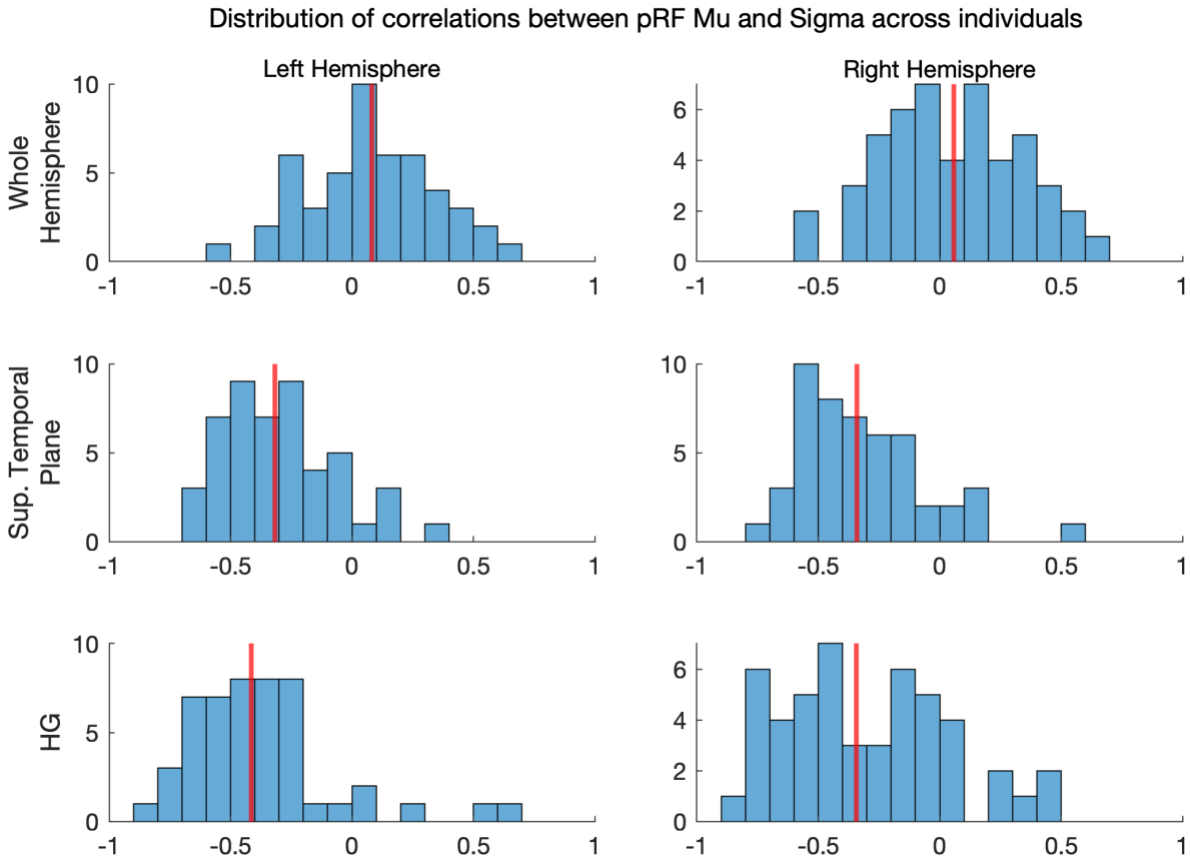

Figure 3.9*: Histogram of the Spearman correlation coefficients between pRF centre frequency and tuning width. The left and right columns correspond to the left and right hemispheres. The three rows correspond to the correlation coefficients calculated including vertices from the whole hemisphere (top row), the superior temporal plane (middle row), and Heschl's gyrus (bottom row). Vertical red lines indicate the average correlation coefficient.*

3.4.4 Individual differences and morphological variability

In this chapter, freesurfer's curvature-based alignment was used to morph individual surfaces onto a common template for averaging or calculating other group-level statistics. However, one recurring issue with the study of the human auditory cortex is the presence of considerable variability in individual cortical morphology, which can result in artefacts or distortion of individual data. Keeping track of which exact region was morphed onto, e.g.

the template's HG for each subject can be difficult, especially in large samples, and it defeats the purpose of using an automated procedure. Gulban et al. (2020) combined curvature-based alignment with explicit anatomical priors to improve cross-subject alignment, which was shown to increase the cross-subject overlap of ex-vivo cytoarchitectonic parcellations of the auditory cortex. However, this approach has two main issues. One of the anatomical priors was defined as the "anterior HG", or the most anterior full HG duplication. Understandably, given the lack of an empirical prior, the authors combined single gyri and partial duplications into a single category, but they admit this is something that requires further investigation. The second issue is the reliance on manual labelling, which is either unfeasible or incredibly expensive in large-scale studies.

In the following chapter, we present an automated procedure for the classification of partial duplications that can be applied inexpensively to large-scale samples. We identify two morphotypes, based on the length of the intermediate sulcus relative to the length of the gyrus, and morph gyri that share a similar morphotype onto a common template. In Chapter 5, we apply this procedure to evaluate differences and similarities across morphotypes using the tonotopic and MPM data presented in this chapter. We explore whether it is possible to define a functional or structural homology between non-duplicated and partially duplicated gyri, and how individual differences in cortical morphology interact with individual tonotopic and quantitative MRI data.

Chapter 4.

Automated classification of Heschl's gyrus' morphology

4.1 Introduction

4.1.1 The morphology of Heschl's gyrus

Through the dissection of some 1087 human brains (Heschl, 1878; Heynckes et al., 2022), Richard Ladislaus Heschl first described the regular occurrence of a gyrus within the lateral fissure, extending from the middle of the dorsal surface of the superior temporal gyrus (STG) transversely across the superior temporal plane. He also noted the morphological variability of this gyrus across individual brains, which most commonly include a posterior duplication (more rarely up to five duplications) or a partial duplication, also known as common stem duplication (CSD), in which the first and second transverse gyri are only separated laterally by a shorter intermediate sulcus and sharing a medial "stem". An additional-yet rare- variant he described consisted of a continuous arc formed by the anterior half of the STG and the anterior transverse gyrus, separated from the posterior half of the STG by an intermediate sulcus. The morphological variability of HG has since been studied extensively (Dalboni da Rocha et al., 2020; Golestani et al., 2007; Leonard et al., 1998; Penhune et al., 1996; e.g. Thompson et al., 1996). One large-scale study (Marie et al., 2015) of 430 healthy volunteers (from the BIL&GIN database; Mazoyer et al., 2016) found an occurrence of duplications in right-handers (n = 232), partial or complete, of 64%, with the number of duplications in the right hemispheres being approximately 1.3 times those in the left hemisphere. They reported CSD being twice as frequent as complete duplications in the left hemisphere, while in the right hemisphere, complete duplications were 10% more

frequent than CSD. In these subjects, the surface area of anterior gyri (i.e. single gyri or anterior duplications) was greater in the left hemisphere, but lower bilaterally in case of duplications (22% smaller in the left hemisphere and 11% in the right hemisphere), while total HG surface area was overall greater in the presence of duplications. In left-handers (n = 198), they found instead lower occurrences of overall duplications and greater HG surface areas (both anterior duplications and total area) in the right hemisphere.

4.1.2 Classification of HG morphology: terminology and methodological issues

One major obstacle in conducting large-scale studies on HG morphology is the reliance on manual labelling, which in turn involves several parcellation techniques (e.g. volume- or surface-based). Furthermore, terminology and classification heuristics of HG's sub-regions, duplications, and the planum temporale (PT) can be inconsistent across studies. The boundaries of HG are commonly defined anteriorly by the first transverse sulcus (FTS) and posteriorly by Heschl's sulcus (HS) or an intermediate sulcus (IS) in case of partial duplications (Abdul-Kareem & Sluming, 2008; Penhune et al., 1996). However; Rademacher et al. (1993) stated that the IS extends "no more than one-third to one-half of the way along the long axis of the gyrus", while Penhune et al. (1996) only considered IS that were *at least* half the length of HG (or one third in other studies; e.g. Marie et al., 2016), which contradicts the first definition, although the two are often cited together. Furthermore, several studies considered partial duplications as part of a single structure (Benner et al., 2017; e.g. Schneider et al., 2005; Wengenroth et al., 2014; Wengenroth et al., 2010), while others defined an anterior HG (aHG) by extending the IS posteromedially,

"completing" the partial duplication[14] (e.g. Schneider et al., 2002), although there is no agreed standard on how to extend the IS and divide the common stem region into an anterior and a posterior halves.

The definition of a boundary between HG and the planum temporale (PT) also varies across studies. PT is often inclusive of any complete HG duplication (Shapleske et al., 1999; Tzourio-Mazoyer & Mazoyer, 2017), although sometimes they are excluded (e.g. Zoellner et al., 2018). The inclusion of complete HG duplications in the PT is largely based on the notion that the primary auditory cortex (PAC), i.e. a primary-like koniocortical and highly myelinated cortical region that receives direct thalamic projections from the medial geniculate nucleus, is located within the medial two-thirds of the crown of the most anterior duplication (Rivier & Clarke, 1997; Wallace et al., 2002). However, in the presence of CSD, the PAC sometimes extends posteriorly into the intermediate sulcus and partial posterior duplications (Hackett et al., 2001; Rademacher et al., 1993), and arguments exist for primary auditory fields also occupying full posterior duplications (Da Costa et al., 2011). Schneider et al. (2005) found no difference in the correlation between interhemispheric PT volume asymmetry and asymmetry in auditory evoked potentials (P50m) in response to tones of varying harmonic complexity regardless of the definition of PT (i.e. whether it included or excluded partial or complete duplications bilaterally). On the other hand; Tzourio-Mazoyer & Mazoyer (2017) found that the inclusion of a posterior duplication (complete or partial) in the PT systematically increased leftward asymmetry of

[14] Somewhat confusingly, the "aHG" label has also been used to define the most anterior *full* duplication, combining all parts of a CSD into a single region (e.g. Benner et al., 2017).

its surface area and that PT asymmetry was correlated to a verbal ability only when HG duplications were excluded from its definition.

4.1.3 An automated pipeline for the classification of partially duplicated gyri

Overall, inconsistent parcellation standards and the reliance on manual labelling limit the ability to conduct large-scale studies and combine findings across research centres. The first fully automated pipeline for the parcellation of HG duplications was published by Dalboni da Rocha et al. (2020). Their toolbox for the automated parcellation of the Heschl's gyrus (TASH) labels all HG full duplications within the superior temporal plane based on variations in local curvature, segmenting gyral and sulcal regions. This parcellation is done within an ROI that comprises the transverse temporal gyrus, transverse temporal sulcus, PT, and posterior Sylvian fissure, as identified by Freesurfer's automatic parcellation using the Destrieux atlas (Destrieux et al., 2010).

This chapter introduces an additional automated pipeline for the classification of partial duplications and extraction of morphometric information such as the size of intermediate sulci and gyral partial duplications. Furthermore, gyri across three morphotypes (i.e. single gyri, CSDs with an IS shorter than half the length of the gyrus, and CSDs with an IS longer than half the length of the gyrus) are morphed and resampled onto a common surface for cross-subject averaging and comparison. These techniques are applied to an original sample of 58 subjects and an additional sample of 100 subjects from the Human Connectome Project (HCP) database. The occurrence of full and partial duplications across hemispheres and samples is reported and discussed along with descriptive statistics of each morphotype, cortical thickness maps, and the relationship between the occurrence of duplications and overall cortical gyrification.

In Chapter 5, I apply this pipeline to compare measures of structural MRI and tonotopy across morphotypes, identify potential homologies, and quantify individual differences.

4.2 Methods

4.2.1 Subjects

Two samples were included in the following analyses. The first sample ("original"), corresponding to the 58 subjects (age (mean ± SD): 23.9 ± 4.9; 32 female) presented in the previous chapter, was used to develop and test the classification pipeline. An additional matched sample of 100 subjects from the Human Connectome Project (HCP) was used as a test set. The HCP sample (age (mean ± SD): 24.1 ± 4.9; 54 female) was obtained from https://db.humanconnectome.org by selecting "100 unrelated subjects" under the option "explore subjects" in the "WU-Minn HCP Data - 1200 Subjects" sample (WU-Minn, 2017).

4.2.2 TASH

The TASH toolbox (Dalboni da Rocha et al., 2020) was used to automatically label Heschl's gyrus and any of its full duplications. This toolbox uses curvature thresholding to discriminate gyri and sulci within the lateral fissure. However, two labelling issues were noted after manually inspecting the output labels.

First, the area that the toolbox uses to run its thresholding out of the box is composed of four labels taken from freesurfer's Destrieux Atlas (i.e. "*aparc.a2009s"*): the transverse temporal gyrus, transverse temporal sulcus, planum temporale, and the posterior ramus of the lateral fissure. However, these did not always include the most posteromedial portion of Heschl's gyrus as it was sometimes mislabelled as circular insula during freesurfer's

automatic segmentation. Despite being undocumented, the toolbox does calculate two additional "expanded" labels: one including the circular insula and one including both the circular insula and planum polare. Including circular insula solved this issue, which can be done by simply changing the input label in the *TASH_opening.m* script from **LT.curv* to **LT_CI.curv*.

The second issue arose from the implementation of curvature thresholding. This process sometimes failed to correctly identify full duplications in cases when these were connected by regions of low curvature, clustering them into one single gyrus. This artefact was resolved by adding a thresholding step in the *TASH_grow.m* script that not only considers absolute curvature values but also how *consistent* these values are within a given region, as areas of consistently low curvature are not likely to be gyri. Specifically, the added step identifies vertices with low curvature (i.e. between -0.1 and 0) and calculates the root mean square and standard deviation of the curvature of all vertices within a range defined by a cube with 10mm edges centred at the vertex being evaluated. A given vertex was removed from the label if the root mean square was lower than 0.1 (i.e. average curvature in the surrounding area is low) and the standard deviation was lower than 0.04 (i.e. curvature is consistently low). These conditions were set after extensive testing, with the overall goal of only removing areas of very consistently low curvature in a relatively large radius, thus avoiding the creation of holes or sharp edges around the label. Specifically, the root mean square performed better than other lower power means as it is more sensitive to large values, making it more likely that a given vertex would be retained in the proximity of a high-curvature vertex. A cubic search area with a 10mm edge produced the best results in terms of label smoothness and sensitivity to local variations, as opposed to other shapes

(e.g. sphere) and smaller volumes, which tended to erode the label too aggressively, cutting into actual gyri.

4.2.3 Preprocessing

To facilitate the assessment of its morphology, the geometric properties (i.e. shape and orientation) of Heschl's gyrus were automatically standardised during preprocessing, which involves four main steps: rotating, refining (i.e. artefact removal), flattening, and warping. First, the most anterior transverse gyrus, including any partial duplications, was imported into MATLAB in its original 3d space in order to process its orientation. Specifically, the vertex coordinates were rotated to align the typical posteromedial-to-anterolateral orientation of Heschl's gyrus with the vertical axis of a Cartesian plane, with the most posteromedial portion at the top, and then centred at the origin.

Second, the outer contour of the gyrus was scanned for any discontinuities, that is groups of vertices whose coordinates were inconsistent with those of surrounding vertices and the overall shape of the gyrus. These were considered artifactual and removed. These types of artefacts were overall rare and mostly corresponded to clusters of vertices with negative curvature that protruded from the main body of the gyrus (Figure 4.1). Third, a region including transverse temporal gyrus, transverse temporal sulcus, planum temporale, posterior lateral fissure, and circular insula was cut from the cortical surface and flattened via Freesurfer's *mris_flatten.* Heschl's gyrus was cut from this flat patch by matching the vertices that remained after artefact removal. The gyrus was then rotated following the same orientation used in 3d space, with the most posteromedial portion at the top. Crucially, orientation assessment and artefact removal were run beforehand in 3d space, as flattening removes orientation information and distorts the contour of the gyrus.

Fourth, a non-rigid transformation was applied in order to achieve vertical symmetry and, in the case of a partially duplicated gyrus, a clear separation of the anterior and posterior branches around the vertical axis. Specifically, the algorithm first calculates the "convex hull" of a given patch, which corresponds to the smallest convex polygon that envelopes all of its vertices. For each vertex, a pair of points was then defined on this polygon which corresponded to the left and right margins at its y-coordinate. A horizontal translation was calculated so that the midpoint of these two points would land on the vertical axis (i.e. $x = 0$). The magnitude of this translation was gradually scaled down towards a more lateral portion of the gyrus in order to preserve morphologically relevant asymmetries. Finally, if an incomplete duplication was identified, this translation was calculated by taking the average coordinates of the midpoints of both the outer and inner contours (i.e. the borders of the gyrus but also the intermediate sulcus). This ensures that anterior and posterior branches are always clearly separated by the vertical axis $x=0$, as the intermediate sulcus can shift considerably off the centre in cases where one branch is much wider than the other if the translation is calculated on outer contours alone.

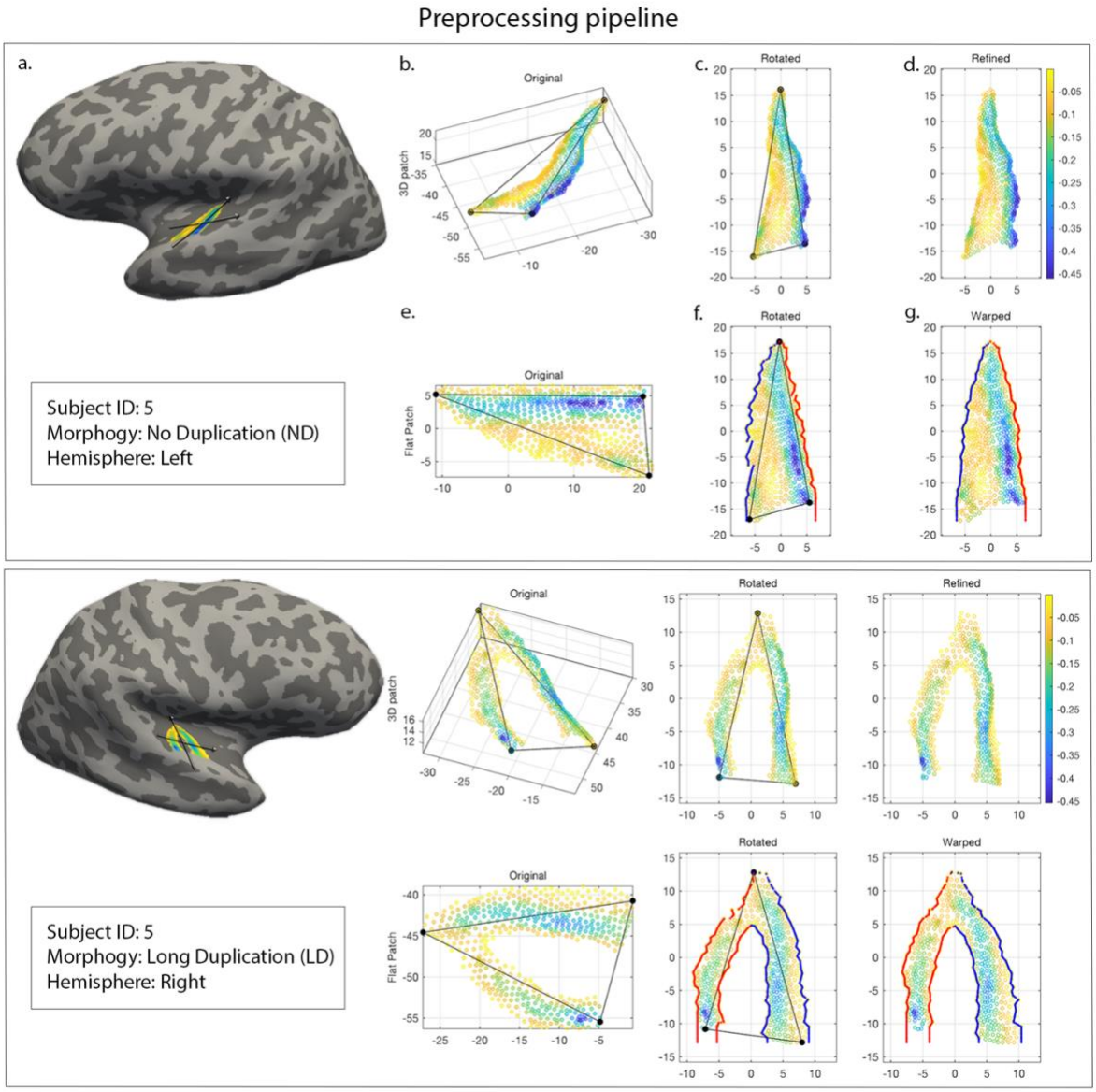

Figure 4.1*: Preprocessing steps. Top row. Horizontal projection of a representative gyrus in 3d space. The left graph shows the gyrus as labelled by the TASH toolbox in its original coordinates. The middle graph displays the output of the rotation applied to the original coordinates, which places the most posteromedial vertices at the top of the vertical axis and the most anterolateral at the bottom. The right graph showcases the effects of artefact removal, which excludes clusters of vertices whose position is inconsistent or generates discontinuities with the main body of the gyrus. Bottom row. The left graph shows the flat patch generated with Freesurfer's* mris_flatten *after artefact removal. The middle graph corresponds to the rotated flat patch using the same reference system as the previous rotation in 3d space. The right graph displayed the effects of a nonlinear horizontal transformation aimed at enhancing the vertical symmetry of the outer and inner contour of the gyrus, dividing vertices evenly at each side of the vertical axis, and improving separation between the branches of incomplete duplications if any are present.*

4.2.4 Morphological assessment

After preprocessing, the morphology of the gyrus was first classified based on the presence or absence of a common stem duplication (CSD). CSDs were further divided into two classes depending on the size of the intermediate sulcus, with one variant ("low split") having a sulcus length of less than half the length of the gyrus, and the other variant ("high split") having a sulcus length of over half the length of the gyrus.

Several classification methods were tested and compared with the manual classification of an expert. Two measures that reached a promising classification rate were the ratio between the area of the gyrus and the area of its convex hull (89% agreement with expert rater), which represents a general measure of a polygon's concavity, and the simple ratio between the length and width of a gyrus (81% agreement with expert rater), as a partially duplicated gyrus can be expected to be wider than a single gyrus. However, these measures have two main flaws. First, they are continuous in nature, which requires an arbitrary threshold[15] to be set. Second, gross indices of gyral geometry don't capture enough information about the specific shapes and sizes of gyri and sulci, which is critical to the description of the morphological variability of Heschl's gyrus.

For these reasons, we designed an algorithm that classifies gyri based on the presence of areas of concavity that fall within specific ranges of size and location. This algorithm first defines a grid of equidistant (1 mm) points within the convex hull that embeds the gyrus and marks all "concave regions", that is areas where no vertices fall within a 1mm-sided square range centred at a given grid point (see regions marked by red squares in Figure

[15] The optimal threshold could be calculated on a much larger database via supervised learning, but it would defeat the purpose of bypassing manual classification entirely.

4.2). The presence of a partial duplication is then determined if there are at least 2 consecutive concave areas in 3 consecutive grid rows, which corresponds to a concave area that measures at least 2x3 mm^2. Concave areas extending all the way to a leftmost or rightmost grid point are excluded as they correspond to regions at the sides of a gyrus rather than an intermediate sulcus. By leveraging these specific anatomical heuristics, this method correctly classified all 118 hemispheres.

A separate algorithm estimates the coordinates of the duplication point with higher precision if a common stem duplication is detected. Sliding a 1 mm-wide horizontal band from the top to the bottom of the preprocessed flat patch, the algorithm measures the minimum distance between any two vertices contained within the band, one on the left half ($x<0$) and one on the right half ($x>0$). Since the intermediate sulcus is expected to be symmetrical around the Y axis after preprocessing, the magnitude of this distance is indicative of the presence of a "gap" corresponding to the intermediate sulcus. To reduce sensitivity to individual differences in vertex density and local variability, the distance is also normalised by subtracting the mean and dividing by the standard deviation of all possible distances between any two vertices within the patch. Finally, a gradient is calculated from top to bottom as the ratio of any two consecutive differences. The maximum value of this gradient, corresponding to the sharpest relative increase in this distance, is then interpreted as the onset of a duplication.

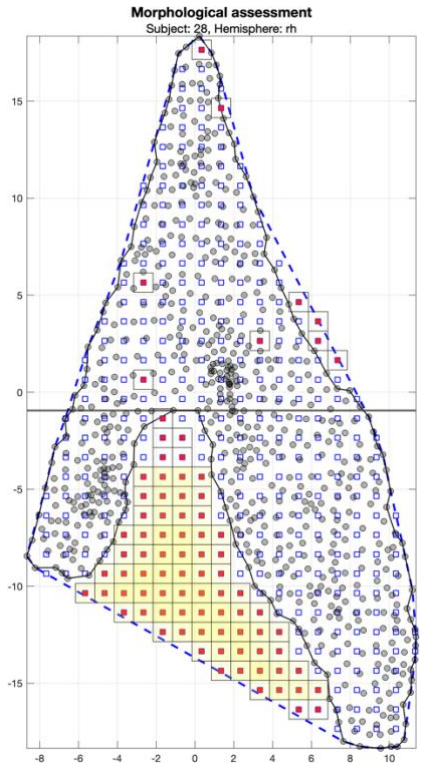

Figure 4.2*: Preprocessed HG and grid matrix points used for classifications. The dashed blue line represents the "convex hull" polygon that contains the entirety of HG and the intermediate sulcus if present. The solid black line marks the outer contour of the gyrus. Black semi-transparent circles represent the surface vertices. The blue squares correspond to the grid of equidistant points defined within the convex hull used to identify concavities. These squares are filled with red if there are no vertices within a 1 mm-sided square region represented by the larger squares, which are coloured in yellow if they are part of a valid concave region (i.e. at least three consecutive squares on three consecutive rows, excluding sequences of consecutive squares adjacent to the sides of the hull). A horizontal line marks the start of a duplication.*

4.2.5 Grid parcellation

In order to compare morphologically equivalent regions across subjects, each preprocessed patch was divided into 24 (6x4) areas that mark its major morphological landmarks (i.e. symmetry, length, width, and presence and position of an incomplete duplication). A unique subdivision was calculated for each individual gyrus based on its morphological class (i.e. single gyrus, low split, and high split; see 4.2.3) and unique anatomy. Vertically, each patch was divided into six regions based on the y coordinate of its duplication point: when a duplication occupied less than half the length of Heschl's gyrus

("low split"), its branches were divided into 2 equal parts; conversely, when duplications occupied more than half the length of the gyrus ("high split"), their branches were divided into 4. The medial region above the duplication was instead divided into either 4 or 2 equal parts respectively, for a total of 6 horizontal bands per gyrus. This type of subdivision generates horizontal regions with similar relative widths (i.e. no region is over or under-represented) independently of individual morphology. Gyri without duplications were simply divided into 6 equal horizontal bands.

Horizontally, patches were first split into halves using the vertical axis (x=0). Because of the transformations applied during preprocessing, the two halves are expected to be symmetrical and, in the case of duplications, correspond to the anterior and posterior branches. These halves were further divided into half using the midpoint between the outer contours and either the vertical axis itself or the inner contours of the branches, if any are present, for a total of 4 vertical sections. This subdivision generates similar-sized regions (average width = 2.2 mm; average height = 5.3 mm) that carry identical morphological meaning across all subjects who share a morphological variant.

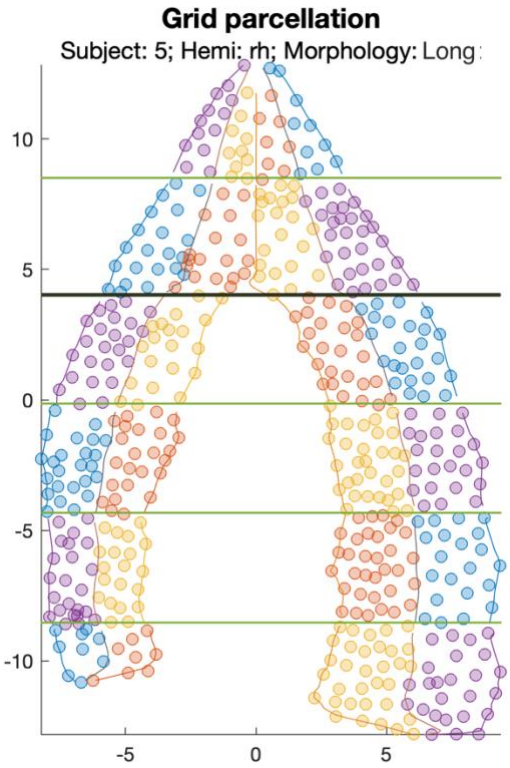

Figure 4.3*: Individual examples of grid parcellation. Coloured circles represent vertices, with colour indicating which area they belong to. Colours are assigned arbitrarily and there is no relation between areas sharing the same colour. The thick black horizontal line marks either the point of duplication or, if no duplication exists, the middle of the gyrus' length. Horizontal green lines mark the rest of the horizontal cut-offs used in the parcellation, which depend on the presence and length of a duplication. The vertical lines represent boundaries that were set based on individual morphology: the outermost lines always correspond to the left and right contours of the gyri; the innermost line represents the Y axis, which splits in two following the inner contours of a duplication if one is present; the remaining 2 lines correspond to the midline between the outermost and innermost boundaries.*

4.2.6 Average patch

Six templates were generated (i.e. one for each hemisphere and morphological type) to visualise multiple individual datasets onto a single common space and calculate group-level statistics. This was done by averaging the coordinates of the contours of individual patches sharing the same hemisphere and morphological type. More specifically, using the same grid parcellation as a reference, 4 equidistant reference points were sampled from the outer contours of each grid area to sample the overall shape of each individual gyrus. These points carry the same morphological information across all subjects, i.e. they represent the

same location relative to the shape of individual gyri. The coordinates of these points for all subjects of the same morphotype and hemisphere were averaged and a smooth spline was drawn between points to create a continuous border. Although any surface (e.g. a hand-drawn surface or a randomly chosen individual patch) could in principle be used to graph individual datasets onto each other, using data from the same sample preserves morphological information such as the average size of duplications and inter-hemispheric differences, which also helps to reduce the overall distortion required to morph individual data.

4.2.7 Morphing

Individual gyri were morphed onto the templates generated in the previous step. This process simply maps the relative position of each vertex within each region of the grid parcellation onto the homologous region of the average patch. Using the regions of the grid parcellation as morphing constraints guarantees that the anatomical landmarks of the original gyrus (i.e. length of the intermediate sulcus, anterior and posterior duplications) are respected and represented in the target patch.

4.2.8 Resampling and smoothing

Morphed patches were resampled onto a common mesh (i.e. one mesh for each morphological type and hemisphere) of equidistant points spaced 0.5 mm apart. Resampling all datasets onto a common set of coordinates is necessary to calculate group statistics and ensure that all participants are equally and uniformly represented at every point on the gyral surface. The resampling algorithm was written to be identical to the "nearest-neighbour, forward and reverse" (nnfr) algorithm implemented in Freesurfer's

mri_surf2surf. Specifically, each node on the target mesh is first assigned the value of the nearest vertex. Then, if there are any vertices left unassigned, their value is assigned to the closes mesh node and averaged with any other vertex that was previously assigned to that node. A single step of smoothing was applied after resampling by averaging the value of each mesh node with those of its immediate neighbours, which is equivalent to using the "–nsmooth-out 1" option of mri_surf2surf. An additional Gaussian kernel smoother was applied to resampled data to improve map visualisation. This procedure calculates for each mesh node the weighted average of all surrounding nodes, with the weights to the values of a 2d Gaussian kernel centred at that node. While nnfr smoothing was used across all analyses, kernel smoothing was solely employed for data visualisation purposes with a fixed full width at half-maximum (FWHM) of 2.5 mm. Both smoothing techniques were extended to handle the averaging of complex values data and correlations. In the case of complex data such as tonotopy, the real (r) and imaginary (i) components of the complex Fourier vectors were averaged separately and the phase (atan2(i,r))and magnitude (sqrt(r^2 + i^2)) of the resulting vector were taken as the average values of phase and magnitude. In the case of correlations (r), a Fisher z-transformation (atanh(r)) was applied before averaging and the inverse transformation (tanh(r)) was applied to the average.

4.2.9 Average and variability maps

Group maps were generated by calculating descriptive statistics at each point of the common surface participants were previously resampled onto. In the case of complex-valued datasets such as tonotopy, average phase and magnitude were calculated as the phase and magnitude of the average vector obtained by averaging the real and imaginary components of all individual vectors. The ratio between the magnitude of the average

vector and the average magnitude of individual vectors was used as an index of dispersion, which represents the loss of magnitude generated by averaging vectors with different phases, as opposed to perfectly aligned vectors. In the case of tonotopy, this index can be interpreted as the consistency of frequency preference across all participants at a given location, with 0 marking complete disagreement and 1 complete agreement.

4.3 Results

4.3.1 HG morphotypes: definition

The TASH-generated HG labels of all 58 subjects were manually inspected to evaluate the output of the labelling procedure across individuals with different morphologies. A total of 5 HG morphotypes were identified (Figure 4.5): Single transverse gyri ("no duplication" or ND); common stem duplications (CSD), characterised by two gyri ("branches") separated laterally by an intermediate sulcus and connected medially by a common "stem"; complete posterior duplications (CPD), defined by at least two parallel gyri fully separated by an intermediate sulcus; co-occurrence of an anterior CSD and a CPD (CSD+CPD); and a rare variant (n = 2, left hemisphere only) defined by a single transverse gyrus (STG) forming a contiguous arc with the anterior half of the superior temporal gyrus ("conjoined STG-HG") and a full posterior transverse sulcus, effectively dividing the superior temporal gyrus into an anterior and a posterior half.

Given the great variability in the length of their intermediate sulci, CSDs were further subcategorised into a short duplication (SD) variant, with an intermediate sulcus less than half the length of HG, and a long (LD) variant, with an intermediate sulcus over half the length of HG. On average, intermediate sulci of the SD type measured one-third of the

length of the gyrus, while sulci of the LD type measured two-thirds the length of the gyrus (Figure 4.4), consistently across cohorts and hemispheres.

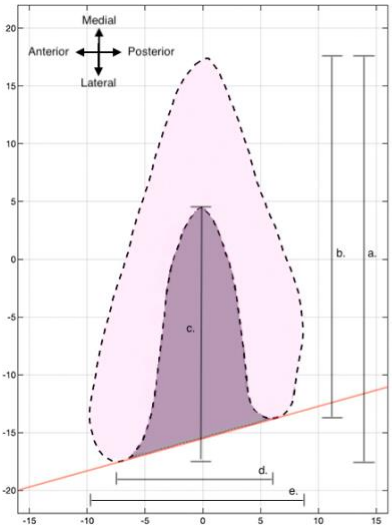

Sample: Original	Left Hemisphere			Right Hemisphere		
	No Duplication	Short Duplication	Long Duplication	No Duplication	Short Duplication	Long Duplication
	Mean (SD)	*Mean (SD)*	*Mean (SD)*	*Mean (SD)*	*Mean (SD)*	*Mean (SD)*
Gyrus						
Length (mm)	34.4 (4.7)	36.6 (6.7)	36.4 (4.9)	32.7 (4.2)	32.7 (4.6)	32.6 (3.4)
Anterior duplication		36.6 (6.7)	36.4 (4.9)		32.7 (4.6)	32.6 (3.4)
Posterior duplication		32.8 (6.4)	30.0 (3.4)		29.3 (4.7)	26.7 (3.0)
Width (mm)	10.9 (3.2)	15.5 (2.4)	21.1 (3.2)	8.1 (2.1)	17.1 (4.4)	19.6 (3.7)
Area (mm^2)	235.9 (76.7)	232.6 (77.1)	265.4 (52.9)	171.2 (52.6)	222.8 (36.8)	227.7 (34.3)
Thickness (mm)	2.9 (0.2)	3.1 (0.2)	3.0 (0.2)	3.0 (0.2)	3.0 (0.2)	3.0 (0.2)
Sulcus						
Length (mm)		10.5 (2.0)	22.8 (4.0)		11.4 (3.2)	21.4 (3.5)
Width (mm)		5.2 (0.8)	7.5 (1.5)		6.5 (2.4)	6.9 (2.0)
Area (mm^2)		21.4 (3.6)	87.7 (30.2)		36.4 (21.3)	80.1 (32.9)
Thickness (mm)		2.9 (0.3)	2.7 (0.3)		2.7 (0.3)	2.8 (0.2)
Sulcus Length / Gyrus Length		31.0% (9.9%)	62.8% (8.6%)		35.0% (10.7%)	65.8% (8.5%)

Sample: HCP	Left Hemisphere			Right Hemisphere		
	No Duplication	Short Duplication	Long Duplication	No Duplication	Short Duplication	Long Duplication
	Mean (SD)	*Mean (SD)*	*Mean (SD)*	*Mean (SD)*	*Mean (SD)*	*Mean (SD)*
Gyrus						
Length (mm)	34.5 (3.6)	35.5 (4.1)	37.4 (3.7)	32.7 (3.2)	32.6 (2.9)	32.0 (4.3)
Anterior duplication		35.5 (4.1)	37.4 (3.7)		32.6 (2.9)	32.0 (4.3)
Posterior duplication		31.2 (3.0)	29.3 (3.8)		28.6 (2.7)	27.9 (3.7)
Width (mm)	10.1 (2.9)	15.9 (1.7)	21.7 (4.0)	8.3 (1.6)	19.0 (3.9)	24.3 (6.0)
Area (mm^2)	221.0 (64.9)	243.2 (30.1)	293.3 (48.9)	174.2 (38.1)	218.0 (46.8)	264.9 (63.5)
Thickness (mm)	2.7 (0.2)	2.8 (0.2)	2.7 (0.2)	2.8 (0.2)	2.9 (0.2)	2.9 (0.2)
Sulcus						
Length (mm)		11.3 (2.6)	25.9 (6.5)		11.9 (3.0)	21.7 (4.3)
Width (mm)		5.1 (1.2)	8.2 (1.7)		7.7 (2.0)	9.2 (3.1)
Area (mm^2)		27.1 (11.3)	101.2 (41.8)		42.3 (14.9)	107.9 (48.3)
Thickness (mm)		2.6 (0.3)	2.7 (0.2)		2.8 (0.3)	2.7 (0.2)
Sulcus Length / Gyrus Length		31.6% (6.8%)	68.8% (13.5%)		36.6% (8.3%)	67.7% (10.8%)

Figure 4.4*: Morphology of common stem duplications (CSD). The graph on the left represents an example of a preprocessed flat patch of a partially duplicated gyrus in the left hemisphere. Labelled horizontal and vertical lines mark its components: a. Anterior duplication length; b. Posterior duplication length, c; Intermediate sulcus length; d. Intermediate sulcus width; e. Gyrus width. The average size (and standard deviation) of these components are reported in the table to the right of the flat patch, separately for each hemisphere, morphological type (no duplication, short duplication, long duplication), and sample. Also reported are average cortical thickness and the ratio of sulcal and gyral length. The oblique red line represents the boundary between HG and the lateral superior temporal gyrus.*

For all analyses, the two cases of a conjoined anterior STG and HG were treated as single gyri. The boundary between STG and HG was drawn automatically as part of the TASH labelling pipeline, which excludes vertices within the lateral STG, as defined by freesurfer's automatic cortical parcellation based on the Destrieux atlas (Destrieux et al., 2010).

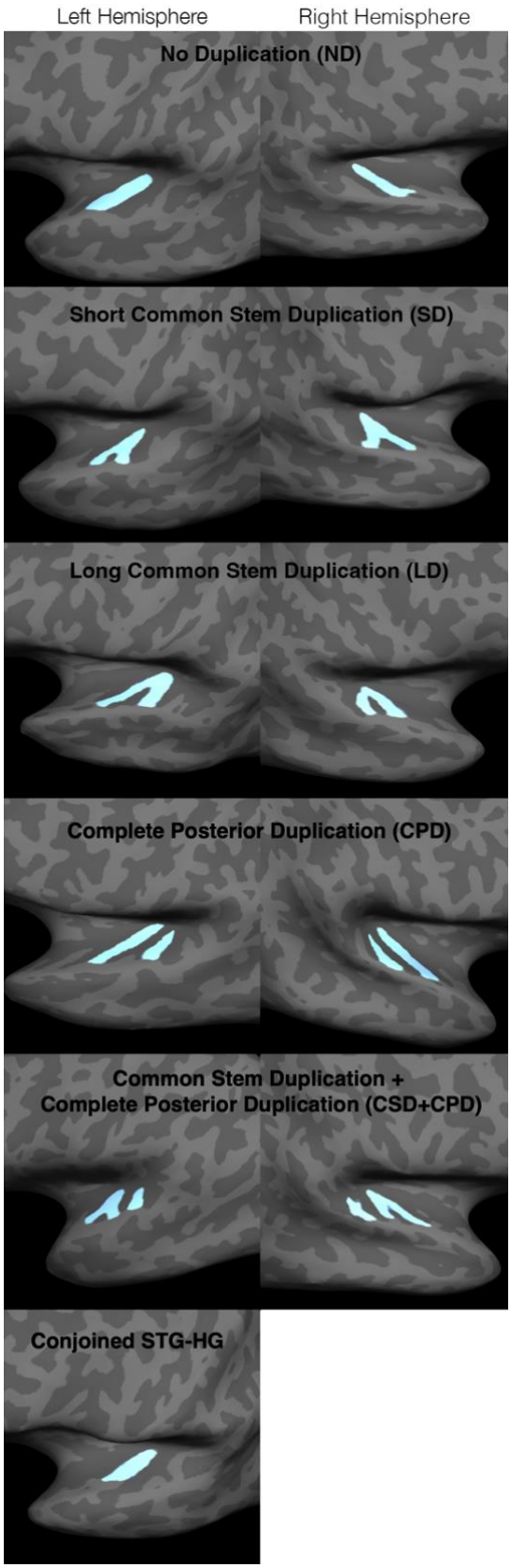

Figure 4.5*: Individual representative examples of each HG morphotype variant. HG labels (in light blue) are drawn on the inflated reconstructed pial surface of individual subjects.*

4.3.2 Surface area and occurrence of HG duplications

Considering both samples in combination (i.e. original and HCP), the occurrence of HG duplications was 57% in the left hemisphere and 66.5% in the right hemisphere, with CSD being the more common variant (left hemisphere, CSD = 30.4%, CPD = 26.6%; right hemisphere, CSD = 39.2%, CPD = 27.2%, see Figure 4.6). Among CSDs, the long duplication variant (LD), defined by an intermediate sulcus longer than half the length of HG, was 53% more frequent than the short variant (SD), while in the right hemisphere, it was 70% more frequent. While in the left hemisphere the relative occurrence of each morphotype was comparable across samples, in the right hemisphere the original sample had a higher incidence of duplications than the HCP sample (72.4% vs 63%). Additionally, while the relative occurrence of CSDs and CPDs was similar in the HCP sample (32% and 31%, respectively), CSDs were much more frequent than CPDs in the original sample (51.7% and 20.7%, respectively).

		Occurrence of duplications			CSD subtypes	
Hemisphere	Sample	ND	CSD	CPD	SD (CSD)	LD (CSD)
Left	Orig	24 (41.4%)	19 (32.8%)	15 (25.9%)	6 (31.6%)	13 (68.4%)
	HCP	44 (44.0%)	29 (29.0%)	27 (27.0%)	13 (44.8%)	16 (55.2%)
	Total	**68 (43.0%)**	**48 (30.4%)**	**42 (26.6%)**	**19 (39.6%)**	**29 (60.4%)**
Right	Orig	16 (27.6%)	30 (51.7%)	12 (20.7%)	12 (40.0%)	18 (60.0%)
	HCP	37 (37.0%)	32 (32.0%)	31 (31.0%)	11 (34.4%)	21 (65.6%)
	Total	**53 (33.5%)**	**62 (39.2%)**	**43 (27.2%)**	**23 (37.1%)**	**39 (62.9%)**

Figure 4.6*: Table displaying the total count and relative occurrence (%) of each HG morphotype across samples and hemispheres. Abbreviations: Orig = original; HCP = Human Connectome Project; ND = no duplication; CSD = common stem duplication; CPD = common posterior duplication; SD = short partial duplication; LD = long partial duplication.*

A 3x2 type III ANOVA was performed to analyse the effect of morphology (ND, CSD, CPD) and hemisphere on total HG surface area. There was a significant main effect of morphotype ($F(2,280) = 76.31$, $p < .001$) and hemisphere ($F(1,280) = 35.07$, $p < .001$),

while the interaction term was not significant ($F(2,280) = 1.9$, $p = .15$). A post-hoc Tukey's HSD revealed that all pairs of morphotypes had significantly different surface areas (Figure 4.7). More specifically, in the left hemisphere, the mean surface area of single gyri ($M = 233.0$ mm^2, $SD = 70.4$ mm^2) was significantly smaller than both partial duplications ($M = 284.9$ mm^2, $SD = 70.9$ mm^2; $p = .004$) and full duplications ($M = 340.6$ mm^2, $SD = 94.3$ mm^2; $p < .001$), and partial duplications were also smaller than full duplications ($p = .005$). Similarly, in the right hemisphere, single gyri ($M = 168.8$ mm^2, $SD = 39.5$ mm^2) had a significantly smaller surface area than both partial duplications ($M = 258.4$ mm^2, $SD = 52.6$ mm^2; $p < .001$) and full duplications ($M = 288.8$ mm^2, $SD = 61.9$ mm^2; $p < .001$), and full duplications had a greater surface area than partial duplications ($p = .01$).

There were also a total of 30 cases (left = 13/158, right = 17/158) of a CSD co-occurring with a CPD (Figure 4.7, white violin plots). These were excluded from previous analyses due to a lack of an empirical prior in the literature and to reduce the number of redundant comparisons. Nonetheless, on an exploratory basis, the occurrence of both partial and full duplications -expectedly- appeared to compound and increase the total HG surface area in both the left ($M = 423.7$ mm^2, $SD = 106.2$ mm^2) and the right ($M = 336.8$ mm^2, $SD = 70.4$ mm^2) hemisphere.

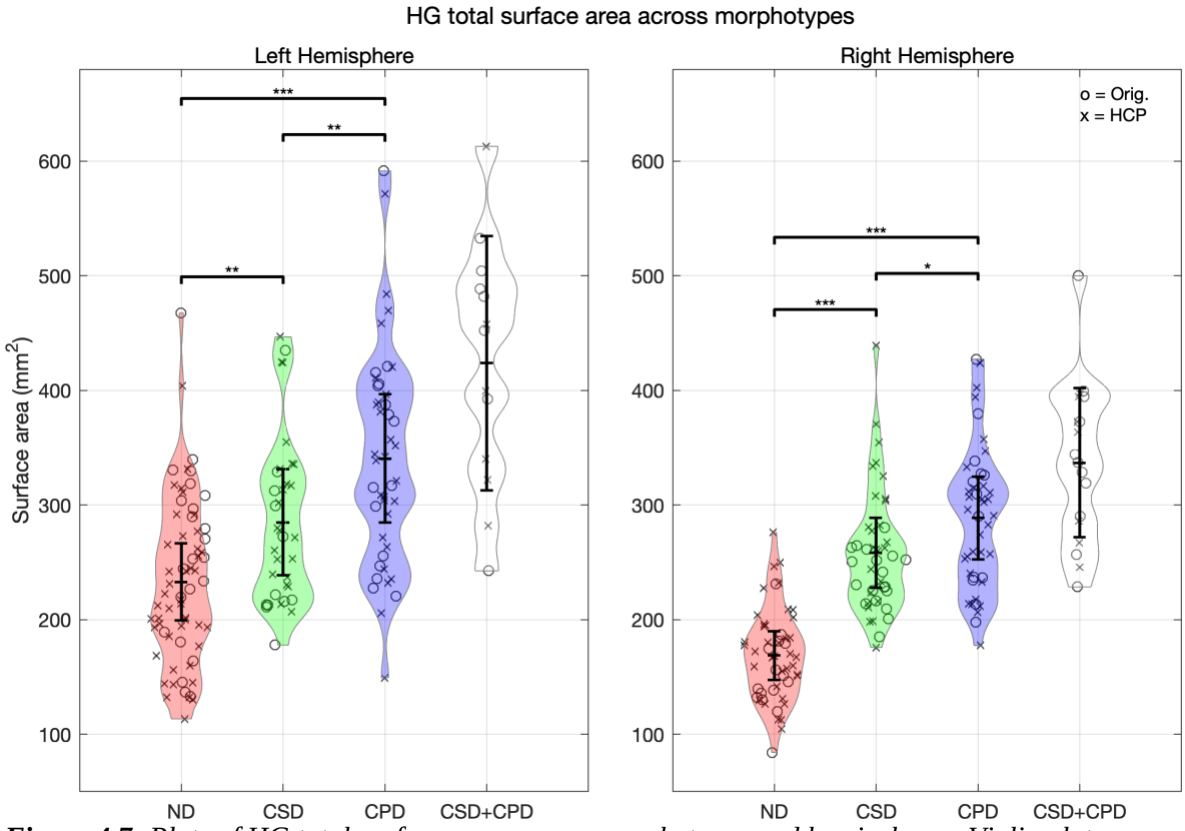

Figure 4.7*: Plots of HG total surface area across morphotypes and hemispheres. Violin plots indicate approximate density distributions for each morphotype, while scattered data points correspond to individual measurements, with different markers for each sample (circles for the original sample, crosses for the HCP sample). Thick vertical line plots indicate the mean and its 95% confidence interval. Horizontal bars connecting pairs of plots indicate a significant difference in mean surface area (post-hoc Tukey HSD test). * = p < .05, ** = p < .01, * p < .001. Abbreviations: Orig = original; HCP = Human Connectome Project; ND = no duplication; CSD = common stem duplication; CPD = common posterior duplication; CSD+CPD = co-occurrence of CSD and CPD*

4.3.3 Transverse gyrus duplications and gyrification index

A 2x2 ANOVA was performed to test whether the presence of large full duplications or partial duplications of the transverse gyrus in a given hemisphere was predictive of the mean gyrification for that hemisphere. The local gyrification index was calculated using Freesurfer's *recon-all* command with the *-localGI* flag. There was no main effect for either number of full duplications ($F(1,115) = 0.08$, $p = 0.77$), partial duplications ($F(1,115) = 2.1$, $p = 0.15$), or their interaction ($F(1,115) = 0.16$, $p = 0.69$).

4.3.4 Curvature

4.3.4.1 Group averages

Curvature gradients appeared to follow expected gyral and sulcal morphology (Figure 4.8). A posterior shift in curvature was visible in non-duplicated gyri as well as the stem of gyri with short partial duplications. This shift corresponds to a real morphological quality of transverse gyri which tend to fold over posteriorly rather than in a symmetric fashion. Maps calculated from the HCP sample appear remarkably similar, including the posterior shift in gyral curvature.

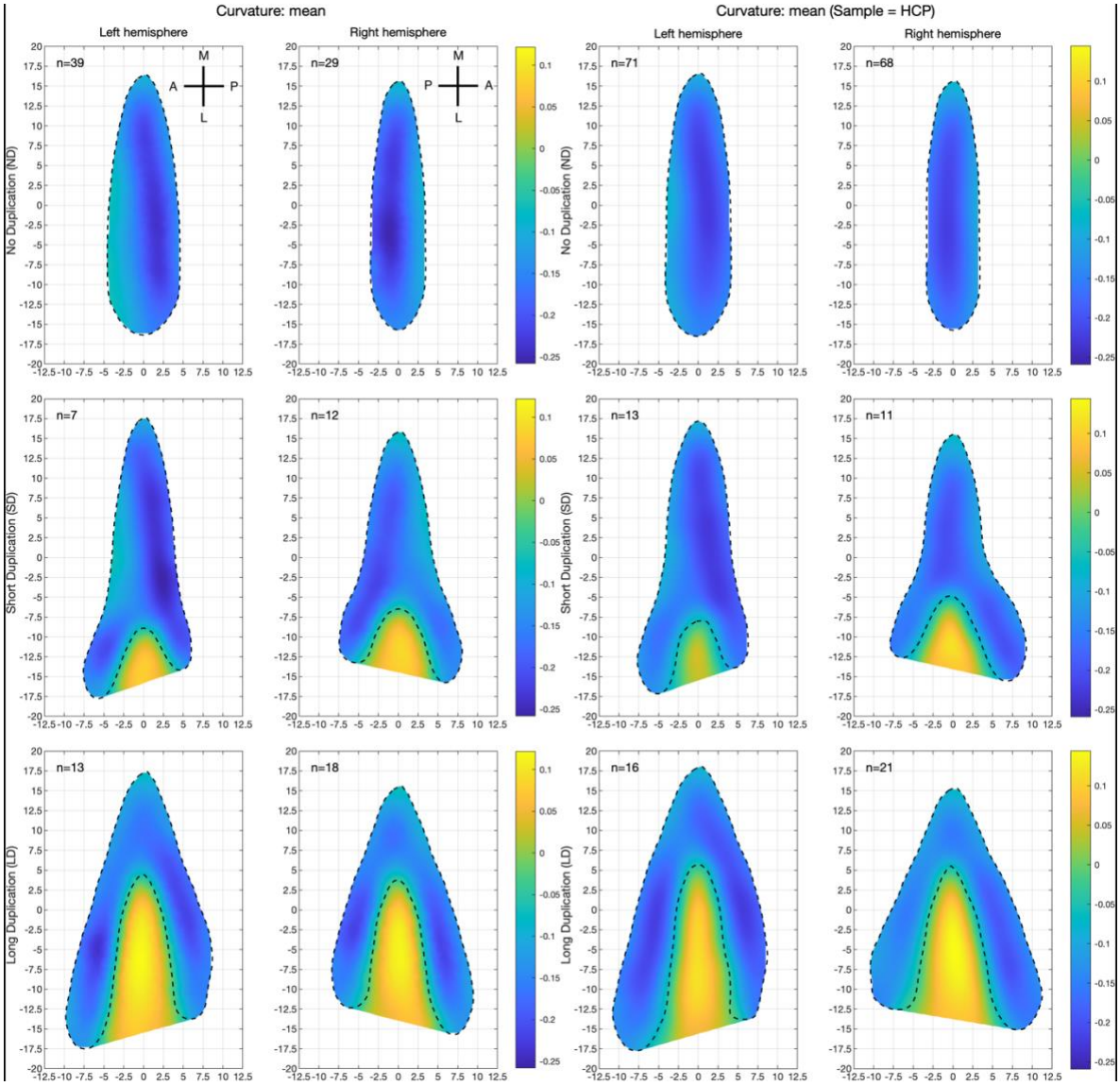

Figure 4.8*: Curvature average maps for all morphological archetypes and hemispheres, calculated separately for the original and HCP samples. The value of 'n' corresponds to the number of individual hemispheres used to compute each map. Reference axes in the two top-left maps indicate the Anterior, Posterior, Medial, and Lateral directions. Note that the anterior-posterior axes of the left and right hemispheres are mirrored*[16]*.*

4.3.4.2 Inter-subject variability

Although curvature within HG is not a determining factor of inter-subject alignment, curvature gradients still appeared largely consistent across participants. Standard deviation

[16] This reference system is used across all maps in this thesis.

maps (Figure 4.9) showed regions of increased variability towards more lateral portions of the gyri across all morphologies and hemispheres, with peaks located within the branches of gyri with common stem duplications. The overall median standard deviation across all maps was 0.043, with first and third quartiles of 0.036 and 0.052 respectively.

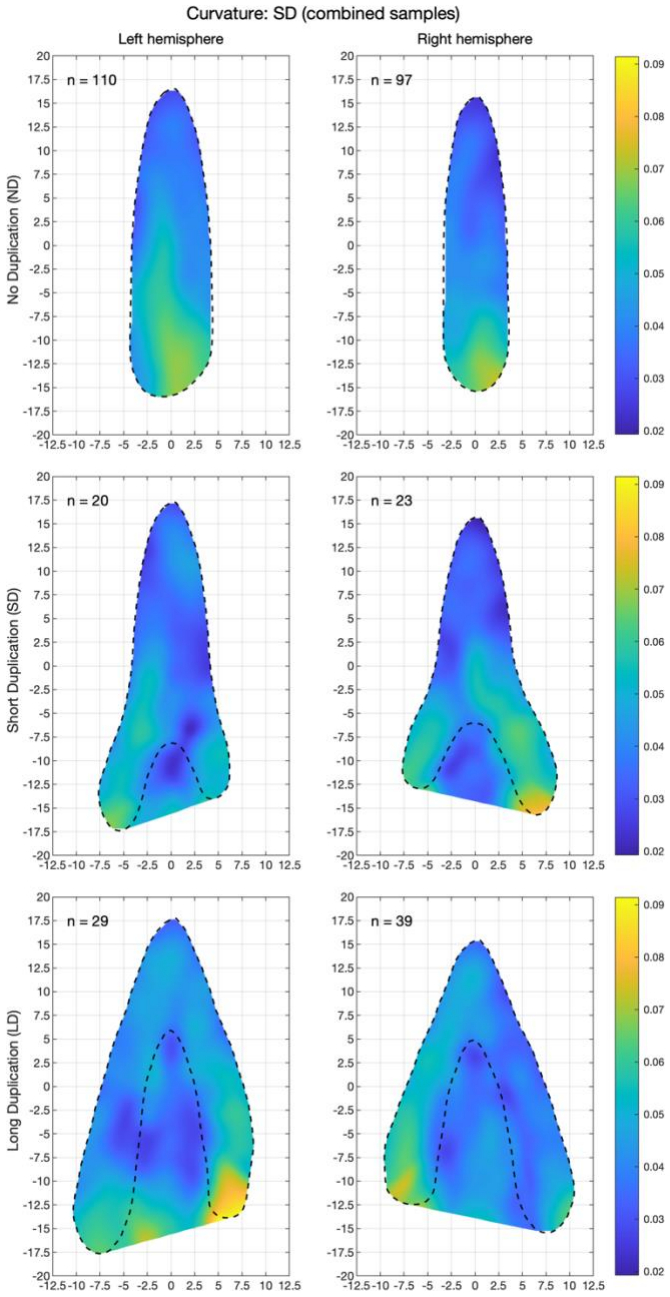

Figure 4.9*: Standard deviation maps of curvature obtained combining subjects from both cohorts. The value of "n" corresponds to the number of individual hemispheres used to compute each map.*

To further quantify the effect of morphing on the inter-subject alignment of curvature gradients, a Spearman correlation coefficient was computed between each individual map and the average map of the corresponding hemisphere and morphological type[17]. The distribution of these correlations is reported in Figure 4.10. The average correlation across all individual maps was[18] 0.78, with approximately 92% of all gyri having a correlation higher than 0.5. The distribution of correlation coefficients appeared to be similar across hemispheres and morphologies, albeit with a longer tail towards lower correlations for gyri with no duplications. Two examples of gyri with a low agreement with their corresponding group average can be seen in Figure 4.11. In the case of the left hemisphere, the morphology of the gyrus appeared to resemble a short partial duplication, with a second anterolateral region of high curvature magnitude. However, the intermediate region between these two curved areas also showed negative curvature and therefore could not be classified as a sulcus by the automated labelling procedure. As a result, the most medial half of the gyrus appeared fairly well aligned with the average curvature, while peak curvature in the lateral half is shifted anteriorly. As for the right hemisphere, although longitudinally the morphology appeared typical, peak curvature was shifted anteriorly rather than posteriorly, generating curvature gradients in the opposite direction as the average map.

[17] The average maps were calculated excluding the individual gyrus being used in the correlation.

[18] Average correlations were calculated by applying a Fisher Z-Transformation to all correlation coefficients and then applying the inverse transformation to their mean.

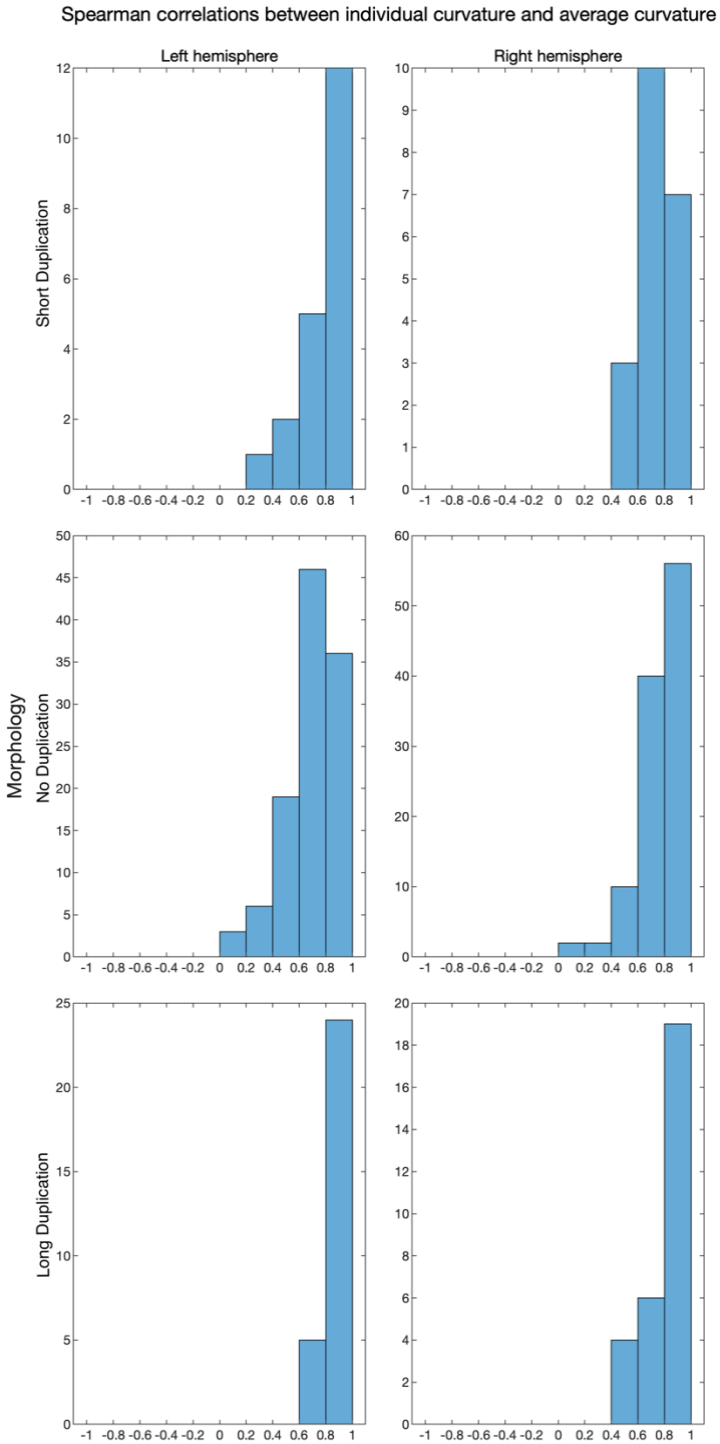

Figure 4.10*: Spearman correlations between individual and average maps across morphotypes and hemispheres. Data from both samples were included.*

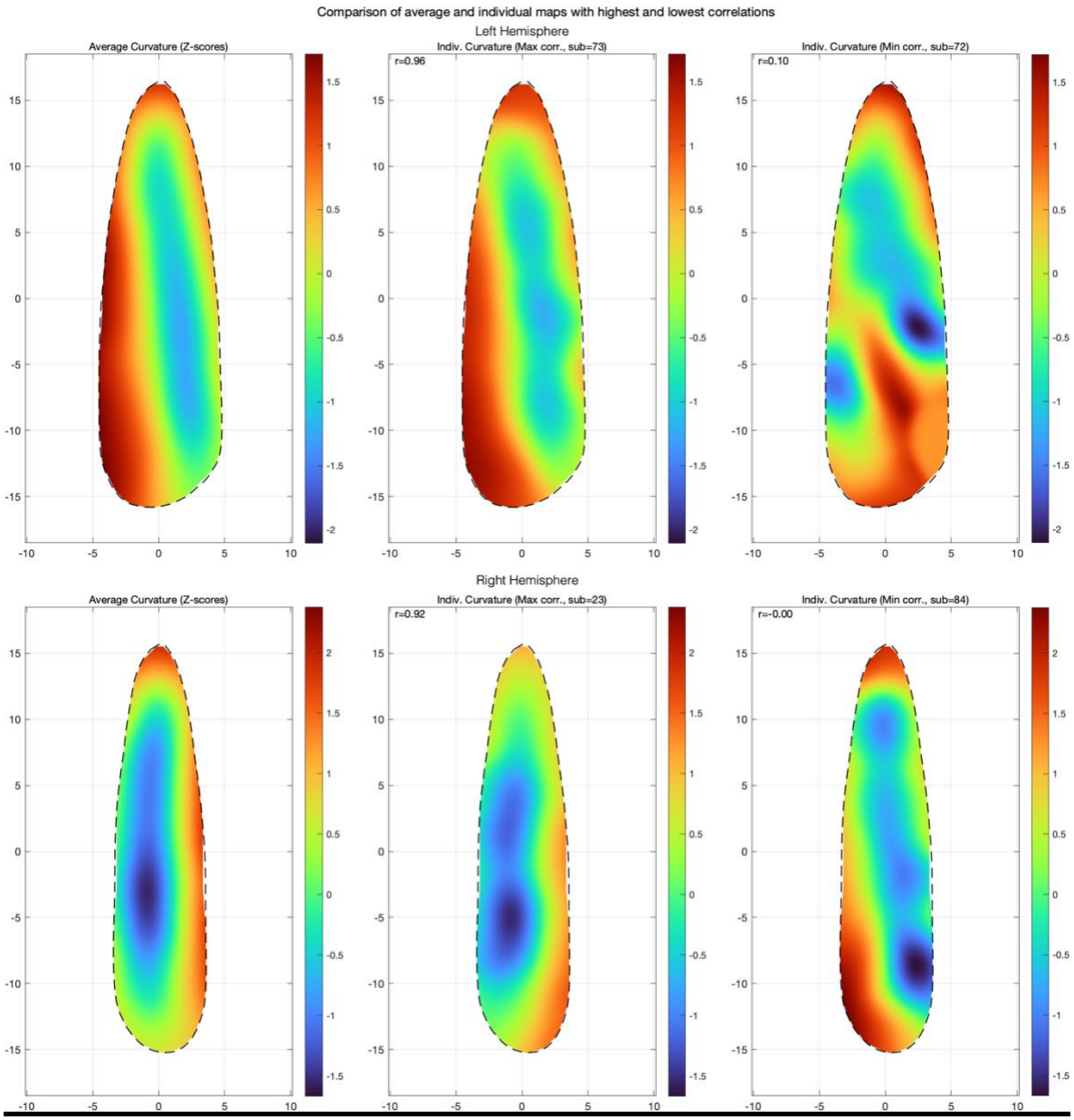

Figure 4.11*: Examples of individual gyri with the highest and lowest correlations with the average map, which is indicative of their alignment with other gyri of the same morphology. Each graph corresponds to a normalised (z) curvature map. Top row: left hemisphere. Bottom row: right hemisphere. Left column: group average maps of non-duplicated gyri. Middle column: individual gyri with the highest correlation with the group-average map. Right column: individual gyri with the lowest correlation with the group-average map.*

4.3.5 Thickness

4.3.5.1 Average cortical thickness maps

Cortical thickness gradients appeared to increase laterally and decrease within sulci across all morphologies (Figure 4.12), following a similar pattern as average curvature gradients. A lateral increase in thickness could also be observed, albeit to varying degrees depending on the hemisphere and morphological variant. In particular, this effect was most apparent within gyri in the right hemisphere, but also gyri with a short duplication in the left hemisphere. Average cortical thickness maps obtained from the HCP dataset followed similar gradients, with thickness increasing posteriorly within gyri and decreasing within sulci.

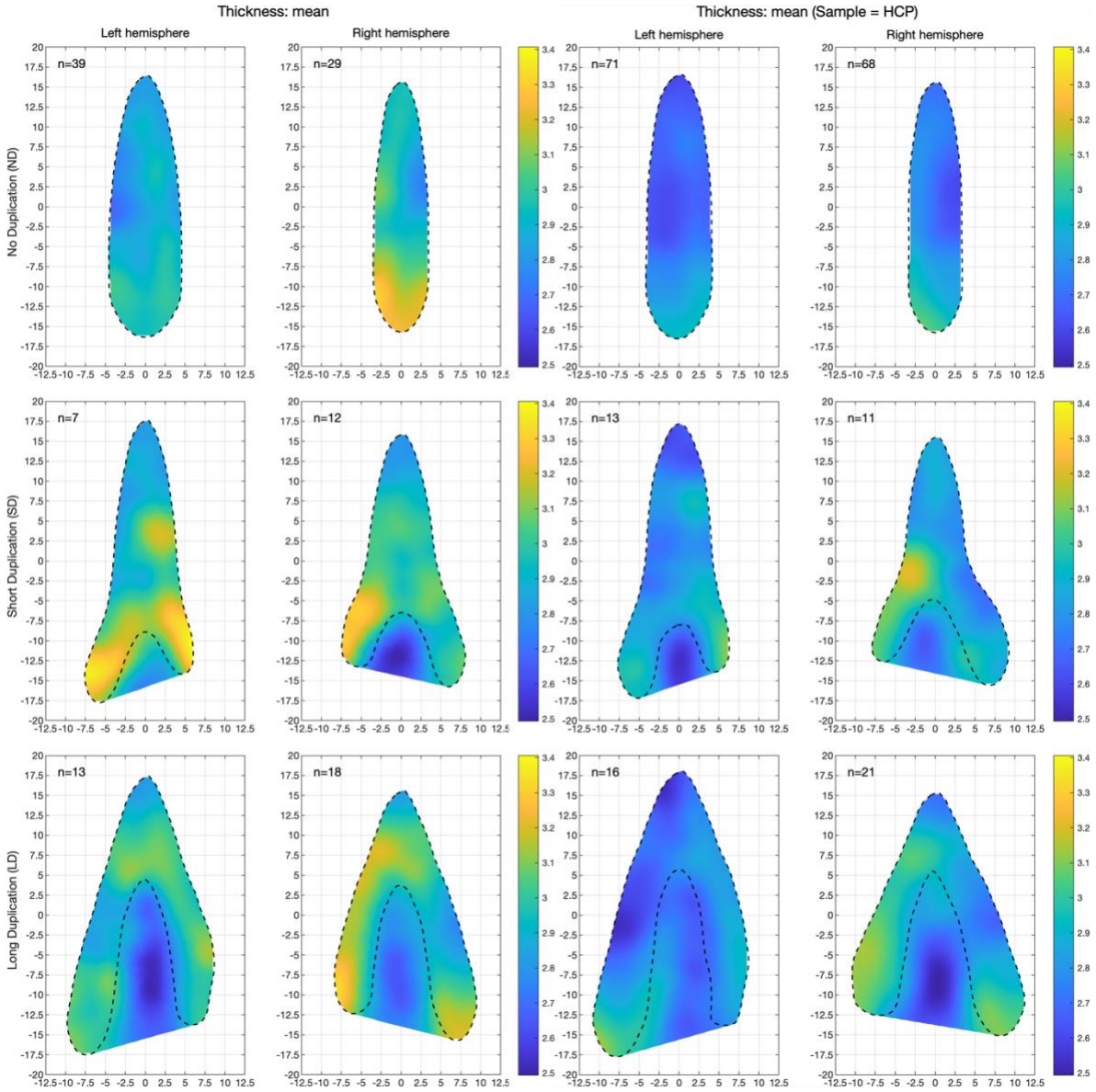

***Figure 4.12**: Thickness average maps for all morphological archetypes and hemispheres, calculated separately for the original and HCP samples. The value of 'n' corresponds to the number of individual hemispheres used to compute each map*

4.3.5.2 Thickness variability across morphologies, hemispheres, and samples

A 3x2x2 type III ANOVA was performed to evaluate the effects of morphological variants, hemispheres, and cohorts on gyral cortical thickness. Results (Figure 4.13) indicated a significant main effect of all three factors, with a significant interaction of morphology and hemisphere. Cohort explained the most variance out of the predictors (partial eta squared,

$\eta_p^2 = 0.092$), while morphology ($\eta_p^2 = 0.036$), hemisphere ($\eta_p^2 = 0.026$) and their interaction ($\eta_p^2 = 0.012$) had a lower effect size. Similarly, data distributions (Figure 4.13) revealed a consistent difference in thickness between cohorts across all morphologies and hemispheres, with cortices sampled from the HCP cohort being on average 0.18mm thinner than the original cohort. Average gyral thickness in the right hemisphere was approximately 0.08mm larger than the left hemisphere in both cohorts, while variability across morphological types appeared to change across hemispheres and cohorts.

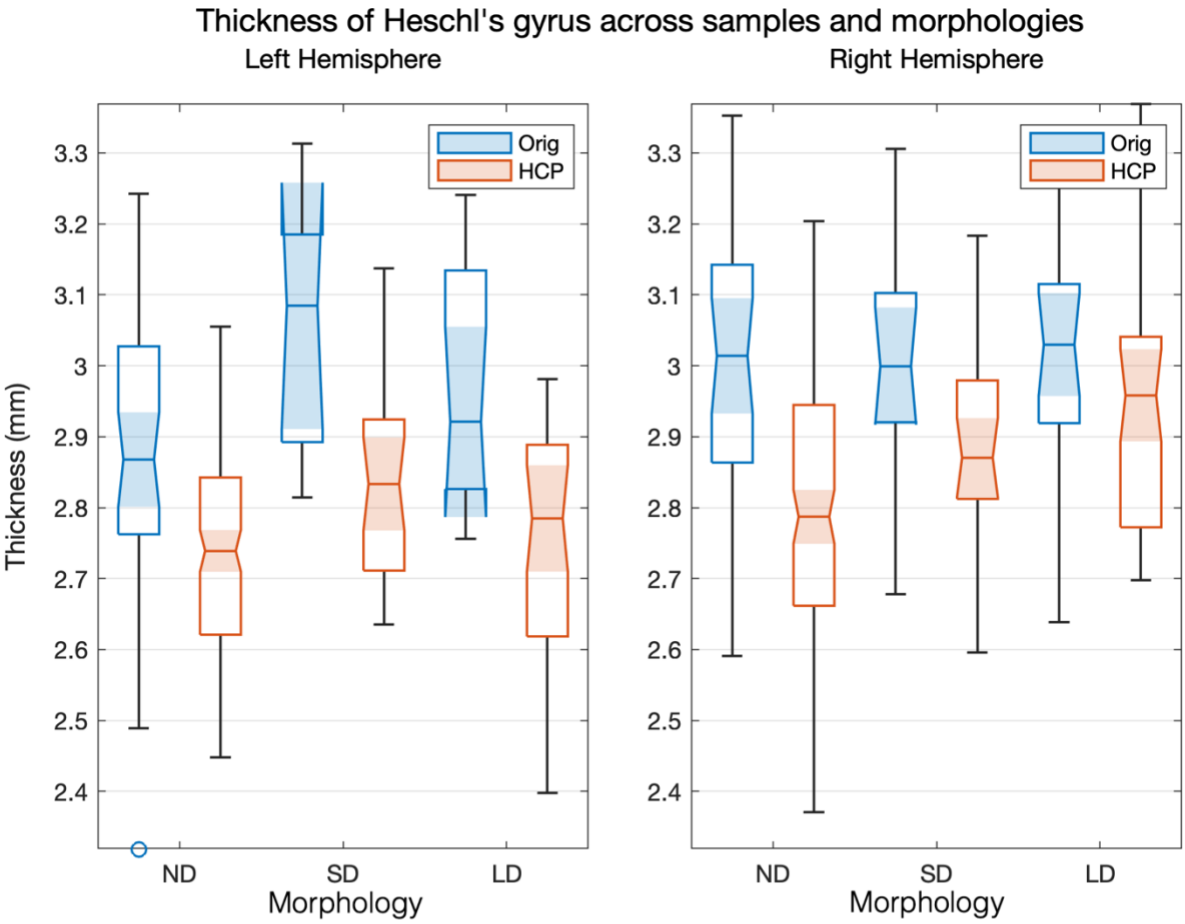

Analysis of Variance

Source	Sum Sq.	d.f.	Mean Sq.	F	Prob>F
Cohort	1.7047	1	1.70475	54.47	0
Morphology	0.5882	2	0.29409	9.4	0.0001
Hemisphere	0.4227	1	0.42266	13.51	0.0003
Cohort*Morphology	0.0132	2	0.00659	0.21	0.8103
Cohort*Hemisphere	0.004	1	0.00396	0.13	0.7223
Morphology*Hemisphere	0.2014	2	0.1007	3.22	0.0409
Error	15.8669	507	0.0313		
Total	20.8743	516			

Figure 4.13*: Comparison of average HG cortical thickness across samples, hemispheres, and morphotypes. The notches on boxplots (blue: original sample; red: HCP sample) represent the mean and its 95% confidence interval. Test results from a 3x2x2 type III ANOVA are reported in the table below the plot*

4.3.5.3 Inter-subject variability in cortical thickness

The standard deviation for average cortical thickness across all gyri measured approximately 0.2mm. However, when calculating the standard deviation across the entire surface of gyri and sulci (Figure 4.14), values appeared to be generally higher, with an

average standard deviation of 0.29mm. Regions of particularly high variability could be observed around the bifurcation of gyri with short duplications in the left hemisphere, the posterior branch of the left gyrus with a long duplication, and the medial portion of intermediate sulci. To verify whether these regions appeared due to the presence of outliers, a set of equivalent maps was generated using median absolute deviation (MAD) as an alternative robust measure of dispersion (Figure 4.15). The particularly high region of variability around the bifurcation of gyri with short duplications in the left hemisphere was not present, while other regions of high variability resembled standard deviation maps. The average Spearman correlation between individual and average maps was approximately 0.42, indicating a moderate degree of alignment across participants, although markedly inferior to curvature. Additionally, 12.9% of all gyri had a negative correlation, in contrast with the exclusively positive correlations identified for curvature.

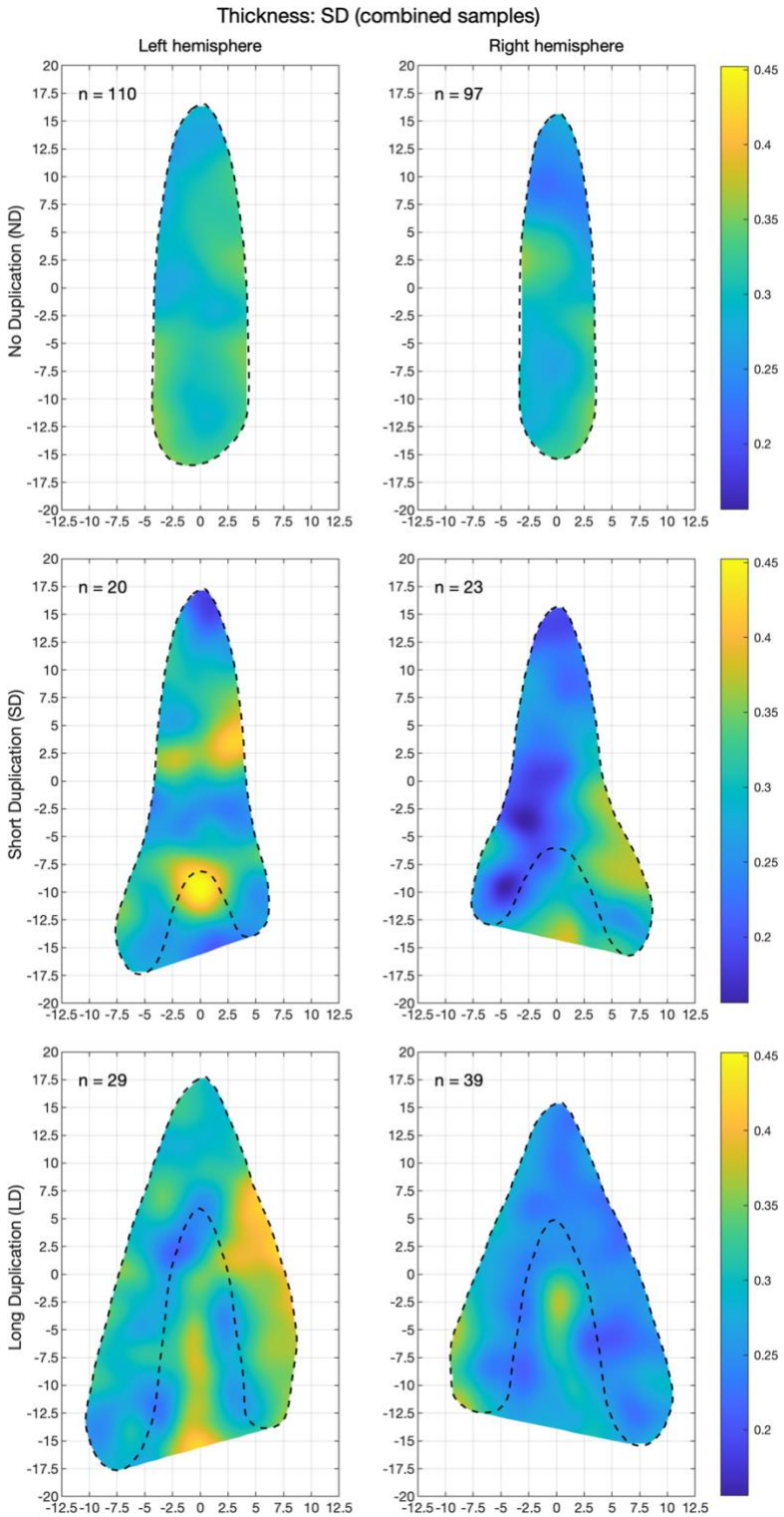

Figure 4.14*: Standard deviation maps of cortical thickness obtained combining subjects from both cohorts. The value of "n" corresponds to the number of individual hemispheres used to compute each map.*

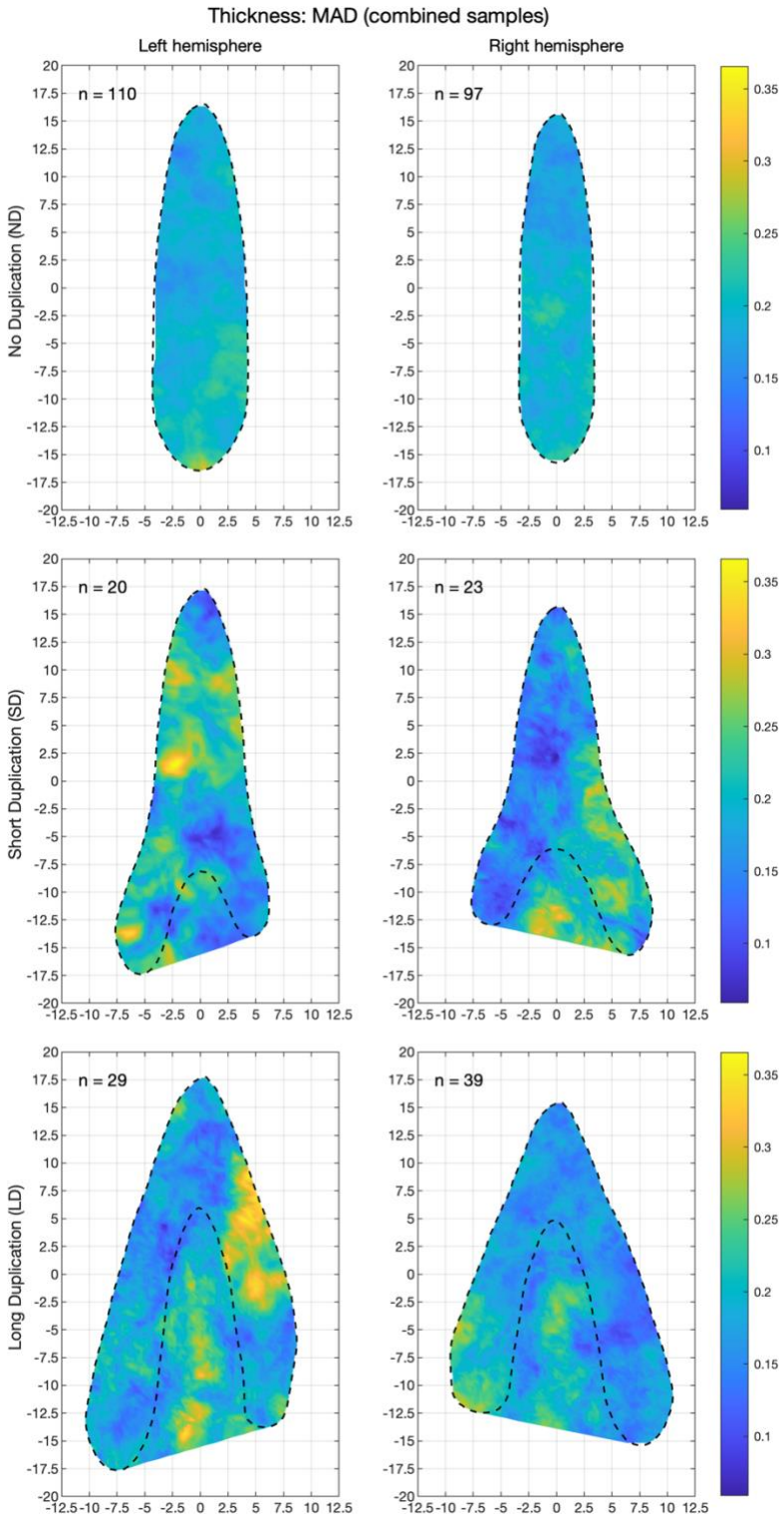

Figure 4.15*: Median absolute deviation (MAD) of cortical thickness obtained by combining subjects from both cohorts. The value of "n" corresponds to the number of individual hemispheres used to compute each map.*

4.4 Discussion

4.4.1 Comparison with benchmark data

The occurrence and size of common stem duplications found in the current sample were only in partial agreement with those reported in the large-scale study by Marie et al. (2015). More specifically, there was a greater occurrence of duplications (of any type) in the right hemisphere compared to the left (right: 66.5%; left: 57%), but the general occurrence was higher than previously reported (right: 49%; left: 37%). Similarly, the total surface area was greater in duplicated gyri, with complete duplications occupying the largest surface area followed by partial duplications and non-duplicated gyri. The surface area was, on average, greater in the left hemisphere. However, this was true across all morphotypes, and not a consequence of the higher occurrence of duplications in the left hemisphere. Marie et al. (2015) also provide a meta-analysis of the occurrence of duplications previously reported in the literature. Although they found a general agreement by pooling results from all previous studies, there was substantial variability across individual studies. For instance, the occurrence of a bilateral absence of duplications ranged from 65% (Penhune et al., 1996) to 10.3% (Campain & Minckler, 1976). This could be due to several variables, such as small sample sizes, different handedness, and varying manual classification criteria. Indeed, although the original sample and HCP sample presented in this chapter had overall comparable occurrences of partial and complete duplications in the left hemisphere (see Figure 4.7), there were notable differences in the overall occurrence of duplications in the right hemisphere (Orig.: 72.4, HCP: 63%), as well as the relative occurrence of partial (Orig.: 51.7%, HCP: 32%) and complete (Orig.: 20.7%, HCP: 31%) duplications. These differences could be explained by both sampling errors and differences in handedness.

Specifically, the original sample was exclusively composed of right-handed individuals, while the HCP sample was sampled from the general population (i.e. an expected proportion of left-handed participants of 10%; Gilbert & Wysocki, 1992), and right-handedness was associated with an overall greater occurrence of duplications, including in the right hemisphere (Marie et al., 2015). Another major difference between the current study and the previous benchmark study was the observed ratio of partial and full duplications. In this study, partial duplications were more common than full duplications in both hemispheres (left: 30.4% vs 26.6%; right: 39.2% vs 27.2%), while in previous data partial duplications were twice more common than full duplications in the left hemisphere, and 10% less common in the right hemisphere. Other than differences in the total occurrence of duplications, the differences in the occurrence of partial duplications could be due to differences in labelling technique. The automated pipeline used in this chapter flags a CSD if it can identify a concavity at least 3mm long on the HG mediolateral axis, which is in most cases less conservative than a classification based on the presence of an intermediate sulcus at least one-third of the length of the gyrus.

4.4.2 Morphological variability

Common stem duplications were characterised by a wide range of shapes and dimensions. For example, the ratio of intermediate sulcus to gyrus length across the original and HCP sample ranged from 17% to 87%. Common classification criteria require this ratio to be one-third to one-half the length of the gyrus (Penhune et al., 1996; e.g. Rademacher et al., 1993). However, given the actual variability in intermediate sulcus length, it is worth asking whether it is appropriate to bundle all CSDs within a single category, as, for instance, CSDs with a short duplication will appear the most similar to a single gyrus, and

CSDs with a long duplication will appear the most similar to full duplications. Using a ratio of 50% to divide CSDs into short and long sub-types is a practical convenience for the purpose of the current study, which is to minimise the distortion needed to morph gyri onto a common template (while keeping the number of sub-categories to a minimum). However, one could also discard all classification categories and simply measure the extent of gyral duplication on a continuous scale from 0%, i.e. no duplication, to 100%, i.e. full duplication, with CSDs representing all the variants in between. Importantly, the occurrence of HG duplications of any type was not associated with a general increase in hemispheric gyrification. This suggests that individual differences in HG morphology may be indicative of developmental differences -whether genetic, epigenetic, or environmental- specific to the auditory cortex, which cannot be traced back to a general trend in gyrogenesis. Finally, this study did not focus on rarer morphotypes such as the co-occurrence of CSDs and CPDs, multiple CPDs, and conjoined STG and HG (see Figure 4.5), although they might also hold important information on the organisation of the human auditory cortex.

4.4.3 Cross-subject alignment

The simple 2d geometric morphing of individual flat patches of the same morphotype onto a common template was overall successful (Figure 4.10). Although curvature within HG was not factored into the calculation of the transformations, curvature gradients aligned well across participants, which was likely due to the general conformity of curvature and gyral geometry. Variability tended to increase laterally, particularly at the junction of HG and STG in partially duplicated gyri. One possible cause is that the lateral boundary of HG labels is the only one that is not based on gyral curvature. Rather, it is the product

freesurfer's automated parcellation (based on the Destrieux atlas), which does not guarantee a smooth curvature gradient between labels. Nonetheless, the procedure was not designed to minimise variability in local curvature. The overarching goal was to visualise the topography of structural and functional data across HG morphologies in order to understand their interaction across individuals, without assuming a correspondence with local curvature gradients (other than the boundaries of HG itself).

Chapter 5.

Correspondence of macro-anatomical landmarks, myeloarchitecture, and tonotopic gradients across Heschl's gyrus' morphotypes

5.1 Introduction

5.1.1 Tonotopy, myelin, and macro-anatomy: individual differences and homologies

The morphological variability of HG is well understood. However, there is no general consensus on the correspondence between specific HG gyral configurations and their underlying cortical cytoarchitecture, myeloarchitecture, or function. The lack of a clear correspondence directly undermines the validity of surface-based (Dale & Sereno, 1993; Essen et al., 1998; Sereno et al., 1995) registration techniques that maximise the similarity of cortical gyral and sulcal patterns across individuals while minimising their overall distortion, such as curvature-based alignment (CBA) (Dale A. M., 1999; Fischl et al., 1999a, 1999b), in the study of individual differences. In fact, in regions as morphologically diverse HG, anatomical landmarks alone are unlikely to be precise markers of functionally or micro-structurally homologous regions across individuals.

In general, the association between cortical micro- and macro-structure has been shown to be fairly reliable across several cortical regions in humans (Fischl, 2013), although with a greater degree of variability for higher-order or phylogenetically younger structures (Amunts et al., 1999; Fischl et al., 2008; Morosan et al., 2005), including HG (Rademacher et al., 2001). Nonetheless, as detailed cytoarchitecture is not accessible -yet[19]- in-vivo,

[19] MRI can reach, in principle, resolutions near the same order of magnitude as the size of cell bodies, but the protocols required are not compatible with the in-vivo study of the human brain. For instance,

several other contrasts have been proposed for the identification of regionalisation homologies across individuals, such as cortical myelin density and functional specialisation, both of which have been shown to be related to cytoarchitecture (Amunts et al., 2007; Dinse et al., 2015; Eickhoff et al., 2004; Weiner et al., 2017). For instance, using in-vivo MRI, an increase in myelin density (Sigalovsky et al., 2006; Wallace et al., 2016), reduced cortical thickness (Zoellner et al., 2018), or multimodal combinations of tonotopic mapping and myelin measures (Dick et al., 2012; Dick et al., 2017; Moerel et al., 2014), have been proposed as regional markers of homologous auditory fields across individuals. Other generalised approaches that involve multi-modal inter-subject registration such as multimodal surface matching (MSM; Glasser et al., 2016); Robinson et al., 2014); Robinson et al., 2018), leverage the information provided by several functional, structural, and connectivity datasets to optimise surface distortion, rather than relying solely on curvature. This approach has the benefit of increasing the power of group fMRI statistical tests and creating sharper maps, at the cost of reducing the accuracy of the alignment of cortical folding patterns (Glasser et al., 2016). In other words, the combination of a range of datasets beyond just cortical curvature can improve the clarity of the typical task-related cortical response or structural features but ignores the relationship between these features and variations in cortical morphology at the individual level. Furthermore, the flexibility of these approaches implies a certain degree of arbitrariness in weighing how much each dataset should influence surface warping, tuning model parameters, and the selection of the datasets themselves.

Wei et al. (2016) achieved a nominal isometric resolution of 10μm, which required over 100 hours of scan time at 9.4 T to achieve an appropriate SNR.

At a smaller scale, especially within regions where the variability of the gross anatomical structure is well established such as HG, studying how specific cortical features may vary across individuals in relation to -rather than regardless of- their own morphology would allow the establishment of ad-hoc anatomical priors (i.e. refined parcellations) that would inform cross-subject comparison and alignment in a theory-driven way. This tailored approach would take full advantage of the information included in individual morphology, which is readily available in-vivo and easy to process through well-established pipelines, and introduce explicit assumptions into data analyses, making group-level statistics easier to interpret. For example, Gulban et al. (2020) demonstrated an improvement in the alignment of cytoarchitectonic maps within the superior temporal surface of 10 brains by enhancing CBA with specific anatomical priors, namely the anterior Heschl's gyrus, superior temporal gyrus, superior temporal, sulcus, and middle temporal gyrus. They justified the selection of specifically the most anterior HG duplication based on prior histological evidence of primary auditory fields residing in this region (Hackett et al., 2001)); however, they bundled together, in case of partial duplications, the anterior branches, posterior branches, and intermediate sulci. This choice is based on cytoarchitectonic evidence that, in some cases, the PAC shifts posteriorly towards the intermediate sulcus and posterior duplication (Hackett et al., 2001; Rademacher et al., 1993), although this relationship is not consistent (Morosan et al., 2001). Nonetheless, the size of the intermediate sulci can change considerably across individuals, ranging from very small lateral duplications, which resemble for the most part non-duplicated gyri, and large duplications that only connect at their medial extremity, which appear most similar to full duplications, and it is unknown how these differences in morphology might relate to

cytoarchitecture, mainly due to the low availability of high-resolution HG cytoarchitectonic map reconstructions in humans (Amunts & Zilles, 2015).

On the other hand, structural and functional data such as proxies of cortical myelination or tonotopy are widely available and much easier to collect through in-vivo MRI. Although direct evidence of a correspondence between tonotopy, myeloarchitecture, and cytoarchitecture in humans has not yet been observed, human cortical myelination and tonotopic gradient topographies share similarities with those of non-human primates (Merzenich & Brugge, 1973; Imig et al., 1977; Morel et al., 1993; Bendor & Wang, 2006; Bendor & Wang, 2008; see paragraph 1.2.1), despite the marked differences in anatomical landmarks (Hackett et al., 2001). Specifically, in non-human primates, tonotopic gradient reversals appear to follow the cytoarchitectonic subdivision of auditory core (i.e. high-to-low-to-high-to-low across A1, R, and RT), with core (A1 in particular) being also characterised by higher myelin density compared to the surrounding belt regions (Morel et al., 1993). Similar characteristics have been observed in humans (De Martino et al., 2014; Dick et al., 2012; e.g. Formisano et al., 2003; Moerel et al., 2014) and proposed as an estimate of the location of cytoarchitectonic boundaries. Da Costa et al. (2011b) specifically analysed the association between tonotopic gradients and HG morphotypes (single, CSD, CPD) and found that, in case of duplications, anterior-posterior high-to-low-to-high tonotopic gradients spanned across all duplications, implying that human analogues of auditory core (A1 and R in particular) might extend across all transverse gyri anterior to Heschl's sulcus, rather than just the most anterior gyrus. Parallels between human and non-human PAC topography have long been the object of debate (Baumann et al., 2013; Besle et al., 2019; Saenz & Langers, 2014) and remain, to this day, hypothetical. Nonetheless,

homologies across (human) individuals in myelin density and tonotopy can still be drawn without specific reference to an underlying cytoarchitectonic parcellation.

5.1.2 Current study

In summary, there exist true individual differences in HG's folding patterns, as well as the location of micro-structurally and functionally homologous regions across individuals relative to these patterns. The use of cortical curvature-based registration techniques in group analyses, in the absence of anatomical priors, can potentially obfuscate true individual differences by introducing an additional layer of variability originating from ambiguities in surface curvature matching across brains. This appears to be particularly relevant within the superior temporal surface (Gulban et al., 2020), where the variable number of transverse gyri can result in the alignment of non-homologous regions across individuals. Several techniques allow the automated parcellation of the cerebral cortex, with the TASH toolbox (Dalboni da Rocha et al. (2020)) being specifically designed to identify and number HG full duplications in the superior temporal plane, while the techniques presented in the previous chapter allow the classification of CSDs. However, both TASH and the novel CSD classification pipeline are completely curvature based, in that there is no further evidence of homology between equally labelled regions across individuals other than macro-anatomy. In this chapter, I apply these techniques to investigate whether homologies in HG's cortical structure (quantitative R1, MT) and function (frequency preference and tuning width) across morphotypes (single, short CSD, long CSD) align with specific anatomical landmarks. After quantifying these homologies, an ideal sub-section of partially duplicated gyri is drawn across participants through an automated procedure and morphed onto a common surface with single gyri. Group average

and variability maps are then calculated and compared with those obtained in Freesurfer. Subjects that displayed the least agreement with the group average are analysed individually in the context of an extended region surrounding HG to disentangle potential alignment or parcellation issues from true individual differences. Finally, the same CSD parcellation technique is applied to a set of 10 surface reconstructions of post-mortem cytoarchitectonic maps (the same set used in Gulban et al., 2020) to calculate probabilistic cytoarchitectonic boundaries within HG and characterise each region in terms of cortical myelin density, tonotopic response, and thickness.

5.2 Methods

5.2.1 Processing of tonotopy and MPM data

Tonotopy and MPM were morphed and resampled using a kernel FWHM of 2.5mm, following the same procedures described in Chapter 4. When averaging tonotopic data (i.e. during resampling or group-averaging), the imaginary (im) and real (r) components of the Fourier vector were averaged first and then used to obtain new average values for phase and magnitude. The phase was calculated as the 2-argument arctangent of the two vector components ('atan2(im,r)'), while the length of the complex vector ('sqrt($r^2 + im^2$)') corresponded to tonotopic magnitude.

5.2.2 Removing effect of curvature and thickness

Measures sensitive to tissue myeloarchitecture such as R1 and MT tend to be positively correlated with cortical convexity (i.e. higher myelin content in gyral peaks) and thickness (Dick et al., 2012; Sereno et al., 2013; Wähnert et al., 2014). To draw a comparison of the variations in cortical myelin and macromolecular content across morphologies that is

independent of the variability in HG morphology across individuals, the effects of curvature and thickness on MT and R1 were removed by calculating the residuals of a multiple linear regression model using thickness and curvature as predictors. A separate model was fitted for each individual hemisphere using only data within HG and the intermediate sulcus. To restore the original scale of R1 and MT data, individual averages were added to the residuals. Curvature and thickness residualised values for R1 and MT are referred to in-text as "decurv-dethick".

5.2.3 Assessing homologies across morphologies

The functional and histological homology between gyri with common stem duplications and non-duplicated gyri was quantified using a custom procedure described below. Datasets included in the procedure were tonotopy (phase and magnitude), R1, and MT (residualised for curvature and thickness). A summary of the steps involved in this procedure can be found in Figure 5.1.

5.2.3.1 Partitioning of partially duplicated gyri

This procedure first defines a set of sub-regions within gyri with common stem duplications and their intermediate sulci using the average shape of non-duplicated gyri from the same hemisphere as a reference outline (see Figure 5.1). The range of possible sub-regions was obtained by transforming the reference outline according to three degrees of freedom: a rotation around the origin, a horizontal translation, and a horizontal dilation. First, the reference outline was rotated around the origin following an angle between -15 and 15 degrees, in 5 degrees intervals. This range of values (i.e. 30 degrees) was selected to approximate the angle formed between the stem and the branches of partially duplicated

gyri, with -15 and 15 degrees aligning with the anterior and posterior branches. Second, the outline was translated horizontally (i.e. along the anterior-posterior axis) in 1mm intervals. Third, the outline was dilated horizontally using scaling factors of 0.8, 1, and 1.2. The application of a contraction or dilation allows the reference outline to adapt to the different sizes of stems and branches across partially duplicated morphologies. Finally, the validity of the geometry of each sub-region was established based on two principles: each sub-region should include vertices near the most medial portion of the gyrus (i.e. within 1% of the maximum y coordinate) and its vertical range should be at least 75% that of its gyrus. These limitations were defined to ensure that the stem of all partial duplications would always be included in each sub-region and that there were no drastic differences in the size of each sub-region and the corresponding non-duplicated reference outline. Any combination of transformations leading to an invalid sub-region was discarded.

5.2.3.2 Processing of valid sub-regions

The vertices of each valid sub-region were morphed (see paragraph 4.2.7) onto the average flat patch of non-duplicated gyri within the same hemisphere. Tonotopic (phase and magnitude) and MPM data (R1 and MT) were then resampled (see paragraph 4.2.8) onto the coordinates of these average flat patches using a normal kernel FWHM of 2.5mm. As previously described, the resampled values of the tonotopic phase were calculated by resampling the imaginary and real components of the Fourier vectors independently first and taking their resulting angles and lengths as phase and magnitude respectively.

5.2.3.3 Searchlight cross-correlations

After resampling each sub-region to the same surface as the reference flat patch, the similarity between their respective datasets was quantified using a searchlight cross-correlation procedure. For any two datasets sampled onto the same surface, this procedure calculates a Pearson correlation coefficient between them within a square "searchlight" area with a side 5mm centred at each point of that surface. This generates a map where each value represents the local correlation within a relatively small region surrounding each surface point. Compared to finding the sub-region that maximises the overall correlation with the non-duplicated gyrus, this approach

5.2.3.4 Average cross-correlations across subjects and parameters

For each subject, the overlapping correlation coefficients obtained from all possible sub-regions were averaged using a Fisher z-transformation, generating a single average cross-correlation map for each participant Figure 5.1. Individual cross-correlation maps were then averaged to obtain group averages for each common stem duplication type, hemisphere, and parameter (i.e. tonotopic phase and magnitude, R1, and MT). A final map was calculated for each morphological type and hemisphere by averaging cross-correlation maps obtained from each parameter. This map represents the average similarity in both tonotopic and histological gradients across the whole surface of the partially duplicated gyri and their intermediate sulcus.

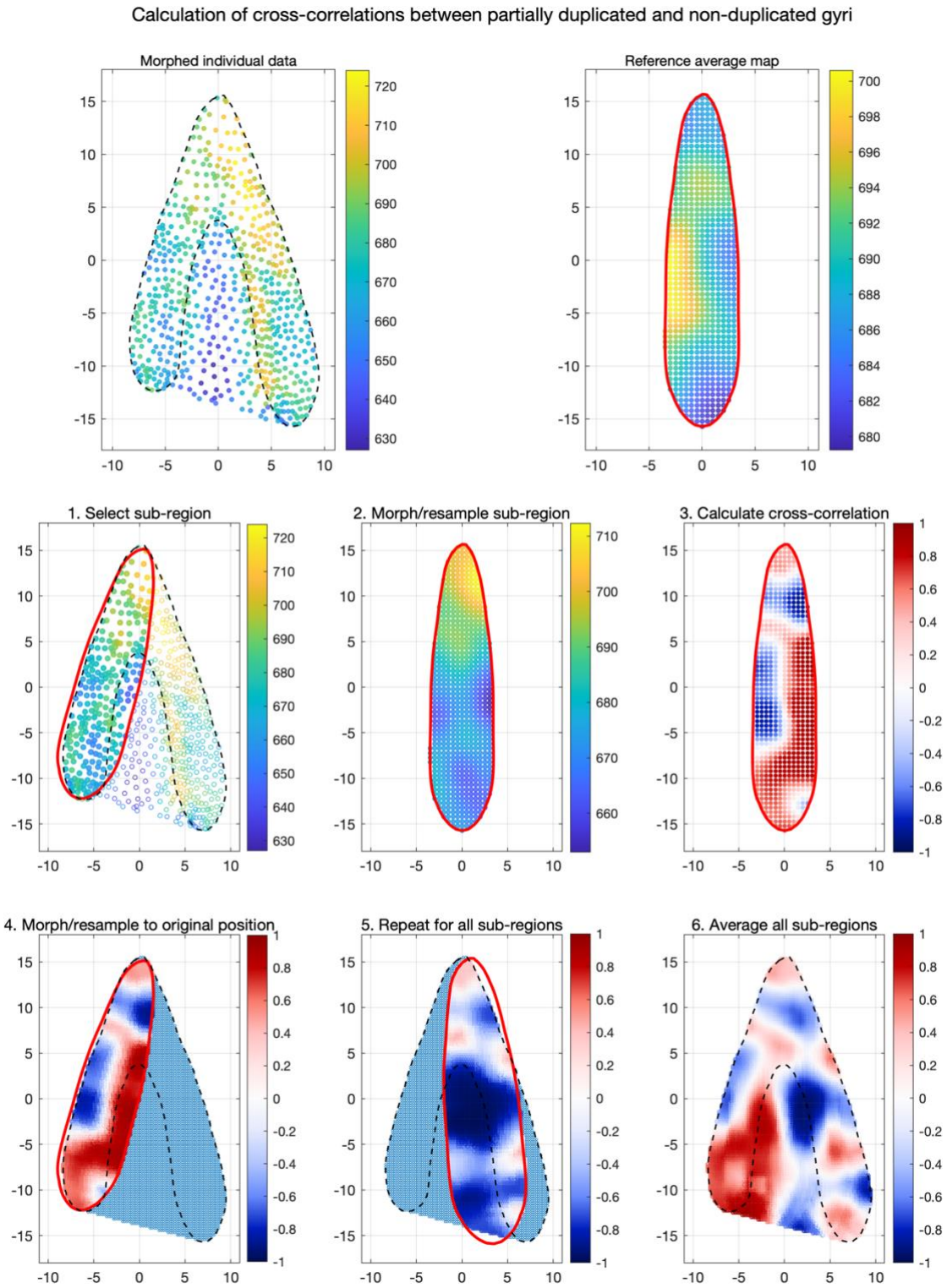

Figure 5.1*: Individual example of the steps involved in the calculation of cross-correlations between partially duplicated and non-duplicated gyri using R1 data (residualised for curvature and thickness). The graphs in the top row represent the two datasets being correlated: on the left, the vertices of a representative subject morphed onto its corresponding standard flat patch (i.e. right hemisphere, long duplication); on the right, the average map obtained from all non-duplicated gyri of the same hemisphere. Graphs in the middle and bottom rows represent the main steps required to*

calculate the cross-correlation between these two datasets. 1. Definition of a possible sub-region, marked by a red line and filled vertices. 2. Vertices within the sub-region are morphed and uniformly resampled onto the non-duplicated average flat patch. 3. Calculation of cross-correlations between the sub-region and average map using a 2.5 mm searchlight radius. 4. Morphing and resampling of the cross-correlation map back onto its original position. 5. Additional example of a cross-correlation map obtained from a different sub-region. 6. Average cross-correlation map obtained by averaging data from all overlapping sub-regions.

5.2.3.5 Combining different morphologies

Compared to approaches that involve maximising or minimising certain statistics (e.g. finding sub-regions that maximise the overall correlation or minimise the sum of squared differences between datasets), searchlight cross-correlations have the advantage of retaining nuance across the entire surface of each sub-region. However, the definition of an 'optimal' section (i.e. most similar in tonotopy and histology) is required in order to morph individuals with different morphologies onto a common surface. For this reason, on each partially-duplicated gyrus, a discrete region was delineated based on the combined cross-correlation in tonotopy (phase and magnitude) and histology (R1 and MT, after removing the effect of curvature and thickness). More specifically, sub-regions with the highest cross-correlations were iteratively combined into a single larger region until their combined surface area approached that of non-duplicated gyri (see Figure 5.8). This approach was chosen to improve robustness against small variations in cross-correlation between sub-regions that aren't necessarily indicative of a better or worse similarity, as well as to control the overall size of the putative homologous region.

5.2.3.6 Cytoarchitectonic data

Cytoarchitectonic data were obtained from 10 ex-vivo MR images histologically labelled by Morosan et al. (2001); Morosan et al. (2005), and Zachlod et al. (2020), which are part of the JuBrain cytoarchitectonic Atlas (Amunts & Zilles, 2015). Reconstructed white matter

cortical surfaces for these brains and their corresponding cytoarchitectonic labels (Gulban et al., 2020) were downloaded from https://search.kg.ebrains.eu/instances/Dataset/ff71a4d1-ea14-4ed6-898e-b92d95b3c446. Surfaces for each hemisphere were imported into csurf, mirrored, and converted from '*.obj*' to freesurfer's surface format. Surfaces were then smoothed, inflated, and processed using the pipeline described in 4.2, which includes HG labelling, flattening, preprocessing, and classification. Vertices for each cytoarchitectonic area were extracted from the '*.poi*' annotation files provided with the same database.

After combining the optimal sub-region of duplicated gyri and non-duplicated gyri, the overlap of each cytoarchitectonic label across specimens was utilised to reconstruct a probabilistic atlas (Figure 5.19) to be used as an estimate of the cytoarchitecture of the in-vivo dataset.

5.2.4 Comparison with curvature-based alignment

Group average and variability maps generated in AFNI and Freesurfer were pre-processed according to the same pipeline used for individual data (see paragraph 4.2). To briefly summarise, after calculating group and standard deviation maps and morphing onto the *fsaverage* surface, Heschl's gyri were identified using TASH, flattened and imported into Matlab. The flat patches were then rotated and their vertices morphed onto the reference average flat patch. All datasets, including R1, MT, PD, R2*, tonotopic phase and magnitude, pRF *mu* and *sigma*, curvature, and thickness were then resampled using the same nnfr algorithm used by freesurfer, with one smoothing step applied after resampling.

5.3 Results

5.3.1 Functional and histological homologies across morpholgies

5.3.1.1 Average tonotopic maps

Average maps of the tonotopic phase showed very similar high-to-low frequency gradients across all morphologies, extending anteromedially to posterolaterally (Figure 5.2). A gradient reversal towards higher frequencies could be observed posteriorly in gyri with large duplications, separated by a region of low-frequency preference within the intermediate sulcus. The same reversal could not be clearly observed in gyri with small or no duplications, indicating a functionally equivalent reversal region might extend beyond the boundary of Heschl's gyrus for these morphologies. Tonotopic magnitude (Figure 5.3) followed similar gradients as a phase but in the opposite direction, with values increasing within the intermediate sulci of duplicated gyri and posteriorly for gyri with small or no duplications. Since average tonotopic magnitude depends not only on the magnitude of the individual Fourier vectors but also on their phase agreement, higher magnitude values can be indicative of the local consistency in phase preference across individuals. Indeed, dispersion maps (Figure 5.4) indicated that regions characterised by high magnitude corresponded to regions with high phase agreement across individuals, which also tended to overlap with regions of low-frequency preference.

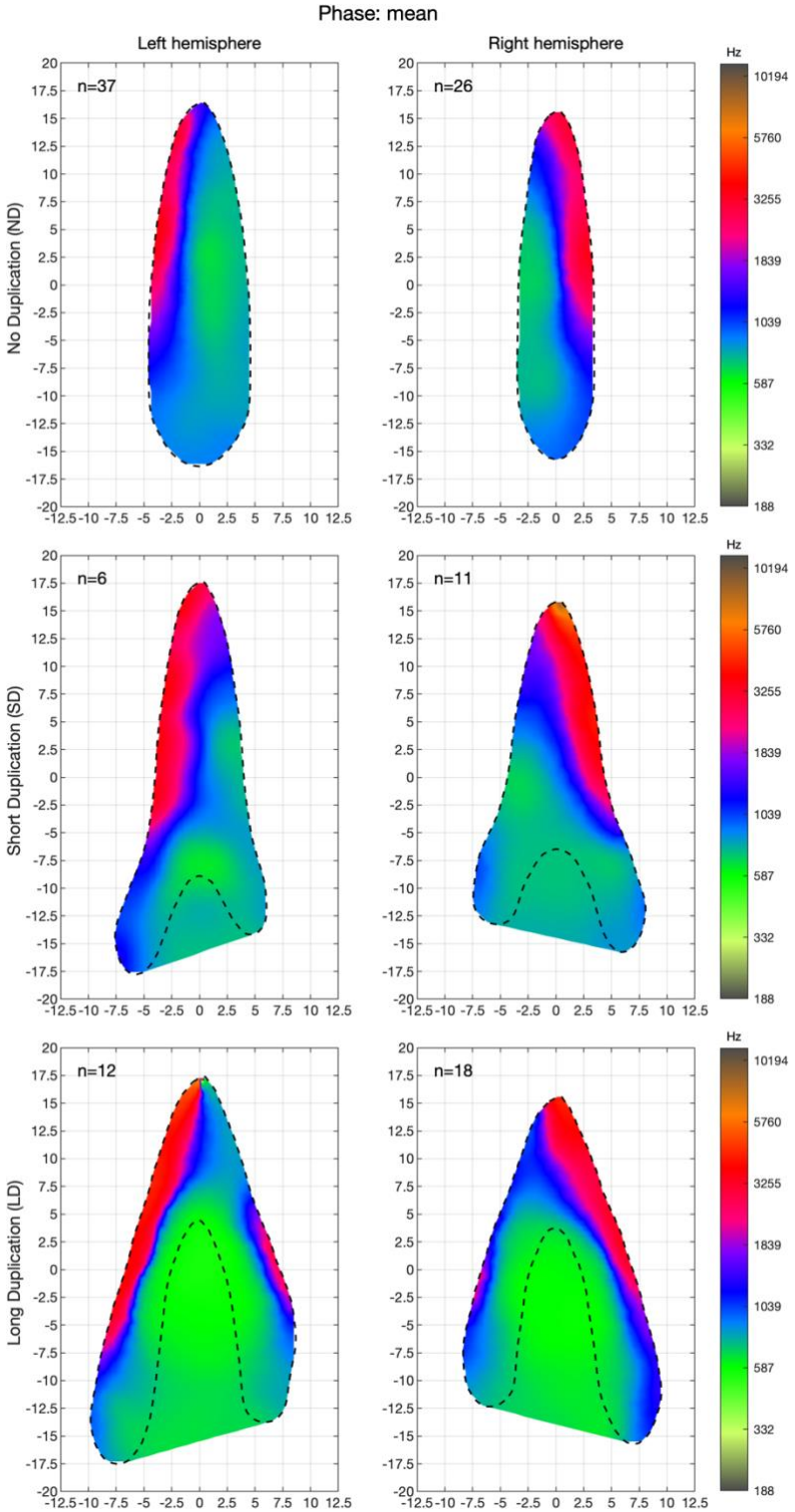

***Figure 5.2**: Average tonotopic phase maps for each morphological type and hemisphere resampled onto average flat patches. Colour represents the average preferred frequency in Hz on a logarithmic scale. The number of hemispheres used to calculate each map is noted in the top-left corner of each graph. Dashed black lines indicate gyral boundaries. Coordinates are in millimetres.*

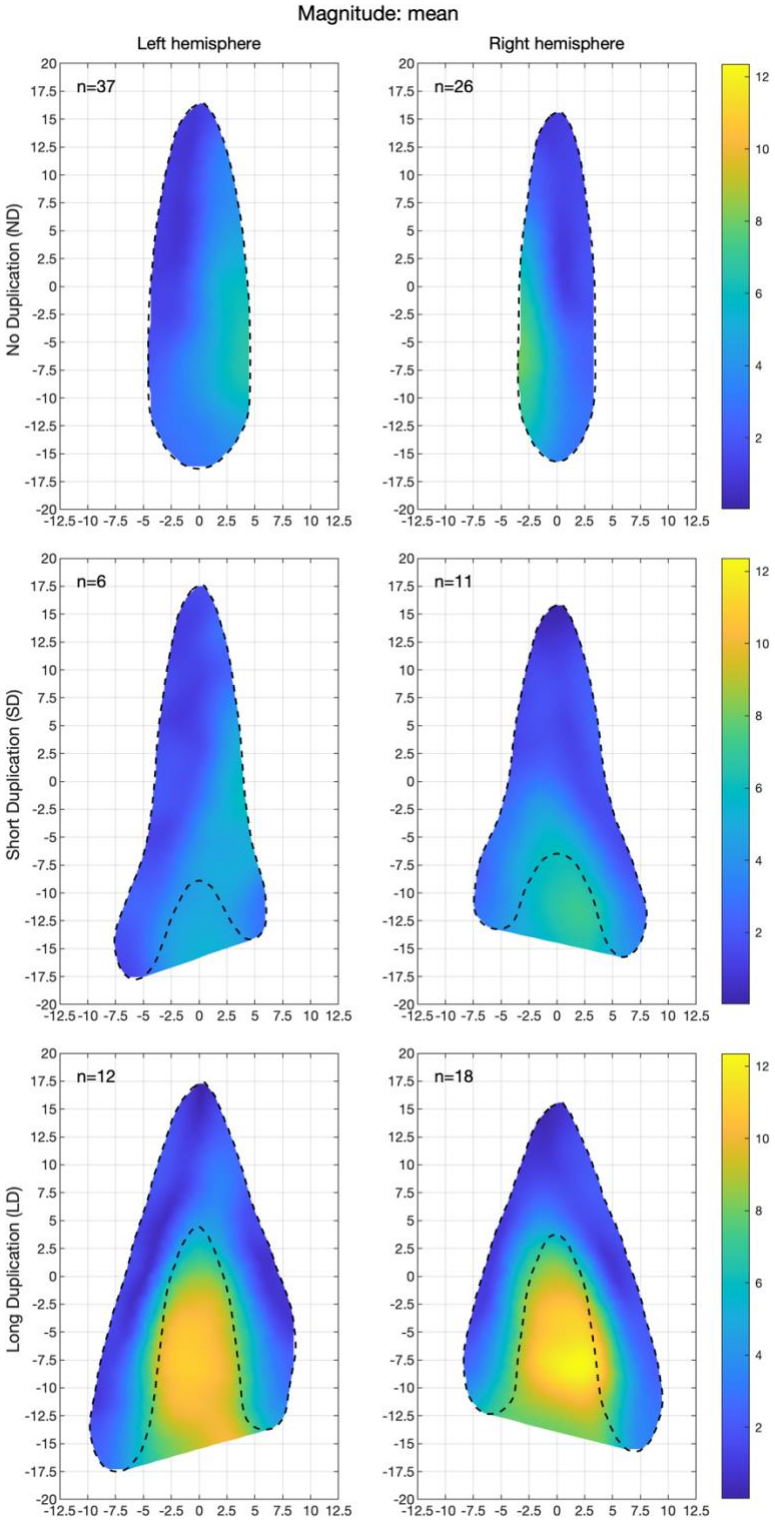

***Figure 5.3**: Average tonotopic magnitude maps for each morphological type and hemisphere resampled onto average flat patches. The number of hemispheres used to calculate each map is noted in the top-left corner of each graph. Coordinates are in millimetres. Dashed black lines indicate gyral boundaries.*

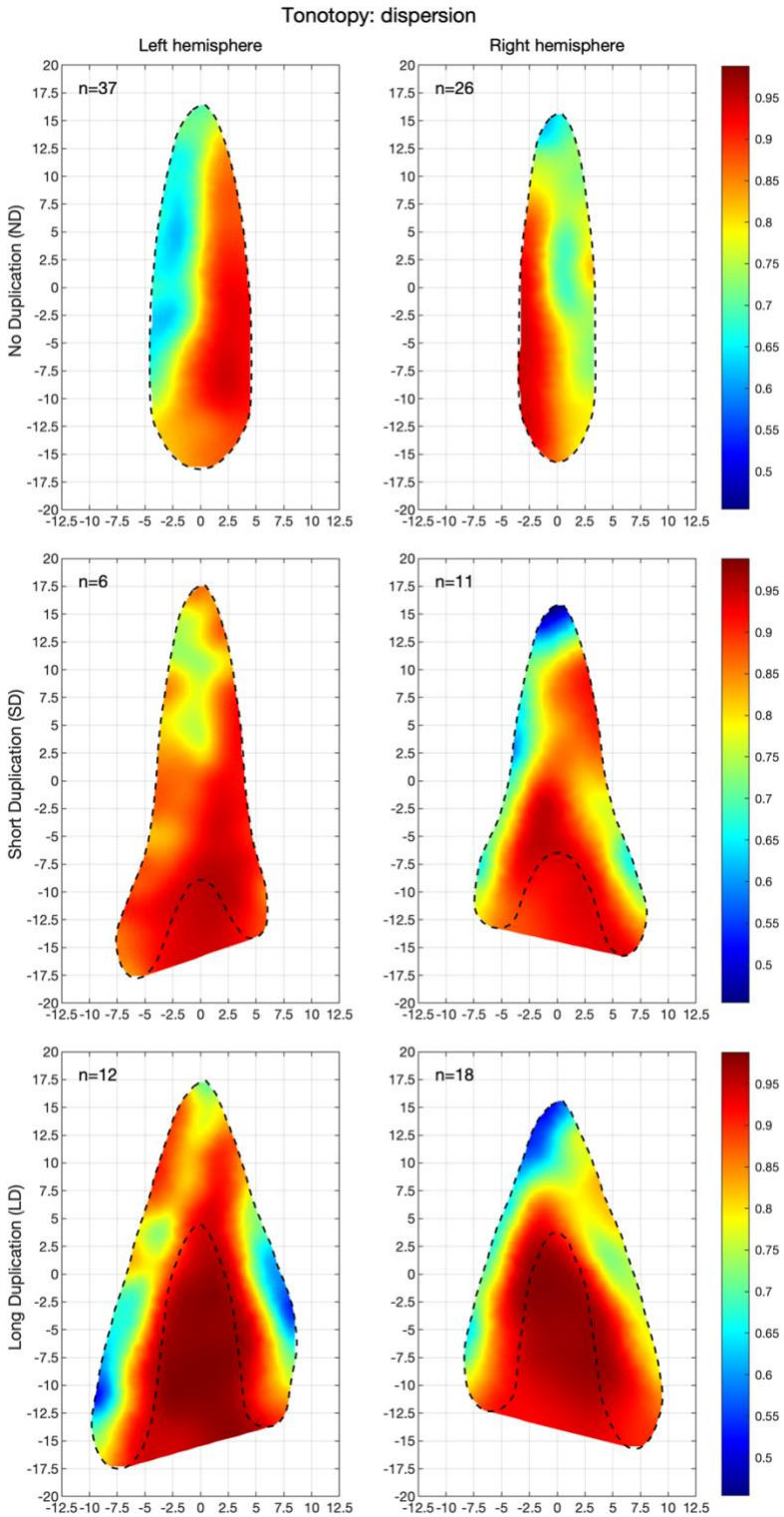

***Figure 5.4**: Tonotopic dispersion index of individuals with similar morphologies, calculated as the ratio between the magnitude of the average vector and the average magnitude of all individual vectors. A higher index corresponds to a greater agreement in frequency preference across individuals. Dashed black lines indicate gyral boundaries.*

5.3.1.2 Multi-Parameter Mapping (MPM)

Both R1 (Figure 5.5) and MT (Figure 5.6) appeared to largely follow curvature gradients, increasing around gyral peaks and decreasing within intermediate sulci, with a posterior shift towards larger values observable in gyri with short or no partial duplications. There were noticeable differences in myelination between the branches of gyri with long partial duplications, with higher values of MT within the anterior branches of both hemispheres and R1 in the right hemisphere. After removing the effect of curvature and thickness (Figure S1; Figure S2), the similarity with curvature gradients was drastically reduced, leaving localised regions of high R1 and MT within the stems of duplicated gyri and a much less pronounced posterior shift in non-duplicated gyri.

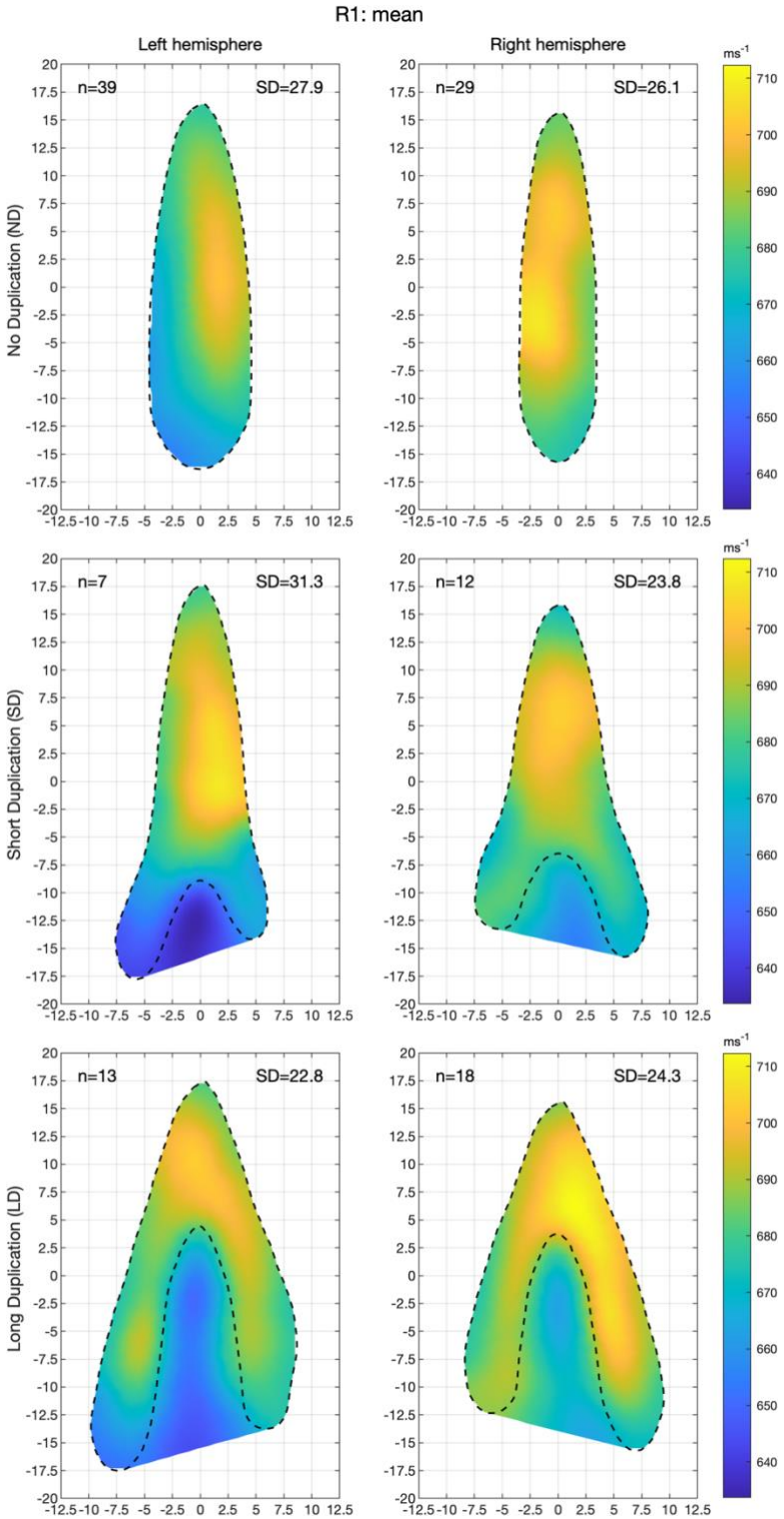

Figure 5.5*: Average R1 maps for each morphological type and hemisphere resampled onto average flat patches. The number on the top-left corner of each plot indicates the number of hemispheres used to calculate each average. The number on the top right indicates the average standard deviation of all the individual datasets used to compute each map. Dashed black lines indicate gyral boundaries. Coordinates are in millimetres.*

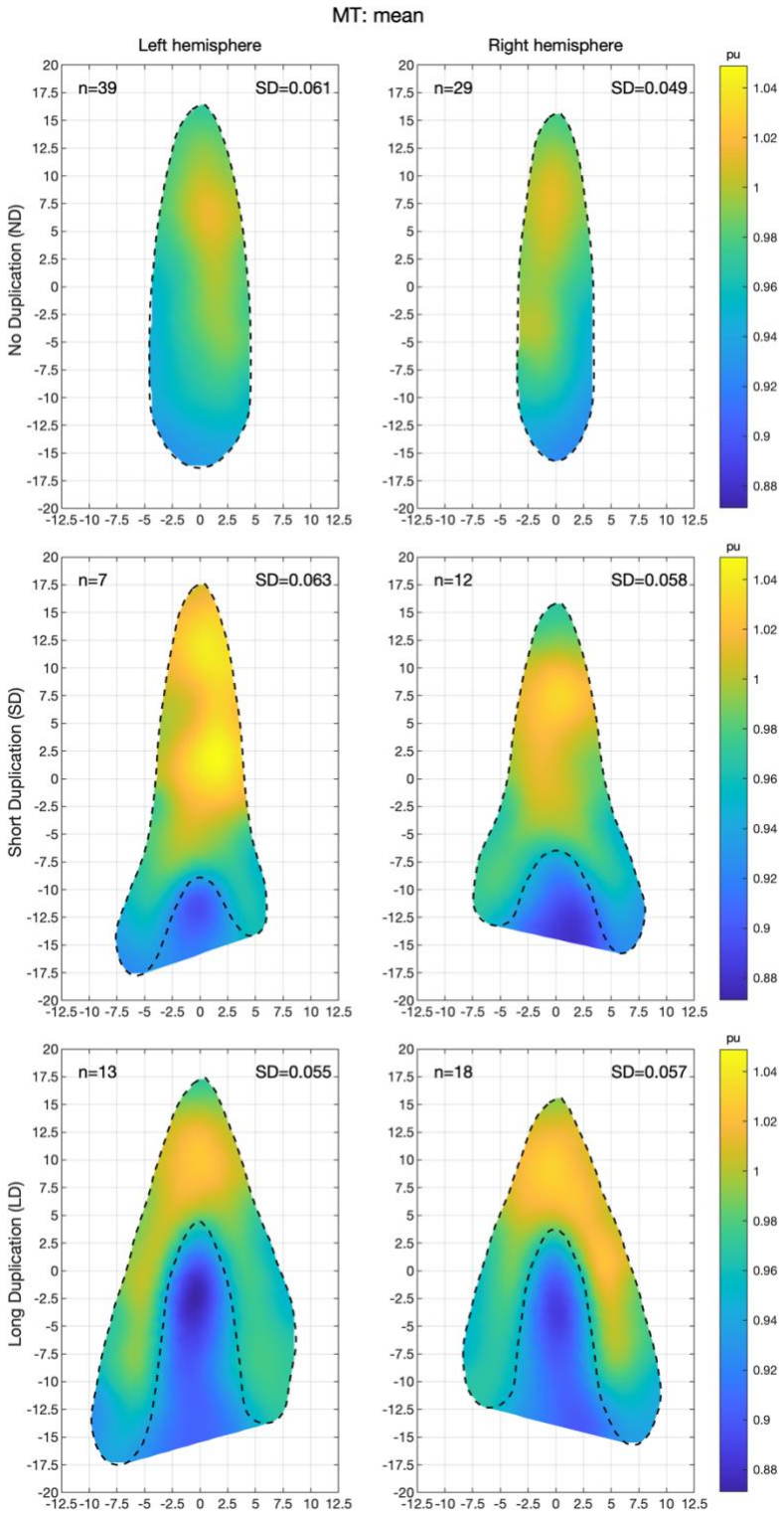

Figure 5.6*: Average MT maps for each morphological type and hemisphere resampled onto average flat patches. The number on the top-left corner of each plot indicates the number of hemispheres used to calculate each average. The number on the top right indicates the average standard deviation of all the individual datasets used to compute each map. Dashed black lines indicate gyral boundaries. Coordinates are in millimetres.*

5.3.1.3 Functional and histological equivalence across morphologies

The functional and structural homology between duplicated and non-duplicated gyri was quantified using searchlight cross-correlations across tonotopic (phase, magnitude) and MPM (R1, MT, residualised for curvature and thickness) data. Average cross-correlation maps (Figure 5.7) showed higher positive correlations towards the anterior half of partially duplicated gyri, spanning across both branches and stems, while regions of lower and negative correlations could be observed posteriorly across both hemispheres. This trend was driven primarily by tonotopic data (Figure S6), specifically the similar anteromedial-to-posterolateral high-to-low gradients of frequency preference and low-to-high magnitude across all morphologies and hemispheres. Conversely, cross-correlations obtained with only R1 and MT appeared more inconsistent, with positive correlations located anteriorly only in gyri with short duplications and a region of negative correlation located between the anterior branches and the intermediate sulci of gyri with long duplications. These negative correlations likely emerged from the contrast between the anterior-posterior increase in R1 and MT that characterises non-duplicated gyri and the decreasing gradients observed between anterior branches and intermediate sulci of gyri with long duplications. Similar results were obtained using the sum of squared differences between duplicated and non-duplicated gyri in the place of cross-correlations (Figure S7). Regions with the lowest sum of squared differences were located mainly in the stem and anterior branches of duplicated gyri, while the posterior branch appeared to be where duplicated and non-duplicated gyri differed the most.

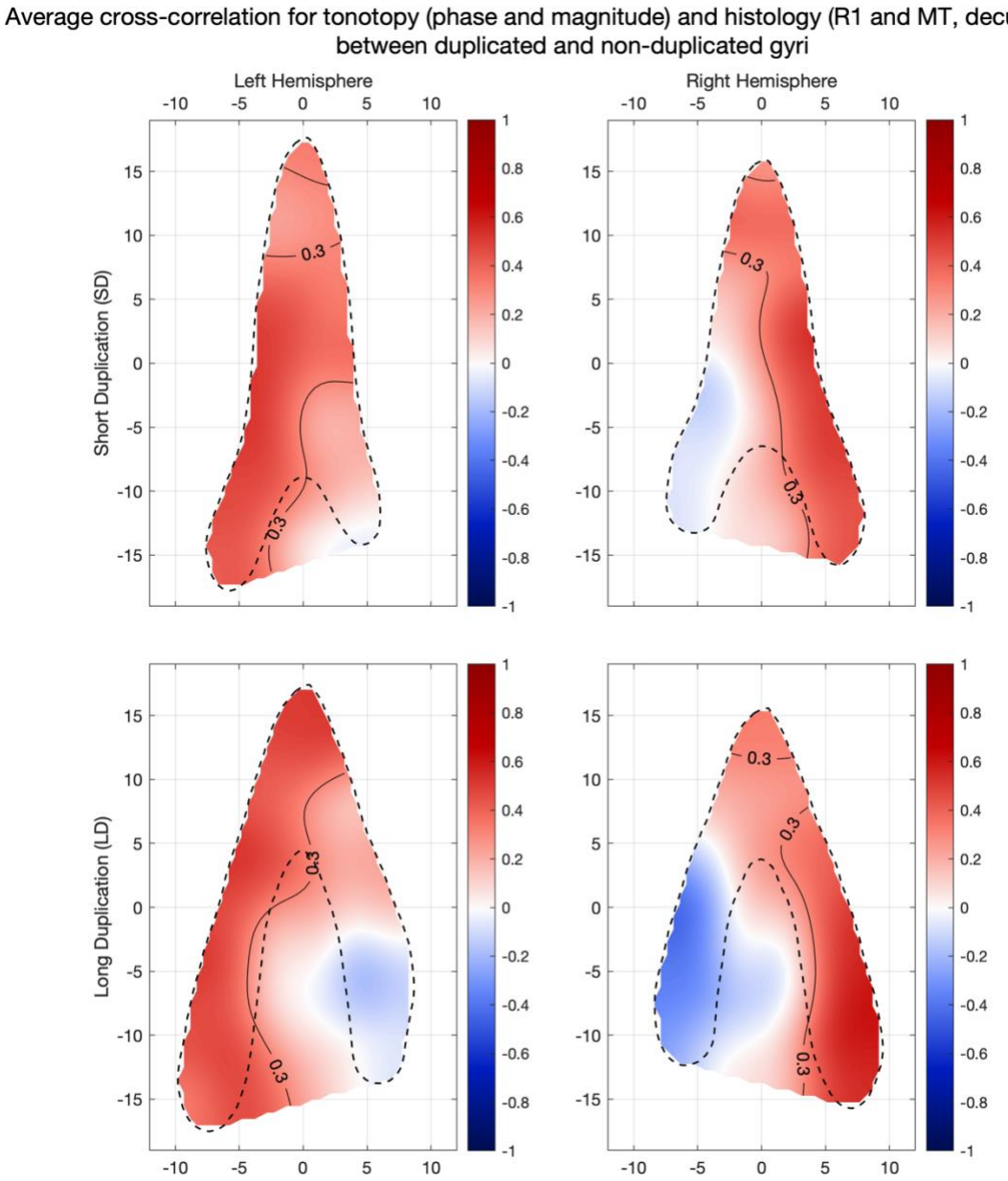

Figure 5.7*: Average cross-correlations between partially duplicated and non-duplicated gyri obtained with tonotopic (phase and magnitude) and MPM (R1 and MT, residualised for curvature and thickness) data. Regions with high cross-correlations (in darker shades of red) represent regions of partially-duplicated gyri whose functional and histological gradients are the most similar to the gradients of non-duplicated gyri. Black contour lines mark correlation values of 0.3*

5.3.1.4 Identifying discrete homologous regions

After calculating the average correlation for each possible sub-region of each morphology, the sub-regions with the highest correlations (i.e. top 5%) were combined into a single larger "optimal" region. These optimal regions (Figure 5.8, marked by a dashed red line)

consistently overlapped with the anterior branch of duplicated gyri in both hemispheres, extending partially into the intermediate sulci, and had similar overall size across morphologies. Although the overall range of correlations differed across morphologies and hemispheres, there was a very consistent and gradual decrease towards posterior sub-regions in all cases, with no posterior sub-region surpassing the selected correlation threshold. After morphing and resampling the identified optimal sub-regions of all subjects with partially duplicated gyri onto the non-duplicated average flat patch, a one-way ANOVA was used to determine whether the resulting alignment of MPM, tonotopy, and cortical thickness with the reference average flat patch[20] was comparable across all three morphologies. A Fisher z-transformation was applied to coefficients before averaging them and performing the ANOVA. There were no statistically significant differences in mean correlation in either hemisphere (left: $F(2,58) = 0.41$, $p = 0.66$; right: $F(2,58) = 1.46$, $p = 0.24$), indicating that the alignment of the selected sub-regions of duplicated gyri was overall comparable to that of non-duplicated gyri for tonotopy, MPM data, and cortical thickness.

[20] In the case of individuals with duplicated gyri, the reference flat patch was calculated as the average map of all non-duplicated gyri. In the case of individuals with non-duplicated gyri, a unique reference flat patch was calculated for each individual as the average of all non-duplicated gyri except themselves, to prevent inflating correlation values.

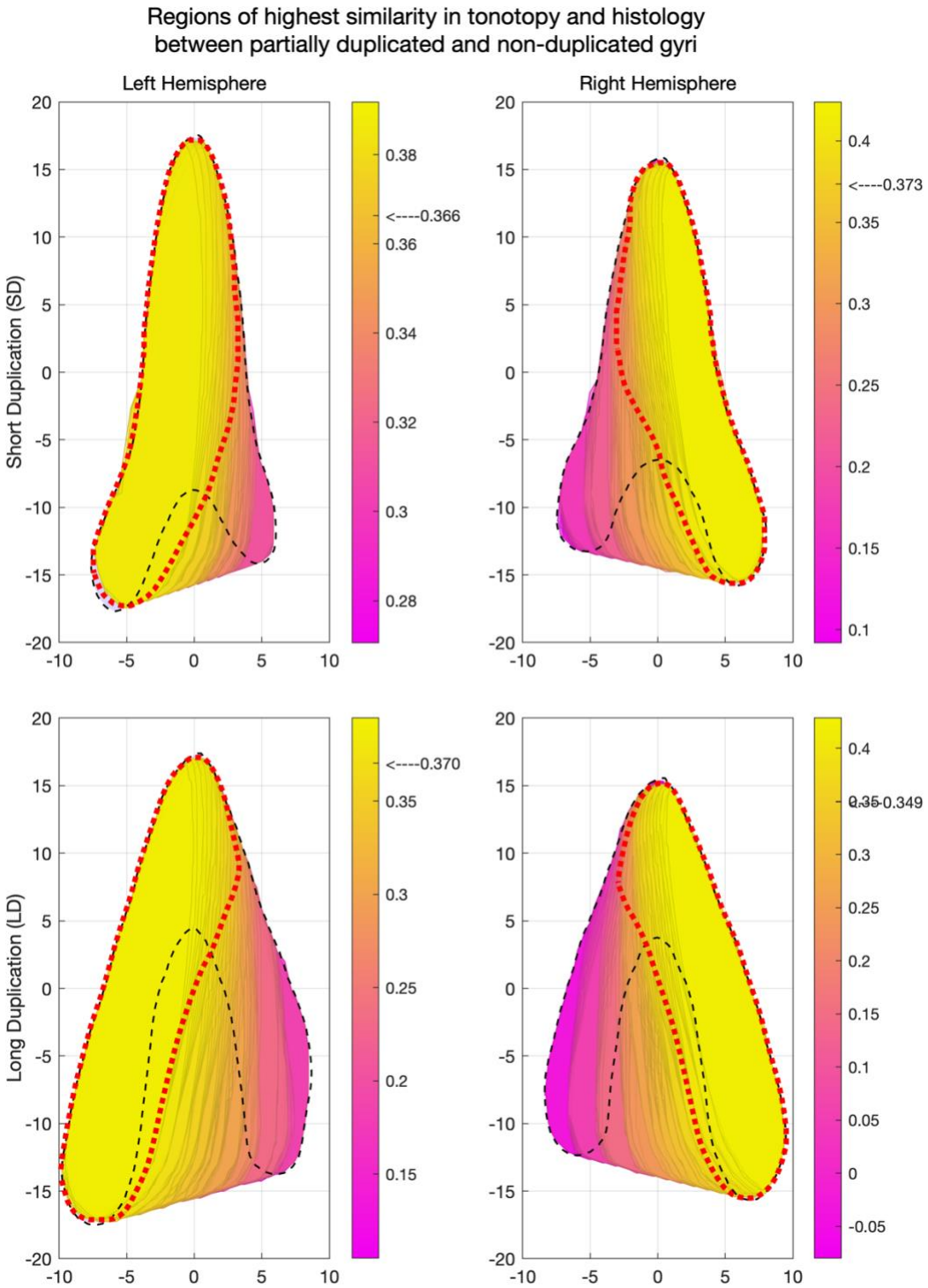

Figure 5.8*: Plots of all sub-regions within partially duplicated gyri that show the highest correlation in tonotopy (phase, magnitude) and histology (R1, MT, after removing the effect of thickness and curvature) with non-duplicated gyri. Sub-regions with average cross-correlation coefficients above the 95th percentile are plotted semi-transparently using a fill colour representing the value of their individual coefficients, with yellow indicating higher and purple lower correlations. Dotted red lines represent the contours of the region obtained by combining all these sub-regions. The remaining surface of all flat patches, including gyri and intermediate sulci, is shaded in blue. The dashed black lines indicate the gyral contours of each flat patch.*

5.3.1.5 Cytoarchitecture

The probabilistic cytoarchitectonic maps obtained from post-mortem data (see 5.2.3.6), despite the relatively small number of brains (n = 10), showed a remarkable similarity in their configuration across non-duplicated gyri and the anterior branches of duplicated gyri (Figure 5.9). Namely, TE 1.1 occupied the medial one-third to one-half of the gyri across morphologies, TE 1.0 was adjacent laterally and extended along the length of the gyri or the anterior branch of duplicated gyri, TE 1.2 was located anterolaterally within 5 to 10 mm from the lateral extremity of both non-duplicated gyri and anterior duplications, while TE 2.1 extended posteriorly in the lateral half of either non-duplicated gyri and anterior duplications. In the case of duplicated gyri, TE 2.1 also extended posteriorly into the intermediate sulcus and the anterior half of posterior duplications, while TE 2.2 occupied the posterior half of posterior duplications, mainly within their lateral two-thirds.

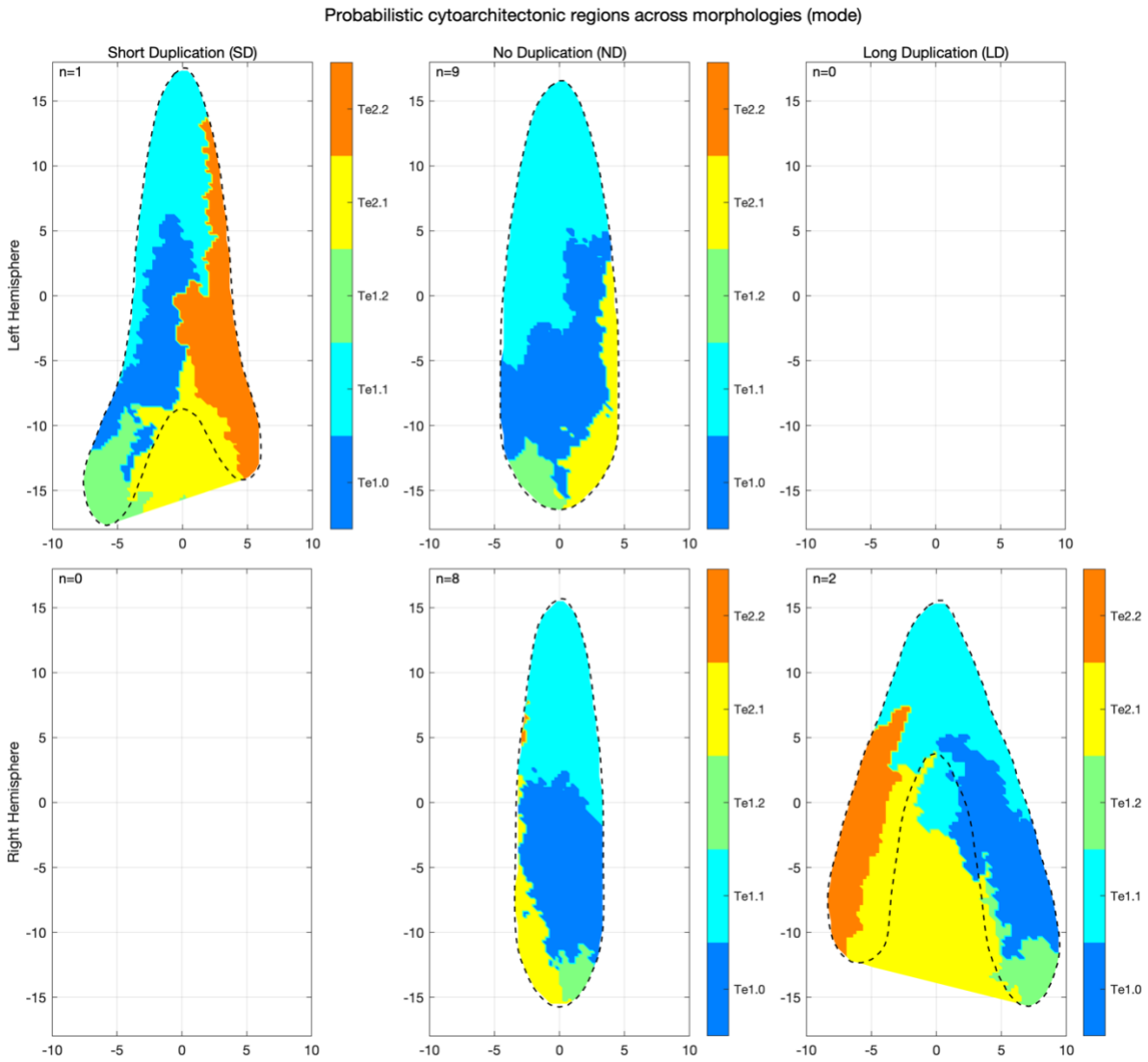

Figure 5.9*: Probabilistic cytoarchitectonic regions within Heschl's gyrus obtained from 10 manually labelled post-mortem brain images (see 5.2.3.6). Regions were obtained by resampling gyri of the same morphological types onto a common surface and calculating the mode at each vertex. The number of brains for each hemisphere and morphology is indicated in the top-left corner of each graph.*

5.3.2 Averages and individual differences of homologous regions across morphologies

5.3.2.1 Curvature and cortical thickness

Average curvature maps (Figure 5.10) followed expected gyral gradients, albeit without the same marked posterior shift typical of non-duplicated gyri (Figure 4.8). Standard deviation maps showed increased variability in curvature towards the posterior half of the gyri,

further pointing to a possible discrepancy between the morphology of non-duplicated gyri and the selected optimal regions of gyri with incomplete duplications, which include, posteriorly, a portion of the intermediate sulcus. Average cortical thickness (Figure 5.11) ranged approximately from 2.8 mm to 3.2 mm. In both hemispheres, average maps were characterised by a thicker cortex laterally and within a small region of the posteromedial quadrant[21]. Standard deviation ranged from 0.28 mm and 0.46 mm and also appeared to increase laterally. Marked differences in lateral cortical thickness could in fact be observed across subject subgroups based on their correlation with the group average, with this region being the thickest for the most similar subgroups but the thinnest for the most dissimilar (Figure 5.11).

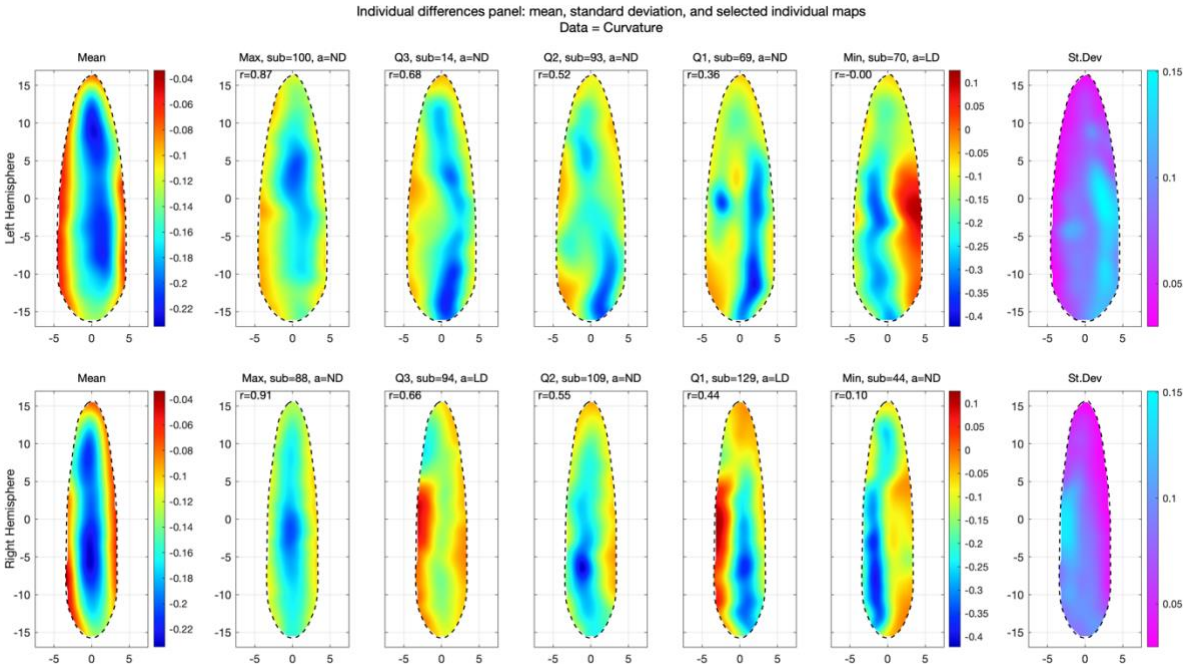

***Figure 5.10**: Panel of individual differences in cortical curvature. Maps in the leftmost column correspond to group average maps. Maps from column two to column six represent the maps of five subjects sorted by descending similarity with the average map. The top and bottom rows correspond to the left and right hemispheres respectively. Colourscales were calculated separately*

[21] The posteromedial quadrant corresponds to x>0 and y>0 coordinates in the left hemisphere and x<0 and y>0 coordinates in the right hemisphere.

for group average and individual maps to improve contrast. Maps in the right column represent the group standard deviation.

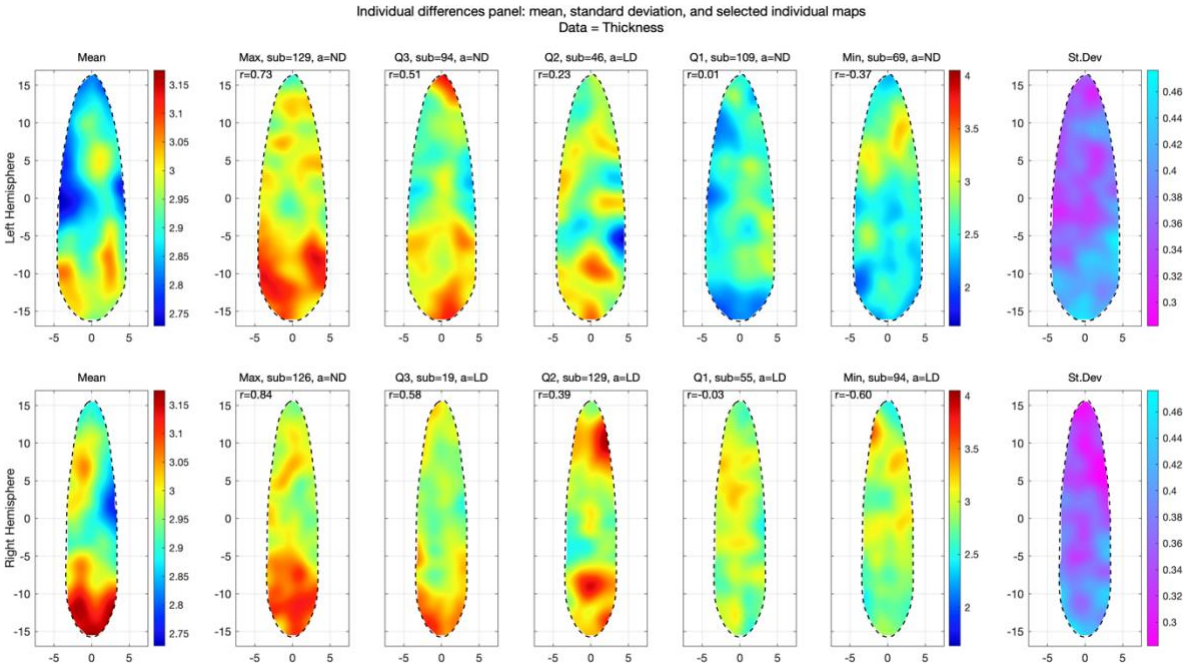

Figure 5.11*: Panel of individual differences in cortical thickness. Maps in the leftmost column correspond to group average maps. Maps from column two to column six represent the maps of five subjects sorted by descending similarity with the average map. The top and bottom rows correspond to the left and right hemispheres respectively. Colourscales were calculated separately for group average and individual maps to improve contrast. Maps in the right column represent the group standard deviation.*

5.3.2.2 R1 and MT

Average R1 (Figure 5.12) and MT maps (Figure 5.13) largely followed the expected curvature gradients, with values increasing along gyral peaks. While both parameters appeared to decrease laterally, a peak within the medial half of the gyrus appeared particularly pronounced in MT maps for both hemispheres. Standard deviation maps showed a higher variability across individuals in the left hemisphere compared to the right hemisphere (Welch's t-test, R1: $t(5473) = 70$, $p < .001$; MT: $t(6056) = 54$, $p < .001$). Furthermore, inter-subject variability appeared lower around the inner surface of the gyral labels compared to their margins, indicating a more consistent histology across individuals

in these regions. Average Spearman correlations between individual and average maps were 0.57 for MT and 0.53 for R1, with individuals who scored a negative correlation ranging between 5% to 6% for both parameters and hemispheres. (Figure 5.12).

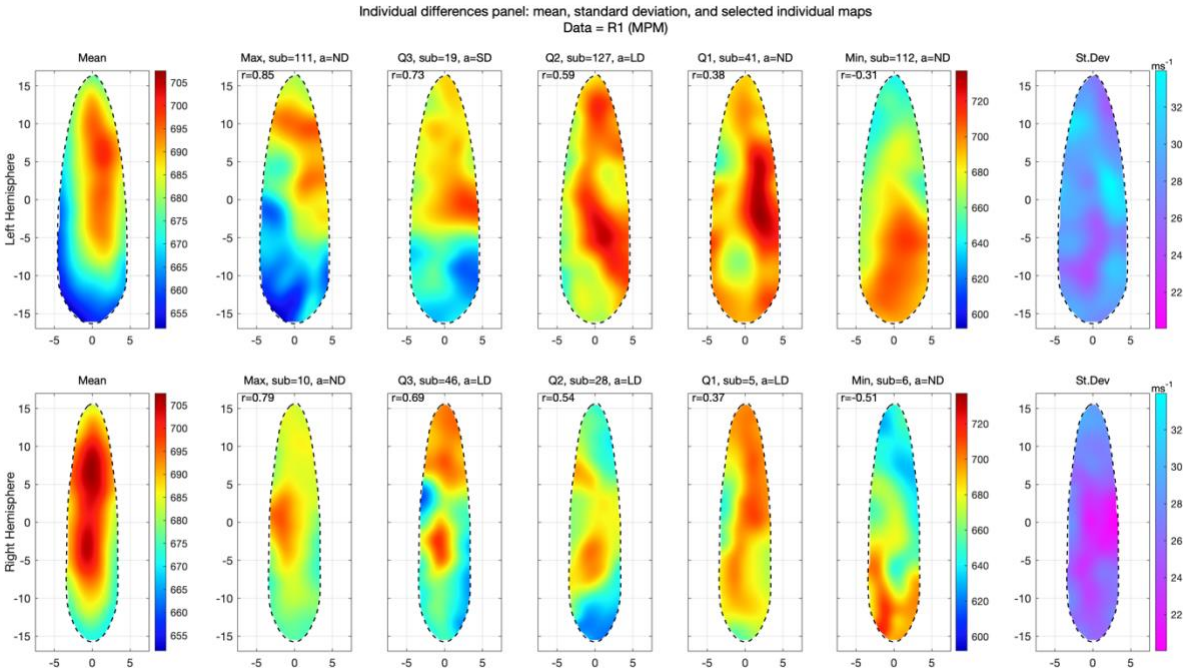

Figure 5.12*: Panel of individual differences in R1 data. Maps in the leftmost column correspond to group average maps. Maps from column two to column six represent the maps of five subjects sorted by descending similarity with the average map. The top and bottom rows correspond to the left and right hemispheres respectively. Colourscales were calculated separately for group average and individual maps to improve contrast. Maps in the right column represent the group standard deviation.*

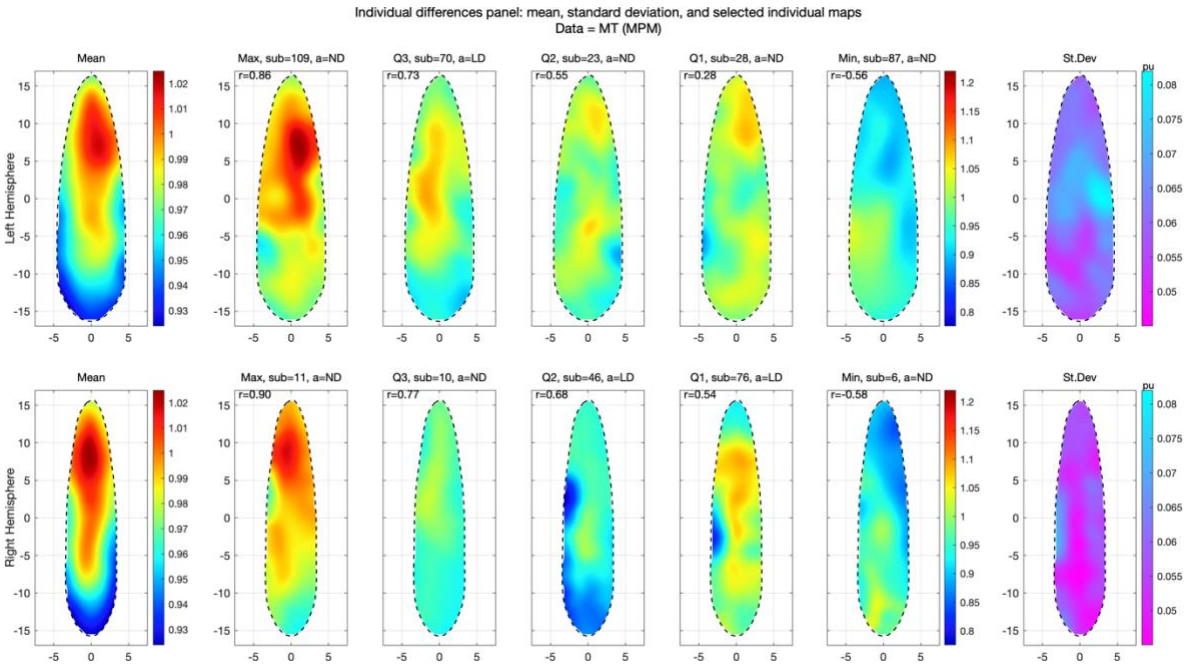

Figure 5.13*: Panel of individual differences in MT data. Maps in the leftmost column correspond to group average maps. Maps from column two to column six represent the maps of five subjects sorted by descending similarity with the average map. The top and bottom rows correspond to the left and right hemispheres respectively. Colourscales were calculated separately for group average and individual maps to improve contrast. Maps in the right column represent the group standard deviation.*

5.3.2.3 Tonotopy

Average tonotopic maps obtained by combining non-duplicated gyri with their putative homologous region within partially duplicated gyri (Figure 5.14) appeared nearly identical to the average maps obtained with only non-duplicated gyri (Figure 5.2), substantiating a possible correspondence between individual morphological landmarks and function across individuals with different gyral morphologies. More specifically, phase maps were characterised by an anteromedial-to-posterolateral high-to-low gradient that was remarkably consistent across the top 80% of individuals most similar to the group average. Average maps of the bottom 20% of subjects appeared to shift anteriorly, with frequency preference between approximately 300 Hz to 600 Hz shifting from the posterior half of the gyrus to its centre, along with high-frequency preference almost disappearing from the

anteromedial quadrant. Phase agreement across individuals decreased anteromedially in both hemispheres, following gradients similar to those of phase maps. More specifically, regions of low inter-subject agreement corresponded to regions of middle to high-frequency preference (i.e. above approximately 1000 Hz), while posterolateral preference for mid-low frequencies was more consistent across individuals. Average tonotopic magnitude (Figure 5.15) also decreased anteromedially, which could be the result of a lower inter-subject phase agreement in this region or an actual decrease in individual magnitude. Maps of the average magnitude of individual Fourier vectors (i.e. as opposed to the magnitude of the average vector, see Figure 5.16) revealed that individual magnitude is indeed lowest anteromedially even without accounting for cross-subject phase disagreement[22]. The average centre frequency maps of pRF tuning functions (Figure 5.17) largely displayed the same characteristics described for average phase maps, albeit with a more prominent anteromedial region centred around the mid-high frequency range. Similarly, tuning widths were greater anteromedially and decreased posterolaterally. Gradients' shape and direction appeared consistent across the whole sample, with increased variability around regions of wider tuning widths. However, the coefficient of variation (i.e. the ratio of tuning function width and centre) was relatively constant across the whole gyrus in both hemispheres (Figure S8), with a mean of 92% and a standard deviation of 2%. In other words, tuning width gradients were overall constant across the gyrus once changes in centre frequency were taken into account.

[22] Even within subjects, this effect could still be enhanced by phase disagreement between each of the four EPI acquisitions.

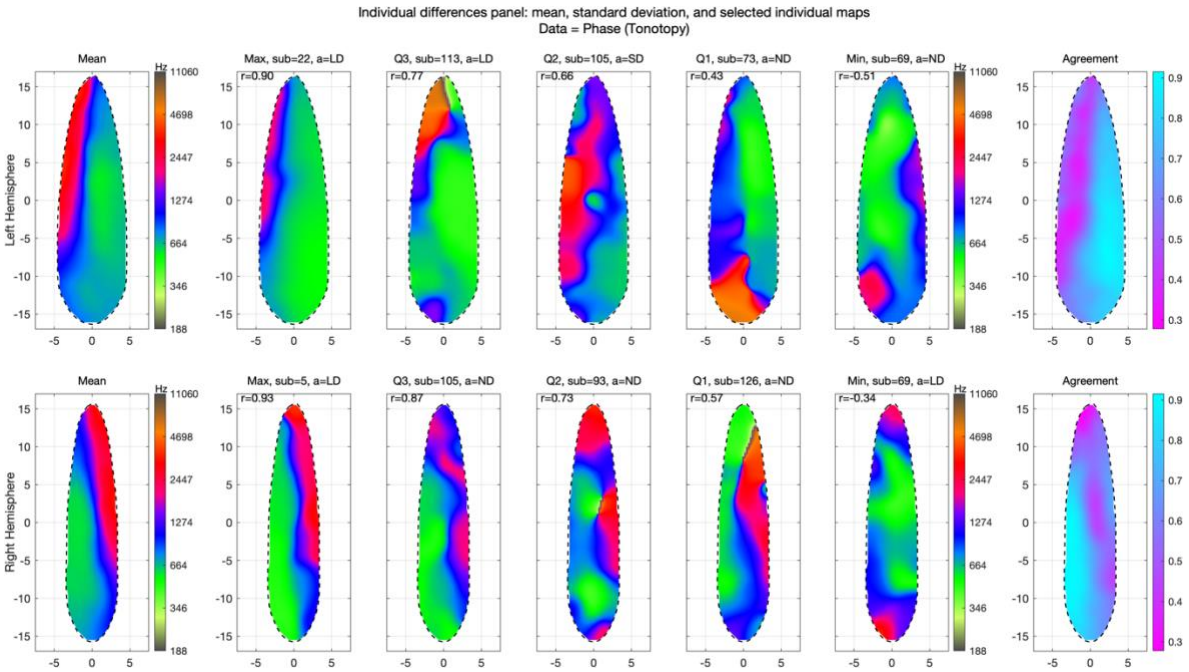

Figure 5.14*: Panel of individual differences in tonotopic phase data. Maps in the leftmost column correspond to group average maps. Maps from column two to column six represent the maps of five subjects sorted by descending similarity with the average map. The top and bottom rows correspond to the left and right hemispheres respectively. Maps in the right column represent cross-subject phase agreement.*

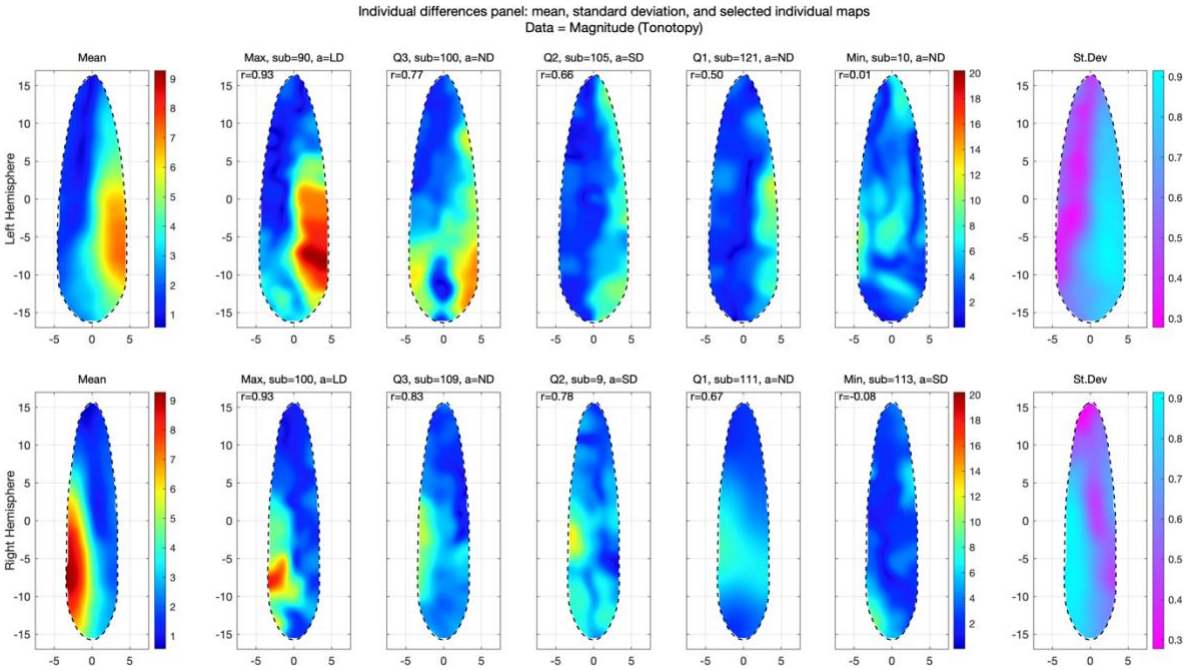

Figure 5.15*: Panel of individual differences in tonotopic magnitude data. Maps in the leftmost column correspond to group average maps. Maps from column two to column six represent the maps of five subjects sorted by descending similarity with the average map. The top and bottom rows correspond to the left and right hemispheres respectively. Maps in the right column represent cross-subject phase agreement.*

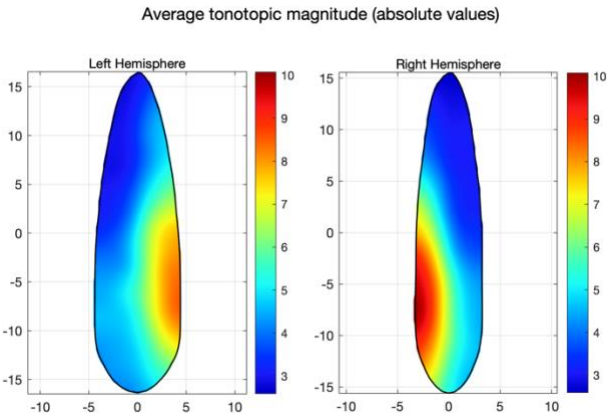

***Figure 5.16**: Group average maps of the absolute values of tonotopic magnitude, i.e. without accounting for the loss in magnitude due to cross-subject divergences in phase. These maps indicate that the lower anteromedial magnitude in average maps (Figure 5.15) is not solely due to cross-subject phase disagreement.*

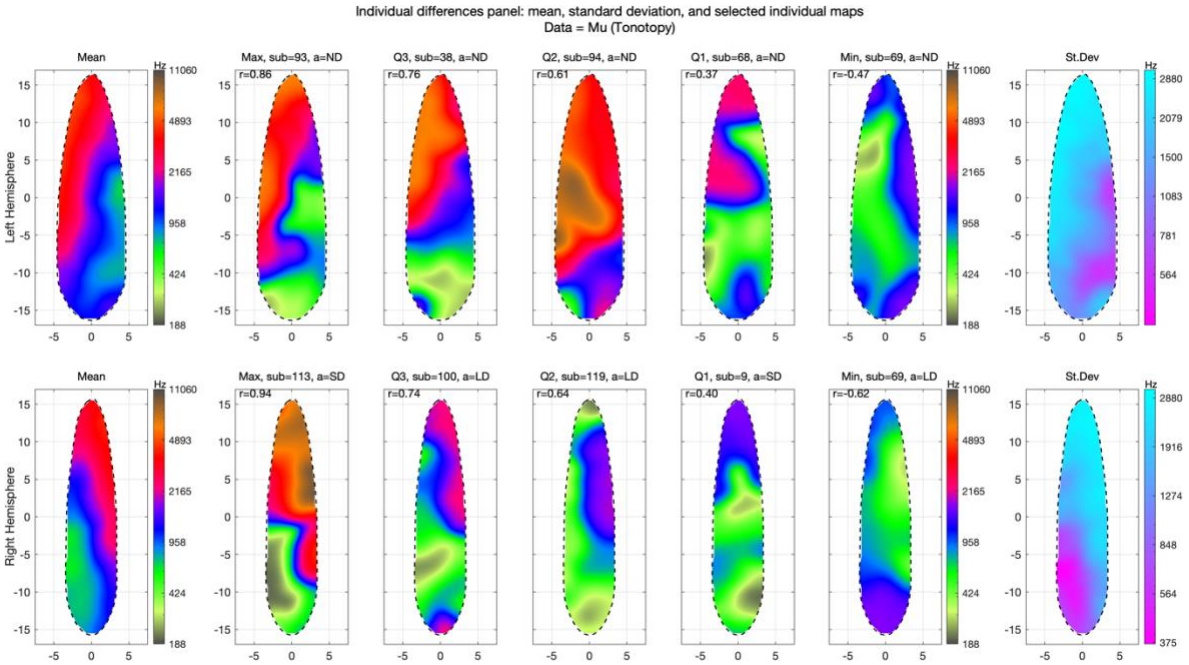

***Figure 5.17**: Panel of individual differences in pRF centre frequencies. Maps in the leftmost column correspond to group average maps. Maps from column two to column six represent the maps of five subjects sorted by descending similarity with the average map. The top and bottom rows correspond to the left and right hemispheres respectively. Maps in the right column represent the group standard deviation.*

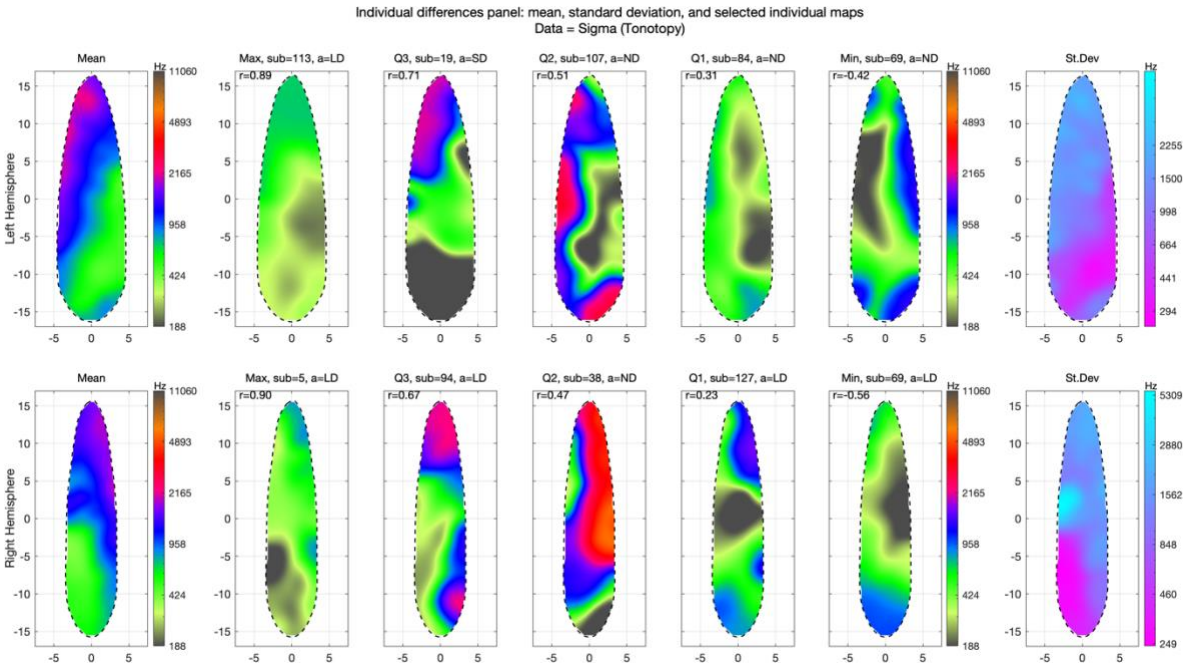

Figure 5.18*: Panel of individual differences in pRF tuning widths. Maps in the leftmost column correspond to group average maps. Maps from column two to column six represent the average maps of five sub-groups of subjects sorted by descending similarity with the average map. The top and bottom rows correspond to the left and right hemispheres respectively. Maps in the right column represent the group standard deviation.*

5.3.2.4 Differences in tonotopy and cortical myelination across cytoarchitectonic regions

The probabilistic cytoarchitectonic maps obtained by combining non-duplicated gyri and the optimal sections of duplicated gyri (Figure 5.19) were almost identical to those of non-duplicated gyri, which could be expected given the small number of duplications in the sample (one for the left hemisphere, two for the right hemisphere), but also the similar cytoarchitecture of anterior duplications and non-duplicated gyri (Figure 5.9). Most cytoarchitectonic regions showed good agreement across subjects, with Te1.0, Te1.1, and Te2.1 showing overlapping areas across 9/10 or 10/10 subjects in both hemispheres. The overall topography appeared to be the same across both hemispheres.

To further investigate the properties of these regions using the in-vivo dataset, for each subject, the weighted averages of R1, MT, tonotopic magnitude, and cortical thickness

within each cytoarchitectonic region were calculated using the overlap data as weights and compared using a one-way ANOVA and post-hoc Tukey's test (Figure 5.20). P-values were further corrected to control the overall FDR of all comparisons across hemispheres, regions, and datasets. There was a significant difference in MT across both hemispheres (left hemisphere: $F(2,171) = 4.78$, $p = 0.001$; right hemisphere: $F(2,171) = 9.96$, $p < 0.001$), with Te1.1 showing significantly higher MT values (left hemisphere: 0.028 ± 0.02 p.u., $p_{FDR} = 0.024$, right hemisphere: 0.033 ± 0.017 p.u., $p_{FDR} < 0.001$). However, there were no significant differences in R1 data between regions. The tonotopic magnitude was also significantly different across cytoarchitectonic regions in both hemispheres (left hemisphere: $F(2, 162) = 36.24$, $p < 0.001$; right hemisphere: $F(2, 162) = 86.77$, $p < 0.001$). Post-hoc tests revealed the same patterns of pairwise differences in tonotopic magnitude in both hemispheres, namely that Te1.0 had significantly higher values than Te1.1 (left hemisphere: 1.44 ± 0.77, $p_{FDR} < 0.001$; right hemisphere: 1.94 ± 0.79, $p_{FDR} < 0.001$), and Te2.1 had significantly higher values than both Te1.0 (left hemisphere: 1.36 ± 0.77, $p_{FDR} < 0.001$; right hemisphere: 2.48 ± 0.79, $p_{FDR} < 0.001$) and Te1.1 (left hemisphere: 2.8 ± 0.77, $p_{FDR} < 0.001$; right hemisphere: 4.42 ± 0.79, $p_{FDR} < 0.001$). Cortical thickness appeared to significantly differ only in the right hemisphere ($F(2,171) = 9.64$, $p < 0.001$), with cortex in Te2.1 being significantly thicker than both Te1.0 (0.11 ± 0.09 mm, $p_{FDR} = 0.008$) and Te1.1 (0.16 ± 0.09 mm, $p_{FDR} < 0.001$).

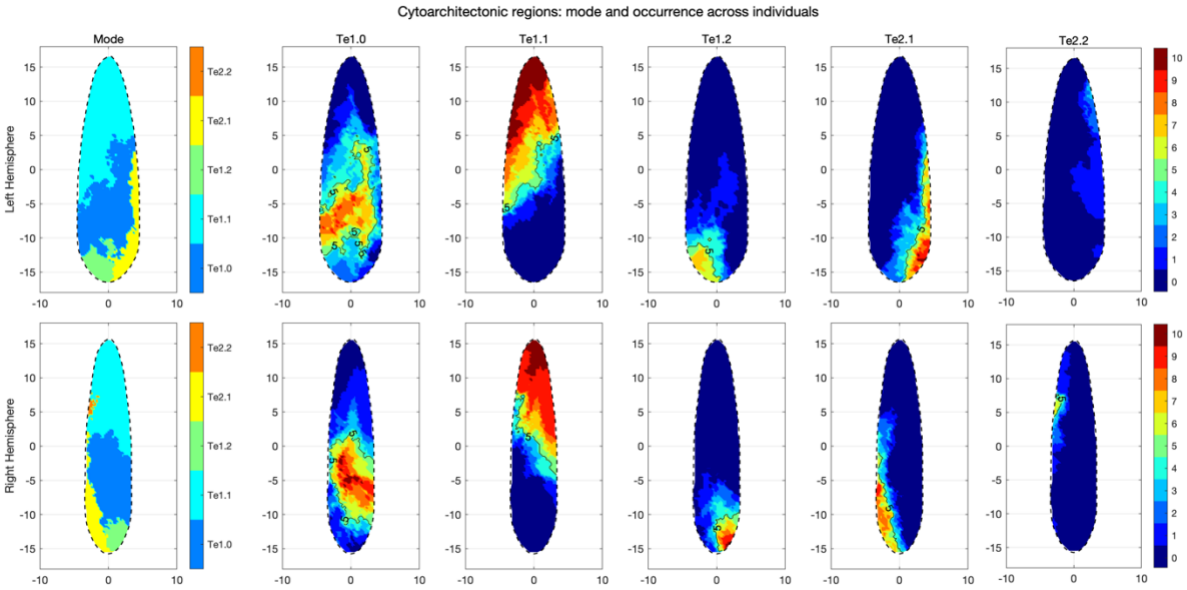

***Figure 5.19**: Probabilistic cytoarchitectonic regions within Heschl's gyrus obtained from 10 manually labelled post-mortem brain images (see 5.2.3.6). Regions were obtained by resampling gyri of the same morphological types onto a common surface and calculating the mode at each vertex. The number of brains for each hemisphere and morphology is indicated in the top-left corner of each graph.*

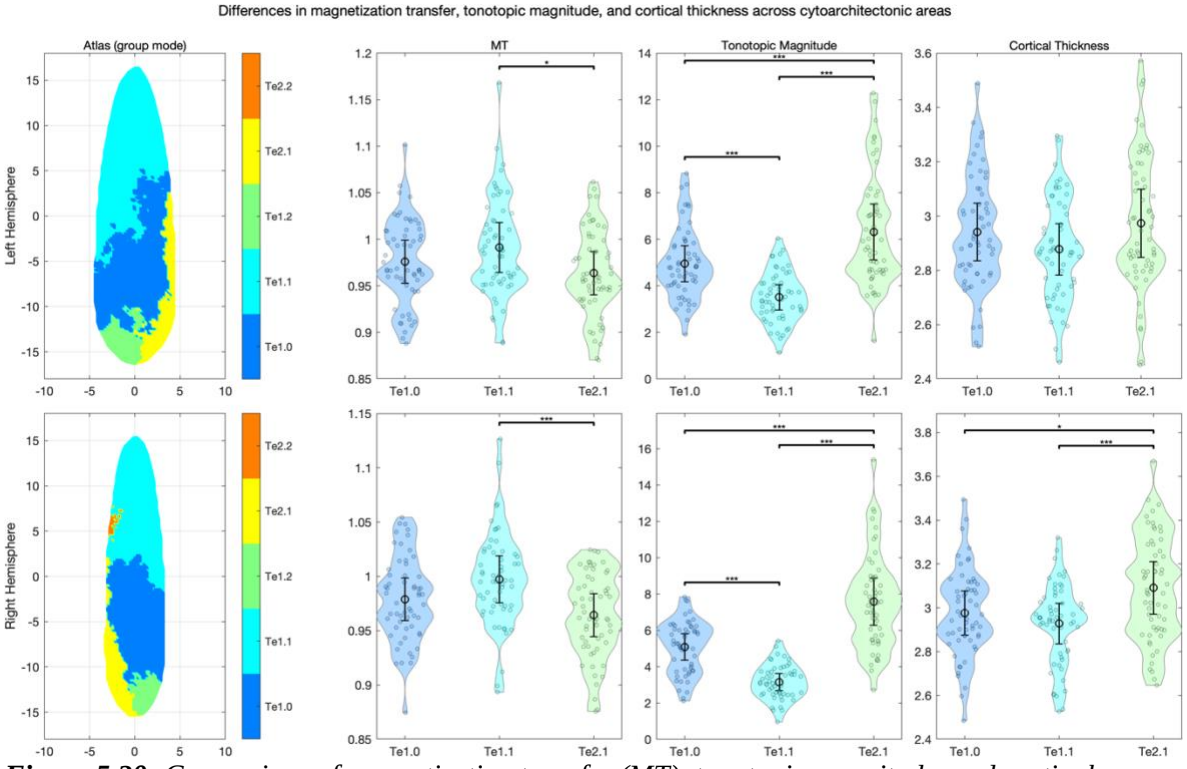

***Figure 5.20**: Comparison of magnetisation transfer (MT), tonotopic magnitude, and cortical thickness measures across three cytoarchitectonic regions: Te1.0, Te1.1, Te2.1. The first column represents the left and right cytoarchitectonic atlases. Columns two to four include jittered data points, violin plots indicating the data distributions, and error bars corresponding to the 95% confidence interval for the mean. Horizontal brackets above plots indicate statistically significant*

differences, with one, two, and three stars corresponding to an FDR-corrected p-value below 0.05, 0.01, and 0.001 respectively.

5.3.3 Individual cases

5.3.3.1 Alignment of tonotopy and R1

Examples of tonotopic mapping and R1 are reported in Figure 5.21 and Figure 5.22 to further explore the interplay of tonotopy, myelination, and morphology across individuals. Individuals in Figure 5.21 represent, for each hemisphere, the four individuals whose tonotopic map diverges the most from the average. In most of these cases, it was possible to identify a "V" shaped high-to-low-to-high gradient surrounding the medial extremity of HG and a region of peak R1 interposed between the high-frequency regions of this gradient. Interestingly, in the case of subject 6 (right hemisphere), although it was possible to identify the same specific pattern of juxtaposition of tonotopic gradients and peak R1, both parameters were equally shifted laterally. On the other hand, the tonotopic gradients of subject 69 (left hemisphere) were typically aligned around the medial extremity of the gyrus, but peak R1 was located posterolaterally. In all these cases (with the exception of subject 6), the regions of high-frequency preference fell mostly outside of the HG label, which might justify their low correlation with the group average. Furthermore, although most of these individuals possessed non-duplicated gyri, their shape deviated considerably from a typical oval shape, which might have affected the quality of their alignment. Conversely, gyri whose tonotopic gradients were best aligned with the group average (Figure 5.22) were mostly of the long-duplication type, with branches that formed typical elongated oval shapes. In most of these individuals, tonotopic gradients followed the expected high-to-low-to-high pattern around the medial half of the gyrus, which also

corresponded to regions of high R1. However, the posterior gradients towards high-frequency preference were not always clearly visible (e.g. subject 22, left hemisphere; subject 90, right hemisphere) and peak R1 was sometimes placed more laterally within the gyrus (e.g. subject 112, left hemisphere; subject 129, right hemisphere), disrupting the pattern. Nonetheless, at least within the label itself, particularly within the anterior branch of partially duplicated gyri, there was a clear anteromedial-to-posterolateral high-to-low tonotopic gradient across all subjects which, along with their streamlined shapes, would justify their high correlation with the group average.

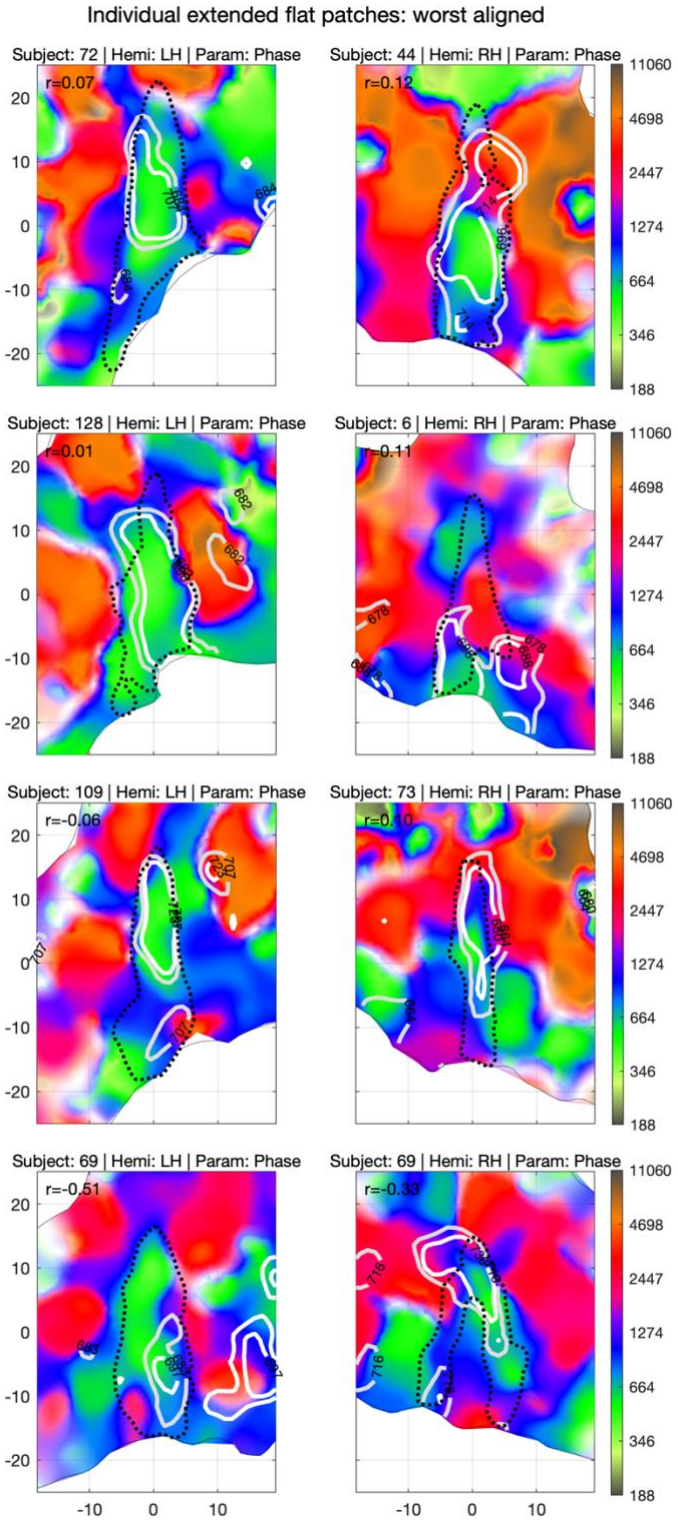

Figure 5.21*: Tonotopic phase maps of the 4 subjects whose HG maps are the worst aligned with the group average. Each map corresponds to the flattened surface of a region of the superior temporal plane surrounding Heschl's gyrus (marked by a dotted black line). White and grey contour lines represent respectively the 95th and 90th percentiles of R1 data. The left and right columns correspond to the left and right hemispheres.*

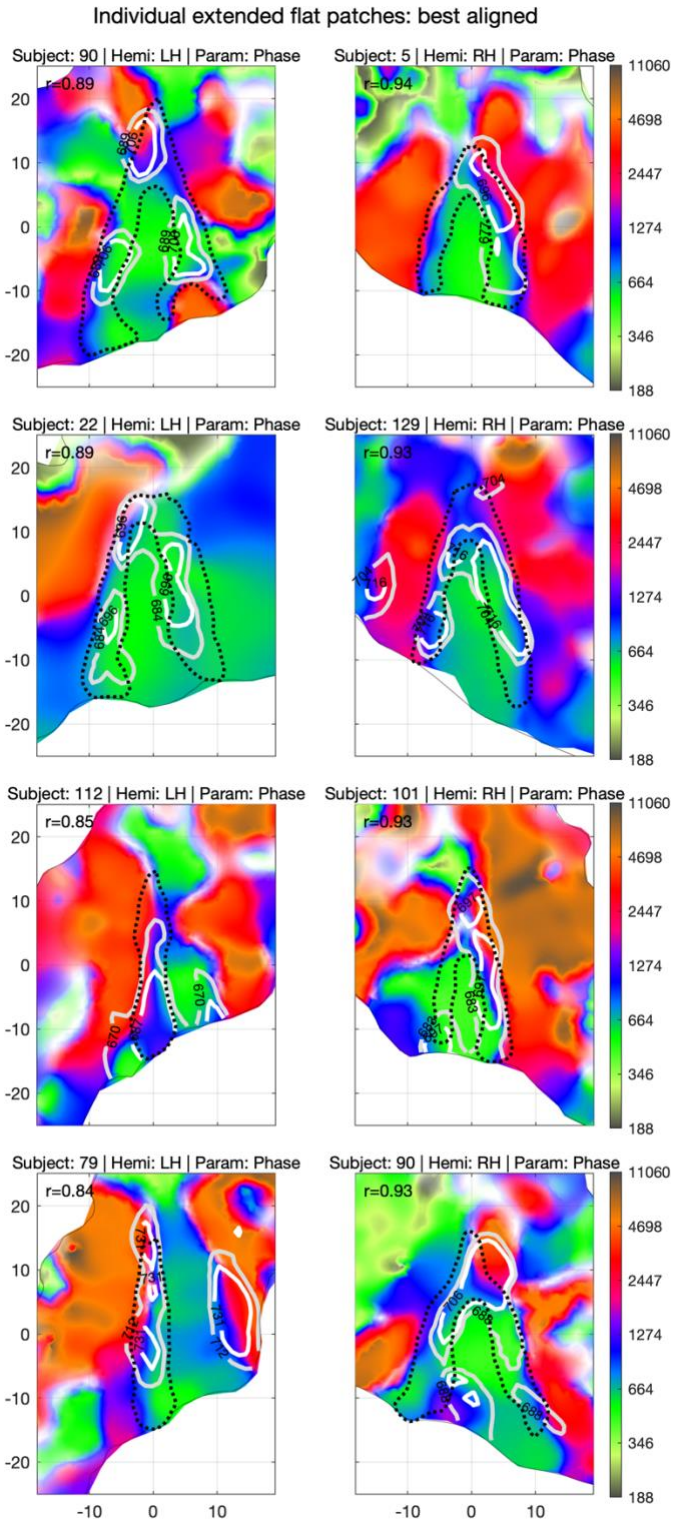

Figure 5.22*: Tonotopic phase maps of the 4 subjects whose HG maps are the best aligned with the group average. Each map corresponds to the flattened surface of a region of the superior temporal plane surrounding Heschl's gyrus (marked by a dotted black line). White and grey contour lines represent respectively the 95th and 90th percentiles of R1 data. The left and right columns correspond to the left and right hemispheres.*

5.3.3.2 Intra-subject variability

To further investigate the variability of tonotopic map alignment across poorly aligned subjects and rule out potential issues with registration or motion artefacts, an additional average map was calculated for each stimulus condition (i.e. sweep up, sweep down), which include two runs each.

Subject 69 (Figure 5.25), whose maps had the poorest alignment with the group average in both hemispheres, appeared extremely consistent across conditions. These maps also appeared very typical once the region surrounding HG was taken into account, just not within the boundaries of HG itself. The right tonotopic map of subject 6 (Figure 5.23), which had a correlation of -0.11 with the group average, also appeared to be consistent across blocks, albeit with a shift towards higher frequencies for the sweep-up condition. The previously observed lateral displacement of the v-shaped high-to-low-to-high gradient for this map was also consistent across conditions. In fact, like subject 6, several other individuals presented a similar lateral displacement of the tonotopic gradients that were consistent across conditions. For instance, subject 44 (Figure 5.24) had poor alignment with the group average in the right hemisphere, with v-shaped tonotopic gradients centred around the middle of the gyrus rather than the medial extremity. However, there were several other cases of consistent tonotopic gradient "lateralisation" in subjects that were strongly positively correlated with the group average (Figure 5.26). Most of these cases consisted of partially duplicated gyri in the right hemisphere, with v-shaped patterns centred around 5 to 10 mm medially of the duplication point. Some of these maps also appeared fairly atypical, lacking clear v-shaped gradient reversals (e.g. subject 28, 78) or

presenting regions of low-frequency preference around the medial apex of HG (e.g. subject 12, 28, 78, 119).

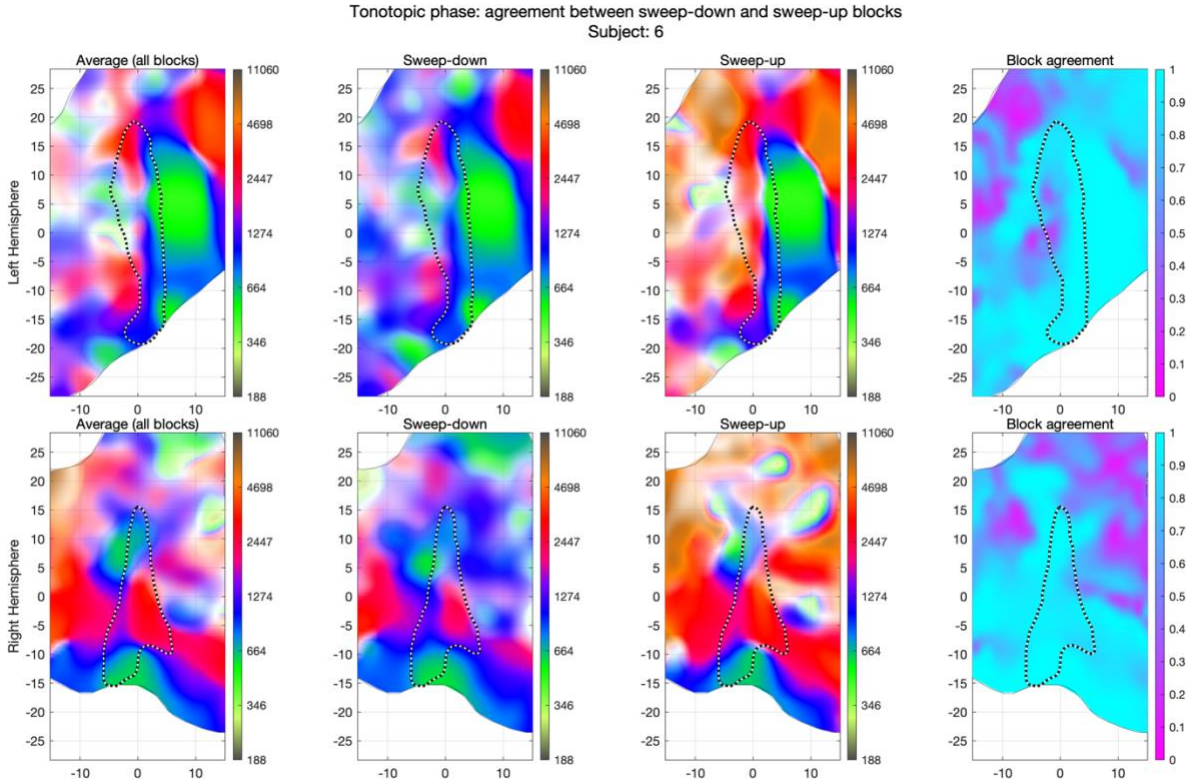

Figure 5.23*: Individual example (subject ID: 6) of average tonotopic maps across conditions. Each map corresponds to a flattened region of the supratemporal plane centred at Heschl's gyrus (marked by a dashes black and white line). The top and bottom rows correspond to the left and right hemispheres respectively. The first column includes maps of the average of both conditions (4 runs total), while columns two and three correspond to the averages of the sweep-down and sweep-up conditions (2 runs each). Maps in column four represent the phase agreement across conditions from 0 (opposite phase) to 1 (same phase).*

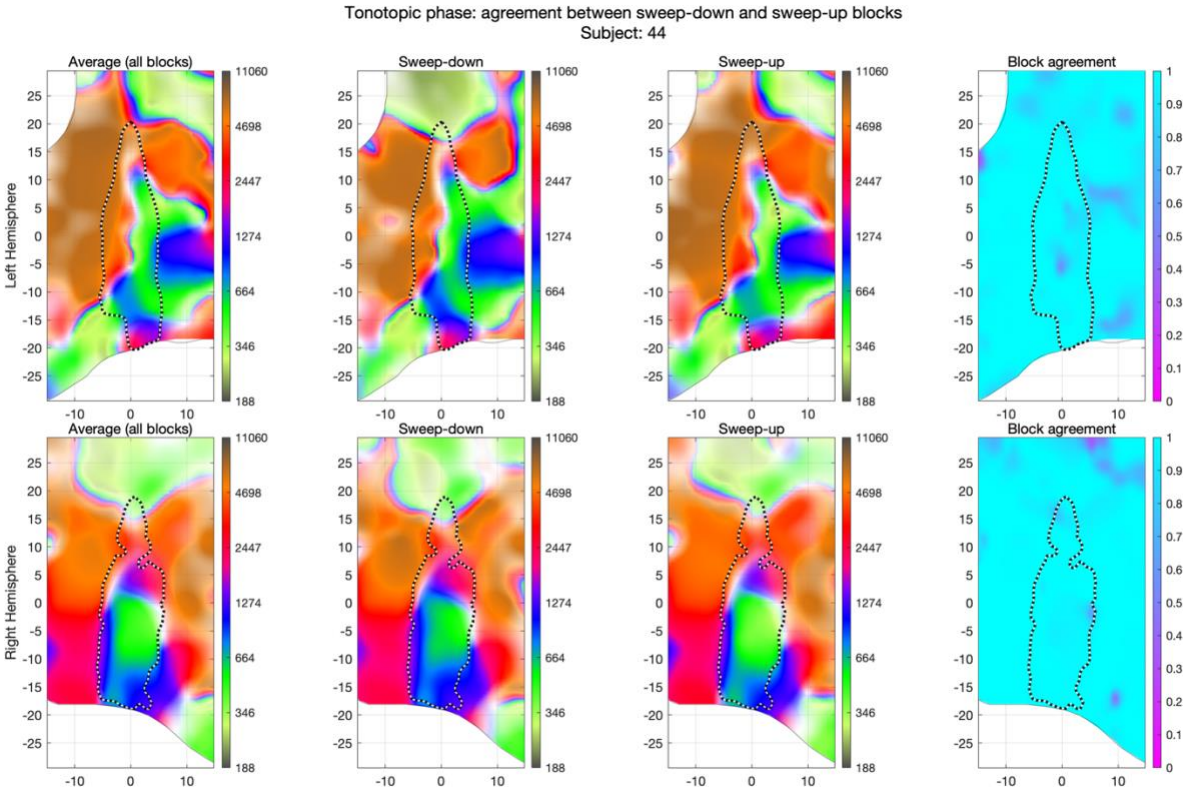

Figure 5.24*: Individual example (subject ID: 44) of average tonotopic maps across conditions: subject 44. Patches correspond to a flattened region of the supratemporal plane centred at Heschl's gyrus (marked by a dashes black and white line). The top and bottom rows correspond to the left and right hemispheres respectively. The first column includes maps of the average of both conditions (4 runs total), while columns two and three correspond to the averages of the sweep-down and sweep-up conditions (2 runs each). Maps in column four represent the phase agreement across conditions from 0 (opposite phase) to 1 (same phase).*

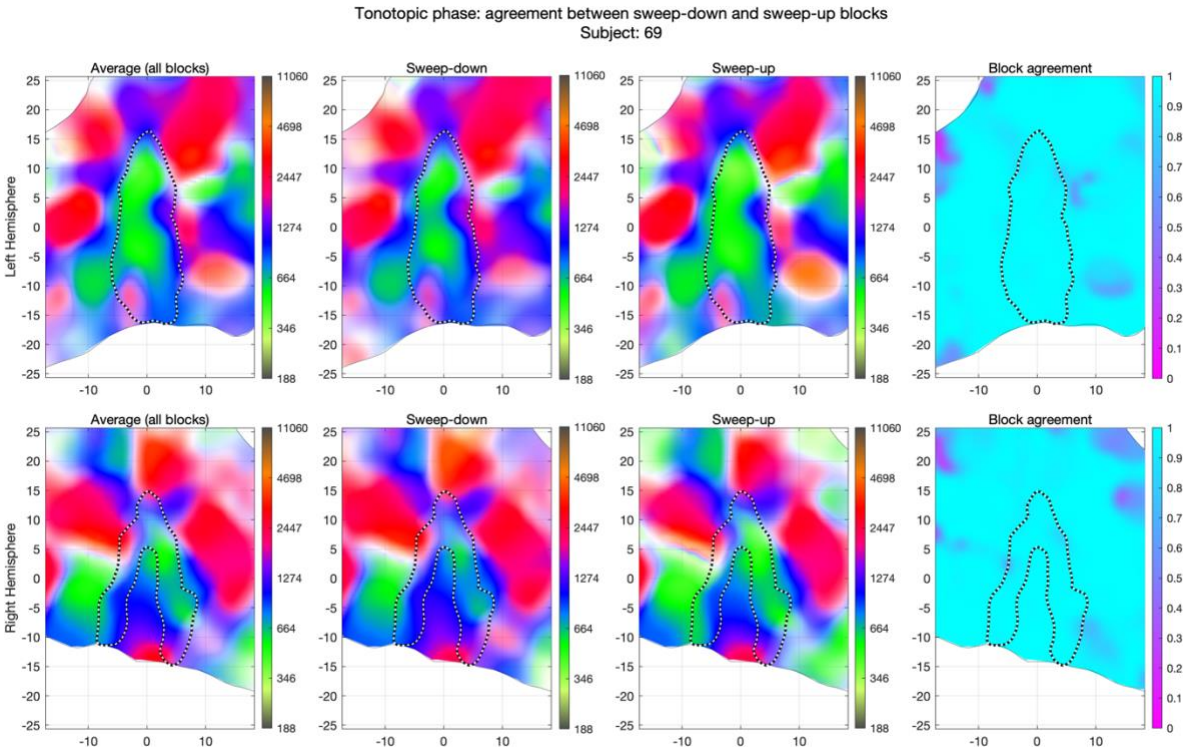

Figure 5.25*: Individual example (subject ID: 69) of tonotopic maps across conditions: subject 69. Patches correspond to a flattened region of the supratemporal plane centred at Heschl's gyrus (marked by a dashes black and white line). The top and bottom rows correspond to the left and right hemispheres respectively. The first column includes maps of the average of both conditions (4 runs total), while columns two and three correspond to the averages of the sweep-down and sweep-up conditions (2 runs each). Maps in column four represent the phase agreement across conditions from 0 (opposite phase) to 1 (same phase).*

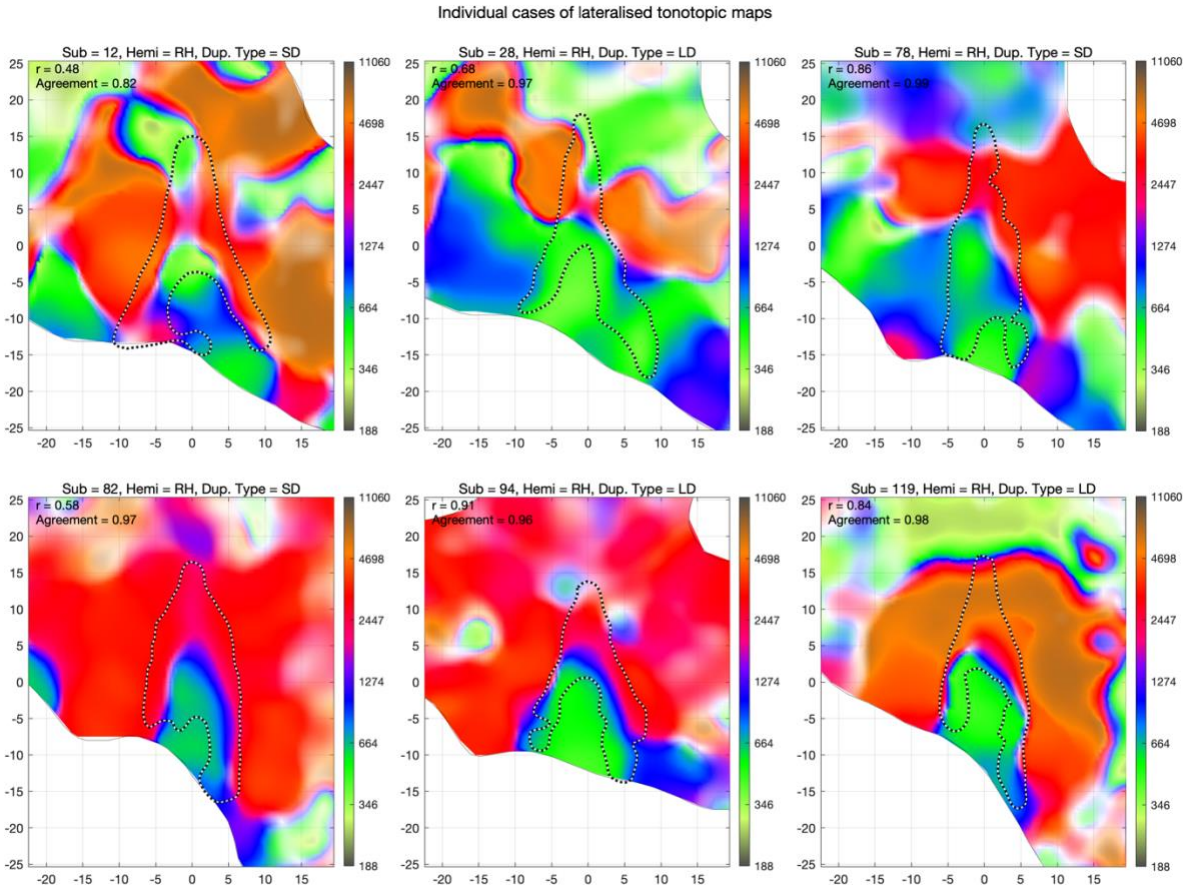

Figure 5.26*: Individual examples of atypical tonotopic gradient configurations or location with respect to Heschl's gyrus. Patches correspond to a flattened region of the supratemporal plane centred at Heschl's gyrus (marked by a dashes black and white line). Titles above each map indicate the subject ID, hemisphere, and duplication type (ND = no duplication; SD = short duplication; LD = long duplication. Spearman correlations with the group average ("r") and average agreement across conditions ("Agreement") are indicated in the top left corner of each map.)*

5.3.4 Comparison with curvature-based analysis

Group average and standard deviation maps obtained using the pipeline described in this chapter were overall comparable to those obtained with *freesurfer*'s curvature-based alignment. The average tonotopic phase (Figure 5.27) displayed the same high-to-low anteromedial-to-posterolateral gradients across both methods, albeit with a minor shift towards higher frequencies using the new pipeline. Similarly, cross-subject phase agreement maps were comparable across methods. Average R1 (Figure 5.28) maps also

displayed similar gradients for both methods. However, regions of peak R1 magnitude obtained with curvature-based alignment appeared more evenly distributed along the length of the gyrus, while the novel approach led to higher values towards the medial half of the gyrus. This difference was also apparent in average MT maps (Figure 5.29). Overall levels of inter-subject variability of R1 and MT appeared similar across methods, although their distribution across the gyrus followed different patterns. More specifically, the new approach led to peaks of increased variability mainly towards the posterior edge of the gyrus for both R1 and MT in both hemispheres, while curvature-based alignment did not appear to follow any specific pattern.

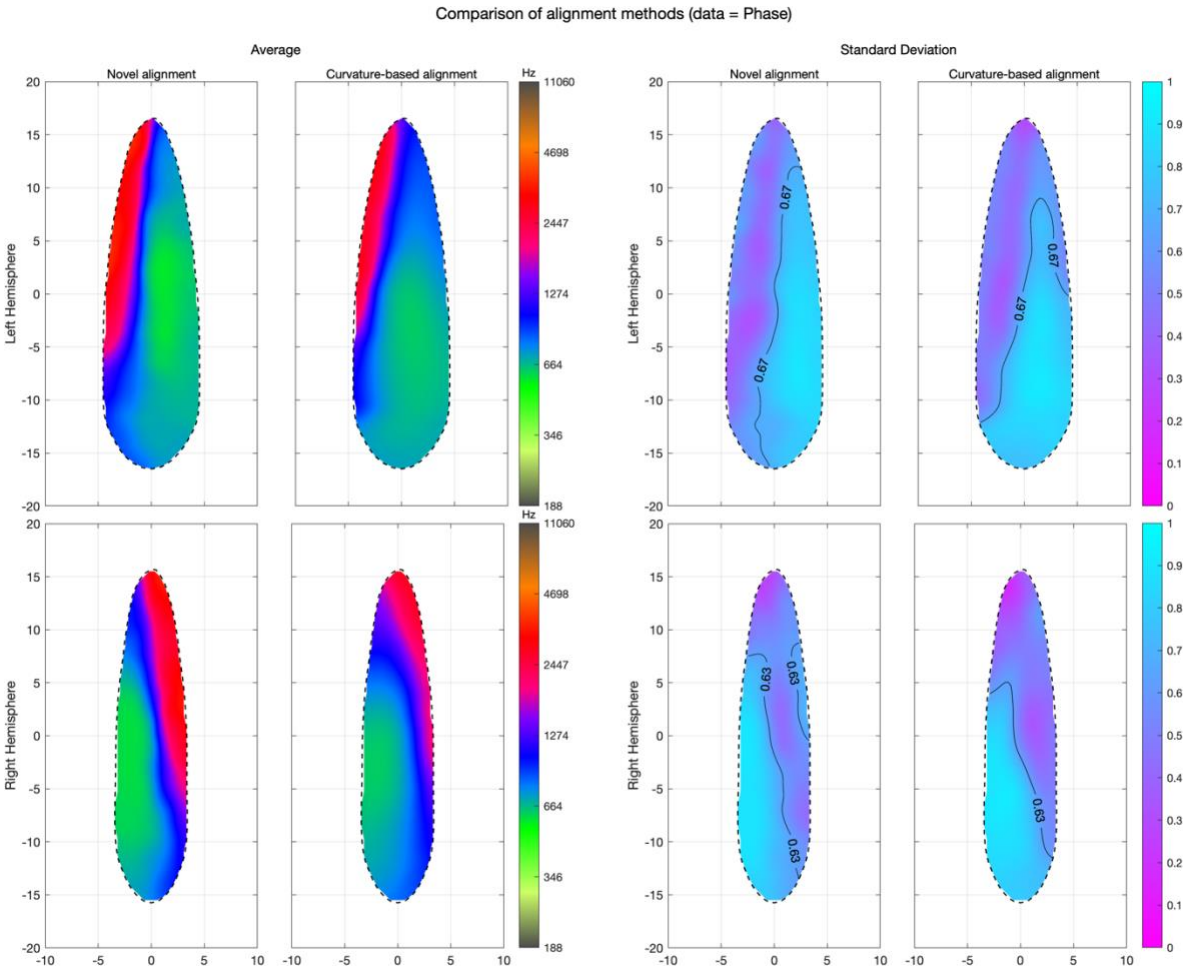

***Figure 5.27**: Comparison of the novel alignment approach and curvature-based alignment. The four plots on the left half of the figure represent the group average maps of the tonotopic phase*

obtained with the novel approach (on the left) and curvature-based alignment (on the right). Similarly, the four plots on the right half of the figure represent cross-subject phase agreement maps for both methods following the same layout. Black contour lines mark the median value calculated separately for each hemisphere. The top and bottom rows correspond to the left and right hemispheres respectively.

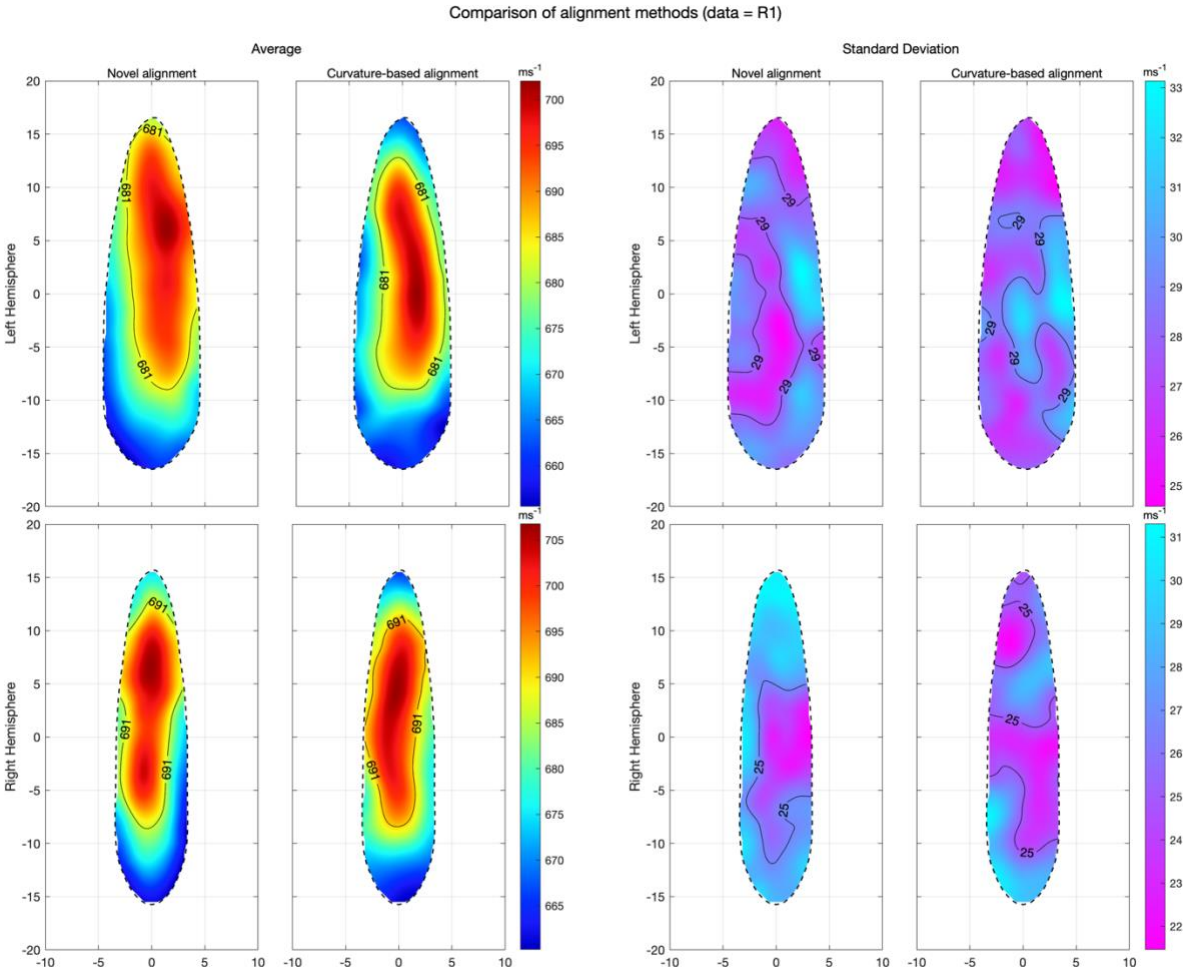

***Figure 5.28**: Comparison of the novel alignment approach and curvature-based alignment. The four plots on the left half of the figure represent the group average maps of R1 obtained with the novel approach on the left and curvature-based alignment on the right. Similarly, the four plots on the right half of the figure represent group standard deviation maps for both methods following the same layout. Black contour lines mark the median value calculated separately for each hemisphere. The top and bottom rows correspond to the left and right hemispheres respectively.*

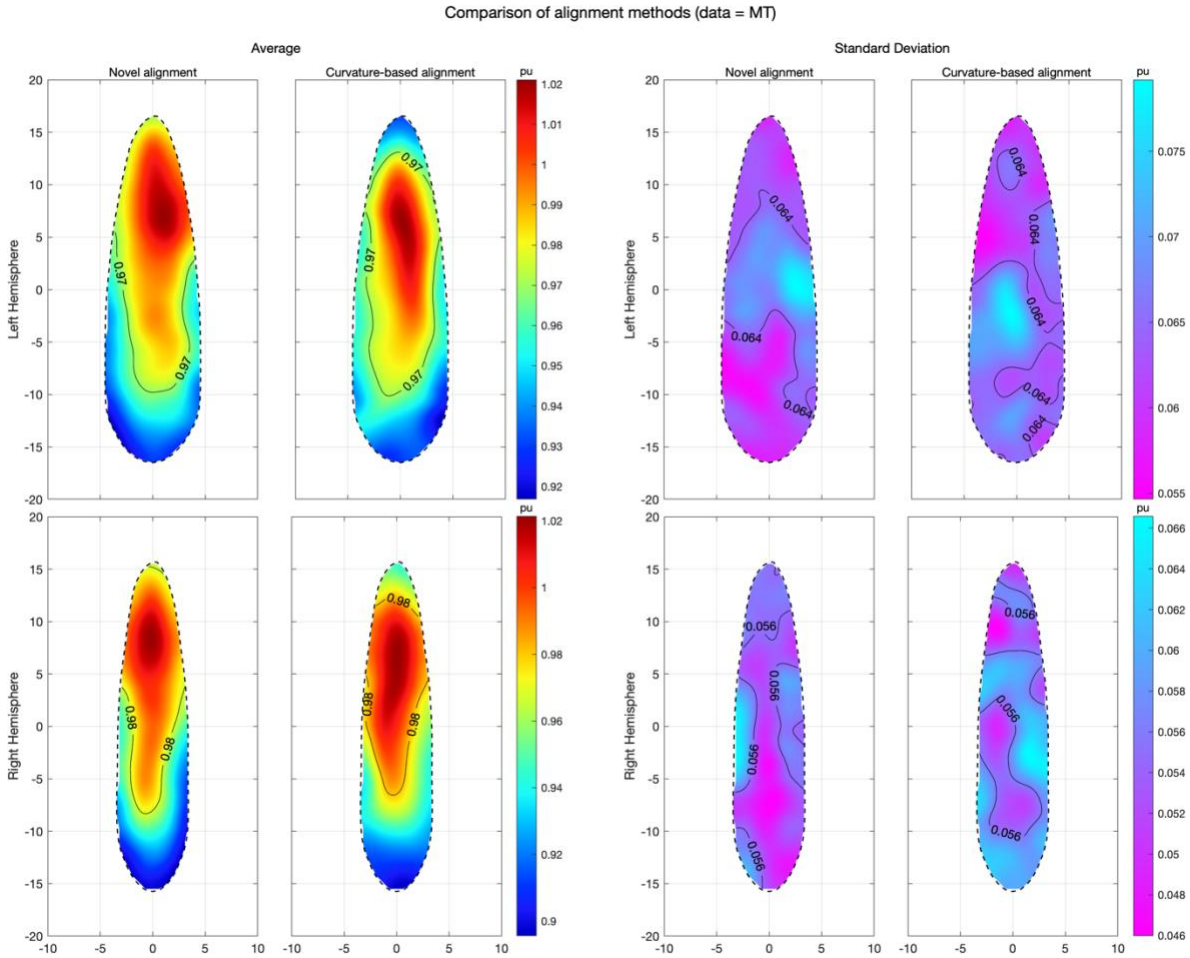

***Figure 5.29**: Comparison of the novel alignment approach and curvature-based alignment. The four plots on the left half of the figure represent the group average maps of MT obtained with the novel approach (on the left) and curvature-based alignment (on the right). Similarly, the four plots on the right half of the figure represent group standard deviation maps for both methods following the same layout. Black contour lines mark the median value calculated separately for each hemisphere. The top and bottom rows correspond to the left and right hemispheres respectively.*

5.4 Discussion

The aim of the analyses presented in the chapter was to provide an extensive description of the individual differences in HG morphology, myelination, and tonotopy in humans, and how they relate to each other. This information was used to determine whether macro-anatomical landmarks alone could be sufficient indicators of homologies in cortical function and structure across individuals. After locating a potential target landmark, putatively homologous regions across individuals were morphed onto a common template

surface and averaged. The resulting tonotopic and quantitative MRI maps within HG were compared with those obtained with curvature-based alignment.

5.4.1 Differences and homologies across morphotypes

5.4.1.1 Tonotopy

Across all morphotypes, average tonotopic maps within HG included one high-low frequency gradient that extended anteromedially to posterolaterally (Figure 5.2). However, in gyri with long duplications, the onset of a reversal towards high frequencies could be observed posteriorly within the surface of the gyrus, while in gyri with short or no duplications, this reversal fell outside the boundaries of HG (see examples in Figure 5.22). The association between tonotopy and anatomical landmarks was also reflected in an increase in tonotopic spatial cross-correlation between single gyri and the anterior branches of duplicated gyri. In other words, based solely on tonotopic data, the anterior border of HG appeared to mark functionally homologous regions across different HG morphologies, while posterior borders of gyri with different morphologies did not. This is in partial contrast with a prior study by Da Costa et al. (2011b), who claimed that high-low-high tonotopic gradients always extend across the entire surface of HG, including any posterior duplication. However, the current study only focused on the most anterior full duplication (i.e. including all regions of partial duplications), a choice that was based on prior myelo- and cytoarchitectonic evidence that the human PAC is located in this region (Hackett et al., 2001; Rademacher et al., 1993). Consequently, non-duplicated gyri and the anterior duplications of fully duplicated gyri were combined into a single category, excluding posterior duplications from analyses. Nonetheless, even in gyri with a short partial duplication, there was no clear gradient reversal spanning across the whole surface of HG,

suggesting that a reversal might occur around the posterior border of these gyri and progress into the planum temporale. Although this may seem a minor detail, tonotopic reversals have been used - somewhat controversially - to infer the location of the underlying auditory fields in humans (Baumann et al., 2013; Besle et al., 2019; Saenz & Langers, 2014). For instance, based on their observations, Da Costa et al. (2011b) suggested that a border between the human homologues of macaque's A1 and R fields is systematically located on the crown of non-duplicated gyri or the intermediate or full posterior sulci of duplicated gyri. However, evidence from the current study would not support that statement. Rather, it supports the notion of assigning not only full posterior HG duplications to the planum temporale but also partial posterior duplications.

5.4.1.2 Cytoarchitecture

Cytoarchitectonic data (Figure 5.9) also supported the notion that anterior branches of partially duplicated gyri are homologous to non-duplicated gyri. More specifically, the topography of Te1.0, Te1.1, Te 1.2, and Te2.1 was remarkably similar between gyri with no duplications and anterior branches of partially duplicated gyri. Conversely, Te2.2 was virtually absent from non-duplicated gyri but occupied a large portion of posterior duplications of CSD. Additionally, while the tonotopic gradients of gyri with short or no duplication appeared fairly similar, this was not the case for cytoarchitectonic data. Specifically, Te2.2 occupied a large portion of the posterior half of the common stem region, not just the posterior branch, indicating a possible homology across common stem duplications, regardless of the size of the intermediate sulcus. However, since only one gyrus of this type was included in the sample, more data are needed to corroborate this finding.

5.4.1.3 Quantitative MRI

The homologies of myelin-sensitive quantitative R1 and MT across morphotypes were not as straightforward as tonotopy or cytoarchitecture. Peaks in R1 and MT were shifted posteriorly in both non-duplicated gyri and the common stem of gyri with short duplications, but there was no clear homology with respect to CSDs of the long type (Figure S5). Additionally, spatial cross-correlation analyses were not fully suited for these datasets, given their correlation with curvature (Dick et al., 2012; Sereno et al., 2013; Wähnert et al., 2014). Even after removing the effect of curvature, intermediate sulci appeared systematically less myelinated than gyri (Figure S4), which influenced the calculation of spatial cross-correlations between duplicated and non-duplicated gyri. However, by calculating the sum of squared differences instead of spatial cross-correlations (Figure S7) the posterior branches of duplicated gyri appeared the most dissimilar to single gyri, which is in line with tonotopic and cytoarchitectonic data.

Furthermore, it is questionable whether removing the effect of curvature on R1 and MT data using linear regression is appropriate when comparing gyri with different morphologies. On the one hand, examining local variations in myelin density that exceed what would be predicted by curvature can be used to identify the potential location of myeloarchitectonically-defined regions such as the auditory core (Dick et al., 2012) in gyri with comparable morphologies. On the other hand, the correlation between curvature and myelination could be indicative of the systematic differences observed in the functional properties of gyri and sulci (Jiang et al., 2021; Warrier et al., 2009b).

5.4.2 Co-localisation of curvature, R1, and tonotopic gradients

Across several individual examples (Figure 5.21; Figure 5.22), it was possible to identify regions of increased myelination in the medial half of HG, which also corresponded to a region of low-frequency preference surrounded anteriorly, medially, and posteriorly by regions of high-frequency preference. Interestingly, a lateral shift in peak R1 also corresponded to a lateral shift in tonotopic gradients across multiple individual cases, indicating a possible relationship between these measures that is stronger than the position relative to the boundaries of HG. Furthermore, this was true for both best- and worst-aligned individual tonotopic maps. In fact, when the area surrounding HG was taken into account, the were no obvious differences in the R1 and tonotopic maps of best- or worst-aligned gyri. This is likely a consequence of the relatively low resolution of tonotopic data (i.e. 3 mm^3 isometric) and the sensitivity of spatial cross-correlation to small but global shifts in tonotopic gradients. For instance, in the tonotopic maps of the participant who had the worst-aligned tonotopic maps in both hemispheres (i.e. subject 69), the anteromedial-posterolateral high-low gradient is not visible within the boundaries of HG itself, but it's clearly visible by expanding the boundaries of the gyrus anteromedially by just a few millimetres. Therefore, although gyral landmarks (i.e. anterior branches of CSDs) represent a good approximation[23] for the alignment of tonotopic maps, introducing some flexibility would improve the overall alignment of subjects whose curvature does not match the expected tonotopic gradients. Notably, these individual differences in tonotopic gradients

[23] The overall median Spearman correlation between individual and group-average maps was 0.58. The phase maps of each subject were correlated with the group average calculated with all remaining subjects.

with respect to HG morphology were very consistent within subjects across the 4 runs, indicating these differences do not arise from differences in alignment or poor quality data.

5.4.3 Cross-subject alignment

Interestingly, group-average maps obtained with the novel pipeline and Freesurfer were remarkably similar for both tonotopy and MPM data, even though Freesurfer tends to consider all parts of a partial duplication as a single gyrus (see e.g. Figure 5.31). It is possible that with a big enough sample, variability in HG morphology does not have a noticeable effect on the average gradients. Therefore, curvature-based alignment could be considered a good-enough approximation if the only goal is to obtain an average map of a large sample.

There were however small differences across methods in the estimation of inter-subject variability. Specifically, inter-subject variability estimated with the novel alignment was slightly lower than those obtained with Freesurfer for R1, MT, and tonotopic phase in the right hemisphere and MT in the left hemisphere (Figure 5.30). Conversely, Freesurfer estimated slightly lower inter-subject variability for R1 in the left hemisphere. It is possible that specifying an explicit anatomical prior (i.e. anterior duplication of CSDs) had a more consistent -albeit small- positive effect on cross-subject alignment in the right hemisphere, which had a greater occurrence of partial duplications. The different effects of the alignment method on R1 across hemispheres (i.e better alignment with Freesurfer in the left hemisphere and worse in the right hemisphere) could be instead due to the sensitivity of R1 not only macromolecular content (e.g. myelin) but also iron. Variations in local vasculature could therefore increase signal variability across individuals, without necessarily reflecting a difference in cortical structure.

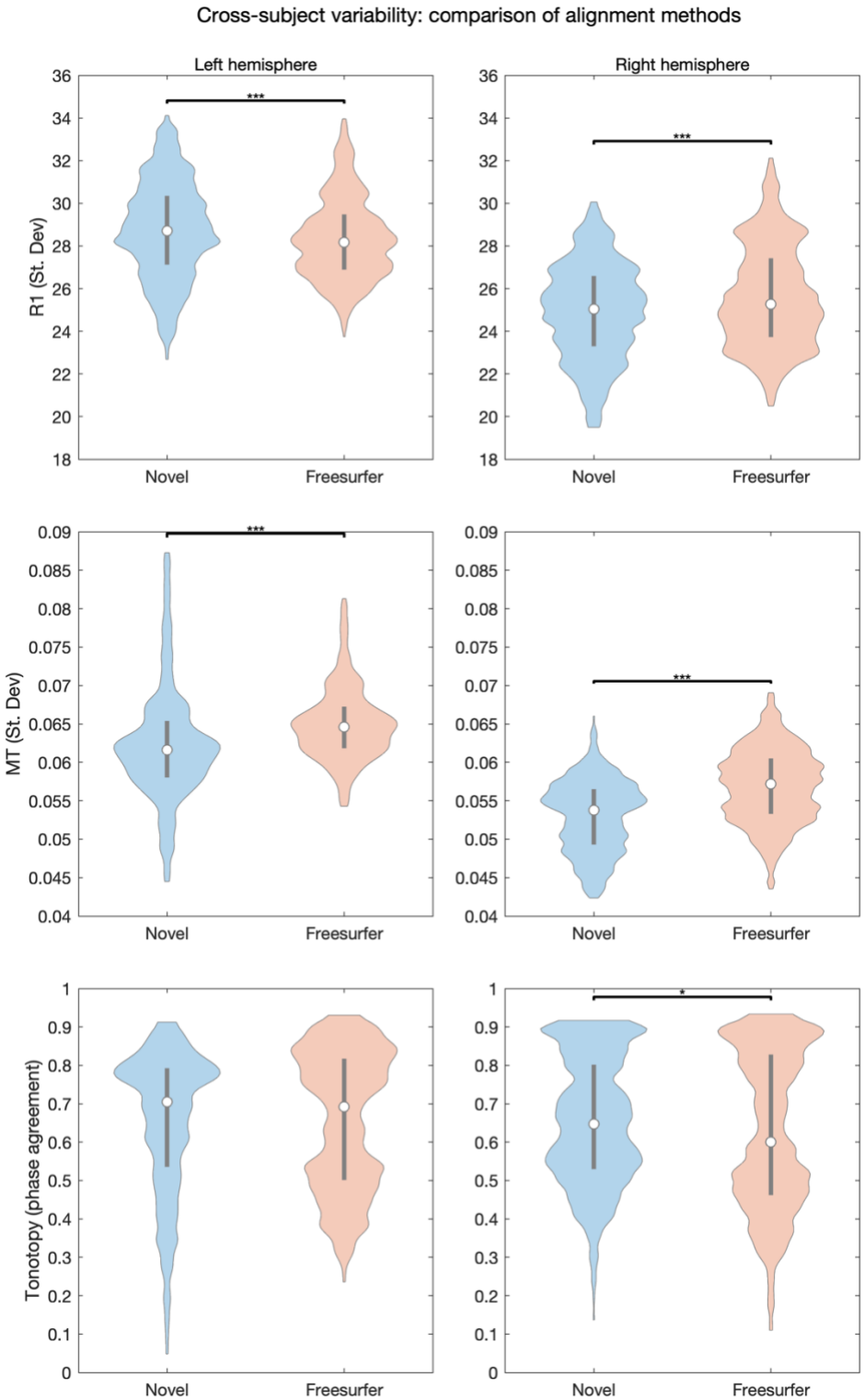

Figure 5.30*: Comparison of the novel alignment procedure and curvature-based alignment (Freesurfer). Values on the Y axis correspond to the cross-subject variability across all vertices for R1 (standard deviation), MT (standard deviation), and tonotopic phase (phase agreement). Horizontal bars above the violin plots represent the significance of a Mann-Whitney U test (1 star: p < .05; 2 stars: p < .01; 3 stars: p < .001).*

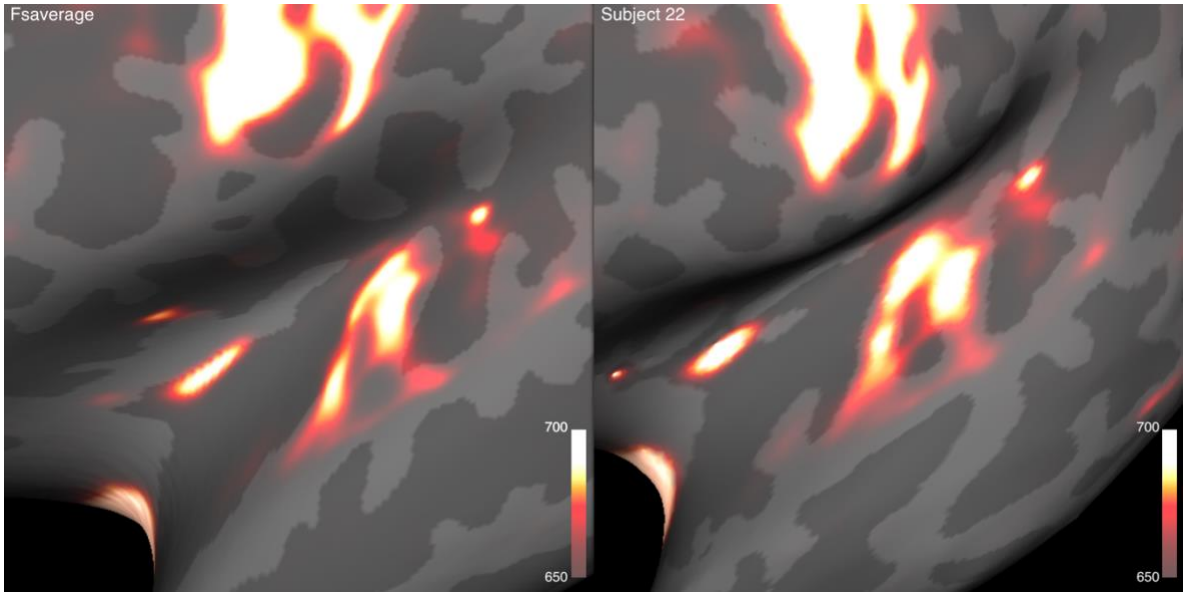

Figure 5.31*: Example of cortical-based alignment of the R1 maps of a partially duplicated gyrus (subject 22, left hemisphere) onto a single gyrus (fsaverage, left hemisphere) generated with Freesurfer's command mri_surf2surf. The entire surface of the partially duplicated gyrus was morphed onto the single gyrus, including the intermediate sulcus.*

Chapter 6.

Association between the structural properties of Heschl's gyrus, auditory perception, and musical training

6.1 Introduction

Variations in the morphology of HG have been associated with behavioural differences in auditory perception, language skills, and musicianship, as well as neurodevelopmental and psychiatric disorders. For instance, the occurrence of duplications of the left HG was also found to be greater in expert phoneticians (Golestani et al., 2011), musicians (Benner et al., 2017; Schneider et al., 2002), and fast learners of non-native speech sounds compared to slow learners (Golestani et al., 2007). Right HG duplications have also been associated with musical training (Benner et al., 2017), musicality and the ability to accurately vocalise foreign words (Turker et al., 2017), as well as foreign language aptitude (Turker et al., 2019). In terms of HG morphometry, an increase in left HG volume was found to correlate with increased speed in learning non-native speech sounds (Golestani et al., 2007; Wong et al., 2008) and early exposure to a second language (Ressel et al., 2012). The volume of the right HG has also been associated with greater activation in response to tonal processing (Warrier et al., 2009a), musical training (Bermudez et al., 2009; Gaser & Schlaug, 2003; Seither-Preisler et al., 2014), and foreign language aptitude (Turker et al., 2019). Individual preference for fundamental pitch or whole-spectrum "holistic" listening of complex sounds was also found to be related to HG morphology. Specifically, the left HG volume was greater in fundamental pitch listeners, while spectral listeners had greater right HG volume

and occurrence of right HG duplications (Schneider et al., 2005; Schneider & Wengenroth, 2009).

A potential link between HG duplication patterns and neurodevelopmental and psychiatric disorders has also been reported. Occurrence of right HG complete duplication has been associated with dyslexia, although the actual incidence of duplication in this population varies tremendously across studies, i.e. from 20% (Altarelli et al., 2014) to 84% (Serrallach et al., 2016). Takahashi et al. (2022b) found a higher occurrence of bilateral HG duplications in participants diagnosed with bipolar disorder compared to controls but also increased severity of anxiety and depression in individuals with major depressive disorder with single HG. The same group also found a higher incidence of bilateral HG duplications in schizophrenic patients (Takahashi et al., 2022a), as well as a specific association between CSDs and decreased verbal fluency (Takahashi et al., 2021). Finally, a greater occurrence of duplications was also observed in Williams-Beuren syndrome (Wengenroth et al., 2010), a genetic disorder associated with heightened interest in musical activity and emotional response to music (Thakur et al., 2018), indicating a possible interaction of genetic effects, musicality, and HG morphology.

In summary, prior evidence points to a possible association between HG duplications, phonetic ability, musical training, but also psychopathology. However, the laterality, type, and incidence of HG duplications appear to vary greatly across studies. Several issues might contribute to this variability, including differences in HG labelling procedures and use of different behavioural constructs. The first objective of this chapter is to test whether the occurrence of both left and right duplications of HG can predict two psychophysical

measures of auditory perception (pitch and duration discrimination), while also accounting for the effect of musical training.

Additionally, data on the association between myelination of HG and auditory perceptual abilities are generally missing from the literature. One study (Kim & Knösche, 2016) reported an association between myelination in the anterolateral HG and pitch discrimination thresholds, although the cluster the authors describe appeared to be located largely on the superior temporal gyrus. Additionally, a large number of studies that previously reported an association between HG's morphology (mainly white or grey matter volume) and auditory-based abilities or musicality don't factor in the presence of HG duplications in their measurements, while it is known that the presence of HG duplications affects the cortical morphology of the superior temporal plane (e.g. cortical thickness; Marie et al., 2016). Additionally, the variety of manual techniques used to label HG, in particular the definition of its posterior border, makes it difficult to compare results across studies. Therefore, the second objective is to explore potential correlations between auditory perceptual ability and HG structural and functional properties, namely cortical thickness, tonotopic magnitude, and myelin-sensitive R1 and MT, using the automated classification and alignment procedures proposed in the previous chapters. The localisation of these associations across the surface of HG is also explored.

6.2 Methods

6.2.1 Subjects and procedures

A total of 51 subjects (27 female, mean age ± SD: 23.3 ± 4.6) from the previous MRI cohort completed a behavioural test battery that included a pitch discrimination task, a

duration discrimination task, and the Gold-MSI questionnaire to quantify musical training. The details of the two psychophysical tests and the questionnaire were identical to those presented in the methods of Chapter 2. All subjects were tested in a sound-insulated room at the Institute of Cognitive Neuroscience (ICN) in London (UK) and were compensated for their participation. Prior to each session, participants' hearing thresholds were measured with an Amplivox 240 diagnostic audiometer. Pure tones were presented monaurally following a 10 dB-down, 5 dB-up adaptive staircase procedure (British Society of Audiology, 2018). The order of tone frequency was: kHz, 1.5 kHz, 2 kHz, 3 kHz, 4 kHz, 6 kHz, 8 kHz, 125 Hz, 250 Hz, 500 Hz, and 750 Hz. None of the 51 participants presented signs of hearing loss.

6.2.2 Statistical analyses

Before all analyses, the values of pitch and duration discrimination thresholds were log-transformed and their sign was inverted in order for a positive value to always correspond to lower thresholds (i.e. better performance).

A multiple least-squared regression was conducted to test the a priori hypothesis that the occurrence of HG duplications and musical training would explain variability in auditory perception across participants. The independent variables included left duplication type (LH_Splittype), right duplication type (RH_Splittype), the musical training dimension of the Gold-MSI questionnaire (MusTrn), and the interactions of musical training and left (MusTrn*LH_Splittype) and right (MusTrn*RH_Splittype) duplications. Given the previously reported association between musical training and HG duplications, two additional ANOVAs were conducted to test the potential collinearity of these two variables in each hemisphere.

A second exploratory analysis was conducted to evaluate the association between average HG myelination, as measured by myelin-sensitive R1 and MT, tonotopic magnitude, cortical thickness, and auditory thresholds. To further qualify any association between MRI and behavioural data, correlations were also calculated across the whole surface of the average HG templates (i.e. a correlation coefficient at each node) onto which all individual data (i.e. the most anterior HG duplication or optimal section, as defined in Chapter 5) were previously morphed and resampled. Correlation peaks on the HG surface were identified using an uncorrected p-value of 0.05.

6.3 Results

6.3.1 Auditory perception, HG duplications, and musical training

Two factorial ANCOVAs were used to test the effect of HG morphology on pitch discrimination and duration discrimination thresholds (i.e. one separate model for each task) while accounting for the effect of musical training. For each hemisphere, the full model included the main effects of musical training, the type of duplication (partial or full) in each hemisphere, and their interaction.

This model significantly predicted pitch discrimination performance ($F(9, 41) = 4.22$, $p < .001$; see (Figure 6.2). Of the five predictors, musical training had a statistically significant effect (FDR-corrected $p = .004$), as well as the presence of duplications in the left hemisphere (FDR-corrected $p = .036$). In contrast, duplication in the right hemisphere and interaction terms were not statistically significant. The full model explained 48% of the variability in pitch discrimination (37% after adjusting for non-significant predictors). To further investigate the effect of specific types of duplication in the left hemisphere on pitch

discrimination performance, a post-hoc test using the Tukey HSD method was conducted to test the significance of all pairwise comparisons while controlling the family-wise error rate. Individuals with a single gyrus in the left hemisphere had significantly lower thresholds than those with common stem duplications (0.65 ± 0.23, p = 0.022). On the other hand, participants with left complete duplications were not significantly different from those with either partial duplications or single gyri (Figure 6.1).

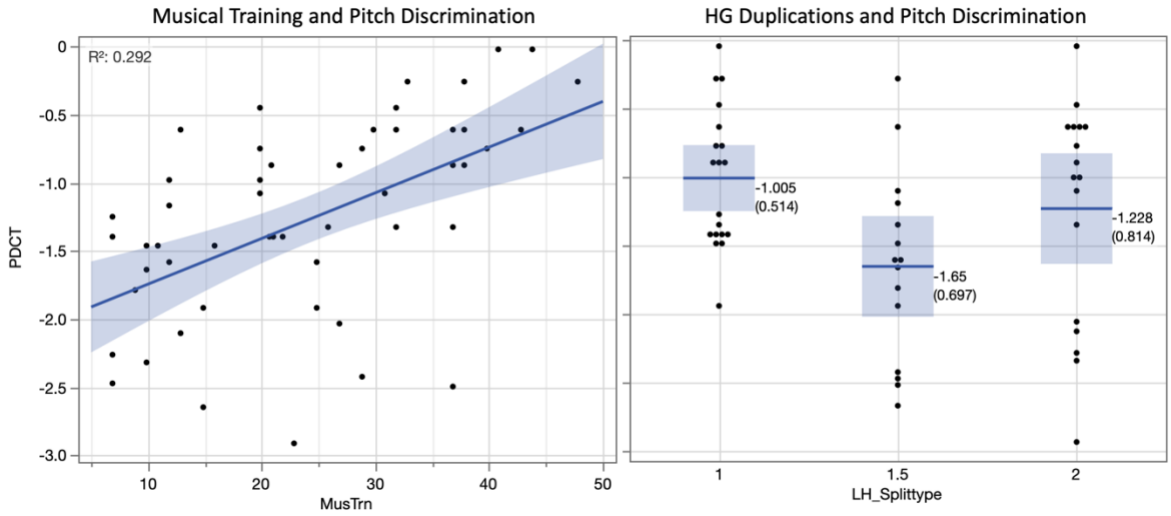

Figure 6.1*: Relationship between musical training, HG duplications in the left hemisphere, and pitch discrimination thresholds. In the left scatterplot, pitch discrimination is represented on the vertical axis and musical training on the horizontal axis, with a line of best fit and its 95% confidence interval. The plot on the right represents pitch discrimination thresholds across the three types of duplications (1 = no duplication; 1.5 = partial duplication; 2 = complete duplication), with blue lines and shaded areas corresponding to each group's mean and their 95% confidence intervals.*

Summary of factorial ANCOVA (Pitch Discrimination)

Source	DF	Sum of Squares	Mean Square	F Ratio
Model	9	12.338462	1.37094	4.2116
Error	41	13.346011	0.32551	Prob > F
C. Total	50	25.684472		0.0007*

Source	DF	Sum of Squares	F Ratio	Prob > F
MusTrn	1	4.1919071	12.8779	0.0009*
LH_Splittype	2	3.0738118	4.7215	0.0143*
RH_Splittype	2	0.6821481	1.0478	0.3599
MusTrn*LH_Splittype	2	0.9593589	1.4736	0.2410
MusTrn*RH_Splittype	2	0.1758622	0.2701	0.7646

Summary of Fit	
RSquare	0.480386
RSquare Adj	0.366324
Root Mean Square Error	0.570537
Mean of Response	-1.26885
Observations (or Sum Wgts)	51

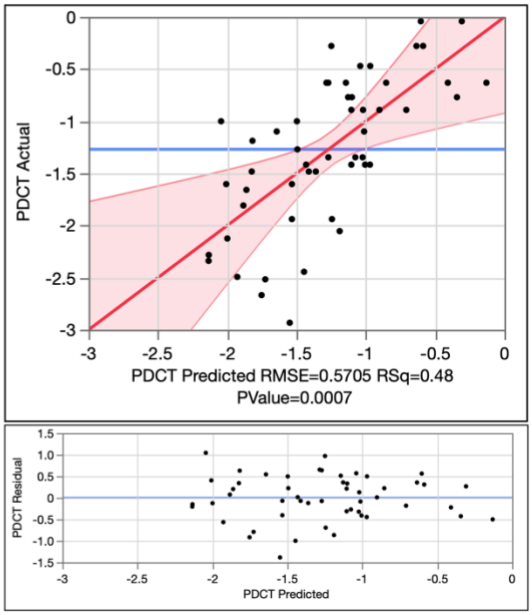

Figure 6.2*: Multiple least squared regression model for pitch discrimination data using bilateral duplication type and musical training as predictors and interaction effects. Tables include F-tests for the full model and individual predictors, as well as indices of fit (R^2, adjusted R^2, RMSE). The top scatterplot shows the relationship between predicted and actual pitch discrimination thresholds, with a blue line indicating the overall sample mean and a red line and shaded region corresponding to the best-fit line and its 95% confidence interval. The bottom scatterplot represents the residuals of the full model. Variable names: PDCT = pitch discrimination; MusTrn = Gold-MSI Musical Training component; LH_Splittype = type of duplication (no duplication, partial, complete) in the left hemisphere; RH_Splittype = type of duplication in the right hemisphere.*

However, the same model did not significantly predict duration discrimination performance

(F(9, 14) = .79, p = .623; see Figure 6.3).

Summary of factorial ANCOVA (Duration Discrimination)

Source	DF	Sum of Squares	Mean Square	F Ratio
Model	9	2.111191	0.23457	0.7946
Error	41	12.103585	0.29520	Prob > F
C. Total	50	14.214776		0.6230

Source	DF	Sum of Squares	F Ratio	Prob > F
MusTrn	1	0.15828379	0.5362	0.4682
LH_Splittype	2	0.39408592	0.6675	0.5185
RH_Splittype	2	0.19407645	0.3287	0.7217
MusTrn*LH_Splittype	2	0.68693804	1.1635	0.3225
MusTrn*RH_Splittype	2	0.19549254	0.3311	0.7200

Summary of Fit	
RSquare	0.148521
RSquare Adj	-0.03839
Root Mean Square Error	0.543332
Mean of Response	-3.44662
Observations (or Sum Wgts)	51

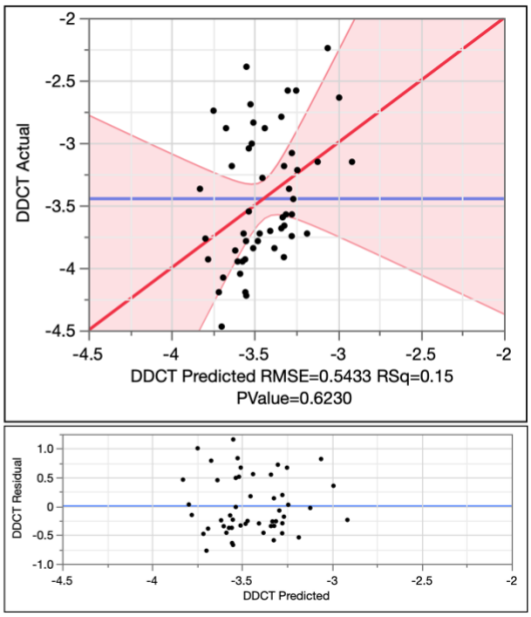

Figure 6.3*: Multiple least squared regression model for duration discrimination data using bilateral duplication type and musical training as predictors and interaction effects. Tables include F-tests for the full model and individual predictors, as well as indices of fit (R^2, adjusted R^2, RMSE). The top scatterplot shows the relationship between predicted and actual duration discrimination thresholds, with a blue line indicating the overall sample mean and a red line and shaded region corresponding to the best-fit line and its 95% confidence interval. The bottom scatterplot represents the residuals of the full model. Variable names: DDCT = duration discrimination; MusTrn = Gold-MSI Musical Training component; LH_Splittype = type of HG duplication (no duplication, partial, complete) in the left hemisphere; RH_Splittype = type of duplication in the right hemisphere.*

Notably, there were no differences in musical training across HG morphologies in either hemisphere (left hemisphere: F(2,48) = .601, p = .553; right hemisphere: F(2,48) = 0.498, p = .611), indicating the independence of the effects of HG duplications and musical training on pitch discrimination thresholds.

Finally, two multiple linear regression models were built to test whether the surface area of the most anterior HG duplication (including CSDs) in either hemisphere could predict pitch and/or duration discrimination thresholds (one model for each task). Neither model reached statistical significance (pitch discrimination: F(2, 48) = 2.23, p = .12; duration

discrimination: $F(2,48) = 0.17$, $p = .84$), indicating the bilateral surface area was not predictive of either behavioural measure.

6.3.2 Auditory perception and HG cortical properties

Another set of analyses was conducted to explore the relationship between auditory perception and the functional-structural properties of HG.

The first analysis focused on the correlations between pitch discrimination, duration discrimination, and the average values of cortical thickness, tonotopic magnitude, and MPM data across the whole surface of HG, or its optimal section in case of duplications (i.e. anterior duplication, as defined in paragraph 5.3.1.4). Given the strong correlation between R1 and MT data (left hemisphere: $r = 0.49$; right hemisphere: $r = 0.51$), a principal component analysis was conducted in each hemisphere in order to obtain a composite measure and reduce the overall number of comparisons. The first components of these analyses explained 74.5% of the variability across MT and R1 in the left hemisphere and 75.3% in the right hemisphere. Given the high proportion of explained variance, the scores of these first components were judged ad an adequate representation of R1 and MT data and used in their place in subsequent analyses (referred to in-text as MPM data for simplicity).

In terms of behavioural variables, pitch discrimination thresholds were positively correlated with tonotopic magnitude in the right hemisphere only ($r = 0.33$, $p = .017$), but not cortical thickness nor MPM data in either hemisphere (Figure 6.4). Duration discrimination thresholds had a positive correlation with tonotopic magnitude bilaterally (left hemisphere: $r = 0.28$, $p = .048$; right hemisphere: $r = 0.29$, $p = .039$), and a strong positive correlation with MPM data in the right hemisphere ($r = 0.42$, $p=.002$). There was also a positive but

weak correlation between duration discrimination and MPM data in the left hemisphere (r = 0.26, p = .071).

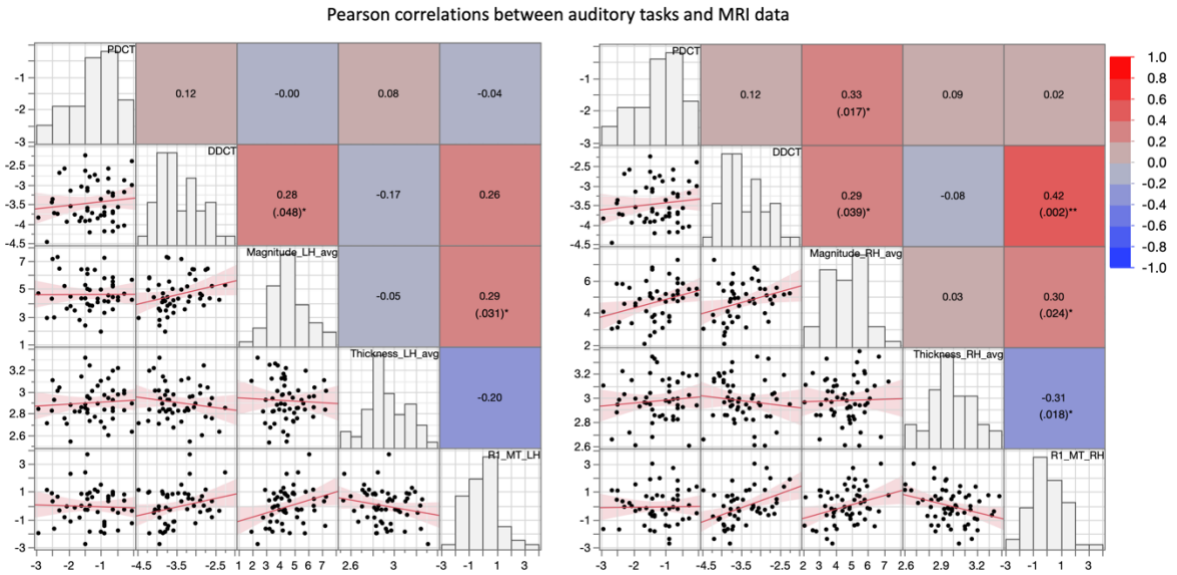

Figure 6.4*: Pearson correlations between pitch discrimination, duration discrimination, tonotopic magnitude, cortical thickness, and MPM data. The left and right correlograms correspond to the left and right hemispheres respectively. In each correlogram, scatterplots and best-fit lines with 95% confidence region are presented in the bottom triangle, histograms for each variable in the diagonal, and correlation indices in the top triangle. Uncorrected p-values are reported below significant correlations (p < .05). Variable names: PDCT = pitch discrimination; DDCT = duration discrimination; Magnitude_xx_avg = tonotopic magnitude; Thickness_xx_avg = cortical thickness; R1_MT_xx = first principal component scores of R1 and MT. "LH" and "RH" in variable names correspond to the left and right hemispheres.*

However, tonotopic magnitude and MPM data were also positively correlated in both hemispheres. The semi-partial correlations between duration discrimination and each MRI variable were then calculated to determine the unique association of duration discrimination with tonotopic magnitude and MPM data. After removing the effect of MPM data, the semi-partial correlation between duration discrimination and tonotopic magnitude in the right hemisphere was no longer significant (r = 0.172, p = .242); on the other hand, after removing the effect of tonotopic magnitude, the association between duration discrimination and MPM data in the right hemisphere was still positive and significant (r =

0.349, p = .015). The same analysis in the left hemisphere resulted in non-significant semi-partial correlation coefficients for both tonotopic magnitude (r = 0.213, p = .144) and MPM data (r = 189, p = .198).

Finally, average cortical thickness, tonotopic magnitude, and MPM data appeared to be largely the same across all duplication types (Figure 6.5), indicating that the effects on auditory perception of HG duplication variants and cortical structure function were not interdependent. Additionally, musical training was also not correlated to any MRI measure in either hemisphere.

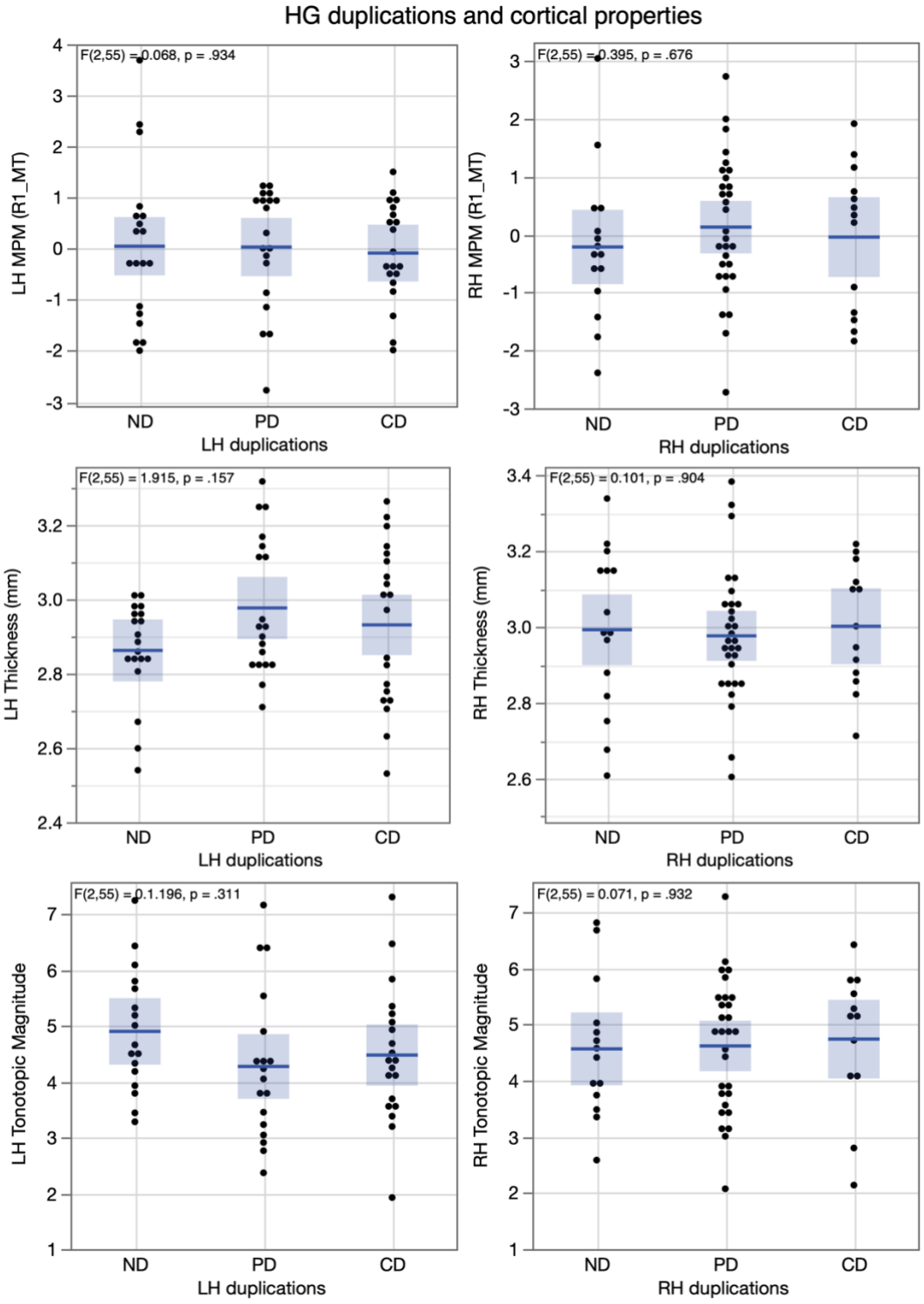

Figure 6.5*: Plots of tonotopic magnitude, cortical thickness, and MPM data across duplication types. The left and right columns correspond to data within the left and right hemispheres respectively. Duplication types are no-duplications (ND), partial duplications (PD), and complete duplications (CD). Plots represent jittered individual data points, group means, and their 95% confidence intervals. "MPM (R1_MT)" in the vertical axis of the first row of plots corresponds to the scores of the first principal component of R1 and MT data.*

6.3.3 Localisation of the association between auditory perception and cortical data

To further investigate the relationship between auditory ability and cortical data and localise its source with more precision, pitch and duration discrimination thresholds were correlated with R1, MT, and tonotopic magnitude data at each individual vertex of the average HG template.

The resulting correlation maps for pitch discrimination (Figure 6.6) were largely composed of small positive and negative correlations, with only tonotopic magnitude in the right hemisphere showing a peak of positive correlation in the centre of the gyrus. On the other hand, duration discrimination thresholds were more consistently positively correlated with all measures across the whole surface of the gyrus (Figure 6.7). More specifically, in the left hemisphere, a peak of positive correlation could be observed posterolaterally with both R1 and MT. In the right hemisphere, there were strong positive correlations with R1 across the whole surface of the gyrus along with peaks within its most medial third and lateral half. A smaller peak in MT was also present but only within the medial third of the gyrus. Tonotopic magnitude had consistently positive but low correlations, with a small peak in the middle of the right gyrus, similar to pitch discrimination.

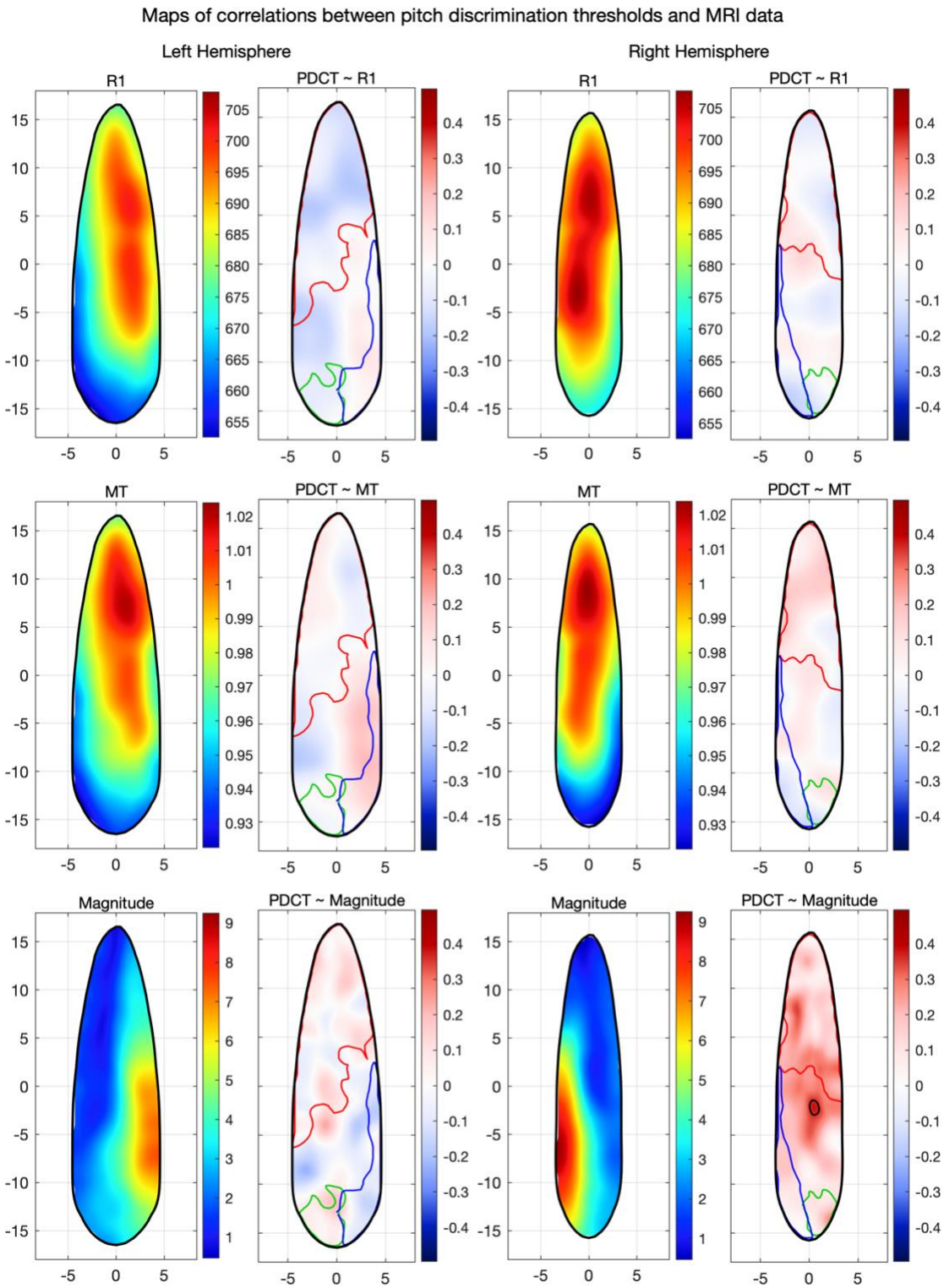

***Figure 6.6**: Correlations between pitch discrimination thresholds and R1, MT, and tonotopic magnitude data. Each average map is paired with its corresponding correlation maps to its right. Black contour lines highlight regions where correlations are statistically significant ($p < .05$, uncorrected). Red, blue, and green lines represent the boundaries of the putative cytoarchitectonic regions Te1.0, Te1.1, Te1.2, and Te2.1 (see Figure 5.19)*

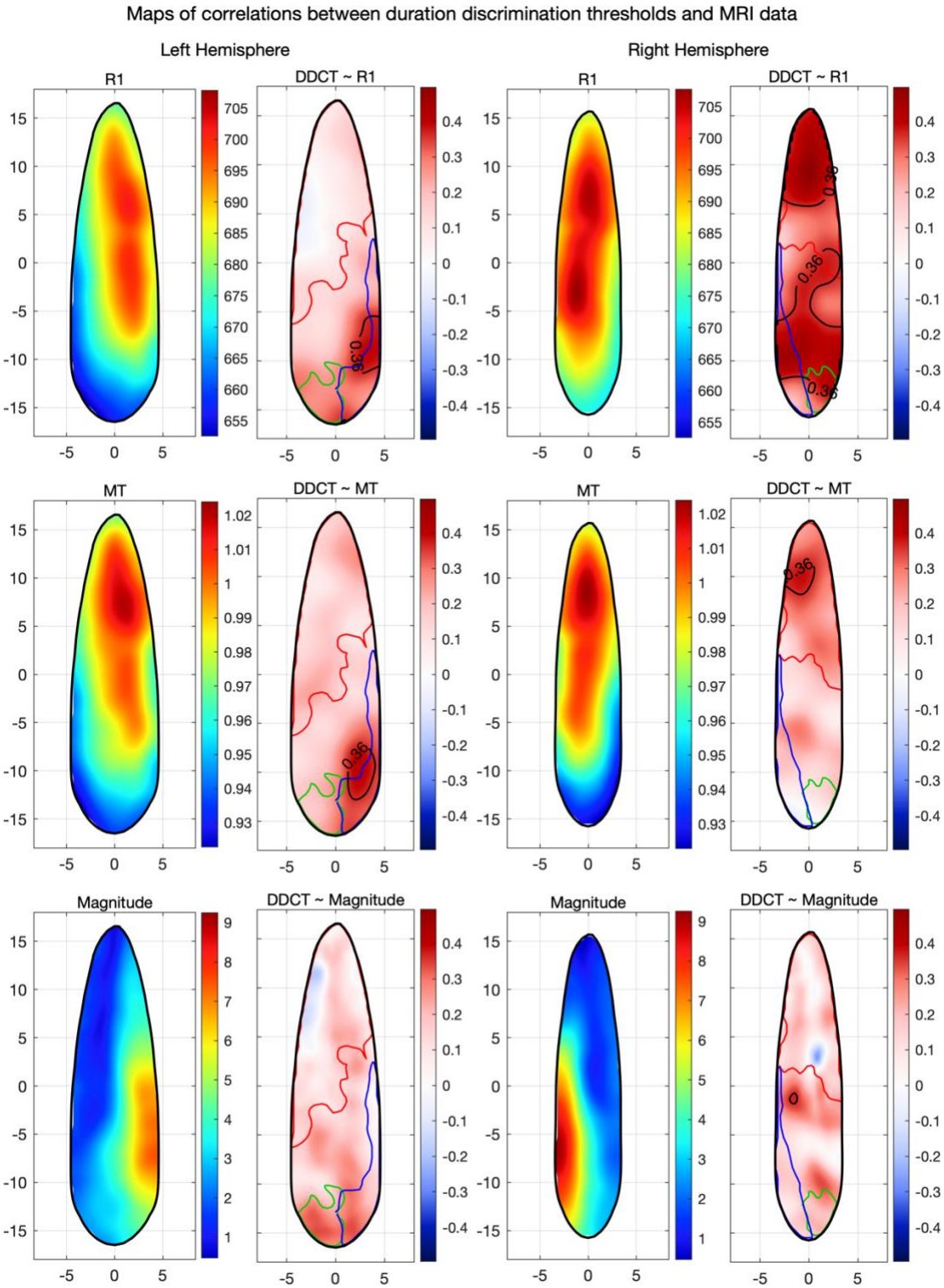

***Figure 6.7**: Correlations between duration discrimination thresholds and R1, MT, and tonotopic magnitude data. Each average map is paired with its corresponding correlation maps to its right. Maps in the first two columns correspond to the left hemisphere, while the third and fourth to the right hemisphere. Black contour lines highlight regions where correlations are statistically significant ($p < .05$, uncorrected). Red, blue, and green lines represent the boundaries of the putative cytoarchitectonic regions Te1.0, Te1.1, Te1.2, and Te2.1 (see Figure 5.19)*

6.4 Discussion

6.4.1 Relationship between HG morphology, musical training, and auditory perception

In this chapter, we found a significant association between pitch discrimination thresholds and HG morphology in the left hemisphere, but not the right hemisphere. More specifically, individuals with a single gyrus had the lowest (i.e. best) thresholds, those with common stem duplications had the highest, and those with full duplications had thresholds in between the other two morphotypes. Additionally, there was no effect of HG gyral surface on either behavioural measure. Although there is no empirical prior in the literature for pitch or duration discrimination specifically, these results are somewhat in contrast with previous related findings. For instance, it was reported that expert phoneticians (Golestani et al., 2011) and musicians (Benner et al., 2017; Schneider et al., 2002) had a greater occurrence of duplications of the left HG. Given the association between musicianship and pitch discrimination thresholds (see paragraph 2.3.1), it might be expected for occurrences of HG duplications in the left hemisphere to predict variations in pitch perception. However, in our sample, there was no association between musical training and the occurrence of HG duplications, and finer pitch perception was associated with a lack of HG duplications. Moreover, no association was found between cortical surface area, cortical thickness, with musical training or auditory perception in either hemisphere, despite previous reports of a correlation in HG morphometry (i.e. grey matter volume) and musicianship (Bermudez et al., 2009; Gaser & Schlaug, 2003; Seither-Preisler et al., 2014). However, participants in the current study were sampled from the general population (Gold-MSI musical training: 24 ± 12). Therefore, variations in musical training did not reflect extensive instrument practice, but rather smaller variations in any training, such as

school music programs or sporadic practice. These variations were still strongly correlated with pitch perception (r = 0.58), but they might not be sufficient to observe a difference in the gyrification of the auditory cortex.

6.4.2 Locating behaviour on the surface of HG

Although not associated with HG morphology, duration discrimination thresholds were correlated with myelin-sensitive R1 and MT in the right hemisphere. They were also correlated with tonotopic magnitude bilaterally, but this effect was mediated by the correlation between tonotopic magnitude and MPM data. The association between cortical myelination of the right HG and duration discrimination thresholds has not been reported before in the literature. Temporal processing of sound had generally been associated with a leftward specialisation of the auditory cortex (Warrier et al., 2009b; Zatorre & Belin, 2001). However, prior studies utilised paradigms that measure the ability to perceive varying rates of tone frequency change in a sequence, which could arguably involve a different type of neuronal circuitry than the comparison of the duration of two tones. Furthermore, it is difficult to draw a direct comparison between cortical activation and myelin density. It is possible to speculate that greater cortical myelination, by increasing the speed of action potential conduction, would allow the detection of shorter differences in tone duration. However, the nature of the association is likely more complex, as intracortical myelination is also related to several other cortical properties, such as neuronal density, soma size, circuitry complexity, intra- and extra-cortical connectivity, and metabolic measures (Glasser et al., 2014). Furthermore, myelination of the right HG could be indicative of differences in myelination elsewhere on the cortical surface but also in subcortical and cortico-cortical connectivity. Nonetheless, dedicated research is needed to confirm the

association between right HG myelination and fine auditory temporal perception and its neurobiological significance.

Chapter 7.

General discussion

7.1 Summary of findings

In this thesis, we have investigated the individual differences in auditory perception, cognition, expertise, and cortical structure, and how they relate to one another. Chapter 2 focused on musicians' and audio engineers' unique patterns of auditory perceptual and cognitive skills. Compared to non-experts, both cohorts displayed advantages in auditory-based tasks from psychoacoustics to auditory scene analysis. However, while audio engineers excelled in identifying sounds based on psychoacoustic features (i.e. pitch and amplitude modulation frequency), musicians displayed greater sensitivity to repetitions in competing melodies and lower SNR thresholds for speech in babble noise perception.

In Chapter 3, 4, and 5, we explored how gyral morphology, cortical myelination, and tonotopic gradients in the human superior temporal plane relate to each other in a sample of 58 subjects drawn from the general population.

In Chapter 3, we replicated a systematic association between cortical myelination and tonotopic magnitude located within Heschl's gyrus bilaterally. We also observed the typical "V" shaped high-low-high tonotopic gradients in group-average maps, a densely myelinated region within the medial half of HG corresponding to the putative location of the human auditory core, and an anteromedial-to-posterolateral gradient of narrow-to-broad pRF tuning widths. A qualitative assessment of individual tonotopic maps revealed

substantial individual differences in tonotopic gradients, namely the relative size of low- and high-frequency preference and the number of gradient reversals.

One defining characteristic of the superior temporal plane in humans is the variability in gyral morphology, which can complicate the study of individual differences and interfere with inter-subject curvature-based alignment techniques. To overcome this issue, in Chapter 4 we presented a pipeline for the automated classification of Heschl's gyrus' common stem duplications (CSD). We tested this pipeline with an independent sample of 100 subjects and found overall similar occurrences of duplications, with smaller differences possibly due to differences in handedness between samples. We found a leftward asymmetry in HG's surface area and an association with the occurrence of duplications. We then defined two CSD variants and morphed similar gyri onto a common template.

In Chapter 5, we applied this technique to compare the average tonotopic and quantitative MRI maps of individuals with different HG morphologies. We found a greater similarity between the anterior branch of CSDs and non-duplicated gyri which was driven mainly by similarities in tonotopic gradients. Based on these observations, we defined a possible homology between non-duplicated gyri and a region of CSDs corresponding approximately to the anterior branch and the common stem. This region of CSDs and non-duplicated gyri were then morphed onto a common template to calculate average maps and evaluate individual differences in tonotopy and cortical myelination. Additionally, the same technique was applied to optimally align the ex-vivo cytoarchitectonic data of 10 brains, which included 3 cases of CSDs (Gulban et al., 2020). We observed a spatial correspondence of the typical "V"-shaped tonotopic gradients and greater cortical myelination which was often, but not always, located at the medial end of HG. The

correlations between individual and average maps were strongly positive for all parameters, albeit with a few individual cases of negative correlations. However, once the region surrounding HG was taken into account, these cases appeared quite typical. Taken together, these results indicated a positive but imperfect correspondence of macro-anatomy, tonotopy, and cortical myelination within HG.

Finally, in Chapter 6 we tested whether the occurrence of HG duplications could predict variability in pitch and duration discrimination thresholds and whether this effect was mediated by musical training. We found a significant association between HG morphology in the left hemisphere and pitch discrimination thresholds, with the non-duplicated variant being associated with the lowest thresholds and CSDs with the highest. Musical training was also associated with lower pitch discrimination thresholds, but this effect was independent of HG morphology. In fact, unlike previous studies, we did not find any association between musical training and HG morphology in either hemisphere. Through post-hoc exploratory analyses, we also found a positive correlation between myelination of the right HG and performance in the duration discrimination task.

7.2 Auditory expertise

Longitudinal studies are the gold standard in the study of expertise and development. Following the trajectory of skill acquisition over time in response to -randomly assigned- training allows us to understand the mechanisms that lead to expert behaviour, such as neural plasticity, and disentangle the effects of nature and nurture. However, the major drawback of longitudinal designs is that they tend to be expensive, logistically challenging, and at times ethically contentious. On the other side of the spectrum, cross-sectional

designs that involve the comparison of expert and naive subjects tend to be less resource-heavy and easier to organise but do not provide conclusive proof of causality of the effects of training on expert behaviour nor any associated differences in brain morphology or function (Schellenberg, 2019). The cross-sectional literature on "the effects of musical training" has been criticised for confusing correlations with causal effects (Schellenberg, 2015). In fact, it has been shown that genetics, socioeconomic status, personality, and general cognitive ability can all predict whether someone will take music lessons in their lifetime and for how long (e.g. Corrigall et al., 2013; Mosing et al., 2014; Schellenberg, 2011; Swaminathan & Schellenberg, 2018) and that an association between musical abilities and speech encoding exists without any actual musical training (Mankel & Bidelman, 2018). Additionally, given the complexity of musical instrument training, it is difficult to track which specific aspect of the training might lead to any given outcome. One possible solution is to compare musicians not only with non-musicians, but with sub-populations of experts within the same domain who might share some of the same baseline characteristics that drive self-selection (i.e. genetics, socioeconomic status, etc.), but undergo different types of training. For instance, perceptual and neural qualities associated with performing particular music genres (Kishon-Rabin et al., 2001; Tervaniemi et al., 2016; Vuust et al., 2012) or playing different musical instruments (Butler & Trainor, 2015; Carey et al., 2015; Micheyl et al., 2006; Slater et al., 2017; Zaltz et al., 2017). In Chapter 2, we analysed differences between young musical instrument students and audio engineering students. Based on the nature of their training (see 2.1.2.1), we hypothesised that audio engineers would possess an advantage for fine auditory perception and auditory scene analysis when compared to musicians. However, we found that both musicians and audio

engineers performed better than controls in auditory scene analysis but differently so across tasks. Specifically, musicians showed an advantage at detecting repetitions in two simultaneous melodies, while audio engineers could more effectively recognise and remember sounds based on elementary features such as pitch and amplitude modulation. Although they don't provide conclusive proof of causality, these advantages are coherent with the nature of the training of these populations and warrant further investigation. Musicians also displayed an advantage for speech in noise perception, although this effect was independent of any other measure in the test battery. Future experiments should employ more than one measure of speech in noise perception to disambiguate which aspect might be facilitated by musical expertise. Finally, comparing audio engineers and instrumentalists at the beginning of their careers might not reveal the full differential effects of their training. In fact, most audio engineers, and certainly all musicians, had received extensive musical training or practised a musical instrument by the time they enrolled in university, normally over a decade. Conversely, most audio engineers began their specialised training at the start of university. Therefore, future studies on audio engineering expertise should include senior professionals who have undergone several years of training.

7.3 Individual differences in development and behaviour: insights from cortical structure

Musical training has also been associated with several neural traits (Olszewska et al., 2021), one of which is the morphology of Heschl's gyrus (HG). More specifically, musical training has been associated with HG duplications in both the left (Benner et al., 2017; Schneider et al., 2002) and the right (Benner et al., 2017; Turker et al., 2017) hemisphere. In Chapter 6, we did not observe an association between musical training and HG

morphology (i.e. neither duplications nor surface area). Since the subjects in our sample were drawn from the general population, we utilised the musical training dimension of the Gold-MSI questionnaire to capture variations in musical instrument experience beyond formal training. 12 participants (i.e. 24%) scored over 37 in this dimension, which is the threshold that was used to match musicians with equally trained audio engineers, indicating the presence of a good number of extensively trained participants. Furthermore, replicating the results of Chapter 2, musical training was also strongly associated with lower pitch perception thresholds, supporting the construct validity of the Gold-MSI dimension. Therefore, although the design of the study was not cross-sectional in nature, we should have captured enough variability in musical training to detect an effect of HG morphology, which we did not observe. However, we did observe an effect of HG morphology on pitch discrimination thresholds, albeit not in the expected direction, in that the absence of any duplications in the left hemisphere was associated with finer pitch perception. This is somewhat in contrast with prior evidence not only on musicians but also on expert phoneticians (Golestani et al., 2011), which generally supports the notion of an association between auditory expertise and the occurrence of HG duplications.

Variations in cortical gyrification have been associated with several functional differences in brain function, both normal and pathological (e.g. Sasabayashi et al., 2021; Amiez et al., 2006; Li et al., 2015; Lopez-Persem et al., 2019; for a review, see paragraph 1.1.5), as well as different patterns of gene expression at birth (Ball et al., 2020). Nonetheless, there is no established framework to interpret how the occurrence of HG duplications might relate to pitch discrimination, musicianship (Benner et al., 2017), learning non-native speech sounds (Golestani et al., 2007), dyslexia (Serrallach et al., 2016), and schizophrenia (Takahashi et

al., 2022a) at the same time. In other words, on the one hand, HG morphology is a potential neural marker, already present at birth, of a predisposition to developing certain traits, which could help differentiate innate and environmental risks. On the other hand, there is no convergence in the current literature on which exact traits HG duplications are supposed to predict.

Other than statistical power, one potential culprit of this divergence is the reliance on manual labelling and the variety of techniques that have been adopted to classify HG's morphology.

7.4 Automated classification of HG morphology

An automated procedure for the classification of HG's partial duplications was presented in Chapter 4. This technique builds on the Tool for the Automated Segmentation of Heschl's gyrus (TASH; Dalboni da Rocha et al., 2020), which automatically labels all transverse gyri on the superior temporal plane. After identifying the most anterior duplication, this procedure normalises its shape and flags the presence of concavities in the contours of the gyrus. So far, manual labelling has been the only option. But despite the commendable effort in recent studies to manually label hundreds of brains (Marie et al., 2015), it remains an expensive and unscalable solution. Subjective judgements are also likely to introduce differences across research centres, especially when sample sizes are in the order of tens rather than hundreds, which is reflected in the vast differences across previous studies in the reported rates of HG duplication occurrences (see 4.4.1). Working towards an automated parcellation of HG's morphology would help advance our understanding of its variability in the general population and special target populations. Importantly, this

procedure could also be applied retrospectively to any prior sample in cases where HG morphology might be a variable of interest.

7.5 Individual differences and homologies in the human auditory cortex: future directions

After classifying common stem duplications, we identified a potential homology between their anterior duplications and gyri with no duplications, based on the similarity of their tonotopic gradients. There have been different definitions of what anatomical landmark should be considered the boundary between HG and the planum temporale (see 4.1.2). We found the intermediate sulcus to be an optimal anatomical landmark to minimise the cross-subject differences in tonotopic gradients in our sample and, to a lesser degree, also quantitative MRI measures sensitive to myelin density such as R1 and MT. More data are needed to fully corroborate this finding. For example, recent developments in ultra-high field MRI (Moerel et al., 2020) have allowed the detailed analysis of tonotopic response across cortical depths (Ahveninen et al., 2016; De Martino et al., 2015) and subcortical regions (Moerel et al., 2015; Sitek et al., 2019), cortical fibre orientation (Gulban et al., 2018), and to improve our understanding of how MR signals might relate to variations in cortical cytoarchitecture (Dinse et al., 2015; McColgan et al., 2021). Obtaining a detailed picture of the human auditory cortex in vivo would allow the formulation of a comprehensive model of its regionalisation, creating a common reference system for the study of homologies and differences between individuals and across species.

Bibliography

Abdul-Kareem, I. A., & Sluming, V. (2008). Heschl gyrus and its included primary auditory cortex: Structural MRI studies in healthy and diseased subjects. *Journal of Magnetic Resonance Imaging*, *28*(2), 287–299. https://doi.org/10.1002/jmri.21445

Adcock, R. A., Dale, C., Fisher, M., Aldebot, S., Genevsky, A., Simpson, G. V., Nagarajan, S., & Vinogradov, S. (2009). When Top-Down Meets Bottom-Up: Auditory Training Enhances Verbal Memory in Schizophrenia. *Schizophrenia Bulletin*, *35*(6), 1132–1141. https://doi.org/10.1093/schbul/sbp068

Ahrens, M. B., Linden, J. F., & Sahani, M. (2008). Nonlinearities and Contextual Influences in Auditory Cortical Responses Modeled with Multilinear Spectrotemporal Methods. *The Journal of Neuroscience*, *28*(8), 1929–1942. https://doi.org/10.1523/JNEUROSCI.3377-07.2008

Ahveninen, J., Chang, W. T., Huang, S., Keil, B., Kopco, N., Rossi, S., Bonmassar, G., Witzel, T., & Polimeni, J. R. (2016). Intracortical depth analyses of frequency-sensitive regions of human auditory cortex using 7T fMRI. *NeuroImage*, *143*, 116–127. https://doi.org/10.1016/j.neuroimage.2016.09.010

Aitkin, L. M., Dickhaus, H., Schult, W., & Zimmermann, M. (1978). External nucleus of inferior colliculus: Auditory and spinal somatosensory afferents and their interactions. *Journal of Neurophysiology*, *41*(4), 837–847. https://doi.org/10.1152/jn.1978.41.4.837

Alain, C., Zendel, B. R., Hutka, S., & Bidelman, G. M. (2014). Turning down the noise: The benefit of musical training on the aging auditory brain. *Hearing Research*, *308*, 162–173. https://doi.org/10.1016/j.heares.2013.06.008

Alluri, V., Toiviainen, P., Burunat, I., Kliuchko, M., Vuust, P., & Brattico, E. (2017). Connectivity patterns during music listening: Evidence for action-based processing in musicians. *Human Brain Mapping*, *38*(6), 2955–2970. https://doi.org/10.1002/hbm.23565

Altarelli, I., Leroy, F., Monzalvo, K., Fluss, J., Billard, C., Dehaene-Lambertz, G., Galaburda, A. M., & Ramus, F. (2014). Planum temporale asymmetry in developmental dyslexia: Revisiting an old question. *Human Brain Mapping*, *35*(12), 5717–5735. https://doi.org/10.1002/hbm.22579

Amiez, C., Kostopoulos, P., Champod, A.-S., & Petrides, M. (2006). Local Morphology Predicts Functional Organization of the Dorsal Premotor Region in the Human Brain. *The Journal of Neuroscience*, *26*(10), 2724–2731. https://doi.org/10.1523/JNEUROSCI.4739-05.2006

Amiez, C., Neveu, R., Warrot, D., Petrides, M., Knoblauch, K., & Procyk, E. (2013). The Location of Feedback-Related Activity in the Midcingulate Cortex Is Predicted by Local

Morphology. *Journal of Neuroscience*, *33*(5), 2217–2228. https://doi.org/10.1523/JNEUROSCI.2779-12.2013

Amrhein, V., Korner-Nievergelt, F., & Roth, T. (2017). The earth is flat (p > 0:05): Significance thresholds and the crisis of unreplicable research. *PeerJ*, *2017*(7), 1–40. https://doi.org/10.7717/peerj.3544

Amunts, K., Malikovic, A., Mohlberg, H., Schormann, T., & Zilles, K. (2000). Brodmann's Areas 17 and 18 Brought into Stereotaxic Space and How Variable? *NeuroImage*, *11*(1), 66–84. https://doi.org/10.1006/nimg.1999.0516

Amunts, K., Schleicher, A., Brgel, U., Mohlberg, H., Uylings, H. B. M., & Zilles, K. (1999). Broca's region revisited: Cytoarchitecture and intersubject variability. *The Journal of Comparative Neurology*, *412*(2), 319–341. https://doi.org/10.1002/(SICI)1096-9861(19990920)412:2<319::AID-CNE10>3.0.CO;2-7

Amunts, K., Schleicher, A., & Zilles, K. (2007). Cytoarchitecture of the cerebral cortex than localization. *NeuroImage*, *37*(4), 1061–1065. https://doi.org/10.1016/j.neuroimage.2007.02.037

Amunts, K., & Zilles, K. (2015). Architectonic Mapping of the Human Brain beyond Brodmann. *Neuron*, *88*(6), 1086–1107. https://doi.org/10.1016/j.neuron.2015.12.001

Amunts, K., & Zilles, K. (2006). A multimodal analysis of structure and function in Broca's region. *Broca's Region*, 17–30.

Anthwal, N., & Thompson, H. (2016). The development of the mammalian outer and middle ear. *Journal of Anatomy*, *228*(2), 217–232. https://doi.org/10.1111/joa.12344

Antunes, F. M., & Malmierca, M. S. (2011). Effect of Auditory Cortex Deactivation on Stimulus-Specific Adaptation in the Medial Geniculate Body. *Journal of Neuroscience*, *31*(47), 17306–17316. https://doi.org/10.1523/JNEUROSCI.1915-11.2011

Arai, Y., & Taverna, E. (2017). Neural Progenitor Cell Polarity and Cortical Development. *Frontiers in Cellular Neuroscience*, *11*, 384. https://doi.org/10.3389/fncel.2017.00384

Arribas, M. (2017). The history of cerebrospinal fluid: From classical antiquity to the late modern period. *Neurosciences and History*, *5*(3), 105–113.

Aslin, R. N., Pisoni, D. B., Hennessy, B. L., & Perey, A. J. (1981). Discrimination of Voice Onset Time by Human Infants: New Findings and Implications for the Effects of Early Experience. *Child Development*, *52*(4), 1135–1145.

Baare, W. F. C. (2001). Quantitative Genetic Modeling of Variation in Human Brain Morphology. *Cerebral Cortex*, *11*(9), 816–824. https://doi.org/10.1093/cercor/11.9.816

Babola, T. A., Li, S., Gribizis, A., Lee, B. J., Issa, J. B., Wang, H. C., Crair, M. C., & Bergles, D. E. (2018). Homeostatic Control of Spontaneous Activity in the Developing Auditory System. *Neuron*, *99*(3), 511–524.e5. https://doi.org/10.1016/j.neuron.2018.07.004

Bajo, V. M., Merchán, M. A., Malmierca, M. S., Nodal, F. R., & Bjaalie, J. G. (1999). Topographic organization of the dorsal nucleus of the lateral lemniscus in the cat. *Journal of Comparative Neurology*, *407*(3), 349–366. https://doi.org/10.1002/(SICI)1096-9861(19990510)407:3<349::AID-CNE4>3.0.CO;2-5

Ball, G., Seidlitz, J., O'Muircheartaigh, J., Dimitrova, R., Fenchel, D., Makropoulos, A., Christiaens, D., Schuh, A., Passerat-Palmbach, J., Hutter, J., Cordero-Grande, L., Hughes, E., Price, A., Hajnal, J. V., Rueckert, D., Robinson, E. C., & Edwards, A. D. (2020). Cortical morphology at birth reflects spatiotemporal patterns of gene expression in the fetal human brain. *PLOS Biology*, *18*(11), e3000976. https://doi.org/10.1371/journal.pbio.3000976

Bandettini, P. A. (2012). Twenty years of functional MRI: The science and the stories. *NeuroImage*, *62*(2), 575–588. https://doi.org/10.1016/j.neuroimage.2012.04.026

Barascud, N., Pearce, M. T., Griffiths, T. D., Friston, K. J., & Chait, M. (2016). Brain responses in humans reveal ideal observer-like sensitivity to complex acoustic patterns. *Proceedings of the National Academy of Sciences*, *113*(5), E616–E625. https://doi.org/10.1073/pnas.1508523113

Bard, J. B., & Rhee, S. Y. (2004). Ontologies in biology: Design, applications and future challenges. *Nature Reviews Genetics*, *5*(3), 213–222. https://doi.org/10.1038/nrg1295

Barnett, S. M., & Ceci, S. J. (2002). When and where do we apply what we learn? A taxonomy for far transfer. *Psychological Bulletin*, *128*(4), 612–637. https://doi.org/10.1037/0033-2909.128.4.612

Barron, D. H. (1950). An experimental analysis of some factors involved in the development of the fissure pattern of the cerebral cortex. *Journal of Experimental Zoology*, *113*(3), 553–581. https://doi.org/10.1002/jez.1401130304

Bartley, A. (1997). Genetic variability of human brain size and cortical gyral patterns. *Brain*, *120*(2), 257–269. https://doi.org/10.1093/brain/120.2.257

Bathke, A. C., & Harrar, S. W. (2008). Nonparametric methods in multivariate factorial designs for large number of factor levels. *Journal of Statistical Planning and Inference*, *138*(3), 588–610. https://doi.org/10.1016/j.jspi.2006.11.004

Baumann, N., & Pham-Dinh, D. (2001). Biology of oligodendrocyte and myelin in the mammalian central nervous system. *Physiological Reviews*, *81*(2), 871–927. https://doi.org/10.1152/physrev.2001.81.2.871

Baumann, S., Griffiths, T. D., Rees, A., Hunter, D., Sun, L., & Thiele, A. (2010). Characterisation of the BOLD response time course at different levels of the auditory

pathway in non-human primates. *NeuroImage*, *50*(3), 1099–1108. https://doi.org/10.1016/j.neuroimage.2009.12.103

Baumann, S., Joly, O., Rees, A., Petkov, C. I., Sun, L., Thiele, A., & Griffiths, T. D. (2015). The topography of frequency and time representation in primate auditory cortices. *eLife*, *4*(4), 1–15. https://doi.org/10.7554/eLife.03256

Baumann, S., Petkov, C. I., & Griffiths, T. D. (2013). A unified framework for the organization of the primate auditory cortex. *Frontiers in Systems Neuroscience*, *7*. https://doi.org/10.3389/fnsys.2013.00011

Bayly, P. V., Okamoto, R. J., Xu, G., Shi, Y., & Taber, L. A. (2013). A cortical folding model incorporating stress-dependent growth explains gyral wavelengths and stress patterns in the developing brain. *Physical Biology*, *10*(1), 016005. https://doi.org/10.1088/1478-3975/10/1/016005

Behrens, J. T. (1997). Principles and Procedures of Exploratory Data Analysis. *Psychological Methods*, *2*(2), 131–160. https://doi.org/10.1037/1082-989X.2.2.131

Belin, P., Fillion-Bilodeau, S., & Gosselin, F. (2008). The Montreal Affective Voices: A validated set of nonverbal affect bursts for research on auditory affective processing. *Behavior Research Methods*, *40*(2), 531–539. https://doi.org/10.3758/BRM.40.2.531

Belliveau, J. W., Kennedy, D. N., McKinstry, R. C., Buchbinder, B. R., Weisskoff, Rm., Cohen, M. S., Vevea, J. M., Brady, T. J., & Rosen, B. R. (1991). Functional mapping of the human visual cortex by magnetic resonance imaging. *Science*, *254*(5032), 716–719.

Bench, J., Kowal, Å., & Bamford, J. (1979). The BKB (Bamford-Kowal-Bench) sentence lists for partially-hearing children. *British Journal of Audiology*, *13*(3), 108–112.

Bendor, D., & Wang, X. (2006). Cortical representations of pitch in monkeys and humans. *Current Opinion in Neurobiology*, *16*(4), 391–399. https://doi.org/10.1016/j.conb.2006.07.001

Bendor, D., & Wang, X. (2008). Neural response properties of primary, rostral, and rostrotemporal core fields in the auditory cortex of marmoset monkeys. *Journal of Neurophysiology*, *100*(2), 888–906. https://doi.org/10.1152/jn.00884.2007

Benjamini, Y., & Hochberg, Y. (1995). Controlling the false discovery rate: A practical and powerful approach to multiple testing. *Journal of the Royal Statistical Society. Series B (Methodological)*, *57*(1), 289–300. https://doi.org/10.2307/2346101

Benner, J., Wengenroth, M., Reinhardt, J., Stippich, C., Schneider, P., & Blatow, M. (2017). Prevalence and function of Heschl's gyrus morphotypes in musicians. *Brain Structure and Function*, *222*(8), 3587–3603. https://doi.org/10.1007/s00429-017-1419-x

Berhouma, M. (2013). Beyond the pineal gland assumption: A neuroanatomical appraisal of dualism in Descartes' philosophy. *Clinical Neurology and Neurosurgery*, *115*(9), 1661–1670. https://doi.org/10.1016/j.clineuro.2013.02.023

Bermudez, P., Lerch, J. P., Evans, A. C., & Zatorre, R. J. (2009). Neuroanatomical Correlates of Musicianship as Revealed by Cortical Thickness and Voxel-Based Morphometry. *Cerebral Cortex*, *19*(7), 1583–1596. https://doi.org/10.1093/cercor/bhn196

Besle, J., Mougin, O., Sánchez-Panchuelo, R. M., Lanting, C., Gowland, P., Bowtell, R., Francis, S., & Krumbholz, K. (2019). Is Human Auditory Cortex Organization Compatible with the Monkey Model? Contrary Evidence from Ultra-High-Field Functional and Structural MRI. *Cerebral Cortex*, *29*(1), 410–428. https://doi.org/10.1093/cercor/bhy267

Betizeau, M., Cortay, V., Patti, D., Pfister, S., Gautier, E., Bellemin-Ménard, A., Afanassieff, M., Huissoud, C., Douglas, R. J., Kennedy, H., & Dehay, C. (2013). Precursor Diversity and Complexity of Lineage Relationships in the Outer Subventricular Zone of the Primate. *Neuron*, *80*(2), 442–457. https://doi.org/10.1016/j.neuron.2013.09.032

Bettison, S. (1996). The long-term effects of auditory training on children with autism. *Journal of autism and developmental disorders,* 26(3), 361–374.

Bidelman, G. M., & Yoo, J. (2020). Musicians Show Improved Speech Segregation in Competitive, Multi-Talker Cocktail Party Scenarios. *Frontiers in Psychology*, *11*. https://doi.org/10.3389/fpsyg.2020.01927

Bizley, J. K., Nodal, F. R., Nelken, I., & King, A. J. (2005). Functional organization of ferret auditory cortex. *Cerebral Cortex (New York, N.Y.: 1991)*, *15*(10), 1637–1653. https://doi.org/10.1093/cercor/bhi042

Blackburn, C. C., & Sachs, M. B. (1990). The representations of the steady-state vowel sound /e/ in the discharge patterns of cat anteroventral cochlear nucleus neurons. *Journal of Neurophysiology*, *63*(5), 1191–1212. https://doi.org/10.1152/jn.1990.63.5.1191

Blackmon, K., Kuzniecky, R., Barr, W. B., Snuderl, M., Doyle, W., Devinsky, O., & Thesen, T. (2015). Cortical Gray and Cognitive Morbidity in Focal Cortical Dysplasia. *Cerebral Cortex*, *25*(9), 2854–2862. https://doi.org/10.1093/cercor/bhu080

Boebinger, D., Evans, S., Rosen, S., Lima, C. F., Manly, T., & Scott, S. K. (2015). Musicians and non-musicians are equally adept at perceiving masked speech. *The Journal of the Acoustical Society of America*, *137*(1), 378–387. https://doi.org/10.1121/1.4904537

Borrell, V. (2018). How Cells Fold the Cerebral Cortex. *The Journal of Neuroscience*, *38*(4), 776–783. https://doi.org/10.1523/JNEUROSCI.1106-17.2017

Borrell, V., & Calegari, F. (2014). Mechanisms of brain evolution: Regulation of neural progenitor cell diversity and cell cycle length. *Neuroscience Research*, *86*, 14–24. https://doi.org/10.1016/j.neures.2014.04.004

Borrell, V., & Götz, M. (2014). Role of radial glial cells in cerebral cortex folding. *Current Opinion in Neurobiology*, *27*, 39–46. https://doi.org/10.1016/j.conb.2014.02.007

Borrell, V., & Reillo, I. (2012). Emerging roles of neural stem cells in cerebral cortex development and evolution. *Developmental Neurobiology*, *72*(7), 955–971. https://doi.org/10.1002/dneu.22013

Breiman, L. (2001). Random forests. *Random Forests*, *45*(1), 5–32. https://doi.org/10.1201/9780429469275-8

British Society of Audiology. (2018). *Pure-tone air-conduction and bone- conduction threshold audiometry with and without masking.* https://www.thebsa.org.uk/resources/pure-tone-air-bone-conduction-threshold-audiometry-without-masking/.

Brodmann, K. (1909). *Vergleichende lokalisationslehre der grosshirnrinde in ihren prinzipien dargestellt auf grund des zellenbaues*. Barth.

Brunner, E., Dette, H., & Munk, A. (1997). Box-type approximations in nonparametric factorial designs. *Journal of the American Statistical Association*, *92*(440), 1494–1502. https://doi.org/10.1080/01621459.1997.10473671

Brunner, E., & Munzel, U. (2000). The Nonparametric Behrens-Fisher Problem: Asymptotic Theory and a Small-Sample Approximation - Brunner - 2000 - Biometrical Journal - Wiley Online Library. *Biometrical Journal*, *42*, 17–25.

Bugos, J. A., Perlstein, W. M., McCrae, C. S., Brophy, T. S., & Bedenbaugh, P. H. (2007). Individualized piano instruction enhances executive functioning and working memory in older adults. *Aging & Mental Health*, *11*(4), 464–471. https://doi.org/10.1080/13607860601086504

Butler, B. E., & Trainor, L. J. (2015). The musician redefined: A behavioral assessment of rhythm perception in professional club DJs. *Timing & Time Perception*, *3*(1-2), 116–132. https://doi.org/10.1163/22134468-03002041

Butti, C., Raghanti, M. A., Sherwood, C. C., & Hof, P. R. (2011). The neocortex of cetaceans: Cytoarchitecture and comparison with other aquatic and terrestrial species: Butti et al. *Annals of the New York Academy of Sciences*, *1225*(1), 47–58. https://doi.org/10.1111/j.1749-6632.2011.05980.x

Callaghan, M. F., Freund, P., Draganski, B., Anderson, E., Cappelletti, M., Chowdhury, R., Diedrichsen, J., FitzGerald, T. H. B., Smittenaar, P., Helms, G., Lutti, A., & Weiskopf, N. (2014). Widespread age-related differences in the human brain microstructure

revealed by quantitative magnetic resonance imaging. *Neurobiology of Aging*, *35*(8), 1862–1872. https://doi.org/10.1016/j.neurobiolaging.2014.02.008

Callaghan, M. F., Helms, G., Lutti, A., Mohammadi, S., & Weiskopf, N. (2015). A general linear relaxometry model of R1 using imaging data. *Magnetic Resonance in Medicine*, *73*(3), 1309–1314. https://doi.org/10.1002/mrm.25210

Campain, R., & Minckler, J. (1976). A note on the gross configurations of the human auditory cortex. *Brain and Language*, *3*(2), 318–323. https://doi.org/10.1016/0093-934X(76)90026-2

Cárdenas, A., & Borrell, V. (2020). Molecular and cellular evolution of corticogenesis in amniotes. *Cellular and Molecular Life Sciences*, *77*(8), 1435–1460. https://doi.org/10.1007/s00018-019-03315-x

Cárdenas, A., Villalba, A., de Juan Romero, C., Picó, E., Kyrousi, C., Tzika, A. C., Tessier-Lavigne, M., Ma, L., Drukker, M., Cappello, S., & Borrell, V. (2018). Evolution of Cortical Neurogenesis in Amniotes Controlled by Robo Signaling Levels. *Cell*, *174*(3), 590–606.e21. https://doi.org/10.1016/j.cell.2018.06.007

Carey, D., Caprini, F., Allen, M., Lutti, A., Weiskopf, N., Rees, G., Callaghan, M. F., & Dick, F. (2018). Quantitative MRI provides markers of intra-, inter-regional, and age-related differences in young adult corticwal microstructure. *NeuroImage*, *182*. https://doi.org/10.1016/j.neuroimage.2017.11.066

Carey, D., Rosen, S., Krishnan, S., Pearce, M. T., Shepherd, A., Aydelott, J., & Dick, F. (2015). Generality and specificity in the effects of musical expertise on perception and cognition. *Cognition*, *137*, 81–105. https://doi.org/10.1016/j.cognition.2014.12.005

Case, A. (2012). *Mix Smart: Professional Techniques for the Home Studio*. Focal Press.

Castriota-Scanderbeg, A., Hagberg, G. E., Cerasa, A., Committeri, G., Galati, G., Patria, F., Pitzalis, S., Caltagirone, C., & Frackowiak, R. (2005). The appreciation of wine by sommeliers: A functional magnetic resonance study of sensory integration. *NeuroImage*, *25*(2), 570–578. https://doi.org/10.1016/j.neuroimage.2004.11.045

Chabot, N., Butler, B. E., & Lomber, S. G. (2015). Differential Modification of Cortical and Thalamic Projections to Cat Primary Auditory Cortex Following Early- and Late-Onset Deafness. *The Journal of Comparative Neurology*, *523*(15), 2297–2320. https://doi.org/10.1002/cne.23790

Chang, M., Suzuki, N., & Kawai, H. D. (2018). Laminar specific gene expression reveals differences in postnatal laminar maturation in mouse auditory, visual, and somatosensory cortex. *The Journal of Comparative Neurology*, *526*(14), 2257–2284. https://doi.org/10.1002/cne.24481

Chartrand, J.-P., Filion-Bilodeau, S., & Belin, P. (2007). Brain response to birdsongs in bird experts. *Neuroreport*, *18*(4), 335–340.

Cheema, J. R. (2014). Some general guidelines for choosing missing data handling methods in educational research. *Journal of Modern Applied Statistical Methods*, *13*(2), 53–75. https://doi.org/10.22237/jmasm/1414814520

Chen, J. L., Penhune, V. B., & Zatorre, R. J. (2008). Moving on time: Brain network for auditory-motor synchronization is modulated by rhythm complexity and musical training. *Journal of Cognitive Neuroscience*, *20*(2), 226–239. https://doi.org/10.1162/jocn.2008.20018

Chen, L., Wang, X., Ge, S., & Xiong, Q. (2019). Medial geniculate body and primary auditory cortex differentially contribute to striatal sound representations. *Nature Communications*, *10*(1), 418. https://doi.org/10.1038/s41467-019-08350-7

Chobert, J., François, C., Velay, J. L., & Besson, M. (2014). Twelve months of active musical training in 8-to 10-year-old children enhances the preattentive processing of syllabic duration and voice onset time. *Cerebral Cortex*, *24*(4), 956–967. https://doi.org/10.1093/cercor/bhs377

Chung, Y. S., Hyatt, C. J., & Stevens, M. C. (2017). Adolescent maturation of the relationship between cortical gyrification and cognitive ability. *NeuroImage*, *158*, 319–331. https://doi.org/10.1016/j.neuroimage.2017.06.082

Cicchini, G. M., Arrighi, R., Cecchetti, L., Giusti, M., & Burr, D. C. (2012). Optimal encoding of interval timing in expert percussionists. *Journal of Neuroscience*, *32*(3), 1056–1060. https://doi.org/10.1523/JNEUROSCI.3411-11.2012

Clayton, K. K., Swaminathan, J., Yazdanbakhsh, A., Zuk, J., Patel, A. D., & Kidd, G. (2016). Executive function, visual attention and the cocktail party problem in musicians and non-musicians. *PLoS ONE*, *11*(7), 1–17. https://doi.org/10.1371/journal.pone.0157638

Cliff, N. (1993). Dominance Statistics: Ordinal Analyses to Answer Ordinal Questions. *Psychol Bull*, *114*(3), 494–509.

Coffey, E. B. J., Mogilever, N. B., & Zatorre, R. J. (2017a). Speech-in-noise perception in musicians: A review. *Hearing Research*, *352*, 49–69. https://doi.org/10.1016/j.heares.2017.02.006

Coffey, E. B. J., Mogilever, N. B., & Zatorre, R. J. (2017b). Speech-in-noise perception in musicians: A review. *Hearing Research*, *352*, 49–69. https://doi.org/10.1016/j.heares.2017.02.006

Cohen, J. (1994). *The Earth Is Round ($p < .05$)*.

Corey, J. (2013). Technical ear training: Tools and practical methods Learning acoustic phonetics by listening, seeing, and touching Proceedings. *The Journal of the Acoustical Society of America*, *19*, 25020. https://doi.org/10.1121/1.4795853

Corey, J., & Benson, D. H. (2016). Audio production and critical listening: Technical ear training, second edition. In *Audio Production and Critical Listening: Technical Ear Training*. https://doi.org/10.4324/9781315727813

Correia, A. I., Castro, S. L., MacGregor, C., Müllensiefen, D., Schellenberg, E. G., & Lima, C. F. (2020). Enhanced Recognition of Vocal Emotions in Individuals With Naturally Good Musical Abilities. *Emotion*. https://doi.org/10.1037/emo0000770

Corrigall, K. a, Schellenberg, E. G., & Misura, N. M. (2013). Music training, cognition, and personality. *Frontiers in Psychology*, *4*(April), 222. https://doi.org/10.3389/fpsyg.2013.00222

Cox, R. W. (2012). AFNI: What a long strange trip it's been. *NeuroImage*, *62*(2), 743–747. https://doi.org/10.1016/j.neuroimage.2011.08.056

Cross, I. (2012). Cognitive Science and the Cultural Nature of Music. *Topics in Cognitive Science*, *4*(4), 668–677. https://doi.org/10.1111/j.1756-8765.2012.01216.x

Da Costa, S., van der Zwaag, W., Marques, J. P., Frackowiak, R. S. J., Clarke, S., & Saenz, M. (2011). Human Primary Auditory Cortex Follows the Shape of Heschl's Gyrus. *Journal of Neuroscience*, *31*(40), 14067–14075. https://doi.org/10.1523/JNEUROSCI.2000-11.2011

Da Costa, S., van der Zwaag, W., Miller, L. M., Clarke, S., & Saenz, M. (2013). Tuning In to Sound: Frequency-Selective Attentional Filter in Human Primary Auditory Cortex. *Journal of Neuroscience*, *33*(5), 1858–1863. https://doi.org/10.1523/JNEUROSCI.4405-12.2013

Dalboni da Rocha, J. L., Schneider, P., Benner, J., Santoro, R., Atanasova, T., Van De Ville, D., & Golestani, N. (2020). TASH: Toolbox for the Automated Segmentation of Heschl's gyrus. *Scientific Reports*, *10*(1), 3887. https://doi.org/10.1038/s41598-020-60609-y

Dale A. M., S. M. L., Fischl B. (1999). Cortical Surface-Based Analysis. *NeuroImage*, *194*, 179–194. https://doi.org/10.1006/nimg.1998.0395

Dale, A. M., & Sereno, M. I. (1993). Improved Localization of Cortical Activity by Combining EEG and MEG with MRI Cortical Surface Reconstruction: A Linear Approach. *Journal of Cognitive Neuroscience*, *5*(2), 162–176. https://doi.org/10.1162/jocn.1993.5.2.162

de Juan Romero, C., Bruder, C., Tomasello, U., Sanz-Anquela, J. M., & Borrell, V. (2015). Discrete domains of gene expression in germinal layers distinguish the development of gyrencephaly. *The EMBO Journal*, *34*(14), 1859–1874. https://doi.org/10.15252/embj.201591176

De Kerangal, M., Vickers, D., & Chait, M. (2021). The effect of healthy aging on change detection and sensitivity to predictable structure in crowded acoustic scenes. *Hearing Research*, *399*, 108074.

De Man, B., Boerum, M., Leonard, B., King, R., Massenburg, G., & Reiss, J. D. (2015). Perceptual evaluation of music mixing practices. *138th Audio Engineering Society Convention 2015*, *1*, 129–136.

de Manzano, Ö., Kuckelkorn, K. L., Ström, K., & Ullén, F. (2020). Action-Perception Coupling and near Transfer: Listening to Melodies after Piano Practice Triggers Sequence-Specific Representations in the Auditory-Motor Network. *Cerebral Cortex*, *30*(10), 5193–5203. https://doi.org/10.1093/cercor/bhaa018

De Martino, F., Moerel, M., Ugurbil, K., Goebel, R., Yacoub, E., & Formisano, E. (2015). Frequency preference and attention effects across cortical depths in the human primary auditory cortex. *Proceedings of the National Academy of Sciences*, *112*(52), 16036–16041. https://doi.org/10.1073/pnas.1507552112

De Martino, F., Moerel, M., van de Moortele, P.-F., Ugurbil, K., Goebel, R., Yacoub, E., & Formisano, E. (2013). Spatial organization of frequency preference and selectivity in the human inferior colliculus. *Nature Communications*, *4*, 1386. https://doi.org/10.1038/ncomms2379

De Martino, F., Moerel, M., Xu, J., van de Moortele, P.-F., Ugurbil, K., Goebel, R., Yacoub, E., & Formisano, E. (2014). High-Resolution Mapping of Myeloarchitecture In Vivo: Localization of Auditory Areas in the Human Brain. *Cerebral Cortex*, *25*(10), 3394–3405. https://doi.org/10.1093/cercor/bhu150

De Meo, R., Bourquin, N. M.-P., Knebel, J.-F., Murray, M. M., & Clarke, S. (2015). From bird to sparrow: Learning-induced modulations in fine-grained semantic discrimination. *Neuroimage*, *118*, 163–173.

de Villers-Sidani, E., Alzghoul, L., Zhou, X., Simpson, K. L., Lin, R. C. S., & Merzenich, M. M. (2010). Recovery of functional and structural age-related changes in the rat primary auditory cortex with operant training. *Proceedings of the National Academy of Sciences of the United States of America*, *107*(31), 13900–13905. https://doi.org/10.1073/pnas.1007885107

de Villers-Sidani, E., Chang, E. F., Bao, S., & Merzenich, M. M. (2007). Critical period window for spectral tuning defined in the primary auditory cortex (A1) in the rat. *The Journal of Neuroscience: The Official Journal of the Society for Neuroscience*, *27*(1), 180–189. https://doi.org/10.1523/JNEUROSCI.3227-06.2007

Dehay, C., Giroud, P., Berland, M., Killackey, H., & Kennedy, H. (1996). Contribution of thalamic input to the specification of cytoarchitectonic cortical fields in the primate: Effects of bilateral enucleation in the fetal monkey on the boundaries, dimensions, and gyrification of striate and extrastriate cortex. *The Journal of Comparative Neurology*, *367*(1), 70–89. https://doi.org/10.1002/(SICI)1096-9861(19960325)367:1<70::AID-CNE6>3.0.CO;2-G

Dehay, C., Horsburgh, G., Berland, M., Killackey, H., & Kennedy, H. (1991). The effects of bilateral enucleation in the primate fetus on the parcellation of visual cortex.

Developmental Brain Research, *62*(1), 137–141. https://doi.org/10.1016/0165-3806(91)90199-S

Dehay, C., Kennedy, H., & Kosik, K. S. (2015). The Outer Subventricular Zone and Primate-Specific Cortical Complexification. *Neuron*, *85*(4), 683–694. https://doi.org/10.1016/j.neuron.2014.12.060

Del Maschio, N., Fedeli, D., Sulpizio, S., & Abutalebi, J. (2019). The relationship between bilingual experience and gyrification in adulthood: A cross-sectional surface-based morphometry study. *Brain and Language*, *198*, 104680. https://doi.org/10.1016/j.bandl.2019.104680

del Toro, D., Ruff, T., Cederfjäll, E., Villalba, A., Seyit-Bremer, G., Borrell, V., & Klein, R. (2017). Regulation of Cerebral Cortex Folding by Controlling Neuronal Migration via FLRT Adhesion Molecules. *Cell*, *169*(4), 621–635.e16. https://doi.org/10.1016/j.cell.2017.04.012

Delaney, H. D., & Vargha, A. (2002). Comparing several robust tests of stochastic equality with ordinally scaled variables and small to moderate sized samples. *Psychological Methods*, *7*(4), 485–503. https://doi.org/10.1037/1082-989X.7.4.485

Destrieux, C., Fischl, B., Dale, A., & Halgren, E. (2010). Automatic parcellation of human cortical gyri and sulci using standard anatomical nomenclature. *NeuroImage*, *53*(1), 1–15. https://doi.org/10.1016/j.neuroimage.2010.06.010

Dick, F. K., Lehet, M. I., Callaghan, M. F., Keller, T. A., Sereno, M. I., & Holt, L. L. (2017). Extensive tonotopic mapping across auditory cortex is recapitulated by spectrally directed attention and systematically related to cortical myeloarchitecture. *Journal of Neuroscience*, *37*(50), 12187–12201. https://doi.org/10.1523/JNEUROSCI.1436-17.2017

Dick, F., Taylor Tierney, A., Lutti, A., Josephs, O., Sereno, M. I., & Weiskopf, N. (2012). In Vivo Functional and Myeloarchitectonic Mapping of Human Primary Auditory Areas. *Journal of Neuroscience*, *32*(46), 16095–16105. https://doi.org/10.1523/JNEUROSCI.1712-12.2012

Dinse, J., Härtwich, N., Waehnert, M. D., Tardif, C. L., Schäfer, A., Geyer, S., Preim, B., Turner, R., & Bazin, P.-L. (2015). A cytoarchitecture-driven myelin model reveals area-specific signatures in human primary and secondary areas using ultra-high resolution in-vivo brain MRI. *NeuroImage*, *114*, 71–87. https://doi.org/10.1016/j.neuroimage.2015.04.023

Douglas, K. M., & Bilkey, D. K. (2007). Amusia is associated with deficits in spatial processing. *Nature Neuroscience*, *10*(7), 915–921. https://doi.org/10.1038/nn1925

Dubois, J., Dehaene-Lambertz, G., Kulikova, S., Poupon, C., Hüppi, P. S., & Hertz-Pannier, L. (2014). The early development of brain white matter: A review of imaging studies

in fetuses, newborns and infants. *Neuroscience*, *276*, 48–71. https://doi.org/10.1016/j.neuroscience.2013.12.044

Dumoulin, S. O., & Wandell, B. A. (2008). Population receptive field estimates in human visual cortex. *NeuroImage*, *39*(2), 647–660. https://doi.org/10.1016/j.neuroimage.2007.09.034

Eichert, N., Watkins, K. E., Mars, R. B., & Petrides, M. (2021). Morphological and functional variability in central and subcentral motor cortex of the human brain. *Brain Structure and Function*, *226*(1), 263–279. https://doi.org/10.1007/s00429-020-02180-w

Eickhoff, S. B., Stephan, K. E., Mohlberg, H., Grefkes, C., Gereon R. Fink, Fink, G. R., Amunts, K., & Zilles, K. (2005). A new SPM toolbox for combining probabilistic cytoarchitectonic maps and functional imaging data. *NeuroImage*, *25*(4), 1325–1335. https://doi.org/10.1016/j.neuroimage.2004.12.034

Eickhoff, S., Walters, N. B., Schleicher, A., Kril, J., Egan, G. F., Zilles, K., Watson, J. D. G., & Amunts, K. (2004). High-resolution MRI reflects myeloarchitecture and cytoarchitecture of human cerebral cortex. *Human Brain Mapping*, *24*(3), 206–215. https://doi.org/10.1002/hbm.20082

Ellis, A. R., Burchett, W. W., Harrar, S. W., & Bathke, A. C. (2017). Nonparametric inference for multivariate data: The R package npmv. *Journal of Statistical Software*, *76*(1). https://doi.org/10.18637/jss.v076.i04

Ellis, D. G., & Aizenberg, M. R. (2022). Structural Brain Imaging Predicts Individual-Level Task Activation Maps Using Deep Learning. *Frontiers in Neuroimaging*, *1*. https://doi.org/10.3389/fnimg.2022.834883

Emery, B. (2010). Regulation of Oligodendrocyte Differentiation and Myelination. *Science*, *330*(6005), 779–782. https://doi.org/10.1126/science.1190927

Ericsson, K. A., & Charness, N. (1994). Expert Performance: Its Structure and Acquisition. *American Psychologist*, *49*(8), 725–747. https://doi.org/10.1037/0003-066x.49.8.725

Escobar, J., Mussoi, B. S., & Silberer, A. B. (2020). The Effect of Musical Training and Working Memory in Adverse Listening Situations. *Ear and Hearing*, *41*(2), 278–288. https://doi.org/10.1097/AUD.0000000000000754

Essen, D. C. V., Drury, H. A., Joshi, S., & Miller, M. I. (1998). Functional and Structural Mapping of Human Cerebral Cortex: Solutions are in the Surfaces. *Proceedings of the National Academy of Sciences of the United States of America*, *95*(3), 788–795.

Fame, R. M., Cortés-Campos, C., & Sive, H. L. (2020). Brain Ventricular System and Cerebrospinal Fluid Development and Function: Light at the End of the Tube: A Primer with Latest Insights. *BioEssays*, *42*(3), 1900186. https://doi.org/10.1002/bies.201900186

Fenchel, D., Dimitrova, R., Seidlitz, J., Robinson, E. C., Batalle, D., Hutter, J., Christiaens, D., Pietsch, M., Brandon, J., Hughes, E. J., Allsop, J., O'Keeffe, C., Price, A. N., Cordero-Grande, L., Schuh, A., Makropoulos, A., Passerat-Palmbach, J., Bozek, J., Rueckert, D., … O'Muircheartaigh, J. (2020). Development of Microstructural and Morphological Cortical Profiles in the Neonatal Brain. *Cerebral Cortex*, *30*(11), 5767–5779. https://doi.org/10.1093/cercor/bhaa150

Fernald, A., & Kuhl, P. K. (1987). Acoustic determinants of infant preference for motherese speech. *Infant Behavior & Development*, *10*, 279–293. https://doi.org/10.1016/0163-6383(87)90017-8

Fietz, S. A., Kelava, I., Vogt, J., Wilsch-Bräuninger, M., Stenzel, D., Fish, J. L., Corbeil, D., Riehn, A., Distler, W., Nitsch, R., & Huttner, W. B. (2010). OSVZ progenitors of human and ferret neocortex are epithelial-like and expand by integrin signaling. *Nature Neuroscience*, *13*(6), 690–699. https://doi.org/10.1038/nn.2553

Fischl, B. (2012). FreeSurfer. *NeuroImage*, *62*(2), 774–781. https://doi.org/10.1016/j.neuroimage.2012.01.021

Fischl, B. (2013). Estimating the location of Brodmann areas from cortical folding patterns using histology and ex vivo MRI. In *Microstructural parcellation of the human cerebral cortex* (pp. 129–156). Springer. https://doi.org/10.1007/978-3-642-37824-9_4

Fischl, B., Rajendran, N., Busa, E., Augustinack, J., Hinds, O., Yeo, B. T. T., Mohlberg, H., Amunts, K., & Zilles, K. (2008). Cortical Folding Patterns and Predicting Cytoarchitecture. *Cerebral Cortex*, *18*(8), 1973–1980. https://doi.org/10.1093/cercor/bhm225

Fischl, B., Sereno, M. I., & Dale, A. M. (1999a). Cortical Surface-Based Analysis: II: Inflation, Flattening, and a Surface-Based Coordinate System. *NeuroImage*, *9*(2), 195–207. https://doi.org/10.1006/nimg.1998.0396

Fischl, B., Sereno, M. I., & Dale, A. M. (1999b). Cortical surface-based analysis: II: Inflation, flattening, and a surface-based coordinate system. *Neuroimage*, *9*(2), 195–207.

Fisher, M., Holland, C., Merzenich, M. M., & Vinogradov, S. (2009). Using neuroplasticity-based auditory training to improve verbal memory in schizophrenia. *American Journal of Psychiatry*, *166*(7), 805–811. https://doi.org/10.1176/appi.ajp.2009.08050757

Flaugnacco, E., Lopez, L., Terribili, C., Montico, M., Zoia, S., & Schön, D. (2015). Music training increases phonological awareness and reading skills in developmental dyslexia: A randomized control trial. *PLoS ONE*, *10*(9). https://doi.org/10.1371/journal.pone.0138715

Florio, M., Albert, M., Taverna, E., Namba, T., Brandl, H., Lewitus, E., Haffner, C., Sykes, A., Wong, F. K., Peters, J., et al. (2015). Human-specific gene ARHGAP11B promotes basal progenitor amplification and neocortex expansion. *Science (New York, N.Y.)*, *347*(6229), 1465–1470. https://doi.org/10.1126/science.aaa1975

Florio, M., Namba, T., Pääbo, S., Hiller, M., & Huttner, W. B. (2016). A single splice site mutation in human-specific *ARHGAP11B* causes basal progenitor amplification. *Science Advances*, *2*(12), e1601941. https://doi.org/10.1126/sciadv.1601941

Formisano, E., Kim, D.-S., Di Salle, F., Van de Moortele, P.-F., Ugurbil, K., & Goebel, R. (2003). Mirror-symmetric tonotopic maps in human primary auditory cortex. *Neuron*, *40*(4), 859–869. https://doi.org/10.1016/s0896-6273(03)00669-x

Foubet, O., Trejo, M., & Toro, R. (2019). Mechanical morphogenesis and the development of neocortical organisation. *Cortex*, *118*, 315–326. https://doi.org/10.1016/j.cortex.2018.03.005

Franchini, L. F. (2021). Genetic Mechanisms Underlying Cortical Evolution in Mammals. *Frontiers in Cell and Developmental Biology*, *9*, 591017. https://doi.org/10.3389/fcell.2021.591017

François, C., Grau-Sánchez, J., Duarte, E., & Rodriguez-Fornells, A. (2015). Musical training as an alternative and effective method for neuro-education and neuro-rehabilitation. *Frontiers in Psychology*, *6*(APR), 1–15. https://doi.org/10.3389/fpsyg.2015.00475

Fritz, J., Elhilali, M., & Shamma, S. (2005). Active listening: Task-dependent plasticity of spectrotemporal receptive fields in primary auditory cortex. *Hearing Research*, *206*(1-2), 159–176. https://doi.org/10.1016/j.heares.2005.01.015

Fu, Q. J., Nogaki, G., & Galvin, J. J. (2005). Auditory training with spectrally shifted speech: Implications for cochlear implant patient auditory rehabilitation. *JARO - Journal of the Association for Research in Otolaryngology*, *6*(2), 180–189. https://doi.org/10.1007/s10162-005-5061-6

Fuhrmeister, P., & Myers, E. B. (2021). Structural neural correlates of individual differences in categorical perception. *Brain and Language*, *215*, 104919. https://doi.org/10.1016/j.bandl.2021.104919

Fuller, C. D., Galvin, J. J., Maat, B., Free, R. H., & Başkent, D. (2014). The musician effect: Does it persist under degraded pitch conditions of cochlear implant simulations? *Frontiers in Neuroscience*, *8*(8 JUN), 1–16. https://doi.org/10.3389/fnins.2014.00179

Galaburda, A. M., & Pandya, D. N. (1983). The intrinsic architectonic and connectional organization of the superior temporal region of the rhesus monkey. *J Comp Neurol*, *221*(2), 169–184. https://doi.org/10.1002/cne.902210206

Garcia, K. E., Kroenke, C. D., & Bayly, P. V. (2018). Mechanics of cortical folding: Stress, growth and stability. *Philosophical Transactions of the Royal Society B: Biological Sciences*, *373*(1759), 20170321. https://doi.org/10.1098/rstb.2017.0321

García-Gomar, M. G., Strong, C., Toschi, N., Singh, K., Rosen, B. R., Wald, L. L., & Bianciardi, M. (2019). In vivo Probabilistic Structural Atlas of the Inferior and Superior Colliculi, Medial and Lateral Geniculate Nuclei and Superior Olivary Complex in Humans Based on 7 Tesla MRI. *Frontiers in Neuroscience*, *13*.

Garcia-Moreno, F., Vasistha, N. A., Trevia, N., Bourne, J. A., & Molnar, Z. (2012). Compartmentalization of Cerebral Cortical Germinal Zones in a Lissencephalic Primate and Gyrencephalic Rodent. *Cerebral Cortex*, *22*(2), 482–492. https://doi.org/10.1093/cercor/bhr312

Gaser, C., & Schlaug, G. (2003). Brain structures differ between musicians and non-musicians. *The Journal of Neuroscience : The Official Journal of the Society for Neuroscience*, *23*(27), 9240–9245.

Gaucher, Q., Panniello, M., Ivanov, A. Z., Dahmen, J. C., King, A. J., & Walker, K. M. (2020). Complexity of frequency receptive fields predicts tonotopic variability across species. *eLife*, *9*, e53462. https://doi.org/10.7554/eLife.53462

Gaus, W. (2015). Interpretation of Statistical Significance - Exploratory Versus Confirmative Testing in Clinical Trials, Epidemiological Studies, Meta-Analyses and Toxicological Screening (Using Ginkgo biloba as an Example). *Clinical & Experimental Pharmacology*, *05*(04). https://doi.org/10.4172/2161-1459.1000182

Germann, J., Chakravarty, M. M., Collins, D. L., & Petrides, M. (2020). Tight Coupling between Morphological Features of the Central Sulcus and Somatomotor Body Representations: A Combined Anatomical and Functional MRI Study. *Cerebral Cortex*, *30*(3), 1843–1854. https://doi.org/10.1093/cercor/bhz208

Gilardi, C., & Kalebic, N. (2021). The Ferret as a Model System for Neocortex Development and Evolution. *Frontiers in Cell and Developmental Biology*, *9*, 661759. https://doi.org/10.3389/fcell.2021.661759

Gilbert, A. N., & Wysocki, C. J. (1992). Hand preference and age in the United States. *Neuropsychologia*, *30*(7), 601–608. https://doi.org/10.1016/0028-3932(92)90065-T

Gillespie, W., & Myors, B. (2000). Personality of Rock Musicians. *Psychology of Music*, *28*(2), 154–165. https://doi.org/10.1177/0305735600282004

Gilmore, J. H., Schmitt, J. E., Knickmeyer, R. C., Smith, J. K., Lin, W., Styner, M., Gerig, G., & Neale, M. C. (2010). Genetic and environmental contributions to neonatal brain structure: A twin study. *Human Brain Mapping*, n/a–n/a. https://doi.org/10.1002/hbm.20926

Gingras, B., Honing, H., Peretz, I., Trainor, L. J., & Fisher, S. E. (2015). Defining the biological bases of individual differences in musicality. *Philosophical Transactions of*

the Royal Society B: Biological Sciences, *370*(1664). https://doi.org/10.1098/rstb.2014.0092

Glasser, M. F., Coalson, T. S., Robinson, E. C., Hacker, C. D., Harwell, J., Yacoub, E., Ugurbil, K., Andersson, J., Beckmann, C. F., Jenkinson, M., Smith, S. M., & Van Essen, D. C. (2016). A multi-modal parcellation of human cerebral cortex. *Nature*, *536*(7615), 171–178. https://doi.org/10.1038/nature18933

Glasser, M. F., Goyal, M. S., Preuss, T. M., Raichle, M. E., & Van Essen, D. C. (2014). Trends and properties of human cerebral cortex: Correlations with cortical myelin content. *NeuroImage*, *93*, 165–175. https://doi.org/10.1016/j.neuroimage.2013.03.060

Glasser, M. F., & Van Essen, D. C. (2011). Mapping Human Cortical Areas In Vivo Based on Myelin Content as Revealed by T1- and T2-Weighted MRI. *Journal of Neuroscience*, *31*(32), 11597–11616. https://doi.org/10.1523/JNEUROSCI.2180-11.2011

Glendenning, K. K., & Masterton, R. B. (1998). Comparative Morphometry of Mammalian Central Auditory Systems: Variation in Nuclei and Form of the Ascending System. *Brain, Behavior and Evolution*, *51*(2), 59–89. https://doi.org/10.1159/000006530

Golestani, N., Molko, N., Dehaene, S., LeBihan, D., & Pallier, C. (2007). Brain Structure Predicts the Learning of Foreign Speech Sounds. *Cerebral Cortex*, *17*(3), 575–582. https://doi.org/10.1093/cercor/bhk001

Golestani, N., Price, C. J., & Scott, S. K. (2011). Born with an Ear for Dialects? Structural Plasticity in the Expert Phonetician Brain. *Journal of Neuroscience*, *31*(11), 4213–4220. https://doi.org/10.1523/JNEUROSCI.3891-10.2011

Gonda, Y., Namba, T., & Hanashima, C. (2020). Beyond Axon Guidance: Roles of Slit-Robo Signaling in Neocortical Formation. *Frontiers in Cell and Developmental Biology*, *8*, 607415. https://doi.org/10.3389/fcell.2020.607415

Gosling, S. D., Rentfrow, P. J., & Swann, W. B. (2003). A very brief measure of the Big-Five personality domains. *Journal of Research in Personality*, *37*(6), 504–528. https://doi.org/10.1016/S0092-6566(03)00046-1

Goulas, A., Uylings, H., & Hilgetag, C. C. (2017). Principles of ipsilateral and contralateral cortico-cortical connectivity in the mouse. *Brain Structure and Function*, *222*(3), 1281–1295. https://doi.org/10.1007/s00429-016-1277-y

Grassi, M., & Soranzo, A. (2009). MLP: A MATLAB toolbox for rapid and reliable auditory threshold estimation. *Behavior Research Methods*, *41*(1), 20–28. https://doi.org/10.3758/BRM.41.1.20

Green, C. S., & Bavelier, D. (2008). Exercising your brain: A review of human brain plasticity and training-induced learning. *Psychology and Aging*, *23*(4), 692–701. https://doi.org/10.1037/a0014345

Green, C. S., Strobach, T., & Schubert, T. (2014). On methodological standards in training and transfer experiments. *Psychological Research*, *78*(6), 756–772. https://doi.org/10.1007/s00426-013-0535-3

Greenberg, D. M., Müllensiefen, D., Lamb, M. E., & Rentfrow, P. J. (2015). Personality predicts musical sophistication. *Journal of Research in Personality*, *58*, 154–158. https://doi.org/10.1016/j.jrp.2015.06.002

Greve, D. N., & Fischl, B. (2009). Accurate and robust brain image alignment using boundary-based registration. *NeuroImage*, *48*(1), 63–72. https://doi.org/10.1016/j.neuroimage.2009.06.060

Groussard, M., Viader, F., Landeau, B., Desgranges, B., Eustache, F., & Platel, H. (2014). The effects of musical practice on structural plasticity: The dynamics of grey matter changes. *Brain and Cognition*, *90*, 174–180. https://doi.org/10.1016/j.bandc.2014.06.013

Gruber, T. R. (1993). A translation approach to portable ontology specifications. *Knowledge Acquisition*, *5*(2), 199–220. https://doi.org/10.1006/knac.1993.1008

Güçlü, B., Sevinc, E., & Canbeyli, R. (2011). Duration discrimination by musicians and nonmusicians. *Psychological Reports*, *108*(3), 675–687. https://doi.org/10.2466/11.22.27.PR0.108.3.675-687

Guerrini, R., & Dobyns, W. B. (2014). Malformations of cortical development: Clinical features and genetic causes. *The Lancet Neurology*, *13*(7), 710–726. https://doi.org/10.1016/S1474-4422(14)70040-7

Gulban, O. F., De Martino, F., Vu, A. T., Yacoub, E., Uğurbil, K., & Lenglet, C. (2018). Cortical fibers orientation mapping using in-vivo whole brain 7 T diffusion MRI. *NeuroImage*, *178*, 104–118. https://doi.org/10.1016/j.neuroimage.2018.05.010

Gulban, O. F., Goebel, R., Moerel, M., Zachlod, D., Mohlberg, H., Amunts, K., & de Martino, F. (2020). Improving a probabilistic cytoarchitectonic atlas of auditory cortex using a novel method for inter-individual alignment. *eLife*, *9*, e56963. https://doi.org/10.7554/eLife.56963

Gurung, B., & Fritzsch, B. (2004). Time Course of Embryonic Midbrain and Thalamic Auditory Connection Development in Mice as Revealed by Carbocyanine Dye Tracing. *The Journal of Comparative Neurology*, *479*(3), 309–327. https://doi.org/10.1002/cne.20328

Habibi, A., Ilari, B., Heine, K., & Damasio, H. (2020). Changes in auditory cortical thickness following music training in children: Converging longitudinal and cross-sectional results. *Brain Structure and Function*, *225*(8), 2463–2474. https://doi.org/10.1007/s00429-020-02135-1

Hackett, T. A. (2007). Organization and Correspondence of the Auditory Cortex of Humans and Nonhuman Primates. In *Evolution of Nervous Systems* (pp. 109–119). Elsevier. https://doi.org/10.1016/B0-12-370878-8/00012-4

Hackett, T. A., Barkat, T. R., O'Brien, B. M. J., Hensch, T. K., & Polley, D. B. (2011). Linking topography to tonotopy in the mouse auditory thalamocortical circuit. *The Journal of Neuroscience : The Official Journal of the Society for Neuroscience*, *31*(8), 2983–2995. https://doi.org/10.1523/JNEUROSCI.5333-10.2011

Hackett, T. A., Preuss, T. M., & Kaas, J. H. (2001). Architectonic identification of the core region in auditory cortex of macaques, chimpanzees, and humans. *The Journal of Comparative Neurology*, *441*(3), 197–222. https://doi.org/10.1002/cne.1407

Hackett, T. A., Stepniewska, I., & Kaas, J. H. (1998). Subdivisions of auditory cortex and ipsilateral cortical connections of the parabelt auditory cortex in macaque monkeys. *The Journal of Comparative Neurology*, *394*(4), 475–495. https://doi.org/10.1002/(SICI)1096-9861(19980518)394:4<475::AID-CNE6>3.0.CO;2-Z

Hagiwara, A., Hori, M., Kamagata, K., Warntjes, M., Matsuyoshi, D., Nakazawa, M., Ueda, R., Andica, C., Koshino, S., Maekawa, T., Irie, R., Takamura, T., Kumamaru, K. K., Abe, O., & Aoki, S. (2018). Myelin Measurement: Comparison Between Simultaneous Tissue Relaxometry, Magnetization Transfer Saturation Index, and T1w/T2w Ratio Methods. *Scientific Reports*, *8*(1), 10554. https://doi.org/10.1038/s41598-018-28852-6

Hallam, S. (2001). The Development of Metacognition in Musicians: Implication for Education. *British Journal of Music Education*, *18*(01), 27–39. https://doi.org/10.1017/S0265051701000122

Hallam, S. (2010). Transitions and the Development of Expertise. *Psychology Teaching Review*, *16*(2), 3–32.

Hansen, D. V., Lui, J. H., Parker, P. R. L., & Kriegstein, A. R. (2010). Neurogenic radial glia in the outer subventricular zone of human neocortex. *Nature*, *464*(7288), 554–561. https://doi.org/10.1038/nature08845

Hassler, M., Birbaumer, N., & Feil, A. (1985). Musical talent and visual-spatial abilities: A longitudinal study. *Psychology of Music*, *13*(2), 99–113.

Haukoos, J. S., & Lewis, R. J. (2005). Advanced statistics: Bootstrapping confidence intervals for statistics with "difficult" distributions. *Academic Emergency Medicine*, *12*(4), 360–365. https://doi.org/10.1197/j.aem.2004.11.018

Heide, M., Haffner, C., Murayama, A., Kurotaki, Y., Shinohara, H., Okano, H., Sasaki, E., & Huttner, W. B. (2020). Human-specific *ARHGAP11B* increases size and folding of primate neocortex in the fetal marmoset. *Science*, *369*(6503), 546–550. https://doi.org/10.1126/science.abb2401

Heidekum, A. E., Vogel, S. E., & Grabner, R. H. (2020). Associations Between Individual Differences in Mathematical Competencies and Surface Anatomy of the Adult Brain. *Frontiers in Human Neuroscience*, *14*, 116. https://doi.org/10.3389/fnhum.2020.00116

Helms, G., & Dechent, P. (2009). Increased SNR and reduced distortions by averaging multiple gradient echo signals in 3D FLASH imaging of the human brain at 3T. *Journal of Magnetic Resonance Imaging: JMRI*, *29*(1), 198–204. https://doi.org/10.1002/jmri.21629

Henkelman, R. M., Stanisz, G. J., & Graham, S. J. (2001). Magnetization transfer in MRI: A review. *NMR in Biomedicine*, *14*(2), 57–64. https://doi.org/10.1002/nbm.683

Henshaw, H., & Ferguson, M. A. (2013). Efficacy of Individual Computer-Based Auditory Training for People with Hearing Loss: A Systematic Review of the Evidence. *PLoS ONE*, *8*(5). https://doi.org/10.1371/journal.pone.0062836

Hepper, P. G., & Shahidullah, B. S. (1994). Development of fetal hearing. *Archives of Disease in Childhood Fetal and Neonatal Edition*, *71*(2), F81–F87.

Heschl. (1878). *Ueber die vordere quere Schlafenwindung des menschlichen Grosshirns*.

Hevner, R. F., & Haydar, T. F. (2012). The (Not Necessarily) Convoluted Role of Basal Radial Glia in Cortical Neurogenesis. *Cerebral Cortex*, *22*(2), 465–468. https://doi.org/10.1093/cercor/bhr336

Heynckes, M., Gulban, O. F., & De Martino, F. (2022). On the superior temporal gyrus by R.L. Heschl: English translation of "Über Die Vordere Quere Schläfenwindung Des Menschlichen Großhirns." *Brain Multiphysics*, *3*, 100055. https://doi.org/10.1016/j.brain.2022.100055

Holt, L. L., Tierney, A. T., Guerra, G., Laffere, A., & Dick, F. (2018). Dimension-selective attention as a possible driver of dynamic, context-dependent re-weighting in speech processing. *Hearing Research*, *366*, 50–64. https://doi.org/10.1016/j.heares.2018.06.014

Hong, S. E., Shugart, Y. Y., Huang, D. T., Shahwan, S. A., Grant, P. E., Hourihane, J. O'B., Martin, N. D. T., & Walsh, C. A. (2000). Autosomal recessive lissencephaly with cerebellar hypoplasia is associated with human RELN mutations. *Nature Genetics*, *26*(1), 93–96. https://doi.org/10.1038/79246

Hothorn, T., & Zeileis, A. (2015). Partykit : A Toolkit for Recursive Partytioning. *Journal of Machine Learning Research*, *16*, 3905–3909.

Howard, D. M., & Angus, J. A. S. (2009). Acoustics and Psychoacoustics Fourth Edition. In *Acoustics and Psychoacoustics: Fifth Edition*.

Hribar, M., Suput, D., Carvalho, A. A., Battelino, S., & Vovk, A. (2014). Structural alterations of brain grey and white matter in early deaf adults. *Hearing Research*, *318*, 1–10. https://doi.org/10.1016/j.heares.2014.09.008

Hubbard, E. M. (2003). A discussion and review of Uttal (2001) The New Phrenology. *Cognitive Science Online*, *1*, 22–33.

Huber, P. J. (1973). Robust regression: Asymptotics, conjectures and monte carlo. *The Annals of Statistics*, *1*(5), 799–821. https://doi.org/10.1214/aos/1176342503

Huber, P. J. (2011). Robust statistics. In M. Lovric (Ed.), *International encyclopedia of statistical science* (pp. 1248–1251). Springer Berlin Heidelberg. https://doi.org/10.1007/978-3-642-04898-2$_5$94

Humphries, C., Liebenthal, E., & Binder, J. R. (2010). Tonotopic organization of human auditory cortex. *NeuroImage*, *50*(3), 1202–1211. https://doi.org/10.1016/j.neuroimage.2010.01.046

Hyde, K. L., Lerch, J., Norton, A., Forgeard, M., Winner, E., Evans, A. C., & Schlaug, G. (2009). Musical training shapes structural brain development. *Journal of Neuroscience*, *29*(10), 3019–3025. https://doi.org/10.1523/JNEUROSCI.5118-08.2009

Imaizumi, K., Priebe, N. J., Crum, P. A. C., Bedenbaugh, P. H., Cheung, S. W., & Schreiner, C. E. (2004). Modular Functional Organization of Cat Anterior Auditory Field. *Journal of Neurophysiology*, *92*(1), 444–457. https://doi.org/10.1152/jn.01173.2003

Imig, T. J., Ruggero, M. A., Kitzes, L. M., Javel, E., & Brugge, J. F. (1977). Organization of auditory cortex in the owl monkey(Aotus trivirgatus). *The Journal of Comparative Neurology*, *171*(1), 111–128. https://doi.org/10.1002/cne.901710108

Iwamiya, S. I., Nakajima, Y., Ueda, K., Kawahara, K., & Takada, M. (2003). Technical Listening Training: Improvement of sound sensitivity for acoustic engineers and sound designers. *Acoustical Science and Technology*, *24*(1), 27–31. https://doi.org/10.1250/ast.24.27

Izhaki, R. (2008). *Mixing audio: Concepts, Practices, and Tools*. Focal Press. https://doi.org/10.5860/choice.49-6905

Jansen, A. G., Mous, S. E., White, T., Posthuma, D., & Polderman, T. J. C. (2015). What Twin Studies Tell Us About the Heritability of Brain Development, Morphology, and Function: A Review. *Neuropsychology Review*, *25*(1), 27–46. https://doi.org/10.1007/s11065-015-9278-9

Javad, F., Warren, J. D., Micallef, C., Thornton, J. S., Golay, X., Yousry, T., & Mancini, L. (2014). Auditory tracts identified with combined fMRI and diffusion tractography. *NeuroImage*, *84*, 562–574. https://doi.org/10.1016/j.neuroimage.2013.09.007

Javier-Torrent, M., Zimmer-Bensch, G., & Nguyen, L. (2021). Mechanical Forces Orchestrate Brain Development. *Trends in Neurosciences*, *44*(2), 110–121. https://doi.org/10.1016/j.tins.2020.10.012

Jespersen, S. N., Leigland, L. A., Cornea, A., & Kroenke, C. D. (2012). Determination of Axonal and Dendritic Orientation Distributions Within the Developing Cerebral Cortex by Diffusion Tensor Imaging. *IEEE Transactions on Medical Imaging*, *31*(1), 16–32. https://doi.org/10.1109/TMI.2011.2162099

Jiang, X., Zhang, T., Zhang, S., Kendrick, K. M., & Liu, T. (2021). Fundamental functional differences between gyri and sulci: Implications for brain function, cognition, and behavior. *Psychoradiology*, *1*(1), 23–41. https://doi.org/10.1093/psyrad/kkab002

Jones, Z., & Linder, F. (2015). Exploratory Data Analysis using Random Forests. *73rd Annual MPSA Conference*, 1–31.

Ju, X.-C., Hou, Q.-Q., Sheng, A.-L., Wu, K.-Y., Zhou, Y., Jin, Y., Wen, T., Yang, Z., Wang, X., & Luo, Z.-G. (2016). The hominoid-specific gene TBC1D3 promotes generation of basal neural progenitors and induces cortical folding in mice. *eLife*, *5*, e18197. https://doi.org/10.7554/eLife.18197

Kaas, J. H. (2011). The Evolution of Auditory Cortex: The Core Areas. In J. A. Winer & C. E. Schreiner (Eds.), *The Auditory Cortex*. Springer US. https://doi.org/10.1007/978-1-4419-0074-6

Kaas, J. H., & Hackett, T. A. (2000). Subdivisions of auditory cortex and processing streams in primates. *Proceedings of the National Academy of Sciences*, *97*(22), 11793–11799. https://doi.org/10.1073/pnas.97.22.11793

Kaganovich, N., Kim, J., Herring, C., Schumaker, J., MacPherson, M., & Weber-Fox, C. (2013). Musicians show general enhancement of complex sound encoding and better inhibition of irrelevant auditory change in music: An ERP study. *European Journal of Neuroscience*, *37*(8), 1295–1307. https://doi.org/10.1111/ejn.12110

Kajikawa, Y., de La Mothe, L., Blumell, S., & Hackett, T. A. (2005). A comparison of neuron response properties in areas A1 and CM of the marmoset monkey auditory cortex: Tones and broadband noise. *Journal of Neurophysiology*, *93*(1), 22–34. https://doi.org/10.1152/jn.00248.2004

Kalebic, N., Gilardi, C., Albert, M., Namba, T., Long, K. R., Kostic, M., Langen, B., & Huttner, W. B. (2018). Human-specific ARHGAP11B induces hallmarks of neocortical expansion in developing ferret neocortex. *eLife*, *7*, e41241. https://doi.org/10.7554/eLife.41241

Kalebic, N., Gilardi, C., Stepien, B., Wilsch-Bräuninger, M., Long, K. R., Namba, T., Florio, M., Langen, B., Lombardot, B., Shevchenko, A., Kilimann, M. W., Kawasaki, H., Wimberger, P., & Huttner, W. B. (2019). Neocortical Expansion Due to Increased

Proliferation of Basal Progenitors Is Linked to Changes in Their Morphology. *Cell Stem Cell*, *24*(4), 535–550.e9. https://doi.org/10.1016/j.stem.2019.02.017

Kalebic, N., & Huttner, W. B. (2020). Basal Progenitor Morphology and Neocortex Evolution. *Trends in Neurosciences*, *43*(11), 843–853. https://doi.org/10.1016/j.tins.2020.07.009

Kaller, M. S., Lazari, A., Blanco-Duque, C., Sampaio-Baptista, C., & Johansen-Berg, H. (2017). Myelin plasticity and behaviourconnecting the dots. *Current Opinion in Neurobiology*, *47*, 86–92. https://doi.org/10.1016/j.conb.2017.09.014

Kandler, K. (2019). *The Oxford handbook of the auditory brainstem*. Oxford University Press, USA.

Kandler, K., Clause, A., & Noh, J. (2009). Tonotopic reorganization of developing auditory brainstem circuits. *Nature Neuroscience*, *12*(6), 711–717. https://doi.org/10.1038/nn.2332

Kaniwa, T., Kim, S., Terasawa, H., Ikeda, M., Yamada, T., & Makino, S. (2011). Towards a personalized technical ear training program: An investigation of the effect of adaptive feedback. *Proceedings of the 8th Sound and Music Computing Conference, SMC 2011*.

Kelava, I., Lewitus, E., & Huttner, W. B. (2013). The secondary loss of gyrencephaly as an example of evolutionary phenotypical reversal. *Frontiers in Neuroanatomy*, *7*. https://doi.org/10.3389/fnana.2013.00016

Kelava, I., Reillo, I., Murayama, A. Y., Kalinka, A. T., Stenzel, D., Tomancak, P., Matsuzaki, F., Lebrand, C., Sasaki, E., Schwamborn, J. C., Okano, H., Huttner, W. B., & Borrell, V. (2012). Abundant Occurrence of Basal Radial Glia in the Subventricular Zone of Embryonic Neocortex of a Lissencephalic Primate, the Common Marmoset Callithrix jacchus. *Cerebral Cortex*, *22*(2), 469–481. https://doi.org/10.1093/cercor/bhr301

Kerimoglu, C., Pham, L., Tonchev, A. B., Sakib, M. S., Xie, Y., Sokpor, G., Ulmke, P. A., Kaurani, L., Abbas, E., Nguyen, H., Rosenbusch, J., Michurina, A., Capece, V., Angelova, M., Maricic, N., Brand-Saberi, B., Esgleas, M., Albert, M., Minkov, R., … Tuoc, T. (2021). H3 acetylation selectively promotes basal progenitor proliferation and neocortex expansion. *Science Advances*, *7*(38), eabc6792. https://doi.org/10.1126/sciadv.abc6792

Kidd, G. R., Watson, C. S., & Gygi, B. (2007). Individual differences in auditory abilities. *The Journal of the Acoustical Society of America*, *122*(1), 418–435. https://doi.org/10.1121/1.2743154

Kim, S.-G., & Knösche, T. R. (2016). Intracortical myelination in musicians with absolute pitch: Quantitative morphometry using 7-T MRI. *Human Brain Mapping*, *37*(10), 3486–3501. https://doi.org/10.1002/hbm.23254

Kim, S., Kaniwa, T., Terasawa, H., Yamada, T., & Makino, S. (2013). Inter-subject differences in personalized technical ear training and the influence of an individually

optimized training sequence. *Acoustical Science and Technology*, *34*(6), 424–431. https://doi.org/10.1250/ast.34.424

Kishon-Rabin, L., Amir, O., Vexler, Y., & Zaltz, Y. (2001). Pitch discrimination: Are professional musicians better than non-musicians? *Journal of Basic and Clinical Physiology and Pharmacology*, *12*(2), 125–144. https://doi.org/10.1515/JBCPP.2001.12.2.125

Kisilevsky, B. S., Hains, S. M. J., Lee, K., Xie, X., Huang, H., Ye, H. H., Zhang, K., & Wang, Z. (2003). Effects of experience on fetal voice recognition. *Psychological Science*, *14*(3), 220–224. https://doi.org/10.1111/1467-9280.02435

Kommajosyula, S. P., Bartlett, E. L., Cai, R., Ling, L., & Caspary, D. M. (2021). Corticothalamic projections deliver enhanced responses to medial geniculate body as a function of the temporal reliability of the stimulus. *The Journal of Physiology*, *599*(24), 5465–5484. https://doi.org/10.1113/JP282321

Konietschke, F., Placzek, M., Schaarschmidt, F., & Hothorn, L. A. (2015). Nparcomp: An R software package for nonparametric multiple comparisons and simultaneous confidence intervals. *Journal of Statistical Software*, *64*(9), 1–17. https://doi.org/10.18637/jss.v064.i09

Kosaki, H., Hashikawa, T., He, J., & Jones, E. g. (1997). Tonotopic organization of auditory cortical fields delineated by parvalbumin immunoreactivity in macaque monkeys. *Journal of Comparative Neurology*, *386*(2), 304–316. https://doi.org/10.1002/(SICI)1096-9861(19970922)386:2<304::AID-CNE10>3.0.CO;2-K

Kreutzberg, G. W., Klatzo, I., & Kleihues, P. (1992). Oskar and Cecile Vogt, Lenin's brain and the bumble-bees of the Black Forest. *Brain Pathology*, *2*(4), 363–364.

Krishnan, S., Carey, D., Dick, F., & Pearce, M. T. (2021). Effects of statistical learning in passive and active contexts on reproduction and recognition of auditory sequences. *Journal of Experimental Psychology: General*.

Kroenke, C. D., Taber, E. N., Leigland, L. A., Knutsen, A. K., & Bayly, P. V. (2009). Regional Patterns of Cerebral Cortical Differentiation Determined by Diffusion Tensor MRI. *Cerebral Cortex*, *19*(12), 2916–2929. https://doi.org/10.1093/cercor/bhp061

Kusmierek, P., & Rauschecker, J. P. (2009). Functional specialization of medial auditory belt cortex in the alert rhesus monkey. *Journal of Neurophysiology*, *102*(3), 1606–1622. https://doi.org/10.1152/jn.00167.2009

Laffere, A., Dick, F., & Tierney, A. T. (2020). Effects of auditory selective attention on neural phase: Individual differences and short-term training. *NeuroImage*, *213*, 116717. https://doi.org/10.1016/j.neuroimage.2020.116717

Laguesse, S., Peyre, E., & Nguyen, L. (2015). Progenitor genealogy in the developing cerebral cortex. *Cell and Tissue Research*, *359*(1), 17–32. https://doi.org/10.1007/s00441-014-1979-5

Lamballais, S., Vinke, E. J., Vernooij, M. W., Ikram, M. A., & Muetzel, R. L. (2020). Cortical gyrification in relation to age and cognition in older adults. *NeuroImage*, *212*, 116637. https://doi.org/10.1016/j.neuroimage.2020.116637

Langers, D. R. M., & van Dijk, P. (2012). Mapping the Tonotopic Organization in Human Auditory Cortex with Minimally Salient Acoustic Stimulation. *Cerebral Cortex*, *22*(9), 2024–2038. https://doi.org/10.1093/cercor/bhr282

Lappi, O. (2015). The Racer's Brain How Domain Expertise is Reflected in the Neural Substrates of Driving. *Frontiers in Human Neuroscience*, *9*.

Lavine, M. (2014). Comment on murtaugh. *Ecology*, *95*(3), 642–645. https://doi.org/10.1890/13-1112.1

Law, L. N., & Zentner, M. (2012). Assessing musical abilities objectively: Construction and validation of the Profile of Music Perception Skills. *PloS One*, *7*(12), e52508.

Lazari, A., & Lipp, I. (2021). Can MRI measure myelin? Systematic review, qualitative assessment, and meta-analysis of studies validating microstructural imaging with myelin histology. *NeuroImage*, *230*, 117744. https://doi.org/10.1016/j.neuroimage.2021.117744

Lee, C. C., Imaizumi, K., Schreiner, C. E., & Winer, J. A. (2004). Concurrent Tonotopic Processing Streams in Auditory Cortex. *Cerebral Cortex*, *14*(4), 441–451. https://doi.org/10.1093/cercor/bhh006

Lee, C. C., & Winer, J. A. (2008). Connections of cat auditory cortex: III. Corticocortical system. *The Journal of Comparative Neurology*, *507*(6), 1920–1943. https://doi.org/10.1002/cne.21613

Leonard, C. M., Puranik, C., Kuldau, J. M., & Lombardino, L. J. (1998). Normal variation in the frequency and location of human auditory cortex landmarks. Heschl's gyrus: Where is it? *Cerebral Cortex*, *8*(5), 397–406. https://doi.org/10.1093/cercor/8.5.397

Letowski, T. (1985). Development of Technical Listening Skills: Timbre Solfeggio. *AES: Journal of the Audio Engineering Society*, *33*(4), 240–244.

Lewitus, E., Kelava, I., & Huttner, W. B. (2013). Conical expansion of the outer subventricular zone and the role of neocortical folding in evolution and development. *Frontiers in Human Neuroscience*, *7*. https://doi.org/10.3389/fnhum.2013.00424

Lewitus, E., Kelava, I., Kalinka, A. T., Tomancak, P., & Huttner, W. B. (2014). An Adaptive Threshold in Mammalian Neocortical Evolution. *PLoS Biology*, *12*(11), e1002000. https://doi.org/10.1371/journal.pbio.1002000

Li, Q., Wang, X., Wang, S., Xie, Y., Li, X., Xie, Y., & Li, S. (2018). Musical training induces functional and structural auditory-motor network plasticity in young adults. *Human Brain Mapping*, *39*(5), 2098–2110. https://doi.org/10.1002/hbm.23989

Li, Y., Sescousse, G., Amiez, C., & Dreher, J.-C. (2015). Local Morphology Predicts Functional Organization of Experienced Value Signals in the Human Orbitofrontal Cortex. *Journal of Neuroscience*, *35*(4), 1648–1658. https://doi.org/10.1523/JNEUROSCI.3058-14.2015

Libero, L. E., DeRamus, T. P., Deshpande, H. D., & Kana, R. K. (2014). Surface-based morphometry of the cortical architecture of autism spectrum disorders: Volume, thickness, area, and gyrification. *Neuropsychologia*, *62*, 1–10. https://doi.org/10.1016/j.neuropsychologia.2014.07.001

Lidji, P., Kolinsky, R., Lochy, A., & Morais, J. (2007). Spatial Associations for Musical Stimuli: A Piano in the Head? *Journal of Experimental Psychology: Human Perception and Performance*, *33*(5), 1189–1207. https://doi.org/10.1037/0096-1523.33.5.1189

Liu, J., Liu, W., Yang, L., Wu, Q., Zhang, H., Fang, A., Li, L., Xu, X., Sun, L., Zhang, J., Tang, F., & Wang, X. (2017). The Primate-Specific Gene TMEM14B Marks Outer Radial Glia Cells and Promotes Cortical Expansion and Folding. *Cell Stem Cell*, *21*(5), 635–649.e8. https://doi.org/10.1016/j.stem.2017.08.013

Llinares-Benadero, C., & Borrell, V. (2019). Deconstructing cortical folding: Genetic, cellular and mechanical determinants. *Nature Reviews Neuroscience*, *20*(3), 161–176. https://doi.org/10.1038/s41583-018-0112-2

Lo, C. Y., Looi, V., Thompson, W. F., & McMahon, C. M. (2020). Music Training for Children With Sensorineural Hearing Loss Improves Speech-in-Noise Perception. *Journal of Speech, Language, and Hearing Research : JSLHR*, *63*(6), 1990–2015. https://doi.org/10.1044/2020_JSLHR-19-00391

Logothetis, N. (2008). What we can do and what we cannot do with fMRI. *Nature*.

Lohmann, G. (1999). Sulcal Variability of Twins. *Cerebral Cortex*, *9*(7), 754–763. https://doi.org/10.1093/cercor/9.7.754

Long, P., Wan, G., Roberts, M. T., & Corfas, G. (2018). Myelin development, plasticity, and pathology in the auditory system. *Developmental Neurobiology*, *78*(2), 80–92. https://doi.org/10.1002/dneu.22538

Loo, J. H. Y., Bamiou, D. E., Campbell, N., & Luxon, L. M. (2010). Computer-based auditory training (CBAT): Benefits for children with language- and reading-related learning difficulties. *Developmental Medicine and Child Neurology*, *52*(8), 708–717. https://doi.org/10.1111/j.1469-8749.2010.03654.x

Lopez-Persem, A., Verhagen, L., Amiez, C., Petrides, M., & Sallet, J. (2019). The Human Ventromedial Prefrontal Cortex: Sulcal Morphology and Its Influence on Functional

Organization. *The Journal of Neuroscience*, *39*(19), 3627–3639. https://doi.org/10.1523/JNEUROSCI.2060-18.2019

Lui, J. H., Hansen, D. V., & Kriegstein, A. R. (2011). Development and Evolution of the Human Neocortex. *Cell*, *146*(1), 18–36. https://doi.org/10.1016/j.cell.2011.06.030

Luo, Z.-X. (2007). Transformation and diversification in early mammal evolution. *Nature*, *450*(7172), 1011–1019. https://doi.org/10.1038/nature06277

Lutti, A., Dick, F., Sereno, M. I., & Weiskopf, N. (2014). Using high-resolution quantitative mapping of R1 as an index of cortical myelination. *NeuroImage*, *93*, 176–188. https://doi.org/10.1016/j.neuroimage.2013.06.005

Lutti, A., Hutton, C., Finsterbusch, J., Helms, G., & Weiskopf, N. (2010). Optimization and Validation of Methods for Mapping of the Radiofrequency Transmit Field at 3T. *Magnetic Resonance in Medicine*, *64*(1), 229–238. https://doi.org/10.1002/mrm.22421

MacCutcheon, D., Füllgrabe, C., Eccles, R., van der Linde, J., Panebianco, C., & Ljung, R. (2020). Investigating the Effect of One Year of Learning to Play a Musical Instrument on Speech-in-Noise Perception and Phonological Short-Term Memory in 5-to-7-Year-Old Children. *Frontiers in Psychology*, *10*(January). https://doi.org/10.3389/fpsyg.2019.02865

Macmillan, N. A., & Kaplan, H. L. (1985). Detection theory analysis of group data: Estimating sensitivity from average hit and false-alarm rates. *Psychological Bulletin*, *98*(1), 185–199. https://doi.org/10.1037/0033-2909.98.1.185

Macnamara, B. N., & Maitra, M. (2019). The role of deliberate practice in expert performance: Revisiting Ericsson, Krampe & Tesch-Römer (1993). *Royal Society Open Science*, *6*(8), 190327.

Madeira, N., Duarte, J. V., Martins, R., Costa, G. N., Macedo, A., & Castelo-Branco, M. (2020). Morphometry and gyrification in bipolar disorder and schizophrenia: A comparative MRI study. *NeuroImage: Clinical*, *26*, 102220. https://doi.org/10.1016/j.nicl.2020.102220

Madsen, S. M. K., Marschall, M., Dau, T., & Oxenham, A. J. (2019). Speech perception is similar for musicians and non-musicians across a wide range of conditions. *Scientific Reports*, *9*(1), 1–10. https://doi.org/10.1038/s41598-019-46728-1

Madsen, S. M. K., Whiteford, K. L., & Oxenham, A. J. (2017). Musicians do not benefit from differences in fundamental frequency when listening to speech in competing speech backgrounds. *Scientific Reports*, *7*(1), 1–9. https://doi.org/10.1038/s41598-017-12937-9

Maffei, C., Jovicich, J., De Benedictis, A., Corsini, F., Barbareschi, M., Chioffi, F., & Sarubbo, S. (2018). Topography of the human acoustic radiation as revealed by ex vivo

fibers micro-dissection and in vivo diffusion-based tractography. *Brain Structure & Function*, *223*(1), 449–459. https://doi.org/10.1007/s00429-017-1471-6

Maguire, E. A., Woollett, K., & Spiers, H. J. (2006). London taxi drivers and bus drivers: A structural MRI and neuropsychological analysis. *Hippocampus*, *16*(12), 1091–1101. https://doi.org/10.1002/hipo.20233

Malinowska, M., & Kosmal, A. (2003). Connections of the posterior thalamic region with the auditory ectosylvian cortex in the dog. *The Journal of Comparative Neurology*, *467*(2), 185–206. https://doi.org/10.1002/cne.10919

Malmierca, M. S., & Hackett, T. A. (2010). Structural organization of the ascending auditory pathway. In A. R. Palmer & A. Rees (Eds.), *The Oxford Handbook of Auditory Science: The Auditory Brain* (p. 0). Oxford University Press. https://doi.org/10.1093/oxfordhb/9780199233281.013.0002

Mancini, M., Karakuzu, A., Cohen-Adad, J., Cercignani, M., Nichols, T. E., & Stikov, N. (2020). An interactive meta-analysis of MRI biomarkers of myelin. *eLife*, *9*, e61523. https://doi.org/10.7554/eLife.61523

Mandikal Vasuki, P. R., Sharma, M., Demuth, K., & Arciuli, J. (2016). Musicians' edge: A comparison of auditory processing, cognitive abilities and statistical learning. *Hearing Research*, *342*, 112–123. https://doi.org/10.1016/j.heares.2016.10.008

Manger, P. R., Prowse, M., Haagensen, M., & Hemingway, J. (2012). Quantitative analysis of neocortical gyrencephaly in African elephants (Loxodonta africana) and six species of cetaceans: Comparison with other mammals. *The Journal of Comparative Neurology*, *520*(11), 2430–2439. https://doi.org/10.1002/cne.23046

Mankel, K., & Bidelman, G. M. (2018). Inherent auditory skills rather than formal music training shape the neural encoding of speech. *Proceedings of the National Academy of Sciences of the United States of America*, *115*(51), 13129–13134. https://doi.org/10.1073/pnas.1811793115

Marie, D., Jobard, G., Crivello, F., Perchey, G., Petit, L., Mellet, E., Joliot, M., Zago, L., Mazoyer, B., & Tzourio-Mazoyer, N. (2015). Descriptive anatomy of Heschl's gyri in 430 healthy volunteers, including 198 left-handers. *Brain Structure and Function*, *220*(2), 729–743. https://doi.org/10.1007/s00429-013-0680-x

Marie, D., Maingault, S., Crivello, F., Mazoyer, B., & Tzourio-Mazoyer, N. (2016). Surface-Based Morphometry of Cortical Thickness and Surface Area Associated with Heschl's Gyri Duplications in 430 Healthy Volunteers. *Frontiers in Human Neuroscience*, *10*.

Martínez-Cerdeño, V., Noctor, S. C., & Kriegstein, A. R. (2006). The Role of Intermediate Progenitor Cells in the Evolutionary Expansion of the Cerebral Cortex. *Cerebral Cortex*, *16*(suppl_1), i152–i161. https://doi.org/10.1093/cercor/bhk017

Martínez-Martínez, M. Á., De Juan Romero, C., Fernández, V., Cárdenas, A., Götz, M., & Borrell, V. (2016). A restricted period for formation of outer subventricular zone defined by Cdh1 and Trnp1 levels. *Nature Communications*, *7*(1), 11812. https://doi.org/10.1038/ncomms11812

Marui, A., & Kamekawa, T. (2013). Towards the development of objective difficulty measure in Technical Ear Training tasks. *Proceedings of Meetings on Acoustics*, *19*, 1805. https://doi.org/10.1121/1.4800094

Marui, A., & Kamekawa, T. (2019, May). Does spectral flatness affect the difficulty of the peak frequency identification task in technical ear training? *AES 146th International Convention*.

Mathias, S. R., Knowles, E. E. M., Mollon, J., Rodrigue, A., Koenis, M. M. C., Alexander-Bloch, A. F., Winkler, A. M., Olvera, R. L., Duggirala, R., Göring, H. H. H., Curran, J. E., Fox, P. T., Almasy, L., Blangero, J., & Glahn, D. C. (2020). Minimal Relationship between Local Gyrification and General Cognitive Ability in Humans. *Cerebral Cortex*, *30*(6), 3439–3450. https://doi.org/10.1093/cercor/bhz319

Matsumoto, N., Shinmyo, Y., Ichikawa, Y., & Kawasaki, H. (2017). Gyrification of the cerebral cortex requires FGF signaling in the mammalian brain. *eLife*, *6*, e29285. https://doi.org/10.7554/eLife.29285

Matsumoto, N., Tanaka, S., Horiike, T., Shinmyo, Y., & Kawasaki, H. (2020). A discrete subtype of neural progenitor crucial for cortical folding in the gyrencephalic mammalian brain. *eLife*, *9*, e54873. https://doi.org/10.7554/eLife.54873

Mazoyer, B., Mellet, E., Perchey, G., Zago, L., Crivello, F., Jobard, G., Delcroix, N., Vigneau, M., Leroux, G., Petit, L., Joliot, M., & Tzourio-Mazoyer, N. (2016). BIL&GIN: A neuroimaging, cognitive, behavioral, and genetic database for the study of human brain lateralization. *NeuroImage*, *124*, 1225–1231. https://doi.org/10.1016/j.neuroimage.2015.02.071

McColgan, P., McColgan, P., Helbling, S., Vaculčiaková, L., Pine, K., Wagstyl, K., Attar, F. M., Edwards, L. J., Papoutsi, M., Wei, Y., van den Heuvel, M. P., Martijn P. van den Heuvel, Tabrizi, S. J., Rees, G., Rees, G., & Weiskopf, N. (2021). Relating quantitative 7T MRI across cortical depths to cytoarchitectonics, gene expression and connectomics. *Human Brain Mapping*, *42*(15), 4996–5009. https://doi.org/10.1002/hbm.25595

McConnell, S. K., Ghosh, A., & Shatz, C. J. (1994). Subplate pioneers and the formation of descending connections from cerebral cortex. *The Journal of Neuroscience: The Official Journal of the Society for Neuroscience*, *14*(4), 1892–1907. https://doi.org/10.1523/JNEUROSCI.14-04-01892.1994

McCrae, R. R. (1987). Creativity, divergent thinking, and openness to experience. *Journal of Personality and Social Psychology*, *52*(6), 1258. https://doi.org/10.1037/0022-3514.52.6.1258

McKinnon-Bassett, M., & Martens, W. L. (2013). Experimental comparison of two versions of a technical ear training program: Transfer of training on tone colour identification to a dissimilarity-rating task. *Proceedings of the AES International Conference*, 54–63.

Meng, X., Mukherjee, D., Kao, J. P. Y., & Kanold, P. O. (2021). Early peripheral activity alters nascent subplate circuits in the auditory cortex. *Science Advances*, *7*(7), eabc9155. https://doi.org/10.1126/sciadv.abc9155

Merzenich, M. M., & Brugge, J. F. (1973). Representation of the cochlear partition on the superior temporal plane of the macaque monkey. *Brain Research*, *50*(2), 275–296. https://doi.org/10.1016/0006-8993(73)90731-2

Merzenich, M. M., Knight, P. L., & Roth, G. L. (1975). Representation of the cochlea within primary auditory cortex in cat. *J. Neurohysiology*, *28*(2), 231–249. https://doi.org/10.1121/1.1920046

Mestre, J. (2005). Is transfer ubiquitous or rare? New paradigms for studying transfer. *AIP Conference Proceedings*, *790*, 3–6. https://doi.org/10.1063/1.2084687

Micheyl, C., Delhommeau, K., Perrot, X., & Oxenham, A. J. (2006). Influence of musical and psychoacoustical training on pitch discrimination. *Hearing Research*, *219*(1-2), 36–47. https://doi.org/10.1016/j.heares.2006.05.004

Mihai, P. G., Moerel, M., de Martino, F., Trampel, R., Kiebel, S., & von Kriegstein, K. (2019). Modulation of tonotopic ventral medial geniculate body is behaviorally relevant for speech recognition. *eLife*, *8*, e44837. https://doi.org/10.7554/eLife.44837

Miranda, D. (2020). The emotional bond between neuroticism and music. *Psychomusicology: Music, Mind, and Brain*, *30*(2), 53–63. https://doi.org/10.1037/pmu0000250

Mishra, S., & Khare, D. (2014). On comparative performance of multiple imputation methods for moderate to large proportions of missing data in clinical trials: A simulation study. *Journal of Medical Statistics and Informatics*, *2*(1), 9. https://doi.org/10.7243/2053-7662-2-9

Misra, H., Ikbal, S., Bourlard, H., & Hermansky, H. (2004). Spectral entropy based feature for robust ASR. *2004 IEEE International Conference on Acoustics, Speech, and Signal Processing*, *1*, I–193. https://doi.org/10.1109/ICASSP.2004.1325955

Moerel, M., De Martino, F., & Formisano, E. (2012). Processing of Natural Sounds in Human Auditory Cortex: Tonotopy, Spectral Tuning, and Relation to Voice Sensitivity. *The Journal of Neuroscience*, *32*(41), 14205–14216. https://doi.org/10.1523/JNEUROSCI.1388-12.2012

Moerel, M., De Martino, F., & Formisano, E. (2014). An anatomical and functional topography of human auditory cortical areas. *Frontiers in Neuroscience*, *8*(8 JUL), 1–14. https://doi.org/10.3389/fnins.2014.00225

Moerel, M., De Martino, F., Santoro, R., Ugurbil, K., Goebel, R., Yacoub, E., & Formisano, E. (2013). Processing of Natural Sounds: Characterization of Multipeak Spectral Tuning in Human Auditory Cortex. *The Journal of Neuroscience*, *33*(29), 11888–11898. https://doi.org/10.1523/JNEUROSCI.5306-12.2013

Moerel, M., De Martino, F., Uğurbil, K., Yacoub, E., & Formisano, E. (2015). Processing of frequency and location in human subcortical auditory structures. *Scientific Reports*, *5*(1), 17048. https://doi.org/10.1038/srep17048

Moerel, M., Yacoub, E., Gulban, O. F., Lage-Castellanos, A., & De Martino, F. (2020). Using high spatial resolution fMRI to understand representation in the auditory network. *Progress in Neurobiology*, 101887. https://doi.org/10.1016/j.pneurobio.2020.101887

Mohr, A., Weisbrod, M., Schellinger, P., & Knauth, M. (2004). The similarity of brain morphology in healthy monozygotic twins. *Cognitive Brain Research*, *20*(1), 106–110. https://doi.org/10.1016/j.cogbrainres.2004.02.001

Moore, J. K. (1987). The human auditory brain stem: A comparative view. *Hearing Research*, *29*(1), 1–32. https://doi.org/10.1016/0378-5955(87)90202-4

Moore, J. K., & Linthicum, F. H. (2001). Myelination of the Human Auditory Nerve: Different Time Courses for Schwann Celland Glial Myelin. *Annals of Otology, Rhinology & Laryngology*, *110*(7), 655–661. https://doi.org/10.1177/000348940111000711

Moore, J. K., Perazzo, L. M., & Braun, A. (1995). Time course of axonal myelination in the human brainstem auditory pathway. *Hearing Research*, *87*(1-2), 21–31. https://doi.org/10.1016/0378-5955(95)00073-d

Morel, A., Garraghty, P. E., & Kaas, J. H. (1993). Tonotopic organization, architectonic fields, and connections of auditory cortex in macaque monkeys. *The Journal of Comparative Neurology*, *335*(3), 437–459. https://doi.org/10.1002/cne.903350312

Morel, A., & Kaas, J. H. (1992). Subdivisions and connections of auditory cortex in owl monkeys. *The Journal of Comparative Neurology*, *318*(1), 27–63. https://doi.org/10.1002/cne.903180104

Morosan, P., Rademacher, J., Schleicher, A., Amunts, K., Schormann, T., & Zilles, K. (2001). Human Primary Auditory Cortex: Cytoarchitectonic Subdivisions and Mapping into a Spatial Reference System. *NeuroImage*, *13*(4), 684–701. https://doi.org/10.1006/nimg.2000.0715

Morosan, P., Schleicher, A., Amunts, K., & Zilles, K. (2005). Multimodal architectonic mapping of human superior temporal gyrus. *Anatomy and Embryology*, *210*(5-6), 401–406. https://doi.org/10.1007/s00429-005-0029-1

Mosing, M. A., Madison, G., Pedersen, N. L., Kuja-Halkola, R., & Ullén, F. (2014). Practice Does Not Make Perfect: No Causal Effect of Music Practice on Music Ability. *Psychological Science*, *25*(9), 1795–1803. https://doi.org/10.1177/0956797614541990

Mosing, M. A., Madison, G., Pedersen, N. L., & Ullén, F. (2016). Investigating cognitive transfer within the framework of music practice: Genetic pleiotropy rather than causality. *Developmental Science*, *19*(3), 504–512. https://doi.org/10.1111/desc.12306

Müllensiefen, D., Gingras, B., Musil, J., & Stewart, L. (2014). The musicality of non-musicians: An index for assessing musical sophistication in the general population. *PLoS ONE*, *9*(2). https://doi.org/10.1371/journal.pone.0089642

Nakamura, M., Nestor, P. G., & Shenton, M. E. (2020). Orbitofrontal Sulcogyral Pattern as a Transdiagnostic Trait Marker of Early Neurodevelopment in the Social Brain. *Clinical EEG and Neuroscience*, *51*(4), 275–284. https://doi.org/10.1177/1550059420904180

Neubert, K., & Brunner, E. (2007). A studentized permutation test for the non-parametric Behrens-Fisher problem. *Computational Statistics and Data Analysis*, *51*(10), 5192–5204. https://doi.org/10.1016/j.csda.2006.05.024

Nieuwenhuys, R. (2013). The myeloarchitectonic studies on the human cerebral cortex of the Vogt-Vogt school, and their significance for the interpretation of functional neuroimaging data. *Brain Structure & Function*, *218*(2), 303–352. https://doi.org/10.1007/s00429-012-0460-z

Nixon, K. C., & Carpenter, J. M. (2012). On homology. *Cladistics*, *28*(2), 160–169. https://doi.org/10.1111/j.1096-0031.2011.00371.x

Noctor, S. C., Flint, A. C., Weissman, T. A., Wong, W. S., Clinton, B. K., & Kriegstein, A. R. (2002). Dividing Precursor Cells of the Embryonic Cortical Ventricular Zone Have Morphological and Molecular Characteristics of Radial Glia. *The Journal of Neuroscience*, *22*(8), 3161–3173. https://doi.org/10.1523/JNEUROSCI.22-08-03161.2002

Noguchi, K., Abel, R. S., Marmolejo-Ramos, F., & Konietschke, F. (2020). Nonparametric multiple comparisons. *Behavior Research Methods*, *52*(2), 489–502. https://doi.org/10.3758/s13428-019-01247-9

Nomura, T., Takahashi, M., Hara, Y., & Osumi, N. (2008). Patterns of Neurogenesis and Amplitude of Reelin Expression Are Essential for Making a Mammalian-Type Cortex. *PLoS ONE*, *3*(1), e1454. https://doi.org/10.1371/journal.pone.0001454

Norton, A., Winner, E., Cronin, K., Overy, K., Lee, D. J., & Schlaug, G. (2005). Are there pre-existing neural, cognitive, or motoric markers for musical ability? *Brain and Cognition*, *59*(2), 124–134. https://doi.org/10.1016/j.bandc.2005.05.009

O'Connell, M. N., Barczak, A., Schroeder, C. E., & Lakatos, P. (2014). Layer Specific Sharpening of Frequency Tuning by Selective Attention in Primary Auditory Cortex. *Journal of Neuroscience*, *34*(49), 16496–16508. https://doi.org/10.1523/JNEUROSCI.2055-14.2014

O'Leary, M. A., Bloch, J. I., Flynn, J. J., Gaudin, T. J., Giallombardo, A., Giannini, N. P., Goldberg, S. L., Kraatz, B. P., Luo, Z.-X., Meng, J., Ni, X., Novacek, M. J., Perini, F. A., Randall, Z. S., Rougier, G. W., Sargis, E. J., Silcox, M. T., Simmons, N. B., Spaulding, M., … Cirranello, A. L. (2013). The Placental Mammal Ancestor and the Post of Placentals. *Science*, *339*(6120), 662–667. https://doi.org/10.1126/science.1229237

Oberfeld, D., & Klöckner-Nowotny, F. (2016). Individual differences in selective attention predict speech identification at a cocktail party. *eLife*, *5*, e16747. https://doi.org/10.7554/eLife.16747

Ogawa, S., Lee, T.-M., Kay, A. R., & Tank, D. W. (1990). Brain magnetic resonance imaging with contrast dependent on blood oxygenation. *Proceedings of the National Academy of Sciences*, *87*(24), 9868–9872.

Okamoto, M., Namba, T., Shinoda, T., Kondo, T., Watanabe, T., Inoue, Y., Takeuchi, K., Enomoto, Y., Ota, K., Oda, K., Wada, Y., Sagou, K., Saito, K., Sakakibara, A., Kawaguchi, A., Nakajima, K., Adachi, T., Fujimori, T., Ueda, M., … Miyata, T. (2013). TAG-1assisted progenitor elongation streamlines nuclear migration to optimize subapical crowding. *Nature Neuroscience*, *16*(11), 1556–1566. https://doi.org/10.1038/nn.3525

Olszewska, A. M., Gaca, M., Herman, A. M., Jednoróg, K., & Marchewka, A. (2021). How Musical Training Shapes the Adult Brain: Predispositions and Neuroplasticity. *Frontiers in Neuroscience*, *15*.

Overath, T., Cusack, R., Kumar, S., Kriegstein, K. von, Warren, J. D., Grube, M., Carlyon, R. P., & Griffiths, T. D. (2007). An Information Theoretic Characterisation of Auditory Encoding. *PLOS Biology*, *5*(11), e288. https://doi.org/10.1371/journal.pbio.0050288

Palomar-García, M. Á., Zatorre, R. J., Ventura-Campos, N., Bueichekú, E., & Ávila, C. (2017). Modulation of Functional Connectivity in Auditory-Motor Networks in Musicians Compared with Nonmusicians. *Cerebral Cortex*, *27*(5), 2768–2778. https://doi.org/10.1093/cercor/bhw120

Parbery-Clark, A., Skoe, E., Lam, C., & Kraus, N. (2009). Musician Enhancement for Speech-In-Noise. *Ear & Hearing*, *30*, 653–661.

Parbery-Clark, A., Strait, D. L., Anderson, S., Hittner, E., & Kraus, N. (2011). Musical experience and the aging auditory system: Implications for cognitive abilities and hearing speech in noise. *PLoS ONE*, *6*(5). https://doi.org/10.1371/journal.pone.0018082

Patel, A. D. (2011). Why would musical training benefit the neural encoding of speech? The OPERA hypothesis. *Frontiers in Psychology*, *2*. https://doi.org/10.3389/fpsyg.2011.00142

Patel, A. D. (2014). Can nonlinguistic musical training change the way the brain processes speech? The expanded OPERA hypothesis. *Hearing Research*, *308*, 98–108. https://doi.org/10.1016/j.heares.2013.08.011

Penhune, V. B., Zatorre, R. J., MacDonald, J. D., & Evans, A. C. (1996). Interhemispheric Anatomical Differences in Human Primary Auditory Cortex: Probabilistic Mapping and Volume Measurement from Magnetic Resonance Scans. *Cerebral Cortex*, *6*(5), 661–672. https://doi.org/10.1093/cercor/6.5.661

Peper, J. S., Brouwer, R. M., Boomsma, D. I., Kahn, R. S., & Hulshoff Pol, H. E. (2007). Genetic influences on human brain structure: A review of brain imaging studies in twins. *Human Brain Mapping*, *28*(6), 464–473. https://doi.org/10.1002/hbm.20398

Petkov, C. I., Kayser, C., Augath, M., & Logothetis, N. K. (2006). Functional Imaging Reveals Numerous Fields in the Monkey Auditory Cortex. *PLOS Biology*, *4*(7), 1213–1226. https://doi.org/10.1371/journal.pbio.0040215

Pfefferbaum, A., Sullivan, E. V., & Carmelli, D. (2004). Morphological changes in aging brain structures are differentially affected by time-linked environmental influences despite strong genetic stability. *Neurobiology of Aging*, *25*(2), 175–183. https://doi.org/10.1016/S0197-4580(03)00045-9

Philibert, B., Beitel, R. E., Nagarajan, S. S., Bonham, B. H., Schreiner, C. E., & Cheung, S. W. (2005). Functional organization and hemispheric comparison of primary auditory cortex in the common marmoset (Callithrix jacchus). *Journal of Comparative Neurology*, *487*(4), 391–406. https://doi.org/10.1002/cne.20581

Plailly, J., Delon-Martin, C., & Royet, J.-P. (2011). Experience induces functional reorganization in brain regions involved in odor imagery in perfumers. *Human Brain Mapping*, *33*(1), 224–234. https://doi.org/10.1002/hbm.21207

Poldrack, R. A., & Yarkoni, T. (2016). From Brain Maps to Cognitive Ontologies: Informatics and the Search for Mental Structure. *Annual Review of Psychology*, *67*(1), 587–612. https://doi.org/10.1146/annurev-psych-122414-033729

Poldrack, R., Kittur, A., Kalar, D., Miller, E., Seppa, C., Gil, Y., Parker, D., Sabb, F., & Bilder, R. (2011). The Cognitive Atlas: Toward a Knowledge Foundation for Cognitive Neuroscience. *Frontiers in Neuroinformatics*, *5*.

Polspoel, B., Vandermosten, M., & De Smedt, B. (2020). The association of grey matter volume and cortical complexity with individual differences in children's arithmetic fluency. *Neuropsychologia*, *137*, 107293. https://doi.org/10.1016/j.neuropsychologia.2019.107293

Porcaro, C., Zappasodi, F., Barbati, G., Salustri, C., Pizzella, V., Rossini, P. M., & Tecchio, F. (2006). Fetal auditory responses to external sounds and mother's heart beat: Detection improved by Independent Component Analysis. *Brain Research*, *1101*(1), 51–58. https://doi.org/10.1016/j.brainres.2006.04.134

Porcello, T. (2004). Speaking of sound: Language and the professionalization of sound-recording engineers. *Social Studies of Science*. https://doi.org/10.1177/0306312704047328

Probst, P., Boulesteix, A. L., & Bischl, B. (2019). Tunability: Importance of hyperparameters of machine learning algorithms. *Journal of Machine Learning Research*, *20*, 1–32.

Rademacher, J., Caviness, J. V. S., Steinmetz, H., & Galaburda, A. M. (1993). Topographical Variation of the Human Primary Cortices. *Cerebral Cortex*, *3*(August), 313–329.

Rademacher, J., Morosan, P., Schormann, T., Schleicher, A., Werner, C., Freund, H.-J., & Zilles, K. (2001). Probabilistic Mapping and Volume Measurement of Human Primary Auditory Cortex. *NeuroImage*, *13*(4), 669–683. https://doi.org/10.1006/nimg.2000.0714

Rakic, P. (1988). Specification of cerebral cortical areas. *Science*, *241*(4862), 170–176. https://doi.org/10.1126/science.3291116

Rammsayer, T., & Altenmüller, E. (2006). Temporal information processing in musicians and nonmusicians. *Music Perception*, *24*(1), 37–48. https://doi.org/10.1525/mp.2006.24.1.37

Ramón y Cajal, S. (1923). *Recuerdos de mi vida*. Proyecto Gutemberg.

Rauschecker, J. P., Tian, B., & Hauser, M. D. (1995). Processing of complex sounds in the Macaque nonprimary auditory cortex. *Science*, *268*(5207), 111–114. https://doi.org/10.1126/science.7701330

Reep, R. L., & O'Shea, T. J. (1990). Regional brain morphometry and lissencephaly in the Sirenia. *Brain, Behavior and Evolution*, *35*(4), 185–194. https://doi.org/10.1159/000115866

Reillo, I., de Juan Romero, C., Cárdenas, A., Clascá, F., Martínez-Martinez, M. Á., & Borrell, V. (2017). A Complex Code of Extrinsic Influences on Cortical Progenitor Cells of Higher Mammals. *Cerebral Cortex*, *27*(9), 4586–4606. https://doi.org/10.1093/cercor/bhx171

Reillo, I., de Juan Romero, C., García-Cabezas, M. Á., & Borrell, V. (2011). A Role for Intermediate Radial Glia in the Tangential Expansion of the Mammalian Cerebral Cortex. *Cerebral Cortex*, *21*(7), 1674–1694. https://doi.org/10.1093/cercor/bhq238

Reiss, L. A. J., & Young, E. D. (2005). Spectral Edge Sensitivity in Neural Circuits of the Dorsal Cochlear Nucleus. *Journal of Neuroscience*, *25*(14), 3680–3691. https://doi.org/10.1523/JNEUROSCI.4963-04.2005

Research, E. (2005). *Bamford speech-in-noise test (version 1.03)[Audio CD]*.

Ressel, V., Pallier, C., Ventura-Campos, N., Diaz, B., Roessler, A., Avila, C., & Sebastian-Galles, N. (2012). An Effect of Bilingualism on the Auditory Cortex. *Journal of Neuroscience*, *32*(47), 16597–16601. https://doi.org/10.1523/JNEUROSCI.1996-12.2012

Rice, D. S., & Curran, T. (2001). Role of the Reelin Signaling Pathway in Central Nervous System Development. *Annual Review of Neuroscience*, *24*(1), 1005–1039. https://doi.org/10.1146/annurev.neuro.24.1.1005

Riecke, L., Peters, J. C., Valente, G., Kemper, V. G., Formisano, E., & Sorger, B. (2016). Frequency-Selective Attention in Auditory Scenes Recruits Frequency Representations Throughout Human Superior Temporal Cortex. *Cerebral Cortex*, bhw160. https://doi.org/10.1093/cercor/bhw160

Rivier, F., & Clarke, S. (1997). Cytochrome Oxidase, Acetylcholinesterase, and NADPH-Diaphorase Staining in Human Supratemporal and Insular Cortex: Evidence for Multiple Auditory Areas. *NeuroImage*, *6*(4), 288–304. https://doi.org/10.1006/nimg.1997.0304

Roberts, R. E., Bain, P. G., Day, B. L., & Husain, M. (2013). Individual Differences in Expert Motor Coordination Associated with White Matter Microstructure in the Cerebellum. *Cerebral Cortex*, *23*(10), 2282–2292. https://doi.org/10.1093/cercor/bhs219

Robinson, E. C., Garcia, K., Glasser, M. F., Chen, Z., Coalson, T. S., Makropoulos, A., Bozek, J., Wright, R., Schuh, A., Webster, M., Hutter, J., Price, A., Grande, L. C., Hughes, E., Tusor, N., Bayly, P. V., Van Essen, D. C., Smith, S. M., Edwards, A. D., … Rueckert, D. (2018). Multimodal Surface Matching with Higher-Order Smoothness Constraint. *NeuroImage*, *167*, 453–465. https://doi.org/10.1016/j.neuroimage.2017.10.037

Robinson, E. C., Jbabdi, S., Glasser, M. F., Andersson, J., Burgess, G. C., Harms, M. P., Smith, S. M., Van Essen, D. C., & Jenkinson, M. (2014). MSM: A new flexible framework for Multimodal Surface Matching. *NeuroImage*, *100*, 414–426. https://doi.org/10.1016/j.neuroimage.2014.05.069

Rollins, C. P. E., Garrison, J. R., Arribas, M., Seyedsalehi, A., Li, Z., Chan, R. C. K., Yang, J., Wang, D., Liò, P., Yan, C., Yi, Z., Cachia, A., Upthegrove, R., Deakin, B., Simons, J. S., Murray, G. K., & Suckling, J. (2020). Evidence in cortical folding patterns for prenatal predispositions to hallucinations in schizophrenia. *Translational Psychiatry*, *10*(1), 1–14. https://doi.org/10.1038/s41398-020-01075-y

Román-Caballero, R., Martín-Arévalo, E., & Lupiáñez, J. (2020). Attentional networks functioning and vigilance in expert musicians and non-musicians. *Psychological Research*, 1–15.

Romero, S., Hight, A. E., Clayton, K. K., Resnik, J., Williamson, R. S., Hancock, K. E., & Polley, D. B. (2020). Cellular and Widefield Imaging of Sound Frequency Organization in Primary and Higher Order Fields of the Mouse Auditory Cortex. *Cerebral Cortex (New York, NY)*, *30*(3), 1603–1622. https://doi.org/10.1093/cercor/bhz190

Romiguier, J., Ranwez, V., Douzery, E. J. P., & Galtier, N. (2013). Genomic Evidence for Large, Long-Lived Ancestors to Placental Mammals. *Molecular Biology and Evolution*, *30*(1), 5–13. https://doi.org/10.1093/molbev/mss211

Ronan, L., & Fletcher, P. C. (2015). From genes to folds: A review of cortical gyrification theory. *Brain Structure and Function*, *220*(5), 2475–2483. https://doi.org/10.1007/s00429-014-0961-z

Ronan, L., Voets, N., Rua, C., Alexander-Bloch, A., Hough, M., Mackay, C., Crow, T. J., James, A., Giedd, J. N., & Fletcher, P. C. (2014). Differential Tangential Expansion as a Mechanism for Cortical Gyrification. *Cerebral Cortex*, *24*(8), 2219–2228. https://doi.org/10.1093/cercor/bht082

Ross, M. E., & Walsh, C. A. (2001). Human Brain Malformations and Their Lessons for Neuronal Migration. *Annual Review of Neuroscience*, *24*(1), 1041–1070. https://doi.org/10.1146/annurev.neuro.24.1.1041

Ruggles, D. R., Freyman, R. L., & Oxenham, A. J. (2014). Influence of musical training on understanding voiced and whispered speech in noise. *PLoS ONE*, *9*(1). https://doi.org/10.1371/journal.pone.0086980

Ryugo, D. K., & Parks, T. N. (2003). Primary innervation of the avian and mammalian cochlear nucleus. *Brain Research Bulletin*, *60*(5-6), 435–456. https://doi.org/10.1016/s0361-9230(03)00049-2

Saenz, M., & Langers, D. R. M. (2014). Tonotopic mapping of human auditory cortex. *Hearing Research*, *307*, 42–52. https://doi.org/10.1016/j.heares.2013.07.016

Sanderson, K. J., & Aitkin, L. M. (1990). Neurogenesis in a marsupial: The brush-tailed possum (Trichosurus vulpecula). I. Visual and auditory pathways. *Brain, Behavior and Evolution*, *35*(6), 325–338. https://doi.org/10.1159/000115878

Sanes, D. H., & Constantine-Paton, M. (1985). The sharpening of frequency tuning curves requires patterned activity during development in the mouse, Mus musculus. *The Journal of Neuroscience: The Official Journal of the Society for Neuroscience*, *5*(5), 1152–1166. https://doi.org/10.1523/JNEUROSCI.05-05-01152.1985

Sasabayashi, D., Takahashi, T., Takayanagi, Y., & Suzuki, M. (2021). Anomalous brain gyrification patterns in major psychiatric disorders: A systematic review and

transdiagnostic integration. *Translational Psychiatry*, *11*(1), 176. https://doi.org/10.1038/s41398-021-01297-8

Sasabayashi, D., Takayanagi, Y., Takahashi, T., Nemoto, K., Furuichi, A., Kido, M., Nishikawa, Y., Nakamura, M., Noguchi, K., & Suzuki, M. (2020). Increased brain gyrification in the schizophrenia spectrum. *Psychiatry and Clinical Neurosciences*, *74*(1), 70–76. https://doi.org/10.1111/pcn.12939

Sato, H., Hatakeyama, J., Iwasato, T., Araki, K., Yamamoto, N., & Shimamura, K. (2022). Thalamocortical axons control the cytoarchitecture of neocortical layers by area-specific supply of VGF. *eLife*, *11*, e67549. https://doi.org/10.7554/eLife.67549

Schafer, J. L. (1999). Multiple imputation: A primer. *Statistical Methods in Medical Research*, *8*(1), 3–15. https://doi.org/10.1191/096228099671525676

Schäfer, J., & Strimmer, K. (2005). A shrinkage approach to large-scale covariance matrix estimation and implications for functional genomics. *Statistical Applications in Genetics and Molecular Biology*, *4*(1), 1–30. https://doi.org/10.2202/1544-6115.1175

Schellenberg, E. G. (2011). Examining the association between music lessons and intelligence. *British Journal of Psychology*, *102*(3), 283–302. https://doi.org/10.1111/j.2044-8295.2010.02000.x

Schellenberg, E. G. (2015). Music training and speech perception: A gene-environment interaction. *Annals of the New York Academy of Sciences*, *1337*(1), 170–177. https://doi.org/10.1111/nyas.12627

Schellenberg, E. G. (2019). Correlation = Causation? Music Training, Psychology, and Neuroscience. *Psychology of Aesthetics, Creativity, and the Arts*. https://doi.org/10.1037/aca0000263

Schlaug, G. (2015). Musicians and music making as a model for the study of brain plasticity. *Progress in Brain Research*, *217*, 37–55. https://doi.org/10.1016/bs.pbr.2014.11.020

Schmidt-Wilcke, T., Rosengarth, K., Luerding, R., Bogdahn, U., & Greenlee, M. W. (2010). Distinct patterns of functional and structural neuroplasticity associated with learning Morse code. *NeuroImage*, *51*(3), 1234–1241. https://doi.org/10.1016/j.neuroimage.2010.03.042

Schneider, P., Scherg, M., Dosch, H. G., Specht, H. J., Gutschalk, A., & Rupp, A. (2002). Morphology of Heschl's gyrus reflects enhanced activation in the auditory cortex of musicians. *Nature Neuroscience*, *5*(7), 688–694. https://doi.org/10.1038/nn871

Schneider, P., Sluming, V., Roberts, N., Scherg, M., Goebel, R., Specht, H. J., Dosch, H. G., Bleeck, S., Stippich, C., & Rupp, A. (2005). Structural and functional asymmetry of lateral Heschl's gyrus reflects pitch perception preference. *Nature Neuroscience*, *8*(9), 1241–1247. https://doi.org/10.1038/nn1530

Schneider, P., & Wengenroth, M. (2009). The Neural Basis of Individual Holistic and Spectral Sound Perception. *Contemporary Music Review*, *28*. https://doi.org/10.1080/07494460903404402

Schofield, B. R. (2010). Structural organization of the descending auditory pathway. In A. R. Palmer & A. Rees (Eds.), *The Oxford Handbook of Auditory Science: The Auditory Brain* (p. 0). Oxford University Press. https://doi.org/10.1093/oxfordhb/9780199233281.013.0003

Schön, D., & François, C. (2011). Musical Expertise and Statistical Learning of Musical and Linguistic Structures. *Frontiers in Psychology*, *2*(July), 1–9. https://doi.org/10.3389/fpsyg.2011.00167

Seither-Preisler, A., Parncutt, R., & Schneider, P. (2014). Size and Synchronization of Auditory Cortex Promotes Musical, Literacy, and Attentional Skills in Children. *Journal of Neuroscience*, *34*(33), 10937–10949. https://doi.org/10.1523/JNEUROSCI.5315-13.2014

Sekine, K., Kubo, K., & Nakajima, K. (2014). How does Reelin control neuronal migration and layer formation in the developing mammalian neocortex? *Neuroscience Research*, *86*, 50–58. https://doi.org/10.1016/j.neures.2014.06.004

Sereno, M. I., Dale, A. M., Reppas, J. B., Kwong, K. K., Belliveau, J. W., Brady, T. J., Rosen, B. R., & Tootell, R. B. (1995). Borders of multiple visual areas in humans revealed by functional magnetic resonance imaging. *Science (New York, N.Y.)*, *268*(5212), 889–893. https://doi.org/10.1126/science.7754376

Sereno, M. I., & Huang, R.-S. (2006). A human parietal face area contains aligned head-centered visual and tactile maps. *Nature Neuroscience*, *9*(10), 1337–1343. https://doi.org/10.1038/nn1777

Sereno, M. I., Lutti, A., Weiskopf, N., & Dick, F. (2013). Mapping the human cortical surface by combining quantitative T1 with retinotopy. *Cerebral Cortex*, *23*(9), 2261–2268. https://doi.org/10.1093/cercor/bhs213

Serrallach, B., Groß, C., Bernhofs, V., Engelmann, D., Benner, J., Gündert, N., Blatow, M., Wengenroth, M., Seitz, A., Brunner, M., Seither, S., Parncutt, R., Schneider, P., & Seither-Preisler, A. (2016). Neural Biomarkers for Dyslexia, ADHD, and ADD in the Auditory Cortex of Children. *Frontiers in Neuroscience*, *10*.

Shapleske, J., Rossell, S. L., Woodruff, P. W. R., & David, A. S. (1999). The planum temporale: A systematic, quantitative review of its structural, functional and clinical significance. *Brain Research Reviews*, *29*(1), 26–49. https://doi.org/10.1016/S0165-0173(98)00047-2

Shinmyo, Y., Terashita, Y., Dinh Duong, T. A., Horiike, T., Kawasumi, M., Hosomichi, K., Tajima, A., & Kawasaki, H. (2017). Folding of the Cerebral Cortex Requires Cdk5 in

Upper-Layer Neurons in Gyrencephalic Mammals. *Cell Reports*, *20*(9), 2131–2143. https://doi.org/10.1016/j.celrep.2017.08.024

Shitamukai, A., Konno, D., & Matsuzaki, F. (2011). Oblique Radial Glial Divisions in the Developing Mouse Neocortex Induce Self-Renewing Progenitors outside the Germinal Zone That Resemble Primate Outer Subventricular Zone Progenitors. *Journal of Neuroscience*, *31*(10), 3683–3695. https://doi.org/10.1523/JNEUROSCI.4773-10.2011

Sigalovsky, I. S., Fischl, B., & Melcher, J. R. (2006). Mapping an intrinsic MR property of gray matter in auditory cortex of living humans: A possible marker for primary cortex and hemispheric differences. *NeuroImage*, *32*(4), 1524–1537. https://doi.org/10.1016/j.neuroimage.2006.05.023

Sinclair, J. L., Fischl, M. J., Alexandrova, O., He\beta, M., Grothe, B., Leibold, C., & Kopp-Scheinpflug, C. (2017). Sound-Evoked Activity Influences Myelination of Brainstem Axons in the Trapezoid Body. *The Journal of Neuroscience*, *37*(34), 8239–8255. https://doi.org/10.1523/JNEUROSCI.3728-16.2017

Sitek, K. R., Gulban, O. F., Calabrese, E., Johnson, G. A., Lage-Castellanos, A., Moerel, M., Ghosh, S. S., & De Martino, F. (2019). Mapping the human subcortical auditory system using histology, postmortem MRI and in vivo MRI at 7T. *eLife*, *8*, e48932. https://doi.org/10.7554/eLife.48932

Skerritt-Davis, B., & Elhilali, M. (2018). Detecting change in stochastic sound sequences. *PLOS Computational Biology*, *14*(5), e1006162. https://doi.org/10.1371/journal.pcbi.1006162

Skoe, E., Camera, S., & Tufts, J. (2019). Noise exposure may diminish the musician advantage for perceiving speech in noise. *Ear and Hearing*, *40*(4), 782–793. https://doi.org/10.1097/AUD.0000000000000665

Slater, J., Azem, A., Nicol, T., Swedenborg, B., & Kraus, N. (2017). Variations on the theme of musical expertise: Cognitive and sensory processing in percussionists, vocalists and non-musicians. *European Journal of Neuroscience*, *45*(7), 952–963. https://doi.org/10.1111/ejn.13535

Slater, J., & Kraus, N. (2016). The role of rhythm in perceiving speech in noise: A comparison of percussionists, vocalists and non-musicians. *Cognitive Processing*, *17*(1), 79–87. https://doi.org/10.1007/s10339-015-0740-7

Slater, J., Kraus, N., Woodruff Carr, K., Tierney, A. T., Azem, A., & Ashley, R. (2018). Speech-in-noise perception is linked to rhythm production skills in adult percussionists and non-musicians. *Language, Cognition and Neuroscience*, *33*(6), 710–717. https://doi.org/10.1080/23273798.2017.1411960

Slayton, M. A., Romero-Sosa, J. L., Shore, K., Buonomano, D. V., & Viskontas, I. V. (2020). Musical expertise generalizes to superior temporal scaling in a Morse code tapping task. *PLOS ONE*, *15*(1), e0221000. https://doi.org/10.1371/journal.pone.0221000

Smart, I. H., Dehay, C., Giroud, P., Berland, M., & Kennedy, H. (2002). Unique morphological features of the proliferative zones and postmitotic compartments of the neural epithelium giving rise to striate and extrastriate cortex in the monkey. *Cerebral Cortex*, *12*(1), 37–53. https://doi.org/10.1093/cercor/12.1.37

Smith, K. M., Mecoli, M. D., Altaye, M., Komlos, M., Maitra, R., Eaton, K. P., Egelhoff, J. C., & Holland, S. K. (2011). Morphometric Differences in the Heschl's Gyrus of Hearing Impaired and Normal Hearing Infants. *Cerebral Cortex*, *21*(5), 991–998. https://doi.org/10.1093/cercor/bhq164

Smith, R., Holmes-Elliott, S., Pettinato, M., & Knight, R.-A. (2014). Cross-Accent Intelligibility of Speech in Noise: Long-Term Familiarity and Short-Term Familiarization. *Quarterly Journal of Experimental Psychology*, *67*(3), 590–608. https://doi.org/10.1080/17470218.2013.822009

Smith, S., Duff, E., Groves, A., Nichols, T. E., Jbabdi, S., Westlye, L. T., Tamnes, C. K., Engvig, A., Walhovd, K. B., Fjell, A. M., Johansen-Berg, H., & Douaud, G. (2019). Structural Variability in the Human Brain Reflects Fine-Grained Functional Architecture at the Population Level. *The Journal of Neuroscience*, *39*(31), 6136–6149. https://doi.org/10.1523/JNEUROSCI.2912-18.2019

Soranzo, A., & Grassi, M. (2014). Psychoacoustics: A comprehensive MATLAB toolbox for auditory testing. *Frontiers in Psychology*, *5*(JUL). https://doi.org/10.3389/fpsyg.2014.00712

Spalthoff, R., Gaser, C., & Nenadić, I. (2018). Altered gyrification in schizophrenia and its relation to other morphometric markers. *Schizophrenia Research*, *202*, 195–202. https://doi.org/10.1016/j.schres.2018.07.014

Spiegel, M. F., & Watson, C. S. (1984). Performance on frequency-discrimination tasks by musicians and nonmusicians. *The Journal of the Acoustical Society of America*, *76*(6), 1690–1695. https://doi.org/10.1121/1.391605

Stacey, P. C., & Summerfield, a. Q. (2007). Effectiveness of computer-based auditory training in improving the perception of noise-vocoded speech. *The Journal of the Acoustical Society of America*, *121*(5 Pt1), 2923–2935. https://doi.org/10.1121/1.2713668

Stahl, R., Walcher, T., De Juan Romero, C., Pilz, G. A., Cappello, S., Irmler, M., Sanz-Aquela, J. M., Beckers, J., Blum, R., Borrell, V., & Götz, M. (2013). Trnp1 Regulates Expansion and Folding of the Mammalian Cerebral Cortex by Control of Radial Glial Fate. *Cell*, *153*(3), 535–549. https://doi.org/10.1016/j.cell.2013.03.027

Stanislaw, H., & Todorov, N. (1999). Calculation of signal detection theory measures. *Behavior Research Methods, Instruments, & Computers*, *31*(1), 137–149. https://doi.org/10.3758/BF03207704

Steele, C. J., Bailey, J. A., Zatorre, R. J., & Penhune, V. B. (2013). Early musical training and white-matter plasticity in the corpus callosum: Evidence for a sensitive period. *The Journal of Neuroscience: The Official Journal of the Society for Neuroscience*, *33*(3), 1282–1290. https://doi.org/10.1523/JNEUROSCI.3578-12.2013

Steinmetz, H., Fürst, G., & Meyer, B.-U. (1989). Craniocerebral topography within the international 10 system. *Electroencephalography and Clinical Neurophysiology*, *72*(6), 499–506. https://doi.org/10.1016/0013-4694(89)90227-7

Stilp, C. E., & Kluender, K. R. (2010). Cochlea-scaled entropy, not consonants, vowels, or time, best predicts speech intelligibility. *Proceedings of the National Academy of Sciences*, *107*(27), 12387–12392. https://doi.org/10.1073/pnas.0913625107

Strait, D. L., Kraus, N., Parbery-Clark, A., & Ashley, R. (2010). Musical experience shapes top-down auditory mechanisms: Evidence from masking and auditory attention performance. *Hearing Research*, *261*(1-2), 22–29. https://doi.org/10.1016/j.heares.2009.12.021

Strait, D. L., Slater, J., O'Connell, S., & Kraus, N. (2015). Music training relates to the development of neural mechanisms of selective auditory attention. *Developmental Cognitive Neuroscience*, *12*, 94–104. https://doi.org/10.1016/j.dcn.2015.01.001

Strasser, H., & Weber, C. (1999). On the Asymptotic Theory of Permutation Statistics. *Mathematical Methods of Statistics*, *8*, 220–250. https://doi.org/10.1016/S0304-0208(08)70741-2

Striem-Amit, E., Hertz, U., & Amedi, A. (2011). Extensive cochleotopic mapping of human auditory cortical fields obtained with phase-encoding FMRI. *PloS One*, *6*(3), e17832. https://doi.org/10.1371/journal.pone.0017832

Strobl, C., Boulesteix, A. L., Kneib, T., Augustin, T., & Zeileis, A. (2008). Conditional variable importance for random forests. *BMC Bioinformatics*, *9*, 1–11. https://doi.org/10.1186/1471-2105-9-307

Strobl, C., Boulesteix, A. L., Zeileis, A., & Hothorn, T. (2007). Bias in random forest variable importance measures: Illustrations, sources and a solution. *BMC Bioinformatics*, *8*. https://doi.org/10.1186/1471-2105-8-25

Strobl, C., Malley, J., & Tutz, G. (2009). An Introduction to Recursive Partitioning: Rationale, Application, and Characteristics of Classification and Regression Trees, Bagging, and Random Forests. *Psychological Methods*, *14*(4), 323–348. https://doi.org/10.1037/a0016973

Su, P., Kuan, C.-C., Kaga, K., Sano, M., & Mima, K. (2008). Myelination progression in language-correlated regions in brain of normal children determined by quantitative MRI assessment. *International Journal of Pediatric Otorhinolaryngology*, *72*(12), 1751–1763. https://doi.org/10.1016/j.ijporl.2008.05.017

Subramanian, L., Calcagnotto, M. E., & Paredes, M. F. (2020). Cortical Malformations: Lessons in Human Brain Development. *Frontiers in Cellular Neuroscience*, *13*, 576. https://doi.org/10.3389/fncel.2019.00576

Swaminathan, S., & Schellenberg, E. G. (2018). Musical Competence is Predicted by Music Training, Cognitive Abilities, and Personality. *Scientific Reports*, *8*(1), 1–7. https://doi.org/10.1038/s41598-018-27571-2

Szucs, D., & Ioannidis, J. P. A. (2017). When null hypothesis significance testing is unsuitable for research: A reassessment. *Frontiers in Human Neuroscience*, *11*(August). https://doi.org/10.3389/fnhum.2017.00390

Takahashi, T., Sasabayashi, D., Takayanagi, Y., Furuichi, A., Kobayashi, H., Noguchi, K., & Suzuki, M. (2022a). Different Heschl's Gyrus Duplication Patterns in Deficit and Non-deficit Subtypes of Schizophrenia. *Frontiers in Psychiatry*, *13*, 867461. https://doi.org/10.3389/fpsyt.2022.867461

Takahashi, T., Sasabayashi, D., Takayanagi, Y., Higuchi, Y., Mizukami, Y., Nishiyama, S., Furuichi, A., Kido, M., Pham, T. V., Kobayashi, H., Noguchi, K., & Suzuki, M. (2021). Heschl's Gyrus Duplication Pattern in Individuals at Risk of Developing Psychosis and Patients With Schizophrenia. *Frontiers in Behavioral Neuroscience*, *15*.

Takahashi, T., Sasabayashi, D., Yücel, M., Whittle, S., Lorenzetti, V., Walterfang, M., Suzuki, M., Pantelis, C., Malhi, G. S., & Allen, N. B. (2022b). Different Frequency of Heschl's Gyrus Duplication Patterns in Neuropsychiatric Disorders: An MRI Study in Bipolar and Major Depressive Disorders. *Frontiers in Human Neuroscience*, *16*, 917270. https://doi.org/10.3389/fnhum.2022.917270

Talamini, F., Altoè, G., Carretti, B., & Grassi, M. (2017). Musicians have better memory than nonmusicians: A meta-analysis. *PLoS ONE*, *12*(10), 1–21. https://doi.org/10.1371/journal.pone.0186773

Talavage, T. M., Gonzalez-Castillo, J., & Scott, S. K. (2014). Auditory neuroimaging with fMRI and PET. *Hearing Research*, *307*, 4–15. https://doi.org/10.1016/j.heares.2013.09.009

Talavage, T. M., Sereno, M. I., Melcher, J. R., Ledden, P. J., Rosen, B. R., & Dale, A. M. (2004). Tonotopic Organization in Human Auditory Cortex Revealed by Progressions of Frequency Sensitivity. *Journal of Neurophysiology*, *91*(3), 1282–1296. https://doi.org/10.1152/jn.01125.2002

Tallinen, T., Chung, J. Y., Biggins, J. S., & Mahadevan, L. (2014). Gyrification from constrained cortical expansion. *Proceedings of the National Academy of Sciences*, *111*(35), 12667–12672. https://doi.org/10.1073/pnas.1406015111

Tallinen, T., Chung, J. Y., Rousseau, F., Girard, N., Lefèvre, J., & Mahadevan, L. (2016). On the growth and form of cortical convolutions. *Nature Physics*, *12*(6), 588–593. https://doi.org/10.1038/nphys3632

Tanji, K., Leopold, D. A., Ye, F. Q., Zhu, C., Malloy, M., Saunders, R. C., & Mishkin, M. (2010). Effect of sound intensity on tonotopic fMRI maps in the unanesthetized monkey. *NeuroImage*, *49*(1), 150–157. https://doi.org/10.1016/j.neuroimage.2009.07.029

Tavano, S., Taverna, E., Kalebic, N., Haffner, C., Namba, T., Dahl, A., Wilsch-Bräuninger, M., Paridaen, J. T. M. L., & Huttner, W. B. (2018). Insm1 Induces Neural Progenitor Delamination in Developing Neocortex via Downregulation of the Adherens Junction Belt-Specific Protein Plekha7. *Neuron*, *97*(6), 1299–1314.e8. https://doi.org/10.1016/j.neuron.2018.01.052

Teki, S., Kumar, S., von Kriegstein, K., Stewart, L., Lyness, C. R., Moore, B. C. J., Capleton, B., & Griffiths, T. D. (2012). Navigating the auditory scene: An expert role for the hippocampus. *The Journal of Neuroscience: The Official Journal of the Society for Neuroscience*, *32*(35), 12251–12257. https://doi.org/10.1523/JNEUROSCI.0082-12.2012

Tervaniemi, M., Janhunen, L., Kruck, S., Putkinen, V., & Huotilainen, M. (2016). Auditory profiles of classical, jazz, and rock musicians: Genre-specific sensitivity to musical sound features. *Frontiers in Psychology*, *6*(JAN), 1900. https://doi.org/10.3389/fpsyg.2015.01900

Thakur, D., Martens, M. A., Smith, D. S., & Roth, E. (2018). Williams Syndrome and Music: A Systematic Integrative Review. *Frontiers in Psychology*, *9*.

Thomas, K., Silvia, P., Nusbaum, E., Beaty, R., & Hodges, D. (2015). Openness to Experience and Auditory Discrimination Ability in Music: An Investment Approach. *Psychology of Music*, *44*. https://doi.org/10.1177/0305735615592013

Thompson, P. M., Schwartz, C., Lin, R. T., Khan, A. A., & Toga, A. W. (1996). Three-Dimensional Statistical Analysis of Sulcal Variability in the Human Brain. *The Journal of Neuroscience*, *16*(13), 4261–4274. https://doi.org/10.1523/JNEUROSCI.16-13-04261.1996

Tierney, A. T., Bergeson-Dana, T. R., & Pisoni, D. B. (2008). Effects of Early Musical Experience on Auditory Sequence Memory. *Empirical Musicology Review : EMR*, *3*(4), 178–186.

Tierney, A. T., & Kraus, N. (2013). Music training for the development of reading skills. In *Progress in Brain Research*. https://doi.org/10.1016/B978-0-444-63327-9.00008-4

Tierney, A. T., Krizman, J., Kraus, N., & Tallal, P. (2015). Music training alters the course of adolescent auditory development. *Proceedings of the National Academy of Sciences of the United States of America*, *112*(32), 10062–10067. https://doi.org/10.1073/pnas.1505114112

Tierney, A., Rosen, S., & Dick, F. (2020). Speech-in-Speech Perception, Nonverbal Selective Attention, and Musical Training. *Journal of Experimental Psychology:*

Learning Memory and Cognition, *46*(5), 968–979. https://doi.org/10.1037/xlm0000767

Toda, T., Shinmyo, Y., Dinh Duong, T. A., Masuda, K., & Kawasaki, H. (2016). An essential role of SVZ progenitors in cortical folding in gyrencephalic mammals. *Scientific Reports*, *6*(1), 29578. https://doi.org/10.1038/srep29578

Toh, A., Togneri, R., & Nordholm, S. (2005). Spectral entropy as speech features for speech recognition. *Proceedings of PEECS*.

Tollin, D. J. (2003). The lateral superior olive: A functional role in sound source localization. *The Neuroscientist: A Review Journal Bringing Neurobiology, Neurology and Psychiatry*, *9*(2), 127–143. https://doi.org/10.1177/1073858403252228

Torsten, H., Kurt, H., & Achim, Z. (2006). Unbiased Recursive Partitioning: A Conditional Interference Framework. *Journal of Computational and Graphical Statistics*, *15*(3), 651–674.

Turker, S., Reiterer, S. M., Schneider, P., & Seither-Preisler, A. (2019). Auditory Cortex Morphology Predicts Language Learning Potential in Children and Teenagers. *Frontiers in Neuroscience*, *13*.

Turker, S., Reiterer, S. M., Seither-Preisler, A., & Schneider, P. (2017). "When Music Speaks": Auditory Cortex Morphology as a Neuroanatomical Marker of Language Aptitude and Musicality. *Frontiers in Psychology*, *8*.

Tzourio-Mazoyer, N., Maingault, S., Panzieri, J., Pepe, A., Crivello, F., & Mazoyer, B. (2019). Intracortical Myelination of Heschl's Gyrus and the Planum Temporale Varies With Heschl's Duplication Pattern and Rhyming Performance: An Investigation of 440 Healthy Volunteers. *Cerebral Cortex*, *29*(5), 2072–2083. https://doi.org/10.1093/cercor/bhy088

Tzourio-Mazoyer, N., & Mazoyer, B. (2017). Variations of planum temporale asymmetries with Heschl's Gyri duplications and association with cognitive abilities: MRI investigation of 428 healthy volunteers. *Brain Structure and Function*, *222*(6), 2711–2726. https://doi.org/10.1007/s00429-017-1367-5

Ullén, F. (2009). Is activity regulation of late myelination a plastic mechanism in the human nervous system? *Neuron Glia Biology*, *5*(1-2), 29–34. https://doi.org/10.1017/S1740925X09990330

Uttal, W. R. (2001). *The new phrenology: The limits of localizing cognitive functions in the brain*. Cambridge, MA: MIT Press.

Vaag, J., Sund, E. R., & Bjerkeset, O. (2018). Five-factor personality profiles among Norwegian musicians compared to the general workforce. *Musicae Scientiae*, *22*(3), 434–445. https://doi.org/10.1177/1029864917709519

Van Der Meer, D., Kaufmann, T., Shadrin, A. A., Makowski, C., Frei, O., Roelfs, D., Monereo-Sánchez, J., Linden, D. E., Rokicki, J., Alnæs, D., et al. (2021). The genetic architecture of human cortical folding. *Science Advances*, *7*(51), eabj9446. https://doi.org/10.1126/sciadv.abj9446

van Dijk, J. A., de Haas, B., Moutsiana, C., & Schwarzkopf, D. S. (2016). Intersession reliability of population receptive field estimates. *NeuroImage*, *143*, 293–303. https://doi.org/10.1016/j.neuroimage.2016.09.013

Van Essen, D. C. (1997). A tension-based theory of morphogenesis and compact wiring in the central nervous system. *Nature*, *385*(6614), 313–318. https://doi.org/10.1038/385313a0

Van Essen, D. C. (2020). A 2020 view of tension-based cortical morphogenesis. *Proceedings of the National Academy of Sciences*, *117*(52), 32868–32879. https://doi.org/10.1073/pnas.2016830117

Vandermosten, M., Price, C. J., & Golestani, N. (2016). Plasticity of white matter connectivity in phonetics experts. *Brain Structure and Function*, *221*(7), 3825–3833. https://doi.org/10.1007/s00429-015-1114-8

Versnel, H., Zwiers, M. P., & van Opstal, A. J. (2009). Spectrotemporal Response Properties of Inferior Colliculus Neurons in Alert Monkey. *Journal of Neuroscience*, *29*(31), 9725–9739. https://doi.org/10.1523/JNEUROSCI.5459-08.2009

Voegtline, K. M., Costigan, K. A., Pater, H. A., & DiPietro, J. A. (2013). Near-term fetal response to maternal spoken voice. *Infant Behavior & Development*, *36*(4), 10.1016/j.infbeh.2013.05.002. https://doi.org/10.1016/j.infbeh.2013.05.002

Vuust, P., Brattico, E., Seppänen, M., Näätänen, R., & Tervaniemi, M. (2012). The sound of music: Differentiating musicians using a fast, musical multi-feature mismatch negativity paradigm. *Neuropsychologia*, *50*(7), 1432–1443. https://doi.org/10.1016/j.neuropsychologia.2012.02.028

Wähnert, M., Dinse, J., Schäfer, A., Geyer, S., Bazin, P.-L., Turner, R., & Tardif, C. L. (2016). A subject-specific framework for in vivo myeloarchitectonic analysis using high resolution quantitative MRI. *NeuroImage*, *125*, 94–107. https://doi.org/10.1016/j.neuroimage.2015.10.001

Wallace, M. N., Cronin, M. J., Bowtell, R. W., Scott, I. S., Palmer, A. R., & Gowland, P. A. (2016). Histological Basis of Laminar MRI Patterns in High Resolution Images of Fixed Human Auditory Cortex. *Frontiers in Neuroscience*, *10*. https://doi.org/10.3389/fnins.2016.00455

Wallace, M. N., Johnston, P., & Palmer, A. R. (2002). Histochemical identification of cortical areas in the auditory region of the human brain. *Experimental Brain Research*, *143*(4), 499–508. https://doi.org/10.1007/s00221-002-1014-z

Walsh, E. J., McGee, J., & Javel, E. (1986). Development of auditory-evoked potentials in the cat. I. Onset of response and development of sensitivity. *The Journal of the Acoustical Society of America*, *79*(3), 712–724. https://doi.org/10.1121/1.393461

Wang, L., Hou, S., & Han, Y.-G. (2016). Hedgehog signaling promotes basal progenitor expansion and the growth and folding of the neocortex. *Nature Neuroscience*, *19*(7), 888–896. https://doi.org/10.1038/nn.4307

Wang, X., Studholme, C., Grigsby, P. L., Frias, A. E., Cuzon Carlson, V. C., & Kroenke, C. D. (2017). Folding, But Not Surface Area Expansion, Is Associated with Cellular Morphological Maturation in the Fetal Cerebral Cortex. *The Journal of Neuroscience*, *37*(8), 1971–1983. https://doi.org/10.1523/JNEUROSCI.3157-16.2017

Wang, X., Tsai, J.-W., Imai, J. H., Lian, W.-N., Vallee, R. B., & Shi, S.-H. (2009). Asymmetric centrosome inheritance maintains neural progenitors in the neocortex. *Nature*, *461*(7266), 947–955. https://doi.org/10.1038/nature08435

Wang, X., Tsai, J.-W., LaMonica, B., & Kriegstein, A. R. (2011). A new subtype of progenitor cell in the mouse embryonic neocortex. *Nature Neuroscience*, *14*(5), 555–561. https://doi.org/10.1038/nn.2807

Warrier, C., Wong, P., Penhune, V., Zatorre, R., Parrish, T., Abrams, D., & Kraus, N. (2009a). Relating Structure to Function: Heschl's Gyrus and Acoustic Processing. *Journal of Neuroscience*, *29*(1), 61–69. https://doi.org/10.1523/JNEUROSCI.3489-08.2009

Warrier, C., Wong, P., Penhune, V., Zatorre, R., Parrish, T., Abrams, D., & Kraus, N. (2009b). Relating structure to function: Heschl's gyrus and acoustic processing. *The Journal of Neuroscience : The Official Journal of the Society for Neuroscience*, *29*(1), 61–69. https://doi.org/10.1523/JNEUROSCI.3489-08.2009

Wehr, M., & Zador, A. M. (2003). Balanced inhibition underlies tuning and sharpens spike timing in auditory cortex. *Nature*, *426*(6965), 442–446. https://doi.org/10.1038/nature02116

Wei, H., Xie, L., Dibb, R., Li, W., Decker, K., Zhang, Y., Johnson, G. A., & Liu, C. (2016). Imaging whole-brain cytoarchitecture of mouse with MRI-based quantitative susceptibility mapping. *NeuroImage*, *137*, 107–115. https://doi.org/10.1016/j.neuroimage.2016.05.033

Weiner, K. S., Barnett, M. A., Lorenz, S., Caspers, J., Stigliani, A., Amunts, K., Zilles, K., Fischl, B., & Grill-Spector, K. (2017). The Cytoarchitecture of Domain-specific Regions in Human High-level Visual Cortex. *Cerebral Cortex*, *27*(1), 146–161. https://doi.org/10.1093/cercor/bhw361

Weiskopf, N., Callaghan, M. F., Josephs, O., Lutti, A., & Mohammadi, S. (2014). Estimating the apparent transverse relaxation time (R2*) from images with different

contrasts (ESTATICS) reduces motion artifacts. *Frontiers in Neuroscience*, *8*, 278. https://doi.org/10.3389/fnins.2014.00278

Weiskopf, N., Edwards, L. J., Helms, G., Mohammadi, S., & Kirilina, E. (2021). *Quantitative magnetic resonance imaging of brain anatomy and in vivo histology*. *3*(8), 570–588.

Weiskopf, N., Mohammadi, S., Lutti, A., & Callaghan, M. F. (2015). Advances in MRI-based computational neuroanatomy: From morphometry to in-vivo histology. *Current Opinion in Neurology*, *28*(4), 313–322. https://doi.org/10.1097/wco.0000000000000222

Weiskopf, N., Suckling, J., Williams, G., Correia, M. M., & Inkster, B. (2013). Quantitative multi-parameter mapping of R1, PD* ,MT , and R2* at 3T: A multi-center validation. *Frontiers in Neuroscience*, *10*(June), 1–11. https://doi.org/10.3389/fnins.2013.00095

Welker, W. (1990). Why does the cortex fissure and fold: A review of determinants of gyri and sulci. *Cerebral Cortex: Comparative Structure and Evolution of Cerebral Cortex*, 3–136.

Wengenroth, M., Blatow, M., Bendszus, M., & Schneider, P. (2010). Leftward Lateralization of Auditory Cortex Underlies Holistic Sound Perception in Williams Syndrome. *PLOS ONE*, *5*(8), e12326. https://doi.org/10.1371/journal.pone.0012326

Wengenroth, M., Blatow, M., Heinecke, A., Reinhardt, J., Stippich, C., Hofmann, E., & Schneider, P. (2014). Increased Volume and Function of Right Auditory Cortex as a Marker for Absolute Pitch. *Cerebral Cortex*, *24*(5), 1127–1137. https://doi.org/10.1093/cercor/bhs391

Wess, J. M., Isaiah, A., Watkins, P. V., & Kanold, P. O. (2017). Subplate neurons are the first cortical neurons to respond to sensory stimuli. *Proceedings of the National Academy of Sciences of the United States of America*, *114*(47), 12602–12607. https://doi.org/10.1073/pnas.1710793114

White, T., Andreasen, N. C., & Nopoulos, P. (2002). Brain volumes and surface morphology in monozygotic twins. *Cerebral Cortex*, *12*(5), 486–493. https://doi.org/10.1093/cercor/12.5.486

Whitton, J. P., Hancock, K. E., Shannon, J. M., & Polley, D. B. (2017). Audiomotor perceptual training enhances speech intelligibility in background noise. *Current Biology*, *27*(21), 3237–3247.

Wiggins, G. A., Müllensiefen, D., & Pearce, M. T. (2010). On the non-existence of music: Why music theory is a figment of the imagination. *Musicae Scientiae*, *14*(1_suppl), 231–255. https://doi.org/10.1177/10298649100140S110

Williams, V. J., Juranek, J., Cirino, P., & Fletcher, J. M. (2018). Cortical Thickness and Local Gyrification in Children with Developmental Dyslexia. *Cerebral Cortex*, *28*(3), 963–973. https://doi.org/10.1093/cercor/bhx001

Winer, J. A. (1984). Anatomy of layer IV in cat primary auditory cortex (AI). *The Journal of Comparative Neurology*, *224*(4), 535–567. https://doi.org/10.1002/cne.902240405

Wong, C., Chabot, N., Kok, M. A., & Lomber, S. G. (2014). Modified Areal Cartography in Auditory Cortex Following Early- and Late-Onset Deafness. *Cerebral Cortex*, *24*(7), 1778–1792. https://doi.org/10.1093/cercor/bht026

Wong, F. K., Fei, J.-F., Mora-Bermúdez, F., Taverna, E., Haffner, C., Fu, J., Anastassiadis, K., Stewart, A. F., & Huttner, W. B. (2015). Sustained Pax6 Expression Generates Primate-like Basal Radial Glia in Developing Mouse Neocortex. *PLOS Biology*, *13*(8), e1002217. https://doi.org/10.1371/journal.pbio.1002217

Wong, P. C. M., Skoe, E., Russo, N. M., Dees, T., & Kraus, N. (2007). Musical experience shapes human brainstem encoding of linguistic pitch patterns. *Nature Neuroscience*, *10*(4), 420–422. https://doi.org/10.1038/nn1872

Wong, P. C. M., Warrier, C. M., Penhune, V. B., Roy, A. K., Sadehh, A., Parrish, T. B., & Zatorre, R. J. (2008). Volume of Left Heschl's Gyrus and Linguistic Pitch Learning. *Cerebral Cortex (New York, N.Y. : 1991)*, *18*(4), 828–836. https://doi.org/10.1093/cercor/bhm115

Woods, D. L., Stecker, G. C., Rinne, T., Herron, T. J., Cate, A. D., Yund, E. W., Liao, I., & Kang, X. (2009). Functional maps of human auditory cortex: Effects of acoustic features and attention. *PLoS ONE*, *4*(4). https://doi.org/10.1371/journal.pone.0005183

Woods, D., Herron, T., Cate, A., Yund, E. W., Stecker, G. C., Rinne, T., & Kang, X. (2010). Functional Properties of Human Auditory Cortical Fields. *Frontiers in Systems Neuroscience*, *4*.

Woolsey, C. (1971). Tonotopic organization of the auditory cortex. *Physiology of the Auditory System*, 271–282.

Woolsey, C., & Walzl, E. (1942). Topical projection of nerve fibers from local regions of the cochlea to the cerebral cortex of the cat. *Bull. Johns Hopdins Hosp.*, *71*, 315–344.

Wright, B. A., & Fitzgerald, M. B. (2005). Learning and generalization on five basic auditory discrimination tasks as assessed by threshold changes. In *Auditory signal processing* (pp. 509–515). Springer.

Wright, B. A., & Sabin, A. T. (2007). Perceptual learning: How much daily training is enough? *Experimental Brain Research*, *180*(4), 727–736. https://doi.org/10.1007/s00221-007-0898-z

Wright, D. B., London, K., & Field, A. P. (2011). Using Bootstrap Estimation and the Plug-in Principle for Clinical Psychology Data. *Journal of Experimental Psychopathology*, *2*(2), 252–270. https://doi.org/10.5127/jep.013611

WU-Minn, H. (2017). 1200 subjects data release reference manual. *URL Https://Www.humanconnectome.org*.

Xu, G., Knutsen, A. K., Dikranian, K., Kroenke, C. D., Bayly, P. V., & Taber, L. A. (2010). Axons Pull on the Brain, But Tension Does Not Drive Cortical Folding. *Journal of Biomechanical Engineering*, *132*(7), 071013. https://doi.org/10.1115/1.4001683

Yang, S., Wagstyl, K., Meng, Y., Zhao, X., Li, J., Zhong, P., Li, B., Fan, Y.-S., Chen, H., & Liao, W. (2021). Cortical patterning of morphometric similarity gradient reveals diverged hierarchical organization in sensory-motor cortices. *Cell Reports*, *36*(8), 109582. https://doi.org/10.1016/j.celrep.2021.109582

Yarkoni, T. (2009). Big Correlations in Little Studies: Inflated fMRI Correlations Reflect Low Statistical Power on Vul et al. (2009). *Perspectives on Psychological Science*, *4*(3), 294–298. https://doi.org/10.1111/j.1745-6924.2009.01127.x

Yoo, J., & Bidelman, G. M. (2019). Linguistic, perceptual, and cognitive factors underlying musicians' benefits in noise-degraded speech perception. *Hearing Research*, *377*, 189–195. https://doi.org/10.1016/j.heares.2019.03.021

Zachlod, D., Rüttgers, B., Bludau, S., Mohlberg, H., Langner, R., Zilles, K., & Amunts, K. (2020). Four new cytoarchitectonic areas surrounding the primary and early auditory cortex in human brains. *Cortex*, *128*, 1–21. https://doi.org/10.1016/j.cortex.2020.02.021

Zaltz, Y., Globerson, E., & Amir, N. (2017). Auditory Perceptual Abilities Are Associated with Specific Auditory Experience. *Frontiers in Psychology*, *8*. https://doi.org/10.3389/fpsyg.2017.02080

Zatorre, R. (2005). Music, the food of neuroscience? *Nature*, *434*(7031), 312–315. https://doi.org/10.1038/434312a

Zatorre, R. J., & Belin, P. (2001). Spectral and Temporal Processing in Human Auditory Cortex. *Cerebral Cortex*, *11*(10), 946–953. https://doi.org/10.1093/cercor/11.10.946

Zatorre, R. J., Chen, J. L., & Penhune, V. B. (2007). When the brain plays music: Auditory-motor interactions in music perception and production. *Nature Reviews. Neuroscience*, *8*(7), 547–558. https://doi.org/10.1038/nrn2152

Zendel, B. R., & Alain, C. (2009). Concurrent sound segregation is enhanced in musicians. *Journal of Cognitive Neuroscience*, *21*(8), 1488–1498. https://doi.org/10.1162/jocn.2009.21140

Zhang, L. I., Bao, S., & Merzenich, M. M. (2002). Disruption of primary auditory cortex by synchronous auditory inputs during a critical period. *Proceedings of the National Academy of Sciences of the United States of America*, *99*(4), 2309–2314. https://doi.org/10.1073/pnas.261707398

Zhang, L. I., Bao, S., & Merzenich, M. M. (2001). Persistent and specific influences of early acoustic environments on primary auditory cortex. *Nature Neuroscience*, *4*(11), 1123–1130. https://doi.org/10.1038/nn745

Zhao, C., Kao, J. P. Y., & Kanold, P. O. (2009). Functional Excitatory Microcircuits in Neonatal Cortex Connect Thalamus and Layer 4. *The Journal of Neuroscience*, *29*(49), 15479–15488. https://doi.org/10.1523/JNEUROSCI.4471-09.2009

Zilles, K., & Amunts, K. (2010). Centenary of Brodmann's map–conception and fate. *Nature Reviews Neuroscience*, *11*(2), 139–145. https://doi.org/10.1038/nrn2776

Zoellner, S., Benner, J., Zeidler, B., Seither-Preisler, A., Christiner, M., Seitz, A., Goebel, R., Heinecke, A., Wengenroth, M., Blatow, M., & Schneider, P. (2018). Reduced cortical thickness in Heschl's gyrus as an in vivo marker for human primary auditory cortex. *Human Brain Mapping*, *40*(4), 1139–1154. https://doi.org/10.1002/hbm.24434

Zola-Morgan, S. (1995). Localization of brain function: The legacy of Franz Joseph Gall (1758-1828). *Annual Review of Neuroscience*, *18*(1), 359–383.

Zwicker, E., & Zwicker, U. T. (1991). Audio engineering and psychoacoustics. Matching signals to the final receiver, the human auditory system. In *AES: Journal of the Audio Engineering Society* (Vol. 39, pp. 115–126).

Supplementary figures

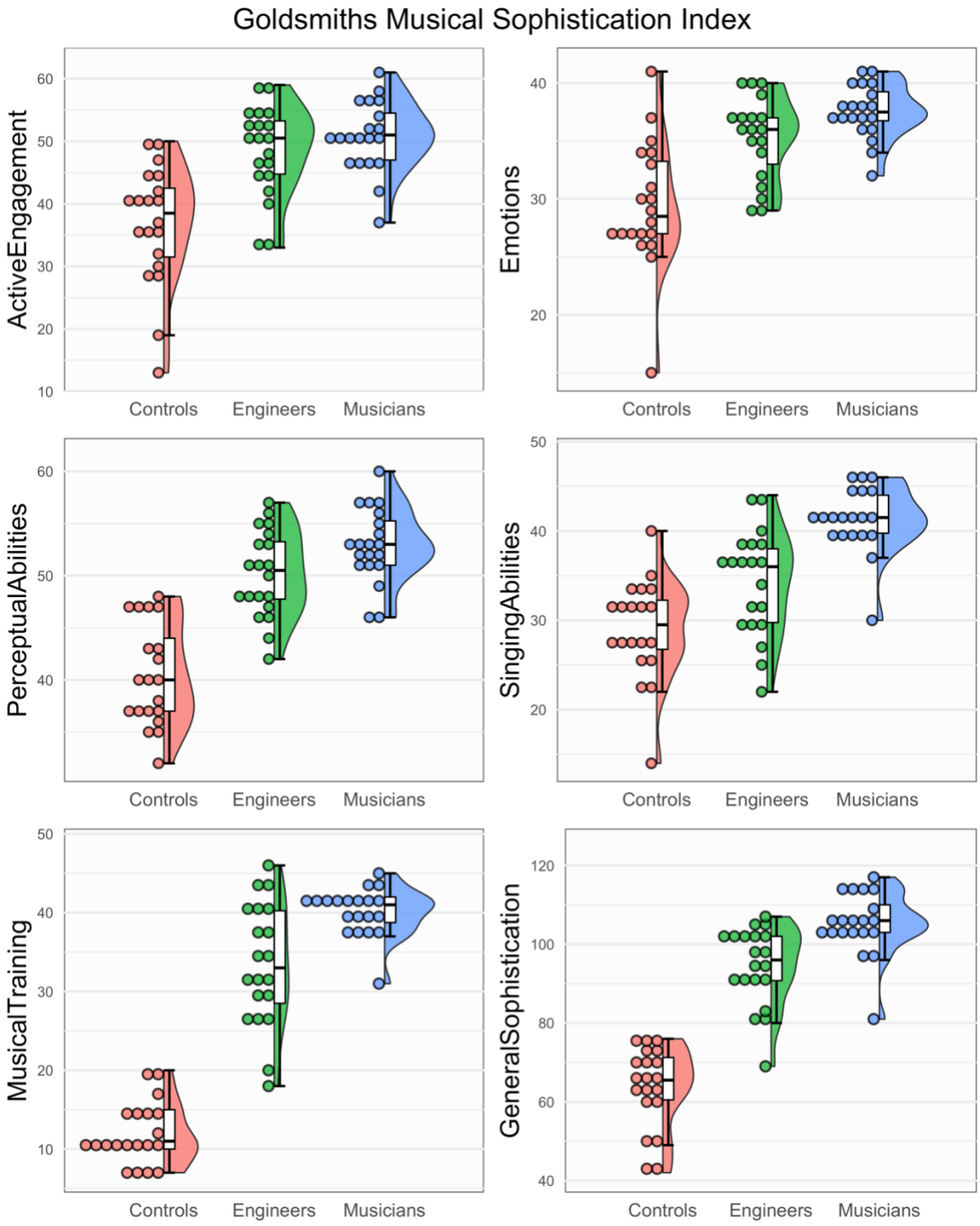

***Figure S1**: Dot plots, same area violin plots, and box plots for the Goldsmiths Musical Sophistication Index (Gold-MSI) scores.*

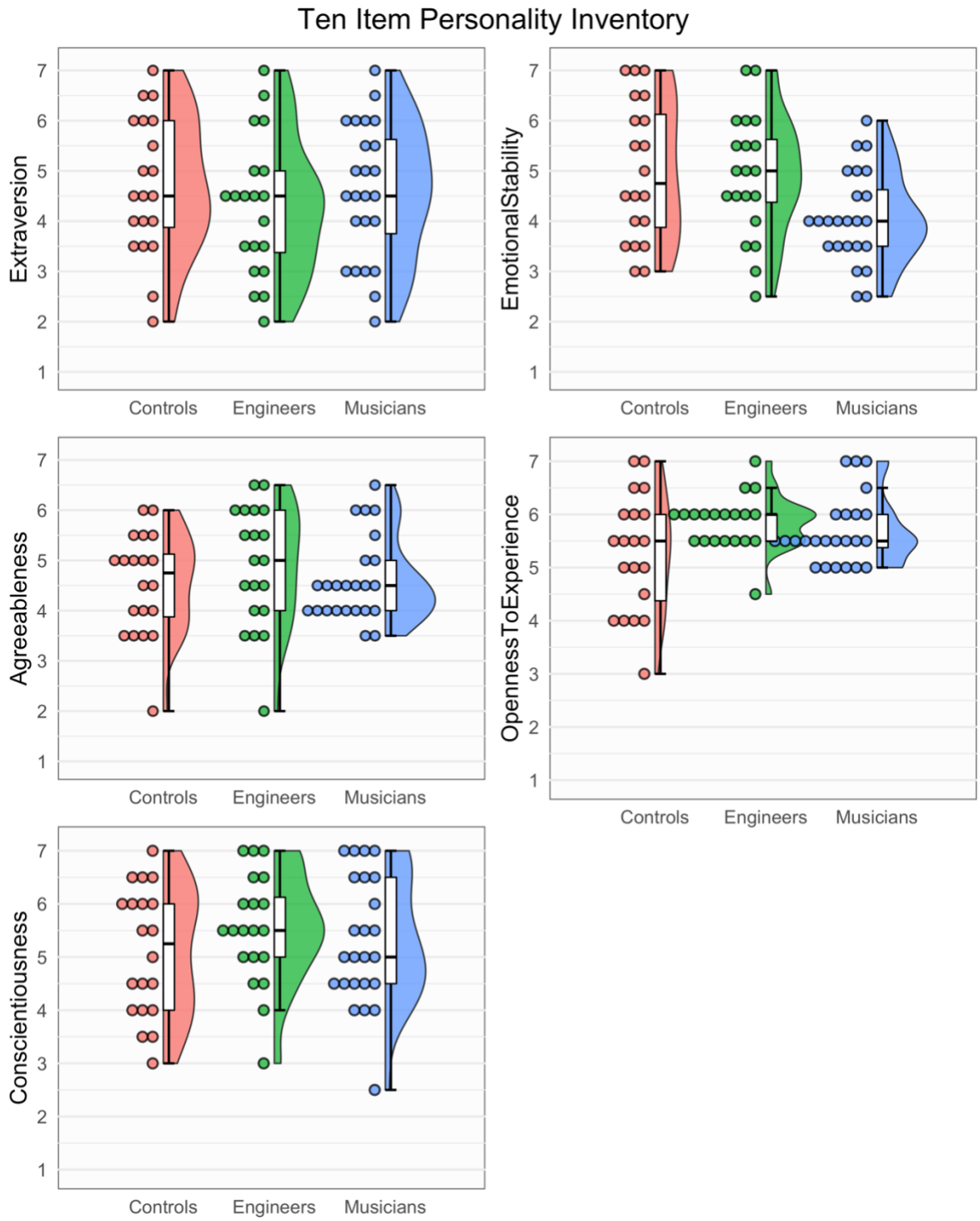

Figure S2*: Dot plots, same area violin plots, and box plots for the Ten Item Personality Inventory (TIPI) scores.*

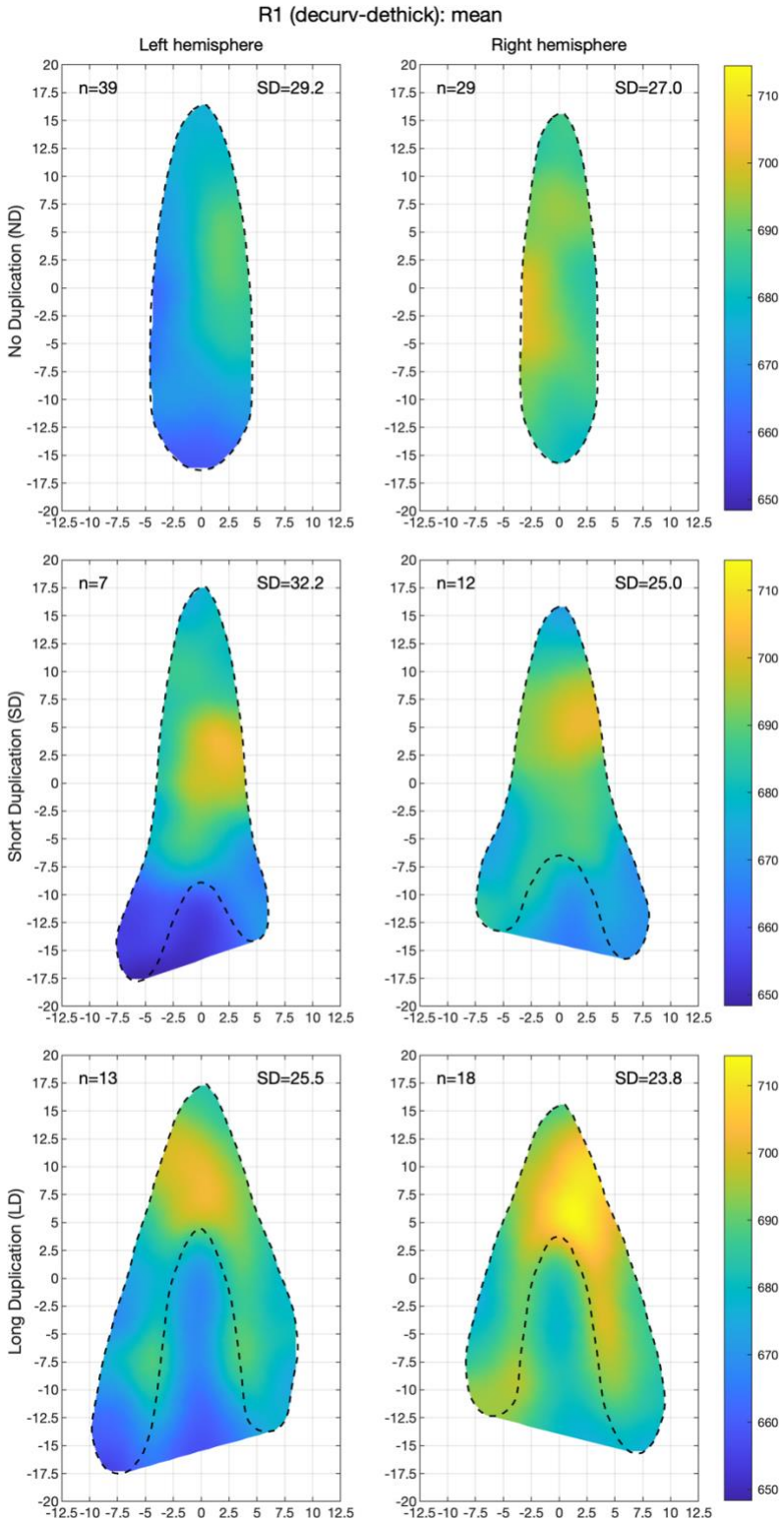

Figure S3*: Average R1 maps for each morphological type and hemisphere resampled onto average flat patches, residualised for curvature and thickness. The number on the top-left corner of each plot indicates the number of hemispheres used to calculate each average. The number on the top right indicates the average standard deviation of all the individual datasets used to compute each map. Dashed black lines indicate gyral boundaries. Coordinates are in millimetres.*

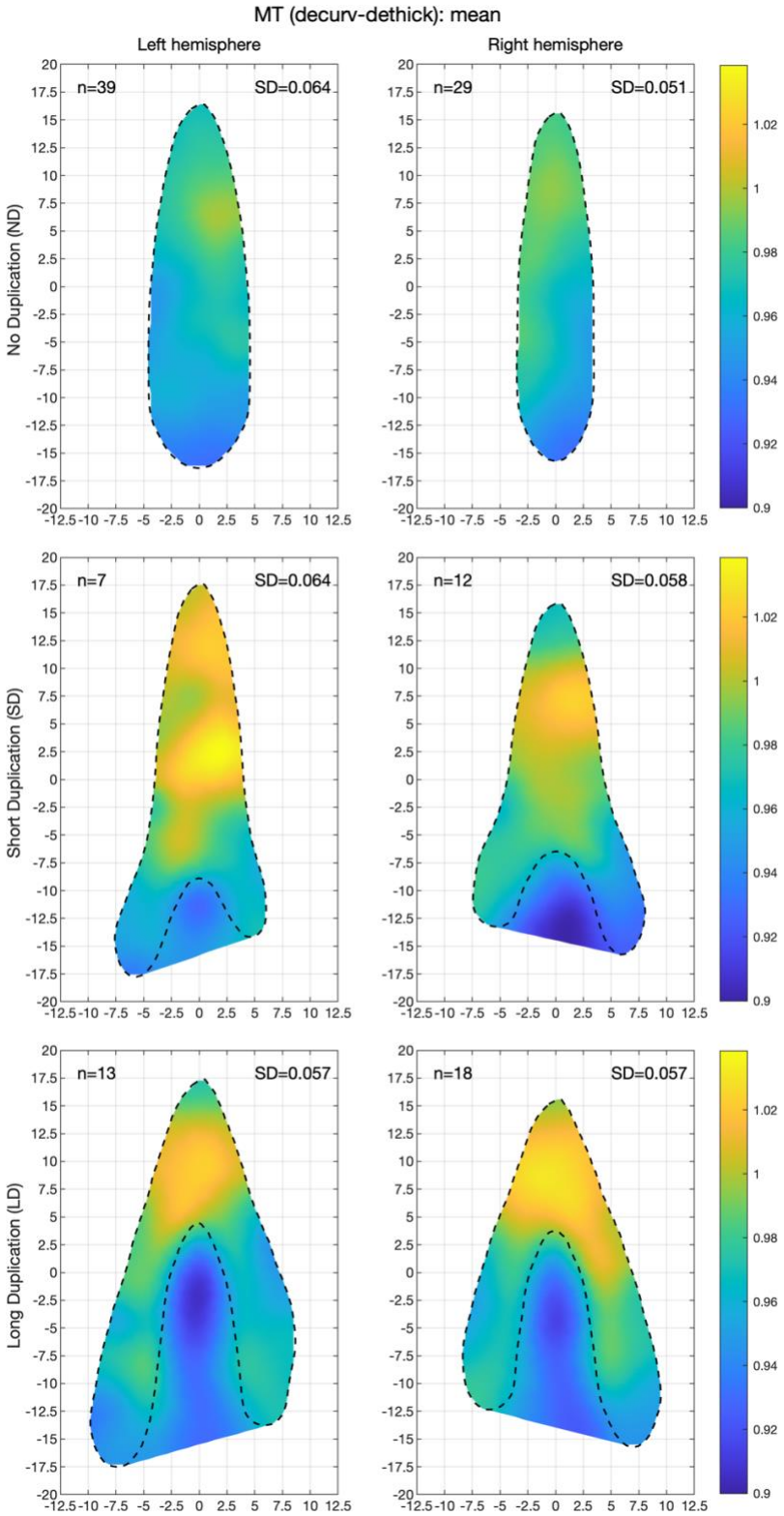

Figure S4*: Average MT maps for each morphological type and hemisphere resampled onto average flat patches, residualised for curvature and thickness. The number on the top-left corner of each plot indicates the number of hemispheres used to calculate each average. The number on the top right indicates the average standard deviation of all the individual datasets used to compute each map. Dashed black lines indicate gyral boundaries. Coordinates are in millimetres.*

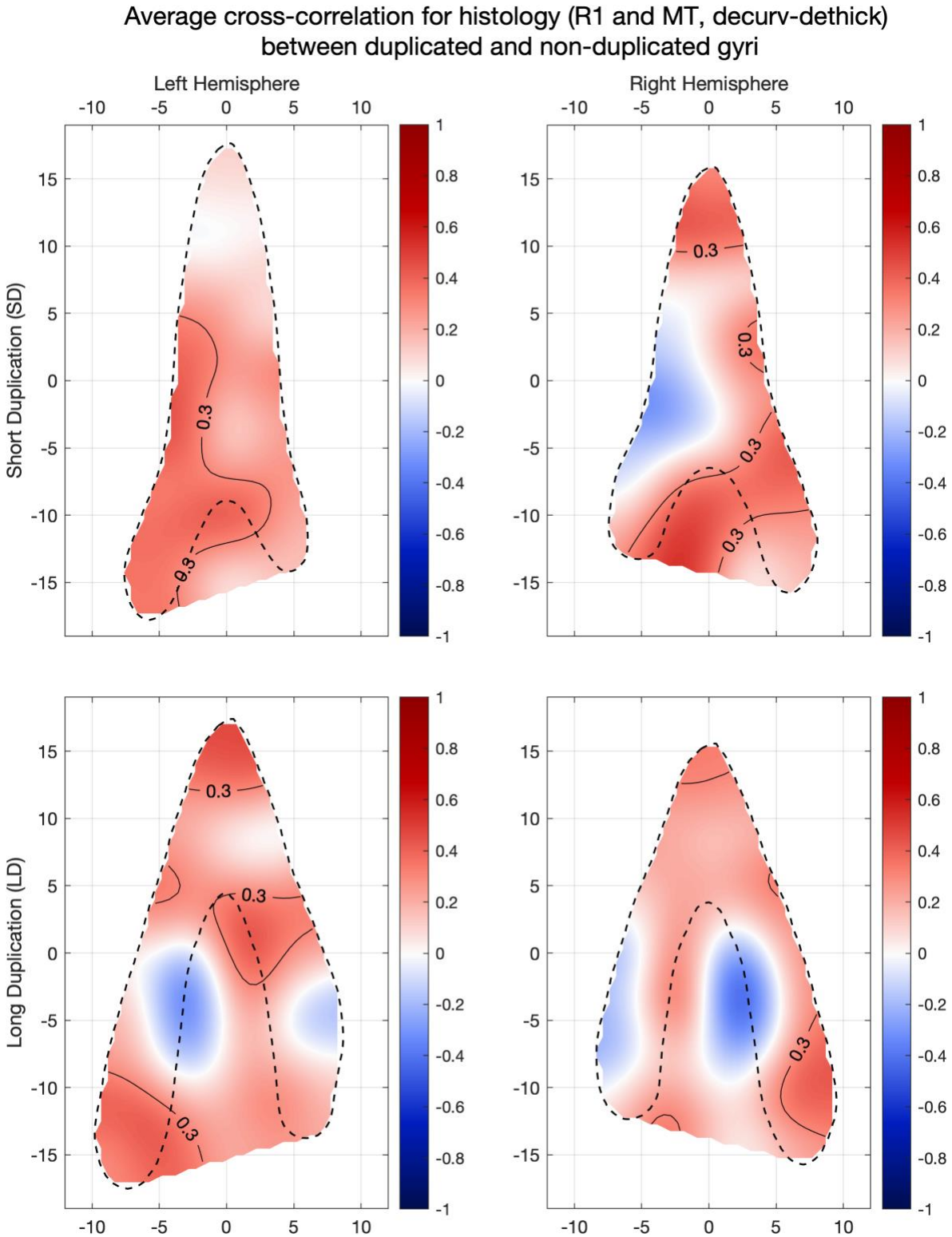

Figure S5*: Average cross-correlations between partially duplicated and non-duplicated gyri obtained with R1 and MT data. Regions with high cross-correlations (in darker shades of red) represent regions of partially-duplicated gyri whose histological gradients are the most similar to the gradients of non-duplicated gyri. Black contour lines mark correlation values of 0.3.*

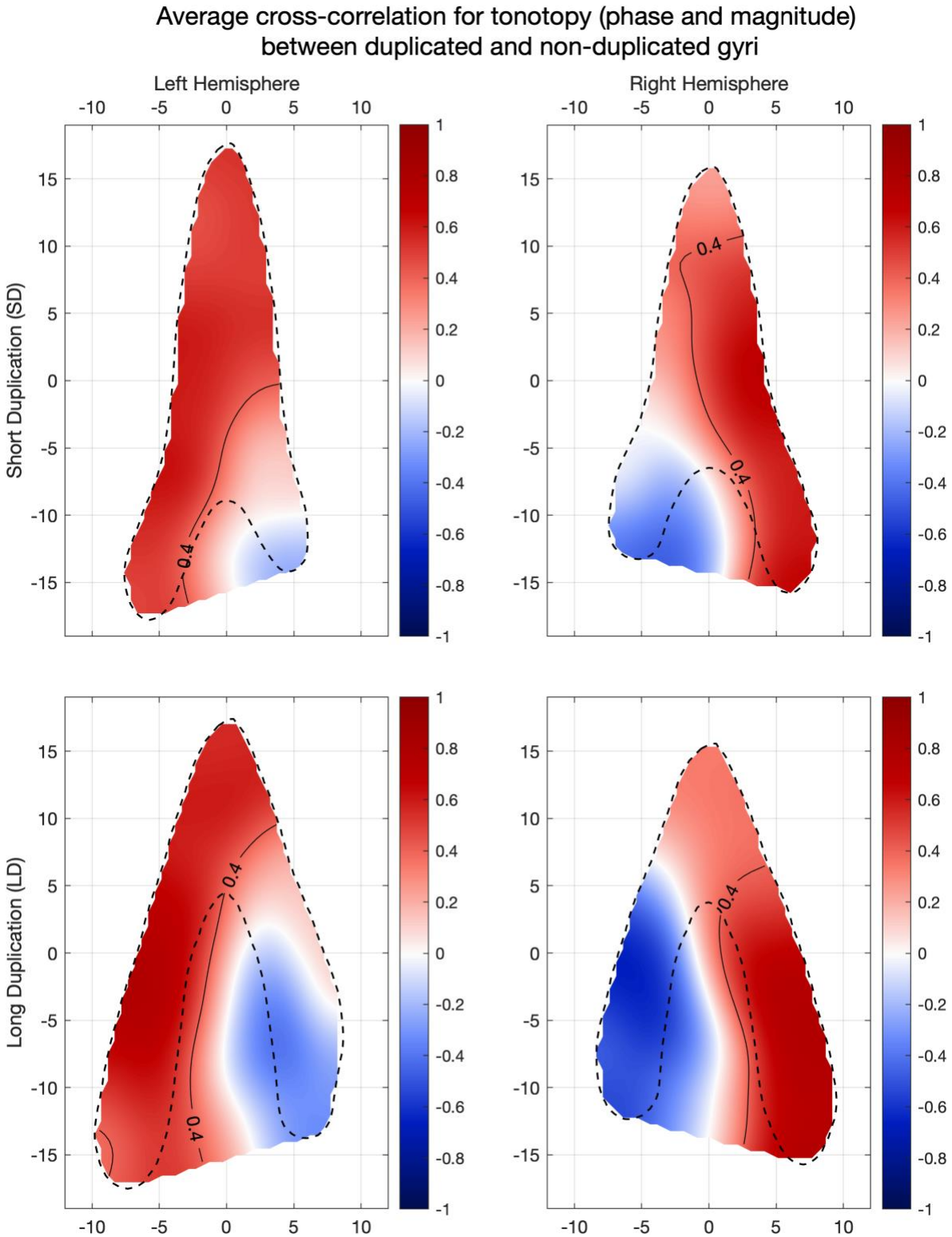

***Figure S6**: Average cross-correlations between partially duplicated and non-duplicated gyri obtained with tonotopic data. Regions with high cross-correlations (in darker shades of red) represent regions of partially-duplicated gyri whose tonotopic gradients are the most similar to the gradients of non-duplicated gyri. Black contour lines mark correlation values of 0.4*

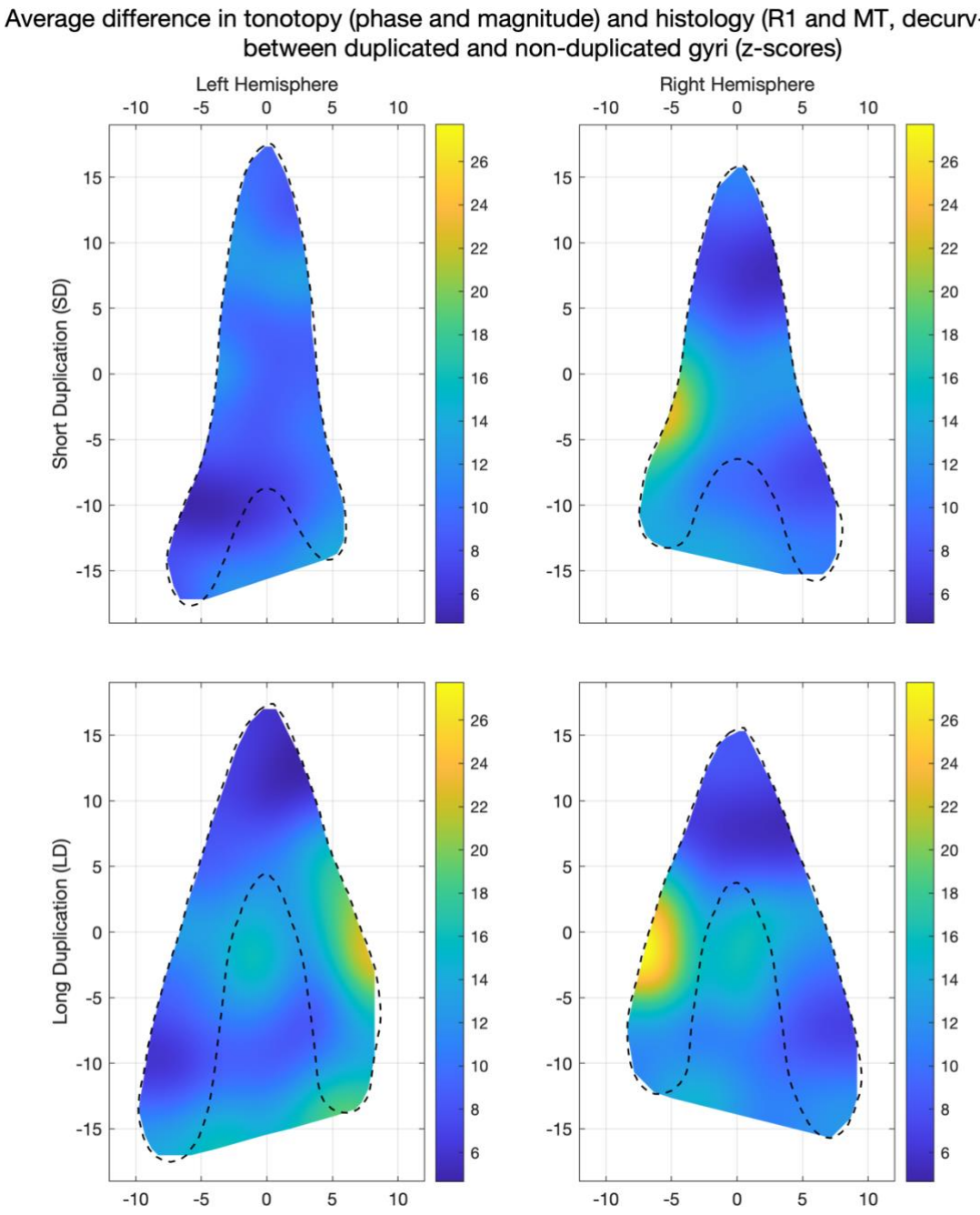

Figure S7*: Average sum of squared differences between partially duplicated and non-duplicated gyri in onotopy (phase and magnitude), R1, and MT data, after correcting for cortical curvature and thickness. Regions with low sum of squared differences (in darker shades of blue) represent regions of partially-duplicated gyri most similar to non-duplicated gyri.*

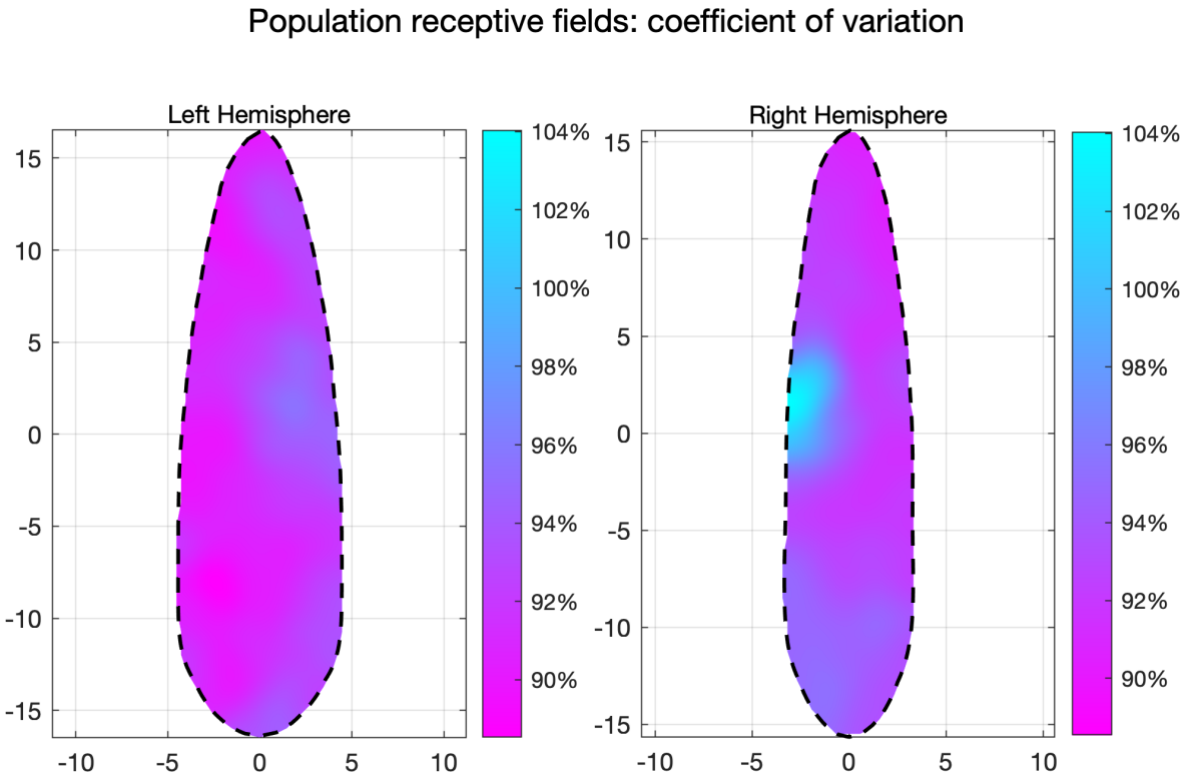

***Figure S8**: Average maps of PRF coefficients of variation, i.e. the ratio of centre frequency and tuning width.*